DEVELOPMENT AND CHARACTERIZATION OF GEL-LIKE STRUCTURES FROM AQUATIC BIOMASS FOR FOOD APPLICATIONS

OBTENCIÓN Y CARACTERIZACIÓN DE ESTRUCTURAS TIPO GEL A PARTIR DE BIOMASA ACUÁTICA PARA APLICACIONES ALIMENTARIAS

DOCTORAL THESIS

Cynthia Fontes Candia

Directed by:
Dra. Amparo López Rubio
Dra. Marta Martínez Sanz

January 2022

UNIVERSITAT POLITÈCNICA DE VALÈNCIA

iata
Instituto de Agroquímica y Tecnología de Alimentos

TESIS DOCTORAL

Doctorado en Ciencias, Tecnología y Gestión Alimentaria

Cynthia Fontes Candia

Development and characterization of gel-like structures from aquatic biomass for food applications

Obtención y caracterización de estructuras tipo gel a partir de biomasa acuática para aplicaciones alimentarias

Directoras:

Dra. Amparo López Rubio

Dra. Marta Martínez Sanz

Diciembre, 2021

A mis padres

Agradecimientos

Quiero dar las gracias a todas las personas que directa o indirectamente fueron parte de esta tesis, gracias por acompañarme durante todo este tiempo y formar parte de mi vida durante esta bonita etapa.

En primer lugar, quiero agradecer a mis directoras, ya que definitivamente esto no sería posible sin ellas. Amparo, gracias por brindarme tu confianza desde el día uno y hacerme parte de este grupo tan lindo que has formado. Gracias por siempre ser esa persona que está dispuesta a ayudar y buscar el bienestar de todos los que te rodean, también gracias por impulsarme siempre a ser mejor y a superarme en cada momento. Marta, como te lo he dicho muchas veces, no que se hubiera hecho si ti, doy gracias porque me tocara compartir esta etapa contigo, gracias por tu apoyo siempre, por compartir todo tu conocimiento y hacerme crecer tanto.

También quiero agradecer a la persona que ha sido mi compañero de aventura, Ever, gracias por todo tu apoyo, por tu paciencia y por nunca solarme. Ha sido una gran experiencia poder compartir esta etapa a tu lado. Y así como tú lo dices, indudablemente lo volvería a hacer. Espero la vida nos siga sorprendiendo gratamente y seguir compartiendo contigo lo que venga.

A mis padres y mis hermanos que siempre estuvieron presente, por su apoyo incondicional, han sido un pilar fundamental en esta etapa de mi vida. Gracias por esas videollamadas que me inyectaban energía al alma, gracias por hacerme sentir cerca en todo momento, por sus palabras de aliento y motivarme siempre a seguir. A mi Leo bebe que con su sonrisa me alegra la vida. A mamá Irma por su cariño, por echarme porras siempre y compartir siempre mis alegrías.

A mis compis de laboratorio, Zaida, Daniel, Vera, Isaac, Hyleene ¿qué haría yo sin ustedes? Gracias por todos los mementos vividos, dentro y fuera del laboratorio. Gracias por las risas, los abrazos de ánimo y hasta las lágrimas que hemos compartido. Han sido una parte muy importante en esta etapa, y aunque esto no es una despedida quiero que sepan que me los llevo para siempre en mi corazón.

Agradecimientos

A mi querida María José, gracias por siempre mostrar esa buena disposición para ayudarme cuando lo necesitaba, ha sido una gran experiencia compartir estos años contigo. Antonio, que siempre con su buen humor y palabras de ánimo hacen el que el día a día en el laboratorio sean mejores. Agustín, gracias por compartir tus conocimientos con nosotros y por hacer que no explotemos en el laboratorio, eres una piensa clave en nuestro laboratorio, ha sido un placer compartir estos años contigo.

A Javier y Pepe por siempre estar dispuestos a ayudar y ser tan dedicados en su trabajo, siempre buscando lo mejor para hacernos más fácil la vida.

A las personas que han formado parte de los trabajos de esta tesis, gracias por compartir sus conocimientos conmigo. Patricia, Anna, Laura, Marisi y Beatriz.

A mi familia política, que me han adoptado como una más y siempre están ahí brindándome su apoyo y cariño.

A mi querida Sandy, por siempre estar presente durante estos años, por tus múltiples detalles y muestras de cariño.

A mi familia y mis amigos que a la distancia siempre estuvieron presentes compartiendo los bueno momentos y alentándome en los no tan buenos.

¡MI ETERNO AGRADECIMIENTO Y CARIÑO PARA TODOS USTEDES!

Abstract

The aim of this doctoral thesis was to design and characterize the structure of gel-like structures based on polysaccharides extracted from aquatic biomass, with interest for food-related applications. The properties of polysaccharides extracted from seaweeds and aquatic plants make them suitable to produce a range of gel-like structures based on the formation of interconnected networks, such as hydrogels, aerogels and emulsion-gels.

In the first part of this thesis, the different gelation mechanism of sulphated polysaccharides and the parameters affecting the structure and functional properties of the obtained hydrogels were investigated. Based on the results, the potential application of agar and κ-carrageenan hydrogels and aerogels to encapsulate a model food protein such as casein was evaluated, thus exploring the protective effect against the enzymatic hydrolysis upon simulated gastrointestinal digestions.

In the second part of this thesis, aerogel structures were developed by valorising an underutilized waste biomass source such as *Arundo donax.* This biomass was used to generate cellulosic fractions with different purification degrees and water-soluble bioactive extracts, which were subsequently used to produce hybrid bioactive aerogels. The highly porous structure and high sorption capacity of aerogels make them excellent candidates for the replacement of absorbent pads to maintain the quality of packaged meat products.

Emulsion-gels are recognized for their great potential as functional ingredients in the food industry to modify texture and for solid fat replacement. Moreover, they can be used as a delivery vehicle for the controlled release of fat-soluble bioactive compounds. Thus, in the last part, the nature of interactions between the components in polysaccharide-based emulsion-gel formulations was investigated and related to their structure and mechanical and rheological behavior. After studying the gelation mechanism of carrageenan emulsion-gels, these systems were adapted and used for two different applications relevant to the food and biomedicine sectors. Firstly, oil-filled gel-like structures from agar and κ-carrageenan emulsion-gels and oil-filled aerogels were produced and evaluated as carriers of a lipophilic bioactive such as

curcumin. The results showed that the polysaccharide type and the physical state of the gel network had an impact on the structure of the digestion products.

On the other hand, the potential of emulsion-gels based on sulphated polysaccharides (κ-carrageenan and agar) for the production of tissue mimicking phantoms was evaluated. The results evidence that the agar emulsion-gels are suitable to produce materials simulating the dielectric properties to mimic low- and high-water content tissues.

Resumen

El objetivo de esta tesis doctoral ha sido el diseño y caracterización estructural de estructuras tipo gel basadas de polisacáridos extraídos de biomasa acuática con interés para aplicaciones relacionadas con la alimentación. Las propiedades de los polisacáridos extraídos de algas y plantas acuáticas son adecuadas para producir diferentes estructuras tipo gel basadas en la formación de redes reticuladas, como hidrogeles, aerogeles y emulsion-gels.

En la primera parte de esta tesis se investigaron los diferentes mecanismos de gelificación de polisacáridos sulfatados, así como los parámetros que afectan a la estructura y las propiedades funcionales de los hidrogeles obtenidos. En base a los resultados, se evaluó la potencial aplicación de los hidrogeles y aerogeles de agar y κ-carragenato para encapsular una proteína alimentaria modelo como la caseína, explorando así el efecto protector contra la hidrólisis enzimática tras digestiones gastrointestinales simuladas.

En la segunda parte de esta tesis, se desarrollaron estructuras de aerogeles mediante la valorización de una fuente de biomasa residual infrautilizada, como es el *Arundo donax*. Con esta biomasa se generaron fracciones celulósicas con diferentes grados de purificación y extractos bioactivos solubles en agua, que posteriormente se utilizaron para producir aerogeles bioactivos híbridos. La estructura altamente porosa y la elevada capacidad de sorción de los aerogeles los convierten en excelentes candidatos para la sustitución de las almohadillas absorbentes para mantener la calidad de los productos cárnicos envasados.

Los emulsion-gels son reconocidos por su gran potencial como ingredientes funcionales en la industria alimentaria como modificadores de textura y como sustitutos de grasas sólidas. Además, pueden utilizarse como vehículo para la liberación controlada de compuestos bioactivos liposolubles. Así, en la última parte de esta tesis, se investigó la naturaleza de las interacciones entre los componentes en las formulaciones de emulsion-gels basadas en polisacáridos y se relacionó con su estructura y comportamiento mecánico y reológico. Después de estudiar el mecanismo de gelificación de los emulsion-gels de carragenato, estos sistemas se adaptaron y utilizaron para dos diferentes aplicaciones relevantes para los sectores de alimentación y biomedicina. En primer lugar, se produjeron y evaluaron estructuras gelificadas a partir de emulsion-gels de agar y κ-carragenato y aerogeles cargados de aceite como

encapsulantes de un bioactivo lipofílico como la curcumina. Los resultados mostraron que el tipo de polisacárido y el estado físico de las redes del gel tenían un impacto en la estructura de los productos de la digestión.

Por otro lado, se evaluó el potencial de los emulsion-gels basados en polisacáridos sulfatados (κ-carragenato y agar) para la producción de un material capaz de simular tejido graso. Los resultados evidencian que los emulsions-gels de agar son adecuadas para producir materiales que simulan las propiedades dieléctricas para imitar tejidos de bajo y alto contenido en agua.

Resum

L'objectiu d'aquesta tesi doctoral ha sigut, el disseny i caracterització estructural d'estructures tipus gel, basades en polisacàrids extrets de biomassa aquàtica amb interès per a aplicacions relacionades amb l'alimentació. Les propietats dels polisacàrids extrets d'algues i plantes aquàtiques, són adequades per a produir diferents estructures tipus gel basades en la formació de xarxes reticulades, com a hidrogels, aerogels i emulsió-gels.

En la primera part d'aquesta tesi es van investigar els diferents mecanismes de gelificació de polisacàrids sulfatats, així com els paràmetres que afecten l'estructura i les propietats funcionals dels hidrogels obtinguts. Sobre la base dels resultats, es va avaluar la potencial aplicació dels hidrogels i aerogels d'agar i κ-carraguenina per a encapsular una proteïna alimentària model com la caseïna, explorant així l'efecte protector contra la hidròlisi enzimàtica després de digestions gastrointestinals simulades.

A la segona part d'aquesta tesi, es van desenvolupar estructures d' aerogels mitjançant la valorització d'una font de biomassa residual infrautilitzada, com és el *Arundo donax*. Amb aquesta biomassa es van generar fraccions cel·lulòsiques amb diferents graus de purificació i extractes bioactius solubles en aigua, que posteriorment es van utilitzar per a produir aerogels bioactius híbrids. L'estructura altament porosa i l'elevada capacitat de sorció dels aerogels els converteixen en excel·lents candidats per a la substitució dels coixinets absorbents per a mantenir la qualitat dels productes carnis envasats.

Els emulsió-gels són reconeguts pel seu gran potencial com a ingredients funcionals en la indústria alimentària com a modificadors de textura i com a substituts de greixos sòlids. A més, poden utilitzar-se com a vehicle per a l'alliberament controlat de compostos bioactius liposolubles. Així, a l'última part d'aquesta tesi, es va investigar la naturalesa de les interaccions entre els components dins les formulacions d' emulsió-gels basades en polisacàrids i es va relacionar amb la seua estructura i comportament mecànic i reològic. Després d'estudiar el mecanisme de gelificació dels emulsió-gels de carraguenina, aquests sistemes es van adaptar i es van utilitzar per a dues aplicacions diferents, rellevants per als sectors de l' alimentació i la biomedicina. En primer lloc, es van produir i van avaluar estructures gelificades a partir de emulsió-gels d'agar i κ-carraguenina i aerogels carregats d'oli com a encapsulants d'un bioactiu

lipofílic com la curcumina. Els resultats van mostrar que el tipus de polisacàrid i l'estat físic de les xarxes del gel tenien un impacte en l'estructura dels productes de la digestió.

D'altra banda, es va avaluar el potencial dels emulsió-gels basats en polisacàrids sulfatats (κ-carraguenina i agar) per a la producció d'un material capaç de simular teixit gras. Els resultats evidencien que els emulsió-gels d'agar són adequats per a produir materials que simulen les propietats dielèctriques podentimitar teixits de baix i alt contingut en aigua.

INDEX

I. INTRODUCTION

1.1 Marine polysaccharides

Marine species comprise approximately one-half of the total global biodiversity. The marine environment and the wide diversity of organisms offers a rich source of valuable functional molecules, including polyunsaturated fatty acids, polysaccharides, minerals and vitamins, antioxidants, enzymes and bioactive peptides (Sun et al., 2020). Amongst marine resources, algae are rich in structurally diverse bioactive compounds with various biological activities. These photosynthetic species constitute multi-cellular structures (Macroalgae) of length up to 60 m and unicellular organisms (Microalgae) with size as small as 0.2 µm (Koyande et al., 2019). Macroalgae are classified into three major groups based on their colour (Figure. 1): green (*Chlorophytes*), brown (*Phaeophytes*) and red algae (*Rhodophytes*) (Devadas et al., 2021). Marine algae have attracted special interest as a good source of nutrients and, particularly, due to their richness in sulphated polysaccharides (Wijesekara et al., 2011). On the other hand, in recent years, aquatic plants have also gained interest as a source of other polysaccharides, such as cellulose and hemicelluloses.

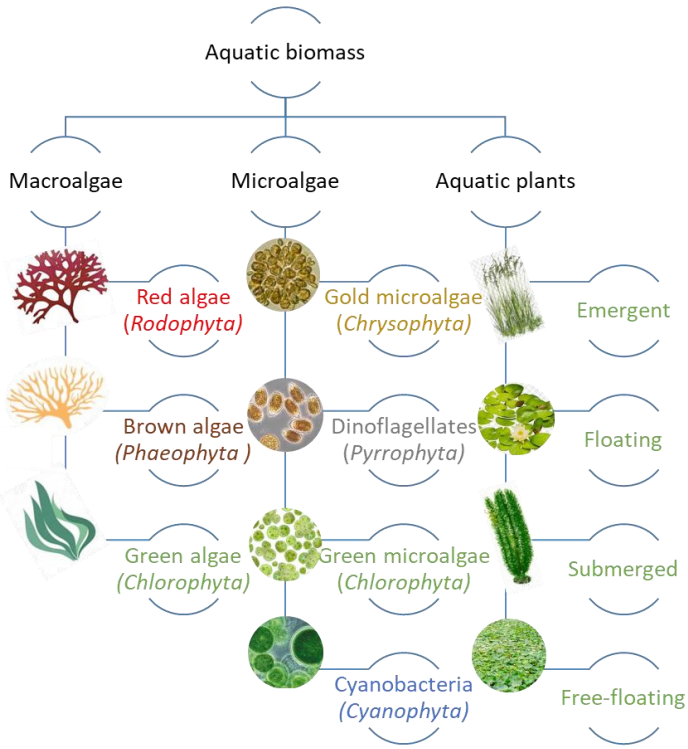

Figure 1. Marine sources of aquatic biomass.

1.1.1 Sulphated polysaccharides in seaweeds

Sulphated polysaccharides are one of the main structural components in the cell walls of seaweeds. Red seaweed galactans are of great commercial importance since they are widely used in the food industry as gelling and thickening agents due to their rheological properties. Amongst these sulphated polysaccharides, the two most abundant types are agarans and carrageenans, which differ in their stereochemistry (Jiao et al., 2011). These polysaccharides exhibit a broad range of interesting properties which makes them useful ingredients for the food, pharmaceutical and cosmetics industries, among others. Furthermore, agarans and carrageenans present several biological activities including antioxidant, anti-inflammatory, anticoagulant, anticancer, anti-thrombogenic, and immunomodulatory (Barros et al., 2013; Jiao et al., 2011). One particular property of several algae-extracted polysaccharides is their capacity to form gel-like structures, making them suitable for several commercial applications.

1.1.1.1 Carrageenans

Carrageenans are sulphated galactans formed by alternate units of 1,3 linked β-D-galactopyranose and 1,4 linked 3,6-anhydro-α-D-galactopyranose (Cunha & Grenha, 2016; Geonzon et al., 2020). Carrageenans are commonly extracted from different species of red seaweeds such as *Chondrus, Eucheuma, Gigartina,* and *Hypnea.* They are normally classified according to their structural characteristics, including the number and position of sulphated groups and the presence or absence of 3,6-anydro-D-galactose. Higher levels of sulphated groups are typically associated with lower solubility at room temperature and lower gel strength (Necas & Bartosikova, 2013). There are at least 15 different carrageenan structures, amongst which κ-, ι- and λ-carrageenan are the most industrially relevant ones (Geonzon et al., 2020; Jiao et al., 2011). While ι- and κ-carrageenan have the same backbone, composed of β-D-galactose and 3,6-anhydro-α-D-galactose (3,6-AG), they differ in their sulphate content; ι-carrageenan possesses sulphated groups on both β-D-galactose and 3,6-AG, while κ-carrageenan features substitution only on β-D-galactose units (Figure. 2). On the other hand, λ-carrageenan presents a distinct backbone, composed of 1,3-linked β-D-galactose and 1,4-linked α-D-galactose substituted with three sulphated groups per disaccharide unit.

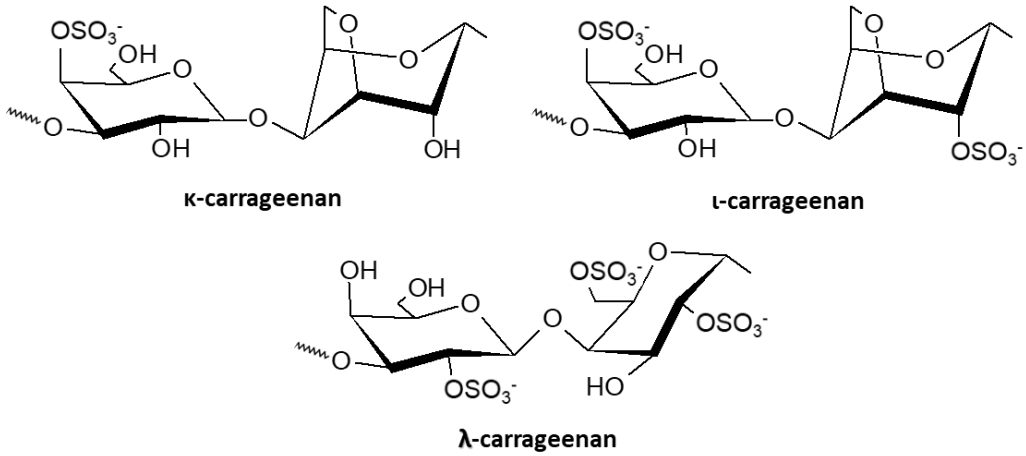

Figure 2. Repeating disaccharide units in the three most commercially relevant types of carrageenan.

To produce a specific type of carrageenan, suitable seaweed species must be selected, and the processing method and conditions should be adapted. While some carrageenans are naturally found in seaweeds, others can only be obtained by chemical modification. Carrageenans are produced as a powder, which slowly dissolves at room temperature, producing a viscous aqueous solution. Viscosity depends on the type of carrageenan, its molecular weight, the concentration, applied temperature and the presence of other solutes (such as cations). The associated cations, together with the conformation of the galactose units in the polymer chain determine the gelling properties of these polysaccharides. The functionality of carrageenans in various applications depends on their rheological properties.

Gelation mechanism of carrageenans

The gelation mechanism of carrageenan depends on many factors, such as the amount and location of sulphated groups, the carrageenan concentration and the presence of counter ions. The carrageenan gelation mechanism is thought to take place in two steps and a schematic representation is shown in the Figure. 3. At higher temperatures, in solution, carrageenan exists as random coils. When the temperature decreases, there is a first transition from random coils to double helices, which is then followed by the aggregation of the double helices to form cross-linking domains which originate the gel network structure (Cunha & Grenha, 2016; Fontes-

Candia et al., 2020). The main structural factors which determine the gelation properties of different carrageenan types are the number and position of ester sulphate groups and the content of 3,6-anhydrogalactose bridges on the galactose residue. These differences affect their respective gelation mechanisms which, in turn, lead to different mechanical properties of the formed hydrogels. While κ-carrageenan gels are strong and brittle, ι-carrageenan gels are softer. The addition of cations has a strong impact on the gelation process, since electrostatic repulsions are inhibited and, thus, the association of carrageenan double helices into bundles is favoured (Beaumont et al., 2021). While monovalent cations are more suitable for κ-carrageenan, divalent cations have been seen to induce the gelation of ι-carrageenan to a greater extent (Thrimawithana et al., 2010). In the case of κ-carrageenan, stronger gels are formed in presence of KCl compared to other salts such as LiCl, NaCl, $MgCl_2$ $CaCl_2$, and $SrCl_2$. Other monovalent cations such as Rb^+, Cs^+, and NH_4^+ also promote the formation of κ-carrageenan gels (Zia et al., 2017). On the other hand, the higher content of sulphated groups in ι-carrageenan requires the addition of a larger salt concentration to inhibit electrostatic repulsions. It has been shown that Ca^{2+} strongly promotes the gelation of ι-carrageenan. However, ι-carrageenan presents sensitivity to the presence of monovalent ions as Rb^+, K^+, Na^+ and Cs^+ (Elfaruk et al., 2021). Since the hydrogel formation is governed by the formation of double helix bundles, addition of different types of ions, which have a strong impact on the formation of these structures, drastically determines the mechanical properties of the gels. Hence, for κ-carrageenan hydrogels, the storage modulus is increased more rapidly in the presence of monovalent cations. Regarding ι-carrageenan hydrogels, the storage modulus increases rapidly with divalent salt and slowly with monovalent salt concentration (Zia et al., 2017).

In the case of λ-carrageenan, lacking the 3,6-anhydro bridge, the C2-sulphated group from the 4-linked residue is oriented towards the internal part, thus hindering the formation of double helices. As a result, λ-carrageenan is thought to adopt a coil conformation whatever the temperature conditions and is unable to form gels (Campo et al., 2009). Although several works reported the non-gelling capacity of λ-carrageenan, recent studies have explored a gelation mechanism based on trivalent cation complexation (Zia et al., 2017). Due to the non-gelling

capacity, the commercial forms of this carrageenan are normally not pure, containing varying amounts of others carrageenan types.

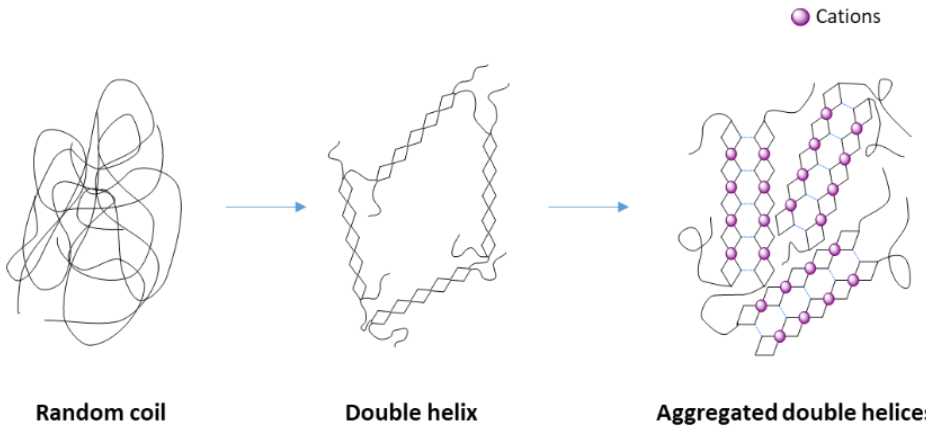

Figure 3. Schematic representation of the general gelation mechanism of carrageenans.

Applications

Carrageenans are widely used in many industries in non-food and food applications. In the food industry, carrageenans are used due to their excellent physical and functional properties, such as their stabilizing, gelling, thickening, and emulsifying capacity (Geonzon et al., 2020). Carrageenans have been used as thickening and protein stabilizers in ice cream, chocolate milk and others milk drinks, improving the quality of dairy products (Hotchkiss et al., 2016; Skryplonek et al., 2019). They can also be used as stabilizers and binders in the meat manufacturing industries for the production of low-calorie products (Cao et al., 2021; Pourashouri et al., 2021). In non-food applications, carrageenans are used for pigment dispersion and as drug encapsulation materials in cosmetics and pharmaceutical formulations (Pacheco-Quito et al., 2020), biomaterials for artificial tissue engineering in the biomedical field (İlhan et al., 2020; Khan et al., 2020) and as bio-based materials for biodegradable packaging (Fabra et al., 2021; Pérez et al., 2021).

1.1.1.2 Agar

Agar (also known within the food industry as agar-agar) is an important commercial phycocolloid, which is constituted by two major components: agarose and agaropectin (Figure.

4). These two polysaccharides have the same monomers but different structures. Agarose is a linear polymer comprising of alternating β-D-galactose and 3, 6-anydro-L-galactose units linked by glycosidic bonds. The second agar component, agaropectin, is heterogeneous agarose consisting of the same repeating units in which some 3, 6-anydro-L-galactose rings are replaced by L-galactose-sulphate or by methoxy or pyruvate residues (Sousa et al., 2012; Sun et al., 2020; Venugopal, 2016). Agar is industrially extracted from different red seaweed species (*Gelidium, Gelidiela*, *Pterocladia*, *Gracilaria*, *Graciliaropsis* and *Ahfeltia*). The structural changes may affect the physical and rheological properties of these biopolymers (Barros et al., 2013). The type of red seaweed species, their environmental growth conditions and the physiological factors, as well as the extraction methods, strongly affect the structure of the extracted agar. The proportion of agarose/agaropectin, as well as the amount of sulphated and anhydrous units, have a strong impact on the gelling and rheological properties of agar, affecting the final mechanical behaviour of the formed gels (Bertasa et al., 2020).

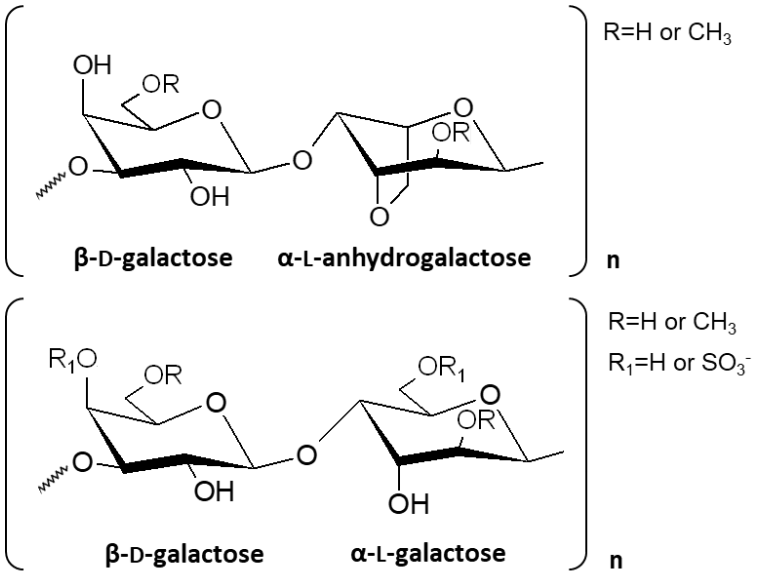

Figure 4. Repeating disaccharide units of agar showing with the different types of units and substitution.

Gelation mechanism of agar

It is generally recognized that the agarose fraction in agar is responsible for the formation of secondary structures, governing its gelation mechanism. Similarly to carrageenans, the gelation

mechanism of agar can occur through a sequential two-step mechanism (Figure. 5). This process involves the formation of double helices in the polymer backbone, followed by the aggregation of these helices into cross-linking points or bundles, creating a 3D hydrogel network (Beaumont et al., 2021; Martínez-Sanz et al., 2020). Many other factors, such as the agar concentration, the amount and type of impurities and the cooling rate, may affect this gelation mechanism (Aymard et al., 2001; Lai & Lii, 1997; Lee et al., 2017; Nishinari & Watase, 1983; Watase & Nishinari, 1983). In particular, the amount and type of substitution in the agaropectin fraction has a strong impact on the formation of bundles, being the sulphate content one of the main factors which determines the rheological and mechanical properties of the hydrogels.

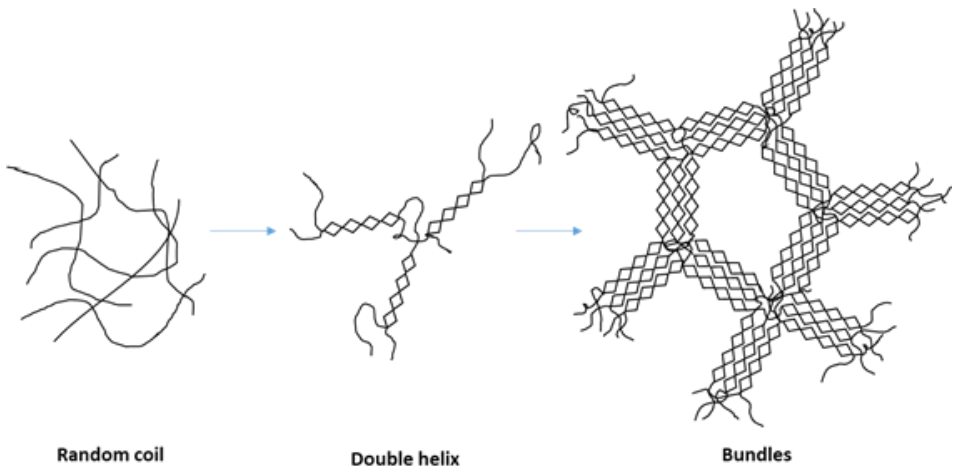

Figure 5. Schematic representation of the gelation mechanism of agar.

Applications

Because of its special characteristics at ambient temperatures, excellent rheological properties, good compatibility with other polysaccharides and low cost, agar has been applied in the fields of food, biomedical, and chemical industries. Agar, as a non-digestible polysaccharide is the food additive with the highest content of soluble gross fibre. The principal use of agar in food is derived from its emulsifying, stabilizing and gelling properties (Alehosseini et al., 2018; Martínez-Sanz et al., 2019). Agar is used in bakery products, such as bakery icings and frostings,

because it is compatible with large amounts of sugar and stable at high storage temperatures. Also, agar is used as a vegetarian gelatin and as an additive in desserts.

In food packaging, agar has been used in combination with other polymers and also incorporating bioactive compounds and has shown to have a reinforcing effect, thus increasing the tensile strength, the mechanical and functional properties of the films (Carina et al., 2021; Mostafavi & Zaeim, 2020).

In non-food applications, agar is the most commonly used growth medium for microorganisms. Moreover, it is also used for tissue engineering applications, and as a gel for denture moulding (Sachlos & Czernuszka, 2003).

1.1.2 Polysaccharides in aquatic plants

As previously mentioned, the composition of aquatic plants is very different from that of seaweeds. The cell walls from aquatic plants resemble to a greater extent to those from terrestrial plants, with cellulose being the main structural component and other biopolymers such as hemicelluloses and lignin, providing different functionalities. One of the main advantages of aquatic plants and seaweeds is that they can produce larger amounts of material in a shorter time than terrestrial-based plants (Knoshaug et al., 2013).

Cellulose is the most abundant biopolymer, as it comprises the major structural component of the cell walls from plants and seaweeds. Cellulose is composed of linear chains of 1,4 β-glucopyranose repeating units at different degrees of polymerization. Hemicelluloses are amorphous and heterogeneous biopolymer structures formed by different monomers such as pentoses and hexoses, among others. Hemicelluloses work as an interconnecting network between cellulose microfibrils and lignin and have different structural roles depending on their specific structure. Lignin is an amorphous aromatic heteropolymer that provides support and impermeability to the plant, as well as resistance to microbial attack and oxidative stress (Martínez-Gutiérrez, 2018).

The structure from cellulose is particularly interesting since it is hierarchically arranged into different structural levels at multiple scales from nano to micro size. Due to its excellent properties and structural characteristics cellulose is one of the most promising materials with the potential to replace conventional plastics within the packaging sector. The main advantages

of cellulosic materials are their renewable character, their low density, low cost and energy consumption, high specific strength, high modulus and reactive surface (Jonoobi et al., 2015). Cellulose and nanocellulose, including its derivatives, are amongst the most abundant and widely used biopolymers in the packaging industry. One of the main functions of cellulose is to serve as reinforcing element in packaging materials, providing selective gas and water vapour barriers (Benito-González et al., 2018), but it can also be used as a carrier for antimicrobial agents, antioxidants or other active molecules, modulating their release from the films (M. Rangaraj et al., 2021; Phoopuritham et al., 2012) and, thus, contributing to increased food product shelf life (Liu et al., 2021).

1.2 Polysaccharide-based gel structures

The structure and properties of polysaccharides extracted from seaweeds and aquatic plants make them suitable to produce a range of gel-like structures based on the formation of interconnected networks, such as hydrogels, aerogels and emulsion gels.

1.2.1 Hydrogels

Hydrogels are defined as a three-dimensional macromolecular network formed by hydrophilic biopolymer chains connected by cross-linking. Hydrogels are highly swollen materials and retain a significant fraction of water within their structure, but do not dissolve (Ahmed, 2015).

Their properties can be strongly modified depending on the biopolymer used as the gelling matrix, the type of cross-linking and the electrical charges provided by the matrix and by the added salts. Polysaccharide-based hydrogels have attracted much attention as biomaterials due to their excellent biocompatibility and biodegradability. Different polysaccharides such as starch, chitosan, carrageenan, agar, cellulose, guar gum and sodium alginate, amongst others, have been investigated as useful hydrogel materials for bio-related applications (Kuang et al., 2011). Hydrogels can be divided into two categories based on the chemical or physical nature of the cross-linking.

1.2.1.1 Hydrogel classification

Chemical hydrogels

Chemically cross-linked networks have permanent junctions and are characterized by their high stability but suffer from the potential presence of chemicals used in their synthesis, which limits their applicability in some industries (especially in food-related applications). In chemical cross-linking, the polymer chains are covalently bonded via a cross-linking agent (Figure. 6). The use of chemically cross-linked hydrogels is limited as the resulting structure in a non-reversible network since the polymer is no longer soluble in solvents and the heating process could degrade the polymer once the cross-linking takes place (A. Patel & Mequanint, 2011).

Physical hydrogels

On the other hand, physical hydrogels, such as the so-called thermogels, present temporary junctions given by the polymer chain entanglements or physical interactions such as hydrophobic associations, chain aggregation, crystallization, ionic interactions and hydrogen bonds (Figure. 6) (Ahmed, 2015; Mahinroosta et al., 2018). The properties of physically cross-linked hydrogels are dependent on several parameters including pH, salt type and ionic strength. Changes in these parameters have a significant impact in their swelling behaviour. The presence of reversible junctions allows solvent casting and thermal processing. Physical hydrogels possess higher compressive strength compared with those obtained by chemical interactions since the mechanical load can be more uniformly distributed through the three-dimensional structure (A. Patel & Mequanint, 2011).

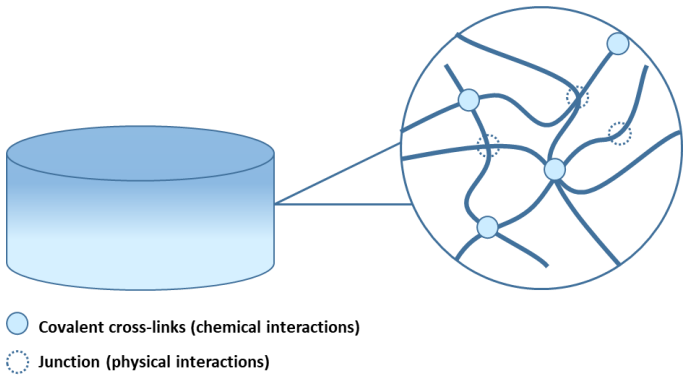

Figure 6. Different types of cross-links forming hydrogel networks.

1.2.1.2 Hydrogel applications

Due to their excellent characteristics, such as its reversible swelling/deswelling behaviour, high environmental sensitivity and adjustable permeability, surface and mechanical properties, hydrogels have found a wide range of applications. Specifically in food products, hydrogels have been explored as encapsulation and delivery systems to release bioactive compounds under certain conditions and in different matrices (Mahinroosta et al., 2018; Zhang et al., 2019). Hydrogels also are used as dietary control ingredients by enhancing satiety or by reducing calorie intake (Jinlong Li et al., 2021). Moreover, hydrogels are also used as food packaging materials for humidity control inside the packages (Batista et al., 2019).

Regarding pharmaceutical and biomedical applications, the lower interfacial tension, tissue-like physical properties, higher permeability and release capacity have become to hydrogels especially attractive in this field (Laftah et al., 2011). In these fields, hydrogels have special interest in certain applications including diagnostic, therapeutic, and implantable devices such as catheters, biosensors, artificial skin, and for tissue engineering (Yegappan et al., 2018).

They can also be used for the controlled release of drugs, agrochemical compounds and nutrients (Akalin & Pulat, 2020; Santamaría Vanegas et al., 2019).

1.2.2 Aerogels

Certain types of hydrogels, when subjected to a drying process, can form structures known as aerogels. These aerogels are microporous solids in which the dispersed phase is a gas, such as air. Aerogels are a special type of nanostructured materials, characterized by their physical properties, with high specific surface area and very low density. Aerogel networks are formed by cross-linked particles or by nanometric fibers which are loosely packed leading to high porosities. Although these materials have been typically prepared using inorganic compounds, an extensive amount of research has been carried out within the last years on the development of bio-based aerogels. In particular, polysaccharides, such as cellulose, starch, chitosan, alginate, carrageenan, and pectin, have been often exploited as the base material for aerogels. The particular interest of polysaccharide-based aerogels lies in their unique properties such as high-water sorption capacity, edibility, renewability, sustainability, biocompatibility, low toxicity, and low cost. Due to their excellent properties, polysaccharide-based aerogels have

attracted wide interest in many fields, such as environmental engineering, construction, electrochemical components and packaging. The functional biocompatibility and low toxicity properties of polysaccharide-based aerogels make them also suitable for the health and medicine fields, where they can be used as controlled delivery systems or to improve the stability of drugs or bioactive compounds throughout the gastrointestinal tract (Ahmadzadeh et al., 2015).

Aerogels are obtained by the removal of the solvent from hydrogels, using methods that allow the preservation of the three-dimensional solid network structure, being the most common methods freeze-drying and supercritical carbon dioxide-assisted drying. They can be produced in a wide variety of shapes, sizes, and textures, using different moulds and gelation conditions. The structure and porosity of aerogels can be modified depending on the base polymer, the preparation technologies, and drying methods (Manzocco, Mikkonen, et al., 2021).

1.2.2.1 Drying methods

Supercritical drying

Supercritical drying is one of the most common procedures to obtain aerogels. This method can be classified into two approaches, (i) high-temperature supercritical drying (HTSCD) and (ii) low-temperature supercritical drying (LTSCD). In HTSCD, the solvent (commonly water) in the hydrogel is firstly replaced by an organic solvent and subsequently, the hydrogel is placed in an autoclave for heating and pressurization. Once the solvent in the hydrogel reaches the supercritical state, it then vents out at constant temperature. On the other hand, in LTSCD, soluble CO_2 is used as a drying medium to replace the organic solvent in the hydrogels. The CO_2 reaches the supercritical point, close to room temperature, leading to the formation of the aerogel (Wang et al., 2019). As supercritical drying uses solvents whose critical point is within a moderate temperature and pressure range, the network material does not degrade, and the conditions can be achieved with standard technical apparatus. Supercritical drying leads to a transition from the liquid phase to a supercritical fluid without crossing a phase boundary. Therefore, controlling the temperature and pressure to get the critical point at which gas and liquid co-exist with the same density and the interface disappears to achieve phase transfer is very important for the retention of the gel network. After that, the liquid in the three-

dimensional network is completely substituted by gas and, hence, an aerogel is obtained (Ziegler et al., 2017). Several factors should be taken into account in supercritical drying. It has been reported that increasing the amount of ethanol in the organic phase and the drying time results in higher surface areas. On the other hand, increasing the drying pressure contributes to decreasing the specific surface area and increasing the density of the aerogels. Furthermore, the rate of depressurization affects the pore growth, leading to the formation of large pores (García-González et al., 2011).

Freeze-drying

The freeze-drying process involves a first step where the solvent in the hydrogel is frozen and a subsequent step where it is removed from the material by sublimation at low pressure (Figure. 7). Freeze-drying is extensively applied for aerogel preparation due to its high safety (Ahankari et al., 2021; Wang et al., 2019). In this process, the aerogel structure and pore size are determined by the ice crystal growth on the gel network, which in turn is affected by the freezing temperature and polysaccharide concentration. During the freeze-drying process, two main phases of crystallization take place. The first step is the nucleation, when the crystal centre, as well as the crystal nucleus, are formed. The second step is the growth of ice crystals. The size of the ice crystals depends on the initial nucleation temperature and the crystallization rate (Wang et al., 2019). The temperature and slurry concentration plays a very important role in ice crystal growth. With temperatures between -15 to 40°C, the mean diameter of ice crystals significantly decreases. In addition, the pressure affects the freezing process. Under high pressure, the freezing point will be decreased, inducing the super-cooling and rapid ice nucleation rates will produce smaller ice crystals.

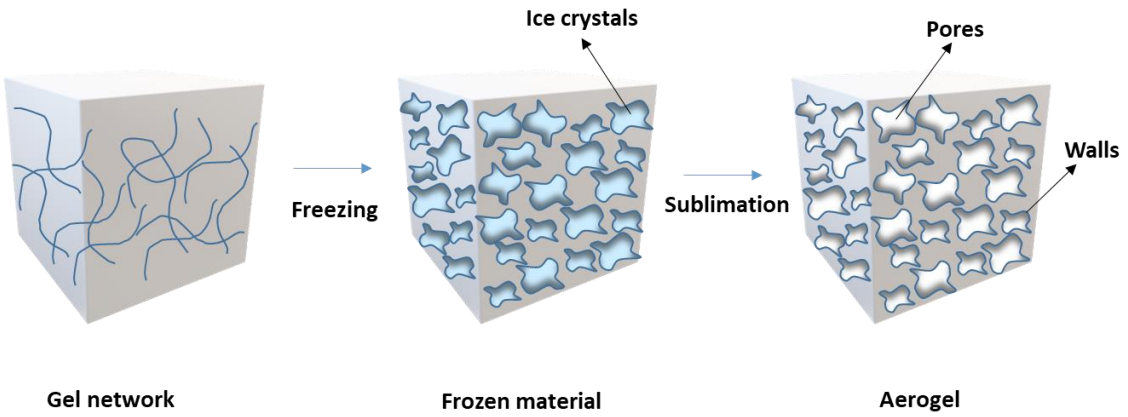

Figure 7. Schematic representation of aerogel formation by means of freeze-drying.

1.2.2.2 Aerogels in food applications

The interest in aerogels in food-related applications has grown significantly in the last years and different bio-based materials have been explored as templates, being polysaccharides the most widely used biopolymers. Cellulose and starch aerogels are considered as promising carrier systems for bioactive compounds in food industries (de Oliveira et al., 2019; García-González et al., 2011; Ubeyitogullari & Ciftci, 2016). Besides them, hemicelluloses, pectin, alginates, xanthan gum, and carrageenans, commonly used in the food industry as thickeners or dietetic fibres, have also been explored as matrices for the production of aerogels (Mikkonen et al., 2013; Nita et al., 2020). Proteins, such as albumin, casein, collagen, gelatin and gluten (Fitzpatrick et al., 2018; Nita et al., 2020), have also been explored for the preparation of aerogels, both as matrices and as additives to modify the internal morphology in composite aerogels (Manzocco, Mikkonen, et al., 2021).

1.2.3 Emulsion gels

Emulsion gels are soft solid-like materials composed of a polymeric gel matrix into which emulsion droplets are incorporated (emulsion-filled gels) or a network of aggregated emulsion droplets (emulsion particle gels). Accordingly, emulsion gels contain a polymer with gelling capacity in the aqueous phase. The formation of a hydrogel network immobilizes the oil phase within the gel structure, thus preventing flocculation and coalescence. This is a great advantage since the stability of emulsions can be greatly improved. These systems can provide the

advantages of both emulsions and hydrogels, i.e. the ability to solubilize both hydrophobic and hydrophilic components, being thus suitable for the controlled delivery of a wide range of compounds. Emulsion gels can be produced with a wide range of rheological properties, which depend on a number of intrinsic factors, such as the nature of interactions between the components, oil volume fraction, and matrix stiffness. The effects of these factors governing the overall rheology of an emulsion gel are of considerable practical importance when utilizing an emulsion gel system for pharmaceutical, cosmetic, and food applications (Farjami & Madadlou, 2019).

1.2.3.1 Emulsion filled-gels

Emulsion-filled gels are systems in which the oil droplets from an emulsion act as the filler particles within a gel matrix. The oil droplets can be classified as either active or inactive fillers depending on their effect on the gel properties. Active fillers, also called bound fillers, are connected to the gel network and contribute to the gel strength, whereas inactive fillers or unbound fillers show low chemical affinity to the gel matrix and do not interact with it.

Emulsion-filled gels can be produced by embedding an emulsion into either a gel phase or a pre-gel polymer solution. They can also be made through gelation of the aqueous continuous phase of an emulsion with low or moderate oil content. The rheological properties of emulsion-filled gels are different from those of conventional hydrogels and depend on several factors such as the characteristics of filler and matrix polymers, the presence of emulsifying agents and the interactions established between the different components (Dickinson, 2012; Yang et al., 2020).

Matrix-filler interactions

Active fillers enhance or diminish emulsion gels modulus depending on the ratio between the modulus from the droplets and the gel matrix. On the other hand, inactive fillers are expected to behave like small holes in the network. Therefore, they may disrupt the network and weaken the gel. The addition of an emulsifying agent can enhance or strengthen the interactions between the matrix and the filler. However, an excess of emulsifying agent can be detrimental due to competition with the matrix polymer to interact with the surface of the oil droplets. In

heat-set emulsion gels where whey protein served as the gelling agent and emulsifier, the protein-covered oil droplets behaved as active filler particles conferring high viscoelasticity to the gel; however, in the presence of an excess amount of a non-ionic surfactant, the droplets behaved as inactive fillers and the gel texture weakened (Farjami & Madadlou, 2019). In emulsion systems containing a mixture of polymer and surfactant, the rheological behaviour becomes more complex because both components contribute to emulsion stability and rheological properties.

Filler concentration and size

The influence of filler concentration on the rheology of emulsion-filled gels depends on the type of filler. It has been reported that gel strength increases with increasing filler concentration for droplets bound to the matrix. Droplet volume fraction can be influenced by the distribution of the droplets within the gel matrix (Oliver et al., 2015). Flocculated droplets possess a higher effective volume fraction as compared with single droplets. For an emulsion gel system with bound and flocculated droplets, a higher effective volume fraction results in greater values of viscoelastic parameters. Regarding the filler size, smaller average particle sizes tend to improve the filler effect due to an increase in the surface area to volume ratio and in the number of filler particles, which reduces the distance between droplets. Several studies conducted on large deformation and fracture properties of emulsion gels have indicated that, at a constant volume fraction, gel strength increases as the size of active fillers decreases (Farjami & Madadlou, 2019; Wu et al., 2011).

Matrix stiffness

The elastic modulus of the gel matrix, which is typically affected by the polymer concentration, has a notable influence on the rheological properties of the emulsion gels. Increasing the gelling agent concentration causes polymer chains to come closer together, resulting in a reduction in the number of voids in the matrix and the formation of more bonds between structural elements. This increases the elastic modulus of the gel matrix. Moreover, the type of polymer utilized as gelling agent can influence matrix stiffness.

Polysaccharide-based emulsion gels

While polysaccharide gels have been extensively investigated, the structures and functionalities of polysaccharide-based emulsion gels have not been much explored yet and only a few works have been published. Carrageenan emulsion gels have been developed and proposed as fat substitutes in meat products (Paglarini et al., 2018). Pectins have been used to produce emulsion gels with the low methylation ones producing emulsion gels more resistant to mechanical deformation (Junhua Li et al., 2020). The stabilizing effect of polysaccharides in a low oil volume fraction is through control of the rheology of the aqueous continuous phase located in the gaps between the individual dispersed oil droplets (Moschakis et al., 2006).

1.2.3.2 Emulsion gels in food applications

Nowadays, in the food industry, emulsion gels represent a great potential as functional ingredients to modify texture, for solid fat replacement and as a template for controlled release of bioactive compounds (Martins et al., 2018). In the food industry, fats are recognised for providing desirable functionality, texture and palatability to food products. However, animal fats and the consumption of saturated fatty acids are related to adverse chronic health effects (A. R. Patel et al., 2014). Therefore, new strategies are currently focused on new alternatives to structure liquid oil to reduce or replace the use of solid fats in edible products. Consequently, one of the challenges is to find oil-structuring materials which are suitable for food applications and with properties as similar as possible to those originally found in animal fats. In this context, polymer gelation has been proposed as a potential alternative method to produce oil-structured materials. The most common direct oil gelation method involves the use of low molecular weight gelling agents that exhibit a high affinity for non-polar solvents. These gelling agents are usually waxes, sterol-based gelling agents, lecithin, and fatty acid derivatives. Due to the legal restrictions on the introduction of new food ingredients and additives, legislation is certainly one of the main issues preventing the application of these materials within the food industry. Recently, several reports have demonstrated the potential of using new sources of polysaccharides and proteins and their combinations to induce oil structuring. In particular, emulsion gels present practical applications in the food industry since they can provide stability and a solid-like functionality to fat-containing products without compromising the functional

and textural properties they impart to the food (Jiang et al., 2019). In addition, emulsion gels provide the possibility of carrying and protecting both hydrophilic and hydrophobic biologically active substances by incorporating these compounds into their structure and can be used to further increase the nutritional value of foods (Martins et al., 2018).

1.2.3.3 Emulsion-oil filled aerogels

The principle of drying hydrogels to obtain aerogels has been extrapolated to organogels to produce novel structures by water removal. Organogels are defined as tridimensional networks entrapping organic liquids. In the particular case of oils, these materials are known as oleogels, which are more interesting for food applications. Some biopolymers such as ethylcellulose and hydrophobic chitin are able to form a gel network even when the liquid phase contains a large proportion of oil, while most polysaccharides are not able to gel in the presence of a liquid phase mostly based on oil. Recent studies have demonstrated that some biopolymers are able to retain their network structure when water is removed from oleogels, thus producing highly lipophilic materials with unique oil sorption features. This approach is particularly interesting for the preparation of oleogels with a very high oil content, which are mainly proposed as fat substitutes to obtain healthier foods with reduced content in saturated/trans fatty acids (Manzocco, Basso, et al., 2021; Manzocco, Mikkonen, et al., 2021).

References

Ahankari, S., Paliwal, P., Subhedar, A., & Kargarzadeh, H. (2021). Recent Developments in Nanocellulose-Based Aerogels in Thermal Applications: A Review. *ACS Nano*, *15*(3), 3849–3874. https://doi.org/10.1021/acsnano.0c09678

Ahmadzadeh, S., Nasirpour, A., Keramat, J., Hamdami, N., Behzad, T., & Desobry, S. (2015). Nanoporous cellulose nanocomposite foams as high insulated food packaging materials. *Colloids and Surfaces A: Physicochemical and Engineering Aspects*, *468*, 201–210. https://doi.org/10.1016/j.colsurfa.2014.12.037

Ahmed, E. M. (2015). Hydrogel: Preparation, characterization, and applications: A review. *Journal of Advanced Research*, *6*(2), 105–121. https://doi.org/10.1016/j.jare.2013.07.006

Akalin, G. O., & Pulat, M. (2020). Preparation and characterization of κ-carrageenan hydrogel for controlled release of copper and manganese micronutrients. *Polymer Bulletin*, *77*(3), 1359–1375. https://doi.org/10.1007/s00289-019-02800-4

Alehosseini, A., del Pulgar, E.-M. G., Gómez-Mascaraque, L. G., Martínez-Sanz, M., Fabra, M. J., Sanz, Y., Sarabi-Jamab, M., Ghorani, B., & Lopez-Rubio, A. (2018). Unpurified Gelidium-extracted carbohydrate-rich fractions improve probiotic protection during storage. *LWT*,

96, 694–703.

Aymard, P., Martin, D. R., Plucknett, K., Foster, T. J., Clark, A. H., & Norton, I. T. (2001). Influence of thermal history on the structural and mechanical properties of agarose gels. *Biopolymers: Original Research on Biomolecules*, *59*(3), 131–144.

Barros, F. C. N., da Silva, D. C., Sombra, V. G., Maciel, J. S., Feitosa, J. P. A., Freitas, A. L. P., & de Paula, R. C. M. (2013). Structural characterization of polysaccharide obtained from red seaweed Gracilaria caudata (J Agardh). *Carbohydrate Polymers*, *92*(1), 598–603. https://doi.org/https://doi.org/10.1016/j.carbpol.2012.09.009

Batista, R. A., Espitia, P. J. P., Quintans, J. de S. S., Freitas, M. M., Cerqueira, M. Â., Teixeira, J. A., & Cardoso, J. C. (2019). Hydrogel as an alternative structure for food packaging systems. *Carbohydrate Polymers*, *205*, 106–116. https://doi.org/10.1016/j.carbpol.2018.10.006

Beaumont, M., Tran, R., Vera, G., Niedrist, D., Rousset, A., Pierre, R., Shastri, V. P., & Forget, A. (2021). Hydrogel-Forming Algae Polysaccharides: From Seaweed to Biomedical Applications. *Biomacromolecules*, *22*(3), 1027–1052. https://doi.org/10.1021/acs.biomac.0c01406

Benito-González, I., López-Rubio, A., & Martínez-Sanz, M. (2018). Potential of lignocellulosic fractions from Posidonia oceanica to improve barrier and mechanical properties of bio-based packaging materials. *International Journal of Biological Macromolecules*, *118*, 542–551.

Bertasa, M., Dodero, A., Alloisio, M., Vicini, S., Riedo, C., Sansonetti, A., Scalarone, D., & Castellano, M. (2020). Agar gel strength: A correlation study between chemical composition and rheological properties. *European Polymer Journal*, *123*, 109442. https://doi.org/https://doi.org/10.1016/j.eurpolymj.2019.109442

Campo, V. L., Kawano, D. F., Braz, D., & Carvalho, I. (2009). Carrageenans : Biological properties , chemical modifications and structural analysis – A review. *Carbohydrate Polymers*, *77*(2), 167–180. https://doi.org/10.1016/j.carbpol.2009.01.020

Cao, C., Feng, Y., Kong, B., Xia, X., Liu, M., Chen, J., Zhang, F., & Liu, Q. (2021). Textural and gel properties of frankfurters as influenced by various κ-carrageenan incorporation methods. *Meat Science*, *176*, 108483.

Carina, D., Sharma, S., Jaiswal, A. K., & Jaiswal, S. (2021). Seaweeds polysaccharides in active food packaging: A review of recent progress. *Trends in Food Science and Technology*, *110*, 559–572. https://doi.org/10.1016/j.tifs.2021.02.022

Cunha, L., & Grenha, A. (2016). Sulfated Seaweed Polysaccharides as Multifunctional Materials in Drug Delivery Applications. *Marine Drugs*, *14*(3), 42. https://doi.org/10.3390/md14030042

de Oliveira, J. P., Bruni, G. P., Fabra, M. J., da Rosa Zavareze, E., López-Rubio, A., & Martínez-Sanz, M. (2019). Development of food packaging bioactive aerogels through the valorization of Gelidium sesquipedale seaweed. *Food Hydrocolloids*, *89*, 337–350. https://doi.org/10.1016/j.foodhyd.2018.10.047

Devadas, V. V., Khoo, K. S., Chia, W. Y., Chew, K. W., Munawaroh, H. S. H., Lam, M. K., Lim, J. W., Ho, Y. C., Lee, K. T., & Show, P. L. (2021). Algae biopolymer towards sustainable circular economy. *Bioresource Technology*, *325*, 124702.

https://doi.org/10.1016/j.biortech.2021.124702

Dickinson, E. (2012). Emulsion gels: The structuring of soft solids with protein-stabilized oil droplets. *Food Hydrocolloids*, *28*(1), 224–241. https://doi.org/https://doi.org/10.1016/j.foodhyd.2011.12.017

Elfaruk, M. S., Wen, C., Chi, C., Li, X., & Janaswamy, S. (2021). Effect of salt addition on iota-carrageenan solution properties. *Food Hydrocolloids*, *113*, 106491. https://doi.org/10.1016/j.foodhyd.2020.106491

Fabra, M. J., Castro-Mayorga, J. L., Gómez-Mascaraque, L. G., & López-Rubio, A. (2021). Novel coatings to improve the performance of multilayer biopolymeric films for food packaging applications. In *Handbook of Modern Coating Technologies* (pp. 259–280). Elsevier. https://doi.org/10.1016/b978-0-444-63240-1.00010-3

Farjami, T., & Madadlou, A. (2019). An overview on preparation of emulsion-filled gels and emulsion particulate gels. *Trends in Food Science & Technology*, *86*, 85–94. https://doi.org/https://doi.org/10.1016/j.tifs.2019.02.043

Fitzpatrick, S. E., Staiger, M. P., Deb-Choudhury, S., & Ranford, S. (2018). Protein-based aerogels: processing and morphology. In *Biobased Aerogels* (pp. 67–102).

Fontes-Candia, C., Ström, A., Gómez-Mascaraque, L. G., López-Rubio, A., & Martínez-Sanz, M. (2020). Understanding nanostructural differences in hydrogels from commercial carrageenans: Combined small angle X-ray scattering and rheological studies. *Algal Research*, *47*, 101882. https://doi.org/https://doi.org/10.1016/j.algal.2020.101882

García-González, C. A., Alnaief, M., & Smirnova, I. (2011). Polysaccharide-based aerogels - Promising biodegradable carriers for drug delivery systems. *Carbohydrate Polymers*, *86*(4), 1425–1438. https://doi.org/10.1016/j.carbpol.2011.06.066

Geonzon, L. C., Descallar, F. B. A., Du, L., Bacabac, R. G., & Matsukawa, S. (2020). Gelation mechanism and network structure in gels of carrageenans and their mixtures viewed at different length scales – A review. *Food Hydrocolloids*, *108*, 106039. https://doi.org/https://doi.org/10.1016/j.foodhyd.2020.106039

Hotchkiss, S., Brooks, M., Campbell, R., Philp, K., & Trius, A. (2016). The use of carrageenan in food. *Carrageenans: Sources and Extraction Methods, Molecular Structure, Bioactive Properties and Health Effects*, 229–243.

İlhan, G. T., Irmak, G., & Gümüşderelioğlu, M. (2020). Microwave assisted methacrylation of Kappa carrageenan: A bioink for cartilage tissue engineering. *International Journal of Biological Macromolecules*, *164*, 3523–3534.

Jiang, Y., Liu, L., Wang, B., Yang, X., Chen, Z., Zhong, Y., Zhang, L., Mao, Z., Xu, H., & Sui, X. (2019). Polysaccharide-based edible emulsion gel stabilized by regenerated cellulose. *Food Hydrocolloids*, *91*, 232–237. https://doi.org/10.1016/j.foodhyd.2019.01.028

Jiao, G., Yu, G., Zhang, J., & Ewart, H. S. (2011). Chemical Structures and Bioactivities of Sulfated Polysaccharides from Marine Algae. *Marine Drugs*, 196–223. https://doi.org/10.3390/md9020196

Jonoobi, M., Oladi, R., Davoudpour, Y., Oksman, K., Dufresne, A., Hamzeh, Y., & Davoodi, R. (2015). Different preparation methods and properties of nanostructured cellulose from various natural resources and residues: a review. *Cellulose*, *22*(2), 935–969. https://doi.org/10.1007/s10570-015-0551-0

Khan, M. U. A., Raza, M. A., Mehboob, H., Kadir, M. R. A., Abd Razak, S. I., Shah, S. A., Iqbal, M.

Z., & Amin, R. (2020). Development and in vitro evaluation of κ-carrageenan based polymeric hybrid nanocomposite scaffolds for bone tissue engineering. *RSC Advances*, *10*(66), 40529–40542.

Knoshaug, E. P., Shi, B., Shannon, T. G., Mleziva, M. M., & Pienkos, P. T. (2013). The potential of photosynthetic aquatic species as sources of useful cellulose fibers-a review. *Journal of Applied Phycology*, *25*(4), 1123–1134. https://doi.org/10.1007/s10811-012-9958-2

Koyande, A. K., Chew, K. W., Rambabu, K., Tao, Y., Chu, D. T., & Show, P. L. (2019). Microalgae: A potential alternative to health supplementation for humans. *Food Science and Human Wellness*, *8*(1), 16–24. https://doi.org/10.1016/j.fshw.2019.03.001

Kuang, J., Yuk, K. Y., & Huh, K. M. (2011). Polysaccharide-based superporous hydrogels with fast swelling and superabsorbent properties. *Carbohydrate Polymers*, *83*(1), 284–290. https://doi.org/10.1016/j.carbpol.2010.07.052

Laftah, W. A., Hashim, S., & Ibrahim, A. N. (2011). Polymer hydrogels: A review. *Polymer-Plastics Technology and Engineering*, *50*(14), 1475–1486.

Lai, M. F., & Lii, C. Y. (1997). Rheological and thermal characteristics of gel structures from various agar fractions. *International Journal of Biological Macromolecules*, *21*(1–2), 123–130. https://doi.org/10.1016/S0141-8130(97)00051-2

Lee, W. K., Lim, Y. Y., Leow, A. T. C., Namasivayam, P., Abdullah, J. O., & Ho, C. L. (2017). Factors affecting yield and gelling properties of agar. *Journal of Applied Phycology*, *29*(3), 1527–1540. https://doi.org/10.1007/s10811-016-1009-y

Li, Jinlong, Jia, X., & Yin, L. (2021). Hydrogel: Diversity of Structures and Applications in Food Science. *Food Reviews International*, *37*(3), 313–372. https://doi.org/10.1080/87559129.2020.1858313

Li, Junhua, Xu, L., Su, Y., Chang, C., Yang, Y., & Gu, L. (2020). Flocculation behavior and gel properties of egg yolk/κ-carrageenan composite aqueous and emulsion systems: Effect of NaCl. *Food Research International*, *132*, 108990. https://doi.org/https://doi.org/10.1016/j.foodres.2020.108990

Liu, Y., Ahmed, S., Sameen, D. E., Wang, Y., Lu, R., Dai, J., Li, S., & Qin, W. (2021). A review of cellulose and its derivatives in biopolymer-based for food packaging application. *Trends in Food Science & Technology*, *112*, 532–546.

M. Rangaraj, V., Rambabu, K., Banat, F., & Mittal, V. (2021). Natural antioxidants-based edible active food packaging: An overview of current advancements. *Food Bioscience*, *43*, 101251. https://doi.org/10.1016/J.FBIO.2021.101251

Mahinroosta, M., Jomeh Farsangi, Z., Allahverdi, A., & Shakoori, Z. (2018). Hydrogels as intelligent materials: A brief review of synthesis, properties and applications. *Materials Today Chemistry*, *8*, 42–55. https://doi.org/10.1016/j.mtchem.2018.02.004

Manzocco, L., Basso, F., Plazzotta, S., & Calligaris, S. (2021). Study on the possibility of developing food-grade hydrophobic bio-aerogels by using an oleogel template approach. *Current Research in Food Science*, *4*, 115–120. https://doi.org/10.1016/j.crfs.2021.02.005

Manzocco, L., Mikkonen, K. S., & García-González, C. A. (2021). Aerogels as porous structures for food applications: Smart ingredients and novel packaging materials. *Food Structure*, *28*, 100188. https://doi.org/10.1016/j.foostr.2021.100188

Martínez-Gutiérrez, E. (2018). Biogas production from different lignocellulosic biomass sources:

advances and perspectives. *3 Biotech*, *8*(5), 233. https://doi.org/10.1007/s13205-018-1257-4

Martínez-Sanz, M., Gómez-Mascaraque, L. G., Ballester, A. R., Martínez-Abad, A., Brodkorb, A., & López-Rubio, A. (2019). Production of unpurified agar-based extracts from red seaweed Gelidium sesquipedale by means of simplified extraction protocols. *Algal Research*, *38*, 101420. https://doi.org/10.1016/j.algal.2019.101420

Martínez-Sanz, M., Ström, A., Lopez-Sanchez, P., Knutsen, S. H., Ballance, S., Zobel, H. K., Sokolova, A., Gilbert, E. P., & López-Rubio, A. (2020). Advanced structural characterisation of agar-based hydrogels: Rheological and small angle scattering studies. *Carbohydrate Polymers*, *236*, 115655. https://doi.org/https://doi.org/10.1016/j.carbpol.2019.115655

Martins, A. J., Pastrana, L. M., Vicente, A. A., & Cerqueira, M. A. (2018). Food Grade Polymers for the Gelation of Edible Oils Envisioning Food Applications. In T. J. Gutiérrez (Ed.), *Polymers for Food Applications* (pp. 591–608). Springer International Publishing. https://doi.org/10.1007/978-3-319-94625-2_22

Mikkonen, K. S., Parikka, K., Ghafar, A., & Tenkanen, M. (2013). Prospects of polysaccharide aerogels as modern advanced food materials. *Trends in Food Science and Technology*, *34*(2), 124–136. https://doi.org/10.1016/j.tifs.2013.10.003

Moschakis, T., Murray, B. S., & Dickinson, E. (2006). Particle tracking using confocal microscopy to probe the microrheology in a phase-separating emulsion containing nonadsorbing polysaccharide. *Langmuir*, *22*(10), 4710–4719. https://doi.org/10.1021/la0533258

Mostafavi, F. S., & Zaeim, D. (2020). Agar-based edible films for food packaging applications - A review. *International Journal of Biological Macromolecules*, *159*, 1165–1176. https://doi.org/10.1016/j.ijbiomac.2020.05.123

Necas, J., & Bartosikova, L. (2013). Carrageenan: a review. *Veterinarni Medicina*, *58*(4), 187–205.

Nishinari, K., & Watase, M. (1983). Effect of alkali pretreatment on the rheological properties of concentrated agar-agar gels. *Carbohydrate Polymers*, *3*(1), 39–52. https://doi.org/10.1016/0144-8617(83)90011-5

Nita, L. E., Ghilan, A., Rusu, A. G., Neamtu, I., & Chiriac, A. P. (2020). New trends in bio-based aerogels. *Pharmaceutics*, *12*(5), 449. https://doi.org/10.3390/pharmaceutics12050449

Oliver, L., Scholten, E., & van Aken, G. A. (2015). Effect of fat hardness on large deformation rheology of emulsion-filled gels. *Food Hydrocolloids*, *43*, 299–310.

Pacheco-Quito, E.-M., Ruiz-Caro, R., & Veiga, M.-D. (2020). Carrageenan: Drug Delivery Systems and Other Biomedical Applications. *Marine Drugs*, *18*(11), 583.

Paglarini, C. de S., Furtado, G. de F., Biachi, J. P., Vidal, V. A. S., Martini, S., Forte, M. B. S., Cunha, R. L., & Pollonio, M. A. R. (2018). Functional emulsion gels with potential application in meat products. *Journal of Food Engineering*, *222*, 29–37. https://doi.org/https://doi.org/10.1016/j.jfoodeng.2017.10.026

Patel, A., & Mequanint, K. (2011). Hydrogel biomaterials. In *Biomedical engineering-frontiers and challenges*. IntechOpen.

Patel, A. R., Cludts, N., Sintang, M. D. Bin, Lesaffer, A., & Dewettinck, K. (2014). Edible oleogels based on water soluble food polymers: preparation, characterization and potential application. *Food & Function*, *5*(11), 2833–2841.

Pérez, M. J., Moreno, M. A., Martínez-Abad, A., Cattaneo, F., Zampini, C., Isla, M. I., López-Rubio,

A., & Fabra, M. J. (2021). Interest of black carob extract for the development of active biopolymer films for cheese preservation. *Food Hydrocolloids*, *113*, 106436. https://doi.org/10.1016/j.foodhyd.2020.106436

Phoopuritham, P., Thongngam, M., Yoksan, R., & Suppakul, P. (2012). Antioxidant Properties of Selected Plant Extracts and Application in Packaging as Antioxidant Cellulose-Based Films for Vegetable Oil. *Packaging Technology and Science*, *25*(3), 125–136. https://doi.org/10.1002/PTS.963

Pourashouri, P., Shabanpour, B., Heydari, S., & Raeisi, S. (2021). Encapsulation of fish oil by carrageenan and gum tragacanth as wall materials and its application to the enrichment of chicken nuggets. *LWT*, *137*, 110334.

Sachlos, E., & Czernuszka, J. T. (2003). Making tissue engineering scaffolds work. Review: the application of solid freeform fabrication technology to the production of tissue engineering scaffolds. *Eur Cell Mater*, *5*(29), 39–40.

Santamaría Vanegas, J., Rozo Torres, G., & Barreto Campos, B. (2019). Characterization of a κ-Carrageenan Hydrogel and its Evaluation as a Coating Material for Fertilizers. *Journal of Polymers and the Environment*, *27*(4), 774–783. https://doi.org/10.1007/s10924-019-01384-4

Skryplonek, K., Henriques, M., Gomes, D., Viegas, J., Fonseca, C., Pereira, C., Dmytrów, I., & Mituniewicz-Małek, A. (2019). Characteristics of lactose-free frozen yogurt with κ-carrageenan and corn starch as stabilizers. *Journal of Dairy Science*, *102*(9), 7838–7848.

Sousa, A. M. M., Morais, S., Abreu, M. H., Pereira, R., Sousa-Pinto, I., Cabrita, E. J., Delerue-Matos, C., & Gonçalves, M. P. (2012). Structural, physical, and chemical modifications induced by microwave heating on native agar-like galactans. *Journal of Agricultural and Food Chemistry*, *60*(19), 4977–4985.

Sun, H., Gao, L., Xue, C., & Mao, X. (2020). Marine-polysaccharide degrading enzymes: Status and prospects. *Comprehensive Reviews in Food Science and Food Safety*, *19*(6), 2767–2796. https://doi.org/10.1111/1541-4337.12630

Thrimawithana, T. R., Young, S., Dunstan, D. E., & Alany, R. G. (2010). Texture and rheological characterization of kappa and iota carrageenan in the presence of counter ions. *Carbohydrate Polymers*, *82*(1), 69–77. https://doi.org/10.1016/j.carbpol.2010.04.024

Ubeyitogullari, A., & Ciftci, O. N. (2016). Formation of nanoporous aerogels from wheat starch. *Carbohydrate Polymers*, *147*, 125–132. https://doi.org/10.1016/j.carbpol.2016.03.086

Venugopal, V. (2016). *Marine polysaccharides: Food applications*. CRC Press.

Wang, Y., Su, Y., Wang, W., Fang, Y., Riffat, S. B., & Jiang, F. (2019). The advances of polysaccharide-based aerogels: Preparation and potential application. *Carbohydrate Polymers*, *226*, 115242. https://doi.org/10.1016/j.carbpol.2019.115242

Watase, M., & Nishinari, K. (1983). Rheological properties of agarose gels with different molecular weights. *Rheologica Acta*, *22*(6), 580–587. https://doi.org/10.1007/BF01351404

Wijesekara, I., Pangestuti, R., & Kim, S. (2011). Biological activities and potential health benefits of sulfated polysaccharides derived from marine algae. *Carbohydrate Polymers*, *84*(1), 14–21. https://doi.org/10.1016/j.carbpol.2010.10.062

Wu, M., Xiong, Y. L., & Chen, J. (2011). Rheology and microstructure of myofibrillar protein-

plant lipid composite gels: Effect of emulsion droplet size and membrane type. *Journal of Food Engineering*, *106*(4), 318–324. https://doi.org/10.1016/j.jfoodeng.2011.05.022

Yang, X., Li, A., Li, X., Sun, L., & Guo, Y. (2020). An overview of classifications, properties of food polysaccharides and their links to applications in improving food textures. *Trends in Food Science and Technology*, *102*, 1–15. https://doi.org/10.1016/j.tifs.2020.05.020

Yegappan, R., Selvaprithiviraj, V., Amirthalingam, S., & Jayakumar, R. (2018). Carrageenan based hydrogels for drug delivery, tissue engineering and wound healing. *Carbohydrate Polymers*, *198*, 385–400.

Zhang, H., Zhang, F., & Yuan, R. (2019). Applications of natural polymer-based hydrogels in the food industry. In *Hydrogels Based on Natural Polymers* (pp. 357–410). Elsevier. https://doi.org/10.1016/B978-0-12-816421-1.00015-X

Zia, K. M., Tabasum, S., Nasif, M., Sultan, N., Aslam, N., Noreen, A., & Zuber, M. (2017). A review on synthesis, properties and applications of natural polymer based carrageenan blends and composites. *International Journal of Biological Macromolecules*, *96*, 282–301. https://doi.org/https://doi.org/10.1016/j.ijbiomac.2016.11.095

Ziegler, C., Wolf, A., Liu, W., Herrmann, A. K., Gaponik, N., & Eychmüller, A. (2017). Modern Inorganic Aerogels. *Angewandte Chemie - International Edition*, *56*(43), 13200–13221. https://doi.org/10.1002/anie.201611552

II. OBJECTIVES

Objectives

The general objective of the present doctoral thesis was to design and investigate the structure of gel-like structures based on polysaccharides extracted from aquatic biomass, with interest for food-related applications.

To achieve this general objective, several specific objectives were proposed:

- To **optimize the formulation of polysaccharide-based hydrogels and emulsion-gels** and understand the effect of different factors on their gelation mechanism, as well as the impact on the formed gel structures.
- To **develop highly porous and adsorbent bioactive aerogels** based on cellulose from aquatic biomass and **evaluate their application as absorbent pads** to improve the preservation of packaged fresh meat.
- To **incorporate bioactive food ingredients** within the optimized gel-like structures and evaluate their release upon gastrointestinal digestion conditions, as well as the structural changes produced on the materials.

These general objectives were materialized in 6 individual case studies, which have been structured in 3 chapters in this thesis.

Chapter 1. Structure and functional properties of sulphated polysaccharide hydrogels.

1.1. Understanding nano structural differences in hydrogels from commercial carrageenans: Combined small angle X-ray scattering and rheological studies.

1.2. Development of polysaccharide-casein gel-like structures resistant to *in vitro* gastric digestion.

Chapter 2. Cellulosic aerogels as adsorbent packaging structures.

2.1. Superabsorbent food packaging bioactive cellulose-based aerogels from *Arundo donax* waste biomass.

Chapter 3. Structure, properties and applications of emulsion gels based on sulphated polysaccharides.

1.3. Rheological and structural characterization of carrageenan emulsion gels.

1.4. Emulsion-gels and oil-filled aerogels as curcumin carriers: nanostructural characterization of gastrointestinal digestion products.

1.5. Maximizing the oil content in polysaccharide-based emulsion gels for the development of tissue mimicking phantoms.

III. RESULTS

Results

This section includes the results from 6 individual case studies, which have been structured in 3 chapters:

Chapter 1. Structure and functional properties of sulphated polysaccharide hydrogels.

1.1. Understanding nano structural differences in hydrogels from commercial carrageenans: Combined small angle X-ray scattering and rheological studies.

1.2. Development of polysaccharide-casein gel-like structures resistant to *in vitro* gastric digestion.

Chapter 2. Cellulosic aerogels as adsorbent packaging structures.

2.1. Superabsorbent food packaging bioactive cellulose-based aerogels from *Arundo donax* waste biomass.

Chapter 3. Structure, properties and applications of emulsion-gels based on sulphated polysaccharides.

3.1. Rheological and structural characterization of carrageenan emulsion-gels.

3.2. Emulsion-gels and oil-filled aerogels as curcumin carriers: nanostructural characterization of gastrointestinal digestion products.

3.3. Maximizing the oil content in polysaccharide-based emulsion-gels for the development of tissue mimicking phantoms.

CHAPTER 1

STRUCTURE AND FUNCTIONAL PROPERTIES OF SULPHATED POLYSACCHARIDE HYDROGELS

3.1.1 Understanding nanostructural differences in hydrogels from commercial carrageenans: combined small angle X-ray scattering and rheological studies

3.1.2 Development of polysaccharide-casein gel-like structures resistant to gastric digestion

INTRODUCTION TO CHAPTER 1

Hydrogels are highly hydrated systems which are typically used within the food industry mainly as templates for the controlled delivery of bioactive compounds and as additives for texture modification in food formulations and for satiety control. Sulphated polysaccharides are particularly interesting for the development of hydrogels due to their excellent gelling capacity. The gelation of sulphated polysaccharides is a complex process that depends on several factors, such as the proportion and location of sulphate groups, the polysaccharide concentration and the presence of counter ions, amongst others. These factors will determine the viscosity of solutions and the strength of the hydrogels formed. The exact mechanism through which different sulphated polysaccharides form hydrogel structures and the interplay of cationic salts in the process are still not fully understood. In this context, this chapter presents an in-depth structural characterization of hydrogel structures formed using different sulphated polysaccharides making use of advanced characterization tools, as well as an innovative application of these materials in the food sector.

In the first work, hydrogels from commercial carrageenans (κ-, ι- and λ-carrageenan) were prepared with and without the addition of cationic salts (KCl and). The effect of carrageenan and salt concentration on the hydrogel strength were evaluated through a response surface design and a detailed structural characterization was carried out by small angle X-ray scattering (SAXS) and rheology. These results evidenced the distinct gelation mechanism of each commercial carrageenan and provided a solid basis for the design and optimization of hydrogels with tuneable properties.

In the second work, the application of polysaccharide-based gel-like structures as templates for the protection of food proteins against the hydrolytic effect of enzymes during gastrointestinal digestion was evaluated. In particular, hybrid hydrogels and aerogels based on agar or κ-carrageenan and casein were developed and subjected to *in vitro* gastrointestinal digestions to evaluate their potential to delay casein hydrolysis. The microstructure evolution of the materials upon the digestions was studied and the molecular weight distribution and peptidomic profile of the digestion products were also determined. This work provides useful information on the parameters which have a strong impact on the protection ability of the

hybrid hydrogels and highlights the potential of these structures to selectively protect food proteins during the gastric phase while promoting the release of peptides during the intestinal phase.

3.1.1

UNDERSTANDING NANOSTRUCTURAL DIFFERENCES IN HYDROGELS FROM COMMERCIAL CARRAGEENANS: COMBINED SMALL ANGLE X-RAY SCATTERING AND RHEOLOGICAL STUDIES

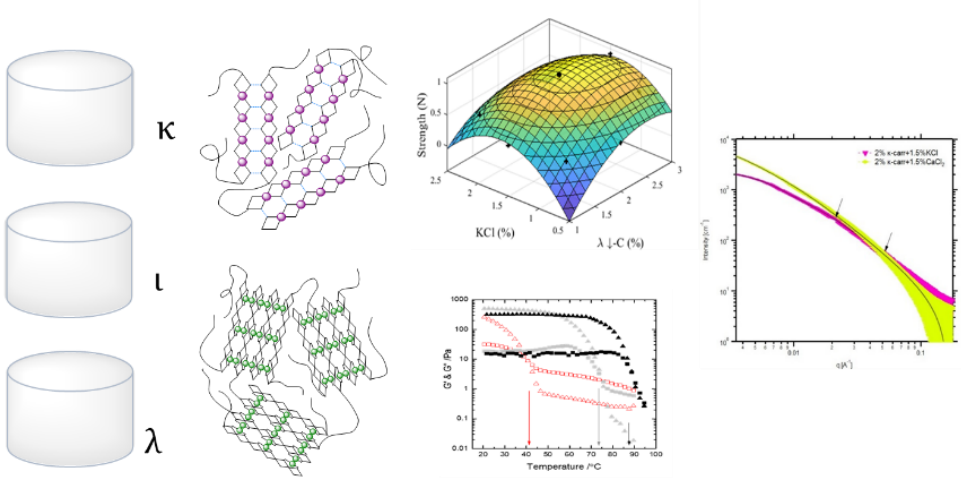

This section is an adapted version of the following published research article:

Fontes-Candia, C., Ström, A., Lopez-Sanchez, P., López-Rubio, A., & Martínez-Sanz, M. (2020). Rheological and structural characterization of carrageenan emulsion gels. Algal Research, 47, 101873.

1 Abstract

Hydrogels from commercial carrageenans (κ-C, ι-C, λ↑-C (high viscosity) and λ↓-C (low viscosity)) were prepared with and without the addition of salts (KCl and $CaCl_2$). FT-IR and ^{1}H-NMR characterization evidenced that while the κ-C and ι-C grades were relatively pure carrageenans, the two λ-C grades were mixtures of λ-, κ-, θ- and μ-carrageenan. The effect of carrageenan and salt concentration on the hydrogel strength were evaluated through a response surface design and a detailed structural characterization was carried out by small angle X-ray scattering (SAXS) and rheology. The low amount of sulphate substitution in κ-C enabled intramolecular association, giving rise to strong hydrogels, even in the absence of salts. On the other hand, ι-C, λ↑-C and λ↓-C produced much weaker hydrogels and required the addition of salts to induce intramolecular association by ionic cross-linking. SAXS results suggested the formation of similar structures of double helices in κ-C and ι-C with the addition of salts; however, distinct network structures were attained. In the case of κ-C, a Gauss-Lorentz gel model was suitable to describe the hydrogel structure and the addition of K^+ promoted the formation of more ordered and densely packed structures. On the other hand, larger but weaker aggregates, with marked periodicity, were observed in ι-C, with Ca^{2+} inducing the formation of more densely packed networks. The complex composition of the λ-C grades gave rise to more heterogeneous branched network structures, properly described by a correlation length model, where the gelation mechanism was mostly governed by the κ-carrageenan component.

2 Introduction

Carrageenans are sulphated polysaccharides present in the cell walls and in the intercellular matrix of red seaweeds (*Rhodophyta*). These polysaccharides contain a backbone of alternating disaccharide repeating units of β-D-galactose (G-units) linked at position 3 and α-D-galactose (D-units) or 3,6-anhydro-α-D-galactose (DA-units) linked at position 4. Depending on the content and position of sulphate groups (SO_3^-), they can be classified into different forms, being the kappa (κ)-, iota (ι)- and lambda (λ)-carrageenans, which contain one, two and three sulphate groups per disaccharide unit, respectively, the three main types commercially available. These carrageenans are obtained from different seaweed species and using different extraction

procedures. κ-carrageenan is typically extracted from the *Eucheuma cottonii* seaweed species, while ι-carrageenan is mainly obtained from *Eucheuma spinosum* (Campo et al., 2009). Their extraction process involves the application of physical separation methods, followed by alkali treatments at high temperatures to transform the naturally occurring μ- and ν-carrageenans (whose backbones are composed of G- and D-units) into κ- and ι-carrageenans. The alkali treatments produce the removal of one sulphate group from the D-units, originating an anhydride bridge and giving rise to the formation of DA-units. It should be noted that most of the extraction protocols described in the literature typically yield κ-/ι- mixtures rather than pure carrageenans (Azevedo et al., 2013; Freile-Pelegrín et al., 2006; Webber et al., 2012). On the other hand, λ-carrageenan is obtained from different species of the *Gigartina* and *Chondrus* genera, although the materials obtained from these seaweeds are typically a mixture of several types of carrageenan (Campo et al., 2009; Hilliou et al., 2012; Pereira & Van de Velde, 2011; Piculell, 1995).

Carrageenans are widely used in the food industry due to their texturizing properties, highlighting their thickening and gelling capacity and their ability to stabilize proteins (Stone & Nickerson, 2012; Zia et al., 2017); additionally, they also find applications in the pharmaceutical (Liu et al., 2015), cosmetic (Fan et al., 2016), printing and textile industries (Imeson, 2000). Of special interest is their use for the production of hydrogels. Hydrogels are three-dimensional, hydrophilic, polymeric networks capable of holding large amounts of water. In the food industry, hydrogels are used as control release systems and as additives for satiety control and texture modification in food formulations (Lopez-Sanchez et al., 2018; Peak et al., 2013; Shewan & Stokes, 2013; Ström et al., 2009). The formation of carrageenan hydrogels is a complex process that depends on the proportion and location of sulphate groups, the carrageenan concentration and the presence of counter ions, amongst others. These factors will determine the viscosity of solutions and the strength of the hydrogels formed (Funami et al., 2007; Robal et al., 2017). The gelation of carrageenans is generally explained by the 'domain model' (Robinson et al., 1980), which describes gelation as a two-step process: (i) the transition from random coils in the solution state to double helices, followed by (ii) the aggregation of double helices to form cross-linking domains which originate the hydrogel network structure

(Mangione et al., 2003). This general mechanism seems to be valid for the most studied gelling carrageenans (e.g. κ- and ι-); however, these two carrageenan types form hydrogels with very distinct properties: whereas κ-carrageenan forms hydrogels that are hard, strong and brittle, ι-carrageenan forms soft and weak hydrogels (Thrimawithana et al., 2010). This must be attributed to structural differences in the hydrogel network, which in turn, should be the result of different processes taking place upon gelation. The presence of the anhydro-galactose bridge in the 4-linked galactose residue (as in κ- and ι-carrageenans) has been proposed to be crucial for the formation of the helical structures, initiating the gelation process (Campo et al., 2009; Piculell, 1995). In the case of λ-carrageenan, lacking the 3,6-anhydro bridge, the C2-sulphate group from the 4-linked residue is oriented towards the internal part, thus hindering the formation of double helices (Campo et al., 2009). As a result, λ-carrageenan is thought to adopt a coil conformation whatever the temperature conditions and is unable to form hydrogels (Piculell, 1995), although it can be used as thickening agent due to its high viscosity. Furthermore, due to the existence of electrical charges in the carrageenan chains, provided by the sulphate groups, the presence of cations plays a very important role in the gelation process (Morris et al., 1980). While monovalent cations have been seen to promote more efficiently hydrogel formation than divalent cations in κ-carrageenan (A.-M. Hermansson, 1989; A. Hermansson et al., 1991; MacArtain et al., 2003; Morris et al., 1980), divalent cations have been proposed as more suitable for the formation of stronger ι-carrageenan hydrogels (Michel et al., 1997; Thrimawithana et al., 2010). The exact mechanism through which specific cations interplay in the gelation mechanism of κ- and ι-carrageenan is still not fully understood and deserves further investigation. Moreover, λ-carrageenan has also been claimed to show gel-like behaviour in presence of trivalent cations (Running et al., 2012); the authors proposed that the neutralization of the sulphate groups by the trivalent cations induced the formation of the hydrogel network structure, which goes against the hypothesis of double helices being essential for the gelation process.

Given the relevance of the hydrogel properties for practical applications, it is of importance to evaluate how the network structure is modified depending on the type of carrageenan and type of cation used. While there are several studies which have focused on these issues for a specific

carrageenan type, models for the mechanisms driving the gelation processes of commercial carrageenans, which are typically mixtures, are still lacking. In this context, the aim of this work was to implement a proper characterization protocol, based on the combination of different techniques, to determine the composition and structural characteristics of different commercial carrageenan grades and optimize the formulation of hydrogels in the presence of mono- and divalent cations (K^+ and Ca^{2+}). For this purpose, the composition of the commercial grades was firstly studied by means of spectroscopy (FT-IR and ^{1}H-NMR) and the influence of the concentration of carrageenan and salts in the hydrogels formed were evaluated through a response surface design, obtaining the optimal formulations for the strongest hydrogels. Moreover, a detailed structural characterization of selected carrageenan hydrogels was carried out using small angle X-ray scattering (SAXS) and rheology. Based on these results and on the models proposed in the literature for the gelation of pure carrageenans, the gelation mechanism for each commercial grade was proposed, which will be particularly useful for the design of hydrogels with target properties for their use in food-related applications.

3 Materials and methods

3.1 Materials

Different commercial carrageenan grades, namely, κ-carrageenan (Ceamgel 90-093) (extracted from *Euchema cottonii*), ι-carrageenan (Ceamvis 3383) (extracted from *Euchema spinosum*) and λ-carrageenan (low viscosity grade Ceamlacta 2270 and low viscosity grade Ceamlacta 2170) (extracted from *Gigartina pistillata* (from Chilean origin for the low viscosity grade and Moroccan origin for the high viscosity grade)), in the form of powders, were kindly donated by CEAMSA (Pontevedra, Spain). The cationic composition of the commercial carrageenans was determined by inductively coupled plasma mass spectrometry (ICP-MS) for the measurement of Ca^{2+}, Na^+, K^+ and Mg^{2+}. The samples were subjected to an acid digestion in an oven at 200°C and analyzed using an Agilent 7900 instrument. $CaCl_2 \cdot 2H_2O$ and KCl were obtained from Panreac and Sigma-Aldrich (Spain), respectively.

3.2 Preparation of carrageenan hydrogels

Hydrogels from the different commercial carrageenan grades (κ-carrageenan (κ-C), ι-carrageenan- (ι-C) and λ-carrageenan with high (λ↑-C) and low viscosity (λ↓-C)) were prepared with and without the addition of two different salts (KCl and $CaCl_2$). The range of carrageenan and salt concentrations tested (cf. Table 1) were established by preliminary experiments and a central composite design was carried out for each combination of carrageenan type and salt. The required amount of carrageenan powder was added to distilled water and heated up to 90 °C for 30 minutes. After that, the required amount of salt was added and the solutions were stirred until the salt was completely dissolved. Aliquots of the hot solutions were directly transferred to quartz capillaries for SAXS analyses or to the rheometer plate. For the penetration tests, the hot solutions were transferred to cylindrical containers (30 mm diameter, 40 mm height) and were cooled down to room temperature and subsequently stored at 4 °C for 24 h prior to the analyses.

3.3 Hydrogel strength

The hydrogel strength was evaluated at room temperature (20–25 °C) through penetration tests in a texture analyser (Stable Micro Systems model TA-XT2, Surrey, UK) equipped with a cylindrical Teflon plunger (1 cm diameter) and operating at a penetration rate of 1 mm/s to a depth of 5 mm. All measurements were performed, at least, in triplicate.

3.4 Statistics

A statistical central composite design was carried out to evaluate the influence of the carrageenan concentration (C) and the concentration of two different added salts (KCl and $CaCl_2$) (S_{KCl} and S_{CaCl2}) in the hydrogel strength (HS). The considered ranges for each variable in this model, which were determined empirically through preliminary tests, are shown in Table 1. According to the central composite design, 13 runs for each combination of carrageenan type and type of salt were carried out. The matrix designs and the graphical analysis were performed using IBM SPSS Statistic software (v.24) (IBM corp., USA) and Matlab (Mathworks, Inc., USA), respectively.

The response values were predicted by the quadratic polynomial equation as follows:

$$\gamma = \beta 0 + \sum_{i=1}^{k} \beta_i + \sum_{i=1}^{k} \beta_{ii} {X_i}^2 + \sum_{i \neq j}^{k} \beta_{ij} X_i X_j \quad (1)$$

were γ correspond to the predicted response: β_0, β_i, β_{ii} and β_{ij} were the constant regression coefficients of the model; X_i and X_j represent the independent variables. The results obtained were analysed by ANOVA to investigate the significance and fitness of the model, as well as the effect of significant individual terms and the interactions on the responses. The optimization of the response was obtained using a response surface methodology.

Table 1. Minimum and maximum level considered in the study for carrageenan and salt concentrations (% wt/v).

Sample	level	C (%)	KCl (%)	$CaCl_2$ (%)
κ-C	Min	1.0	0.0	0.1
	Max	2.0	2.0	2.0
ι-C	Min	1.0	0.5	0.1
	Max	2.0	2.0	2.0
λ↓-C	Min	1.0	0.25	0.25
	Max	2.0	2.0	2.0
λ↑-C	Min	1.0	0.5	-
	Max	3.0	2.5	-
λ↑-C	Min	2.0	-	0.5
	Max	3.0	-	2.5

3.5 Oscillatory rheological measurements

The rheological measurements were performed on a DHR-3 rheometer from TA instruments (USA) using a cone-plate geometry (4 cm diameter, 1º angle and 26 µm of gap). Temperature was controlled using a Peltier plate. The cone was equipped with a solvent trap and an evaporation blocker from TA Instruments. In addition, the samples were covered with a layer

of paraffin oil. Freshly prepared hot carrageenan solutions were loaded onto the rheometer, which plate was pre-heated to 90 ºC. After an equilibration time of 5 minutes, a cooling step from 90 to 20 °C was performed at a constant rate of 1 ºC/min. The storage (G') and loss (G'') moduli were recorded at a strain of 1% and frequency of 1 Hz.

3.6 High performance size exclusion chromatography (HPLC-SEC)

The molecular weight of the different carrageenan grades was estimated by HPLC-SEC analyses, following a method adapted from (Martínez-Sanz et al., 2019). The HPLC system was equipped with a Waters 2695 separations module and a Waters 2414 refractive index detector (Waters, USA). The samples (1 mg/mL) were dissolved in the mobile phase (0.01M LiCl) at 45 °C for 1h, filtered through 0.8 µm pore syringe filters for aqueous media (Sartorius, Germany) and injected into an OHpak SB-806 HQ (8 mm x 300 mm) SEC column (Shodex, Japan) equilibrated at 45 °C. The injection volume was 20 µL and the flow rate was 0.5 mL/min. Calibration was performed using P-82 pullulan standards (Shodex, Japan), and peak molecular weights (M_p) are reported.

3.7 Fourier transform infrared spectroscopy (FT-IR)

FT-IR spectra from the commercial carrageenan powders were recorded in attenuated total reflectance (ATR) mode in a controlled chamber at 21 °C and dry air to avoid humidity and CO_2 using a Thermo Nicolet Nexus (GMI, USA) equipment. The spectra were taken at 4 cm^{-1} resolution in a wavelength range between 650-4000 cm^{-1} and averaging a minimum of 32 scans.

3.8 ^{1}H-NMR analysis

The ^{1}H NMR experiments were performed at a ^{1}H frequency of 500.13 MHz using a Neo-500 Bruker spectrometer, equipped with a 5mm BBO-F-plus probehead. The samples were dissolved in D_2O at 70 °C, at a concentration of 1% (wt./v) and transferred to 5mm NMR tubes. The spectra were acquired at 70 °C, with a 30º pulse sequence (pulse 90º 10 µs), with 2s of relaxation delay and 256 scans. All chemical shifts were referenced to residual non-deuterated solvent (4.82ppm).

3.9 Small angle X-ray scattering (SAXS)

SAXS experiments were carried out in the Non Crystalline Diffraction beamline, BL-11, at ALBA synchrotron light source (www.albasynchrotron.es). Aliquots of carrageenan solutions (containing 2 % (wt./v) of carrageenan and 1.5 % (wt./v) of salt) were placed in sealed 2 mm quartz capillaries (Hilgenburg Gmbh, Germany) and were left to cool down at 25 ºC for 24 h to form gels prior to the experiments. The energy of the incident photons was 12.4 KeV or equivalently a wavelength, λ, of 1 Å. The SAXS diffraction patterns were collected by means of a photon counting detector, Pilatus 1M, with an active area of 168.7x 179.4 mm2, an effective pixel size of 172 x 172 µm2 and a dynamic range of 20 bits. The sample-to-detector distance was set to 6425 mm, resulting in a q range with a maximum value of q = 0.23 Å-1. An exposure time of 0.5 seconds was selected based on preliminary trials. The data reduction was treated by pyFAI python code (ESRF) (Kieffer & Wright, 2013), modified by ALBA beamline staff, to do on-line azimuthal integrations from a previously calibrated file. The calibration files were created from a silver behenate (AgBh) standard. The intensity profiles were then represented as a function of q using the IRENA macro suite (Ilavsky & Jemian, 2009) within the Igor software package (Wavemetrics, Lake Oswego, Oregon). A scattering background (corresponding to a quartz capillary filled with distilled water) was subtracted from all the samples.

Different models were used to fit the experimental data, depending on the type of carrageenan used to prepare the hydrogels. In the case of the κ-C hydrogels, a Gauss-Lorentz gel model was used. This model, described by the scattering function (2), calculates the scattering from a gel structure (typically physical networks) (Evmenenko et al., 2001; Shibayama et al., 1992; Yeh et al., 1998) as the sum of a low-q exponential decay plus a Lorentzian at higher q-values:

$$I(q) = I_G(0) \cdot \exp\left[-\frac{q^2\Xi^2}{2}\right] + I_L(0)/(1 + q^2\xi^2) + bkg \qquad (2)$$

where $I_L(0)$ and $I_G(0)$ are, respectively, the linear coefficients of the Lorentzian and Gaussian terms, Ξ is the characteristic mean size of the static heterogeneities in the system under study, ξ is the correlation length of polymer–polymer interactions between the fluctuating chains of polymer and bkg is the background.

The Gauss-Lorentz gel model was not able to provide satisfactory fits for the scattering curves from the ι-C hydrogels and a two-level unified model was used instead. This model considers that, for each individual level, the scattering intensity is the sum of a Guinier term and a power-law function (Beaucage, 1995, 1996):

$$I(q) = \sum_{i=1}^{N} G_i \exp\left(-q^2 \cdot \frac{R_{g,i}^2}{3}\right) + \frac{B_i\left[\mathrm{erf}(qR_{g,i}/\sqrt{6})\right]^{3P_i}}{q^{P_i}} + bkg \quad (3)$$

where $G_i = c_i V_i \Delta SLD_i{}^2$ is the exponential prefactor (where V_i is the volume of the particle and ΔSLD_i is the scattering length density (SLD) contrast existing between the ith structural feature and the surrounding solvent), $R_{g,i}$ is the radius of gyration describing the average size of the ith level structural feature, B_i is a q-independent prefactor specific to the type of power-law scattering with power-law exponent, P_i, and bkg is the background. An additional term consisting in a Gaussian peak was added to fit the data from the ι-C hydrogel with KCl, resulting in the following function:

$$I(q) = \sum_{i=1}^{N} G_i \exp\left(-q^2 \cdot \frac{R_{g,i}^2}{3}\right) + \frac{B_i\left[\mathrm{erf}(qR_{g,i}/\sqrt{6})\right]^{3P_i}}{q^{P_i}} + I_0 \cdot \exp\left[-\frac{1}{2} \cdot \left(\frac{q - q_0}{B}\right)^2\right] + bkg \quad (4)$$

where q_0 is the peak position, I_0 is the intensity of the peak and B is the standard deviation of the peak position.

In the case of the λ-C hydrogels, a much simpler correlation length model, described by equation (5), could be used to fit the scattering data. This model contains a first term, described by a power-law function, which accounts for the scattering from large clusters in the low q region and a second term, consisting of a Lorentzian function, which describes scattering from polymer chains in the high q region:

$$I(q) = \frac{A}{q^n} + \frac{C}{1 + (q\xi_L)^m} + bkg \quad (5)$$

where n is the power-law exponent, A is the power-law coefficient, m is the Lorentzian exponent, C is the Lorentzian coefficient and ξ_L is the correlation length for the polymer chains (which gives an indication of the gel's mesh size).

4 Results and discussions

4.1 Molecular structure of the different carrageenan grades

The mechanical properties of carrageenan hydrogels are known to be strongly dependent on the content and position of sulphate groups (Stanley, 1990). Furthermore, some studies pointed out towards a possible effect of the molecular weight in some of the parameters describing the hydrogel mechanical performance (Rochas et al., 1989, 1990). Accordingly, different commercial carrageenan grades, potentially presenting different composition and molecular weights, were selected in this work to evaluate the effect of their structural features in the strength of hydrogels formed with and without the addition of salts.

FTIR analyses were firstly carried out to assess the differences between the various carrageenan grades in terms of sulphate group content and distribution. The obtained spectra in the wavelength region where the sulphate-characteristic bands are typically detected (1400-600 cm^{-1}) are shown in Figure 1A. The bands located at 1065 cm^{-1} and 920 cm^{-1}, which are attributed to C-O-C vibrations of the 3,6 anhydrogalactose ring (Pereira et al., 2009), were observed in all the samples. Although the position of these bands was slightly shifted in the two λ-C grades, their appearance indicates that these materials were not of high purity, since no 3,6-anhydride bridges are present in pure λ-carrageenans (Doyle et al., 2010). The appearance of these bands has been reported for θ-carrageenans (Doyle et al., 2010), which can be produced by alkali treatment of λ-carrageenan or found in native seaweed species such as *Sarcothalia crisptata*, *Gigartina skottsbergii* (R Falshaw et al., 2001) and *Callophyllis hombroniana* (Ruth Falshaw et al., 2005). In addition, the band at 890 cm^{-1}, related to the rocking mode of the C6 group of the β-D-galactose unit (Sekkal & Legrand, 1993), was also detected in all carrageenan grades, but it appeared more intense for κ-C and ι-C. As observed, several sulphate-characteristic bands could be detected for all the carrageenan grades, although not all of them were visible for all the samples and their relative intensity was not the same. The absorption band at 1220 cm^{-1},

characteristic of ester sulphate groups from galactans (Robal et al., 2017), was apparent for all the carrageenans; however, its relative intensity was the lowest for κ-C. This is related to the lower amount of sulphate group substitutions in κ-carrageenan (i.e. one sulphate group per disaccharide repeating unit, versus two sulphate groups in ι-C and three sulphate groups in λ-C), which was expected to be the major component in this carrageenan grade. The band located at 840 cm^{-1}, indicative of an axial sulphate ester at the O-4 of a 3–linked galactose (Gómez-Ordóñez & Rupérez, 2011), was visible in κ-C and ι-C, while a broader shoulder was apparent for the two λ-C grades. This shoulder has been assigned to the existence of C–O–SO_3 on the C2 of galactose (Pereira et al., 2009), which is present in λ-, ξ- and θ-carrageenans. The band at 796 cm^{-1}, which is assigned to the sulphate ester substitution at the O-2 of a 4-linked, 3-6 anhydrogalactose (Gómez-Ordóñez & Rupérez, 2011; Prado-Fernández et al., 2003), was clearly visible in ι-C, although it also appeared as a weak shoulder in the two λ-C grades, supporting the presence of a certain fraction of θ-carrageenan. For λ-carrageenan, a broad band corresponding to sulphate ester substitution at the O-6 of a 4-linked galactose has been reported to appear at 867 cm^{-1} (Pereira et al., 2009), but the λ-C samples analysed in this work did not show any sharp peak at this position and instead, they presented a broad band between 780-865 cm^{-1}. This evidences the heterogeneity of the λ-C grades, which seemed to be a mixture of different types of carrageenan. In fact, several studies have reported that the carrageenans extracted from the seaweed species *Gigartina pistillata* consist of a mixture of λ-, κ- and ξ-carrageenans (Pereira et al., 2009; Pereira & Van de Velde, 2011).

To gain further insights on the composition of the commercial carrageenan grades, ^{1}H-NMR analyses were also performed and the obtained results are shown in Figure 1B. Based on the existing literature (Pereira & Van de Velde, 2011; Stortz et al., 1994; Van de Velde et al., 2004), the bands appearing in the region of anomeric protons could be assigned to different carrageenan types. The κ-C grade was characterized by the appearance of a peak at 5.09 ppm, corresponding to the anomeric proton of κ-carrageenan, and a very weak signal at 5.24 ppm, assigned to ι-carrageenan. The relative amount of each carrageenan type was estimated by integrating of the areas under the peaks, suggesting that the material was composed of 92% κ-carrageenan and 8% ι-carrageenan. The ι-C grade showed the ι-carrageenan characteristic band

(accounting for 82%) and a smaller peak at 5.35 ppm, which indicates the presence of floridean starch (corresponding to 18%) (Pereira & Van de Velde, 2011). The two λ-C grades showed a very heterogeneous composition, as reflected by the appearance of multiple peaks in their spectra. In both materials, the λ-carrageenan band was detected at 5.55 ppm; however, additional peaks at 5.09 ppm (κ-carrageenan), 5.14 ppm (non-identified), 5.24 ppm (μ-carrageenan), 5.30 ppm (θ-carrageenan) and 5.35 ppm (floridean starch) were also visible. Accordingly, the composition was determined as 26% λ-carrageenan, 28% κ-carrageenan, 13% μ-carrageenan, 18% θ-carrageenan and 11% starch for λ↓-C and 29% λ-carrageenan, 27% κ-carrageenan, 2% μ-carrageenan, 20% θ-carrageenan and 19% starch for λ↑-C. Thus, the NMR results confirm that while the κ-C and ι-C grades were relatively pure carrageenans, containing a certain amount of starch, the two λ-C grades were actually mixtures.

The cationic composition of all the carrageenan grades was also determined by means of ICP-MS to quantify the amounts of K^+, Na^+, Ca^{2+} and Mg^{2+} in the commercial products. The results, compiled in Table S1, evidence the presence of cations in the four commercial grades, being the total cationic content slightly higher in the ι-C grade. K^+ was the most abundant cation in the κ-C and ι-C grades, while the two λ-C grades contained more Na^+.

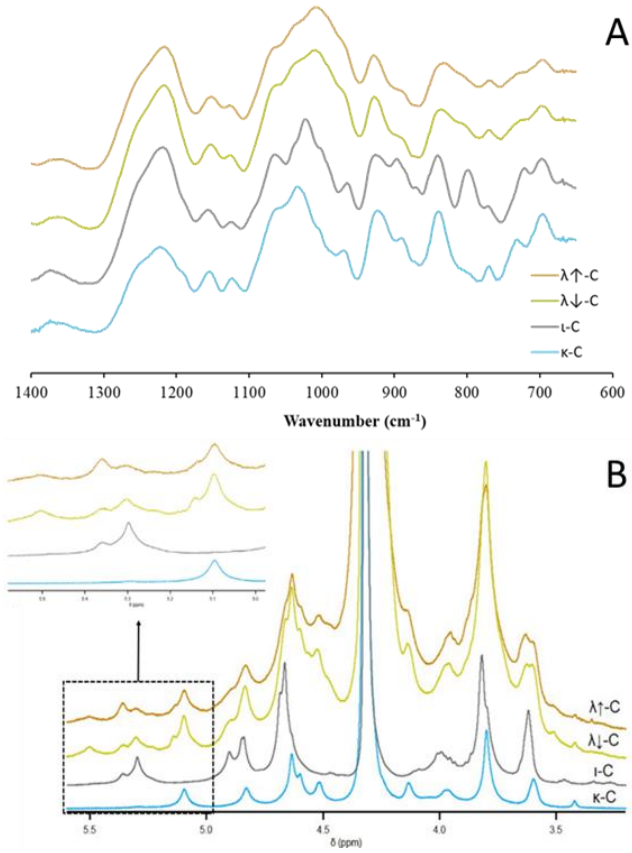

Figure 1. (A) FT-IR spectra and (B) 1H-NMR spectra of the various commercial carrageenan grades used in this work. Spectra have been offset for clarity. Characteristic bands are marked with discontinuous lines.

The molecular weight of the different carrageenan grades was analysed by means of HPLC-SEC. The comparison of the molecular weight of different carrageenans through this technique is complex due to their different aggregation behaviour in the presence of salts, while a certain ionic strength for the eluent is usually required for hydrophilic samples, especially polyelectrolytes (Lecacheux et al., 1985).

The transition of carrageenans from a disordered to an ordered conformation, and subsequent aggregation or gelation, is generally induced by increasing the ionic strength or lowering the temperature, so low ionic strengths and high temperatures were most desirable for the analysis. Accordingly, 0.01M LiCl was selected as eluent, since ι- and κ-carrageenans have been

previously described to exhibit a disordered structure in this medium (Hjerde et al., 1999) (less information is available for λ-carrageenans), and the experiments were carried out at 45 °C, above the aggregation temperature. Figure 2 shows the HPLC-SEC chromatograms obtained for the different carrageenan grades used in this work. As observed, all the samples presented significantly lower retention times than the standard pullulan samples used for calibration, suggesting that their molecular weights were considerably higher. However, it is worth mentioning that, although pullulan standards are commonly used as references for SEC of polysaccharides, the conformation of these neutral carbohydrates in solution is notably different from that of more complex polysaccharides such as carrageenans, precluding the accurate determination of absolute molecular weight values. Nevertheless, relative molecular weight data could be estimated for comparative analysis, and peak molecular weights for each carrageenan grade were calculated by extrapolation from the calibration curve built using the pullulan standards (R^2 = 0.992). The results, shown in Figure 2, evidence strong differences between the carrageenan grades. In particular, the ι-C presented the lowest molecular weight, while the λ↑-C, with the highest molecular weight, showed ca. 2-fold increased value with respect to λ↓-C.

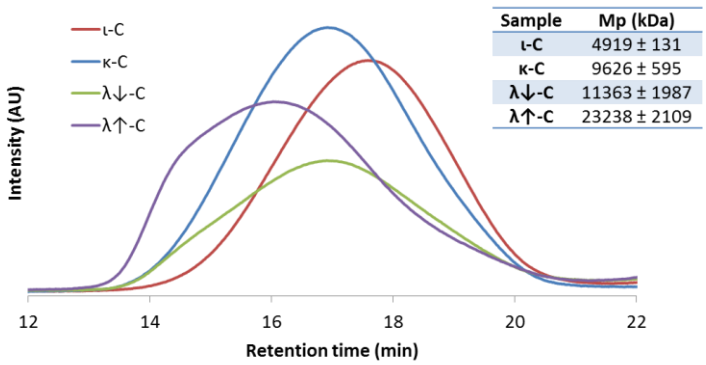

Figure 2. HPLC-SEC chromatograms of the commercial carrageenan grades and the estimated peak molecular weights (Mp). Data shown as mean ± SD, n=3.

4.2 Optimization of hydrogel strength: Effect of carrageenan and salt concentration

The four different commercial carrageenan grades (κ-C, ι-C, λ↓-C and λ↑-C) were used to produce hydrogels, with and without the addition of salts (a monovalent salt such as KCl and a divalent salt such as $CaCl_2$) and the effect of the carrageenan concentration and the salt concentration on the strength of the obtained materials was evaluated. To do so, a central composite design was performed, with the measured hydrogel strength being set as the response variable. Tables S2, S3, S4 and S5 (in the Supplementary Material) present the measured hydrogel strength values for each of the carrageenan and salt concentration combinations determined by the design. For each carrageenan grade and each type of salt, the obtained results were fitted using a quadratic model. The high model correlation coefficients obtained for all the types of hydrogels (R^2>0.99) evidence the accuracy of the theoretical models in describing the experimental data, i.e., they provide a good agreement between the experimental and predicted strength values (see Table S6 for the associated statistical parameters). The response surface plots were also obtained to show visually the dependence of the hydrogel strength on the two studied parameters (i.e., carrageenan and salt concentration) and the results are shown in Figure 3.

In general, it was observed that, as already anticipated due to the lower amount of sulphate substitution in κ-carrageenan, κ-C hydrogels showed the highest strength values from the four commercial grades tested. The results from the statistical analysis indicated that all the factors, except for the quadratic effect of the $CaCl_2$ concentration (P=0.38), had a significant effect on the κ-C hydrogel strength (P ≤0.05) (cf. Figure 3A and 3B). According to the results, higher hydrogel strength values were obtained when increasing the κ-C and salt concentration, where KCl had a stronger effect than $CaCl_2$. This is in agreement with a previous work in which higher strength values were reported for κ-carrageenan hydrogels prepared using monovalent salts as compared to those obtained with the addition of divalent salts (Thrimawithana et al., 2010). This behaviour was explained on the basis of the interference of these salts with the carrageenan double helix association mechanism. While K^+ has been hypothesised to facilitate the formation of strong κ-carrageenan double helix aggregates by neutralizing the repulsive electrostatic forces provided by sulphate groups, Ca^{2+} is thought to induce ionic cross-links

between the κ-carrageenan chains, generating softer hydrogels (Wang et al., 2018). It should be noted that the surface response graphs plotted as a function of ionic strength (cf. Figure S1) showed the same behaviour, in line with KCl and $CaCl_2$ promoting different supramolecular structures. The models obtained for the strength of the κ-C hydrogels with the addition of KCl and $CaCl_2$ could be described by the following equations:

$$HS_{KCl} = -16.72 + 16.19 \cdot \mathrm{C} + 14.79 \cdot \mathrm{S} - 1.16 \cdot C^2 - 4.13 \cdot S^2 + 1.14 \cdot CS \quad (6)$$

$$HS_{CaCl2} = -13.45 + 26.62 \cdot \mathrm{C} + 3.17 \cdot \mathrm{S} - 3.13 \cdot C^2 - 3.36 \cdot S^2 + 2.47 \cdot CS \quad (7)$$

Based on these equations, the maximum hydrogel strength values within the range of the carrageenan and salt concentrations studied were estimated, being ~29 N with the addition of KCl and ~20 N with $CaCl_2$ (cf. Table 2). Hydrogels with the corresponding κ-C and salt concentrations (2.0% κ-C + 2.0% KCl and 2.0% κ-C + 1.2% $CaCl_2$) were prepared and their strength values were measured. As deduced from the values listed in Table 2, the experimental and model-predicted strength values were very similar, highlighting the accuracy of the model. Regarding the ι-C hydrogels, all the measured strength values were significantly lower than those from the κ-C hydrogels. This can be related to the greater sulphate substitution in ι-carrageenan (the main component in the ι-C grade), which in turn impairs the association of the carrageenan double helices due to electrostatic repulsive forces. The statistical analyses indicated that all the considered factors had a significant effect on the hydrogel strength. As deduced from the response surface plots (cf. Figure 3B), the ι-C hydrogels with KCl presented greater strength values when increasing the carrageenan and salt concentrations. On the other hand, the ι-C hydrogels with $CaCl_2$ presented a different behaviour (cf. Figure 3C), showing a maximum strength at intermediate salt concentrations, in agreement with previous work (Funami et al., 2007; Thrimawithana et al., 2010). Moreover, as previously reported (Thrimawithana et al., 2010), lower concentrations were required for hydrogel formation in the presence of $CaCl_2$ as compared with KCl. This observation has been ascribed to the greater capacity of Ca^{2+} to form intramolecular bridges between the sulphate groups of adjacent anhydro-D-galactose and D-galactose residues of ι-carrageenan, as opposed to K^+, which is thought to form an ionic bond with the sulphate group of D-galactose residues (Tako et al.,

1987). The models obtained for the ι-C hydrogels with the addition of KCl and $CaCl_2$ were described by the following equations:

$$HS_{KCl} = -0.22 + 0.34 \cdot \mathrm{C} + 0.07 \cdot \mathrm{S} - 0.07 \cdot C^2 - 0.03 \cdot S^2 + 0.04 \cdot CS \quad (8)$$

$$HS_{CaCl2} = 0.29 - 0.18 \cdot \mathrm{C} - 0.05 \cdot \mathrm{S} + 0.10 \cdot C^2 - 0.03 \cdot S^2 + 0.06 \cdot CS \quad (9)$$

The formulations providing the maximum strength values were predicted as 2.0% ι-C + 2.0% KCl and 2.0% ι-C + 1.0% $CaCl_2$. As shown in Table 2, the corresponding hydrogel strength values (~0.3 N and ~0.4 N for KCl and $CaCl_2$, respectively) were again very close to the theoretical values predicted by the model equations.

The two λ-C grades presented a slightly different behaviour. In particular, $\lambda_{\downarrow}$-C required higher carrageenan and salt concentrations to form hydrogels than $\lambda_{\uparrow}$-C, which is reasonable considering the lower molecular weight of the former. Although the strength values were in general greater for the $\lambda_{\uparrow}$-C hydrogels, the differences were not remarkable as compared with the $\lambda_{\downarrow}$-C hydrogels. The statistical analysis evidenced that all the factors except the linear term of KCl concentration presented a significant effect on the strength of $\lambda_{\downarrow}$-C hydrogels. On the other hand, in the case of the $\lambda_{\uparrow}$-C hydrogels, all the factors presented a significant effect in the response. Figures 3F and 3G show that the highest values of strength for the $\lambda_{\downarrow}$-C hydrogels were obtained increasing the carrageenan concentration and at an intermediate level of KCl concentration, whereas in the case of $CaCl_2$ the highest strength values were obtained by increasing the salt concentration. For the λ↑-C, the strongest hydrogels could be obtained by increasing the concentration of carrageenan and salts (Figures. 3H and 3I). Interestingly, KCl yielded stronger hydrogels than $CaCl_2$ for both λ↑-C and $\lambda_{\downarrow}$-C. Gelation of λ-C using mono- or divalent salts has not been reported to date and only the addition of a trivalent salt ($FeCl_3$) has been described to produce the gelation of λ-C (Running et al., 2012). It was suggested that this type of salt was able to equilibrate the negative charges of sulphate groups in λ-C (three sulphate groups per disaccharide repeating unit), promoting the interaction between the chains and forming a strong gel. The fact that the λ-C grades used in this work were able to form hydrogels confirms that these were actually mixtures of the λ-carrageenan form with other types of carrageenan naturally occurring in the seaweed used for the extraction, such as κ-, μ-

and θ-carrageenans, as previously suggested by the FT-IR and ^{1}H-NMR results. In particular, the presence of gelling κ-carrageenan may have contributed to the capacity of the λ-C grades to form gels. The models that describe the relationship between the hydrogel strength and the factors for $\lambda_{\downarrow}$-C (Eq. 9 and 10) and $\lambda_{\uparrow}$-C (Eq. 11 and 12) were the following:

$$HS_{KCl} = -2.9 + 2.01 \cdot \mathrm{C} + 2.37 \cdot \mathrm{S} - 0.38 \cdot C^2 - 0.67 \cdot S^2 + 0.17 \cdot CS \quad (10)$$

$$HS_{CaCl2} = 1.6 - 1.3 \cdot \mathrm{C} + 0.05 \cdot \mathrm{S} + 0.26 \cdot C^2 - 0.06 \cdot S^2 + 0.07 \cdot CS \quad (11)$$

$$HS_{KCl} = -0.10 + 0.35 \cdot \mathrm{C} + 0.12 \cdot \mathrm{S} - 0.27 \cdot C^2 - 0.72 \cdot S^2 + 1.12 \cdot CS \quad (12)$$

$$HS_{CaCl2} = -0.23 + 0.04 \cdot \mathrm{C} + 0.38 \cdot \mathrm{S} + 0.09 \cdot C^2 - 0.09 \cdot S^2 - 0.12 \cdot CS \quad (13)$$

The formulations that would theoretically produce the highest hydrogel strength values for λ↓-C would be 2.2% λ↓-C + 1.5% KCl (1.1 N) and 3.0% λ↓-C + 2.3% $CaCl_2$ (0.5 N). On the other hand, the optimal formulations in terms of hydrogel strength for $\lambda_{\uparrow}$-C would correspond to 2.0% $\lambda_{\uparrow}$-C + 1.6% KCl (1.4 N) and 2.0% $\lambda_{\uparrow}$-C + 1.1% $CaCl_2$ (0.4 N). In all the cases there was a very good agreement between the model-predicted and the experimental strength values.

Table 2. Model-predicted and experimental strength values for the optimum hydrogel formulations, being C (%) the carrageenan concentration, S (%) the salt concentration and HS (N) the theoretical hydrogel strength. Data shown as mean +/-SD, n=3.

Sample	Salt	C (%)	S (%)	HS (N)	Experimental strength (N)
κ-C	KCl	2.0	2.0	28.6	27.5 ± 1.3
	$CaCl_2$	2.0	1.2	20.1	19.9 ± 0.4
ι-C	KCl	2.0	2.0	0.31	0.34 ± 0.01
	$CaCl_2$	2.0	1.0	0.36	0.35 ± 0.01
λ↓-C	KCl	2.2	1.5	1.07	1.1 ± 0.04
	$CaCl_2$	3.0	2.3	0.47	0.46 ± 0.04
λ↑-C	KCl	2.0	1.6	1.45	1.4 ± 0.1
	$CaCl_2$	2.0	1.1	0.34	0.37 ± 0.02

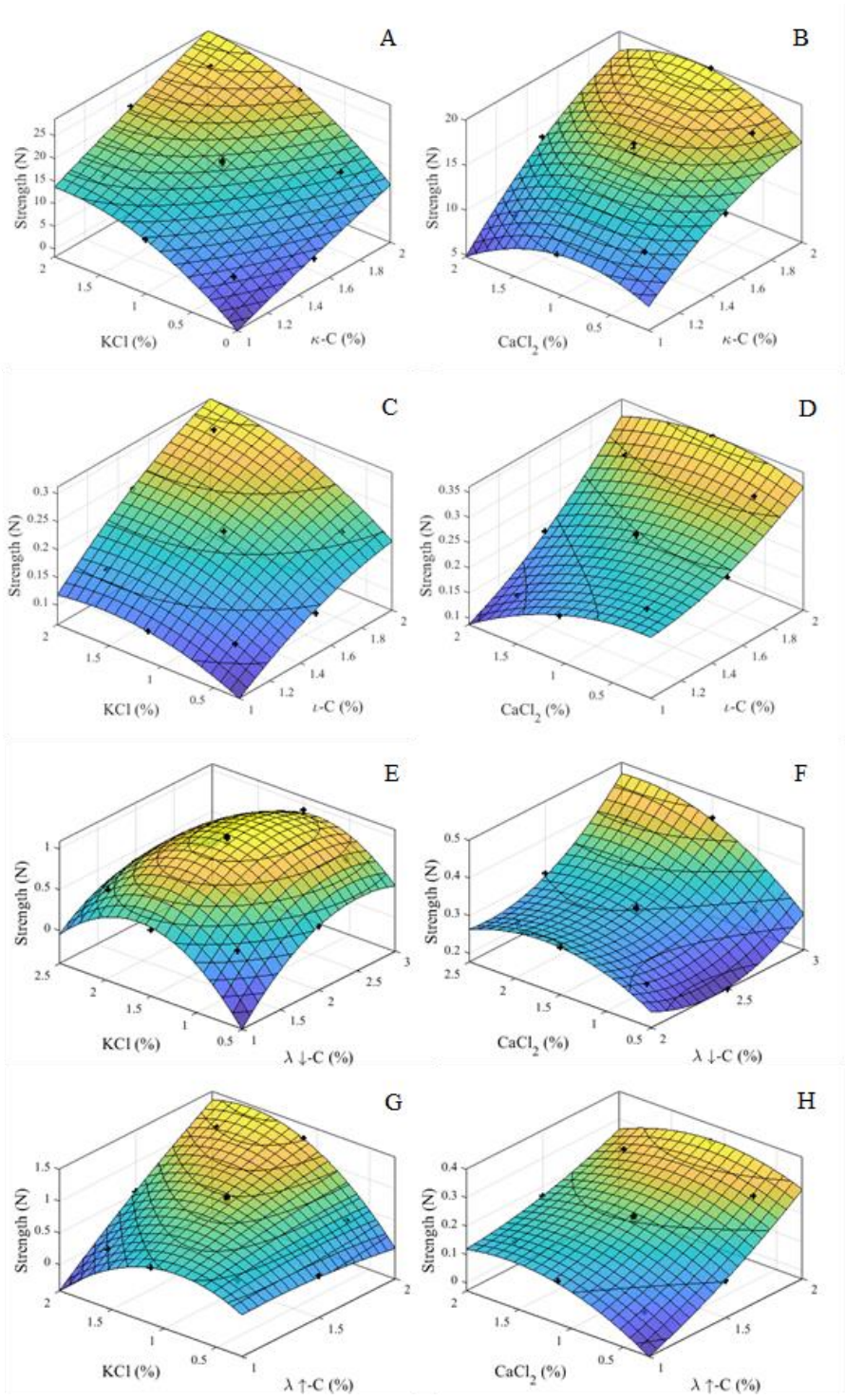

Figure 3. Response surface plots of the hydrogel strength for the different combinations of commercial carrageenans and salts.

4.3 Rheological characterization of selected hydrogels

The effect of the presence of cations and the valency of these in the rheological behaviour of the different carrageenan grades studied were investigated by performing oscillatory rheological measurements on selected hydrogel formulations (using the same carrageenan and salt concentrations for all of them). The elastic modulus (G') and storage modulus (G'') were measured as a function of temperature, at a fixed frequency (1 Hz) and 1 % strain. The gelling temperatures (T_{gel}), which were determined as the cross-over point between G' and G'', as well as G', G'' and tan δ values of the hydrogels at 20 ºC were determined and the results are compiled in Table 3. It should be mentioned that, as opposed to other gelling polysaccharides such as agar (Alehosseini et al., 2018) and agarose (Mohammed et al., 1998), the crossover point between G' and G'' was clearly observed in all the samples, showing all of them a behaviour characteristic of solutions at high temperatures. As a general observation, the addition of salts increased the gelation temperature in the four carrageenan grades, suggesting that the presence of cations facilitated the association of carrageenan molecular chains to originate the network structures responsible for hydrogel formation. Although most of the hydrogels were not fully cured at 20 ºC, in general, the incorporation of salts produced hydrogels with higher strength (as suggested by the higher G' values) and increased their elastic character (as indicated by the lower tan δ values).

Figure 4A shows the temperature sweep plots from the κ-C samples. As observed, the formulations showed a notably different behaviour depending on the nature of the cations added. In particular, the formulation containing KCl was seen to form a hydrogel at much higher temperatures (T_{gel}=79 °C) than the formulation containing $CaCl_2$ (T_{gel}=52 °C) and the plain carrageenan (T_{gel}=44 °C). This is consistent with the hypothesis of K^+ being able to promote the association of κ-carrageenan chains by neutralizing the negative charges from sulphate groups, thus facilitating the sol-gel transition. Wang et al. (Wang et al., 2018) reported the same behaviour, suggesting that K^+ decreases the amount of negative charges in κ-carrageenan, facilitating intermolecular association of carrageenan double helices by hydrogen bonding; on the other hand, divalent cations form ionic cross-links between the sulphate groups of κ-carrageenan. As observed, the plain κ-C and especially the formulation containing KCl showed

a bump in G' after the sol-gel transition, i.e. G' showed a sharp decrease after reaching a maximum value. This phenomenon has been previously reported to take place in κ-carrageenan systems (Ako, 2015; Lai et al., 2000). Despite some works have attributed this bump to syneresis effects, a more in-depth study reported the appearance of this feature as a result of a transient state formed during the gelation process. This structure is reported to consist of a fine network where the junction zones may be double helices. Since it is an unstable structure, when the temperature is further decreased an aggregation process is initiated, forming more tightly packed structures (A.-M. Hermansson, 1989). Although the hydrogels were not fully cured at 20 ºC, the G' and G'' values for the κ-C hydrogels at that temperature were in general much higher than those of the other carrageenan grades, indicating that stronger networks (i.e. stronger interactions between carrageenan chains) were formed in the case of κ-C.

Table 3. Rheological properties of carrageenan hydrogels. Gelation temperature (T_{gel}), elastic modulus ($G'_{20°C}$), viscous modulus ($G''_{20°C}$) and tan δ at 20°C.

Samples	T_{gel} (°C)	G' (Pa)	G'' (Pa)	Tan δ
2.0%κ-C	44	3273	640	0.20
2.0%κ-C+1.5%KCl	79	11364	6950	0.60
2.0%κ-C+1.5%$CaCl_2$	52	134000	2300	0.02
2.0%ι-C	41	300	30	0.10
2.0%ι+1.5%KCl	74	500	20	0.04
2.0%ι+1.5%$CaCl_2$	87	310	10	0.04
2.0%λ↓-C	26	40	30	0.90
2.0%λ↓+1.5%KCl	78	3600	300	0.08
2.0%λ↓+1.5% $CaCl_2$	64	170	40	0.20
2.0%λ↑-C	66	80	50	0.60
2.0%λ↑+1.5%KCl	80	2600	170	0.07
2.0%λ↑+1.5% $CaCl_2$	82	600	100	0.20

As observed in Figure 4B, the ι-C formulations presented a very different behaviour to that of κ-C. The absolute values of the moduli were lower in comparison to those of κ-C after the sol-gel transition. Contrarily to κ-C, the sol-gel transition in ι-C was more strongly promoted by the addition of the divalent salt. Whereas the plain ι-C showed a gelation temperature of ca. 41°C, higher gelation temperatures of 74°C and 87°C were observed with the addition of KCl and $CaCl_2$, respectively. Interestingly, and in agreement with the hydrogel strength values compiled in Table 2, there were no great differences between the G' values of the hydrogels at 20 °C, suggesting that, even though the presence of Ca^{2+} facilitated the association of carrageenan double helices upon cooling to a greater extent than K^+, similar supramolecular structures may have been formed with both cations, which is also confirmed by the same tan δ values for both salts. This is in agreement with previous studies which showed the low cation selectivity of ι-carrageenan in terms of rheological properties (Funami et al., 2007).

With regards to the λ-C samples, Figure 4C shows the results for λ↓-C, whereas the data from λ↑-C are shown in Figure 4D. As deduced from the results listed in Table 3, the hydrogel structure formed at 20 ºC (not fully cured) showed a greater strength for λ↑-C (G'_{20}= 80 Pa) than λ↓-C (G'_{20}=40 Pa), which may be attributed to the higher molecular weight of the former. The addition of salts had a strong impact in the gelation behaviour of λ↓-C, increasing the gelation temperature from 26ºC to 78°C and 64°C with the addition of KCl and $CaCl_2$, respectively. Furthermore, stronger hydrogel networks (not fully cured) were obtained at 20ºC with salt addition, especially with KCl, as indicated by the higher G' values. The addition of salts also had a strong impact on the gelation temperature of λ↑-C, (although to a lower extent than in the case of λ↓-C), which increased from 66ºC to 80ºC and 82ºC with the addition of KCl and $CaCl_2$, respectively. On the other hand, although the systems were still not completely settled at 20ºC, the type of salt strongly affected the rheological properties of the hydrogels, as deduced from the G’ and tan δ values. In agreement with the measured hydrogels strength values (cf. Table 2), KCl was able to promote the formation of stronger λ↑-C hydrogels with higher degree of elastic contribution than $CaCl_2$. These results would suggest that the presence of monovalent cations is more favourable to generate load-bearing cross-links between the carrageenan chains in both λ-C grades.

Since the λ-C grades used in this work were actually mixtures of λ-, κ-, μ- and θ-carrageenans, explaining their gelation behaviour is not straightforward. In principle, one may think that for the same concentration of added salt, Ca^{2+} should be able to neutralize the negative charges from sulphate groups more efficiently than K^{+}. However, it seems that the nature of the intermolecular interactions established was distinct depending on the added salt, with K^{+} promoting stronger interactions than Ca^{2+}. This might be also related to the fact that κ-carrageenan was one of the major components in both λ-C grades and therefore, their gelling behaviour showed some similarities with that from the κ-C grade.

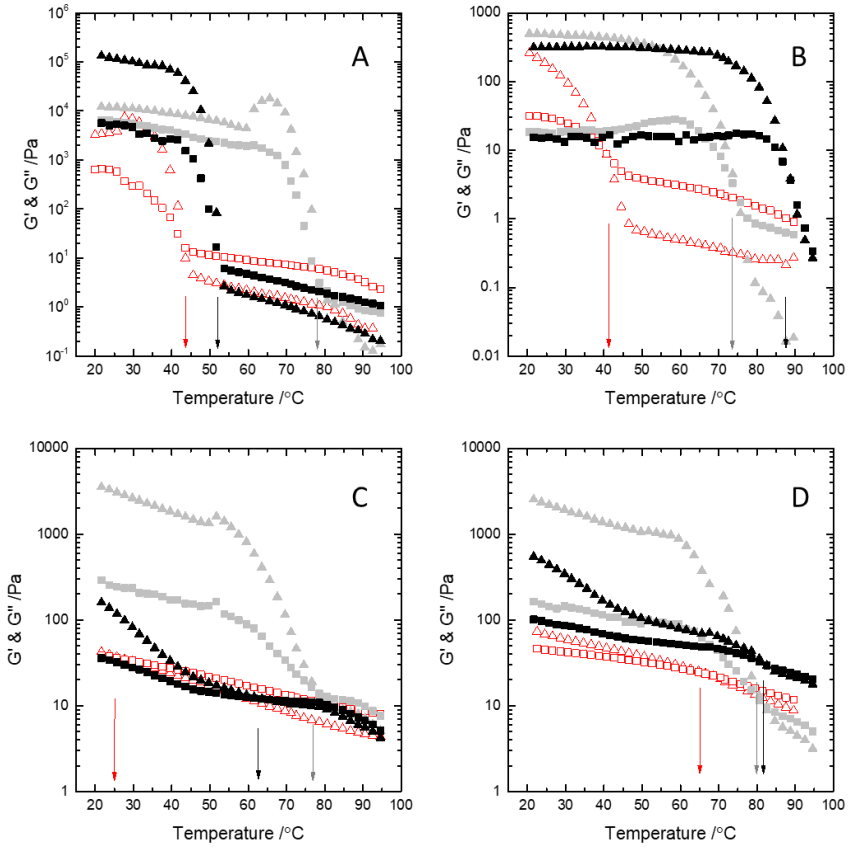

Figure 4. Temperature dependence of G' (triangles) and G'' (squares) moduli of carrageenan solutions upon cooling. (A) κ-C, (B) ι-C, (C) λ↓-C and (D) λ↑-C. 2% carrageenan (red markers), 2% carrageenan + 1.5% KCl (grey markers), 2% carrageenan + 1.5% $CaCl_2$ (black markers).

4.4 Nanostructural characterization of selected hydrogels

To investigate the structural differences between the various hydrogels at the nanoscale level, SAXS experiments were carried out on selected formulations. In particular, hydrogels with 2% of carrageenan and 1.5% of salt were chosen since these concentrations seemed to provide hydrogel strength values relatively close to the optimum for all the carrageenan and salt combinations. Figure 5 shows the scattering patterns for the different hydrogels, which as observed, presented marked differences depending on the type of carrageenan used. Consequently, different models had to be used to fit the experimental data and extract structural information from the scattering results. The SAXS patterns from the κ-C hydrogels could be properly described by means of a Gauss-Lorentz gel model, which to date has been the only model proposed in the literature to fit the small angle scattering data from carrageenan hydrogels over a relatively broad q range (Evmenenko et al., 2001). The obtained fitting parameters are summarized in Table 4a. The Gaussian parameter (Ξ) is the characteristic mean size of the static heterogeneities and can be affected by the introduction of cross-links into the system, whereas the Lorentzian parameter (ξ) is the correlation length for the polymer chains and is related to the interactions between the fluctuating chains of polymer. While values of Ξ ~ 8-10 nm and ξ ~ 3-4 nm have been previously reported for pure 1% κ-carrageenan hydrogels (Evmenenko et al., 2001), the addition of salts had a strong effect and both parameters presented significantly larger values. Although κ-carrageenan chains are able to associate into double helices to form gel-like structures, the addition of salts is known to promote aggregation of carrageenan helices through neutralization of the electrostatic repulsions originated by the presence of sulphate groups (Morris et al., 1980). Thus, the increased values for the structural parameters seem to be indicative of a greater degree of cross-linking taking place in the hydrogels produced in the presence of salts. The correlation length values, which are in agreement with the value of 8.5 nm previously reported for κ-carrageenan hydrogels with KCl (Abad et al., 2006), can be associated to the size of the carrageenan double helices. Similarly to carrageenan, agarose is known to associate into double helices, whose cross-section size has been reported to be within the range of 5-10 nm (Fatin-Rouge et al., 2006), which then further aggregate into bundles, responsible for the formation of strong hydrogels. As observed in Table

4a, the hydrogel prepared in the presence of KCl seemed to present a more compact structure than the hydrogel with $CaCl_2$, as suggested by the smaller values of Ξ and ξ. It should be noted that the hydrogel prepared in the presence of KCl showed two small peaks located at 0.021 $Å^{-1}$ and 0.050 $Å^{-1}$, indicative of the existence of well-ordered structures with real distances of ca. 29 nm and 12 nm. As observed, these values are similar to the structural parameters Ξ and ξ, which may indicate that the association of carrageenan chains into double helices and bundles led to the formation of well-ordered structures arranged with a certain periodicity. This suggests that K^+ is able to promote the formation of more ordered and densely packed κ-C hydrogel networks, which may be the consequence of stronger intermolecular interactions being developed. This denser network could explain the higher strength observed for the κ-C hydrogels obtained with the K^+ as compared with Ca^{2+} (cf. Table S7 for the measured hydrogel strength values).

Although the *Gauss-Lorentz* model provided satisfactory fits for the ι-C hydrogels within the low q range, the data within the region q>0.01 $Å^{-1}$ was not properly described by the model. This confirms that a different type of network structure was originated in the κ-C and ι-C hydrogels. As an alternative, a two-level unified model was suitable to fit the data through the whole q range (cf. Figure 5). In the particular case of the ι-C hydrogel with KCl, an additional term was added to the fitting function to account for an additional shoulder-like feature centred at ca. 0.007 $Å^{-1}$. As deduced from the fitting results (cf. Table 4b), the radius of gyration corresponding to the high q range (Rg_2) could be assigned to the size of the carrageenan double helices, while the radius of gyration calculated from the data within the low q range (Rg_1) could be ascribed to the aggregates of these double helices, giving rise to the gel network structure. Although the gelation of ι-carrageenan has been proposed to take place exclusively as a result of double helix formation (Yuguchi et al., 2002), the addition of salts has been shown to induce further helix aggregation through the establishment of ionic interactions (Grinberg et al., 2001). From the scattering results it is clear that both salts induced the association of carrageenan double helices to form larger structures. The size of the ι-C double helices in the presence of both salts was within the range of values determined for the κ-C hydrogels. On the other hand, larger aggregates were formed as compared to κ-C, as suggested by the Rg_1 values. Comparing the

two different salts, it seems that more densely packed network structures were attained with the addition of $CaCl_2$, which could be related to the greater capacity of Ca^{2+} to neutralize the repulsive forces provided by the sulphate groups in ι-carrageenan. The real distance corresponding to the shoulder-like feature observed in the ι-C hydrogel with KCl (ca. 85 nm), has not been previously attributed to any particular structural feature in ι-C, but it might be associated to the formation of ordered domains in the longitudinal axis of the carrageenan bundles. The differences encountered between the κ-C and ι-C hydrogels are related to the different specific role of the cations on the gelation mechanism of the κ- and ι-carrageenans present in these commercial grades (Thrimawithana et al., 2010). It has been proposed that K^+ forms an ionic bond with the sulphate group of the galactose residues, inducing intermolecular association of κ-carrageenan, subsequently forming an electrostatic bond with the anhydro-bridge oxygen atom of the adjacent galactose residue upon cooling and, at the same time, favouring the association of carrageenan double helices by strong hydrogen bonds. On the other hand, due to its divalent character, Ca^{2+} can form intra-molecular bridges between the sulphate groups of adjacent anhydrogalactose and D-galactose residues of ι-carrageenan. Upon cooling, further aggregation occurs due to intermolecular Ca^{2+} bridging. According to this, and considering the SAXS results, it may be reasonable to hypothesise that in the presence of salts, κ-carrageenan and ι-carrageenan can form similar structures of double helices and bundles, although the nature of the bridges holding together the bundles is different depending on the type of carrageenan and valency of the salt added. K^+ binds more efficiently to κ-carrageenan chains and is able to form strong interactions (most likely hydrogen bonds) between helices to form the bundles. On the other hand, Ca^{2+} is more efficient in creating intermolecular bonds between ι-carrageenan chains and induces the formation of larger aggregates, but weaker ionic cross-links are originated in this case.

The application of the Gauss-Lorentz gel or the unified models for the λ-C hydrogels gave rise to large uncertainties in the errors associated to the obtained fitting parameters. This is not unexpected given the absence of marked scattering features in the data from these heterogeneous samples. Instead, a simpler correlation length model, which has been previously applied to describe the scattering data from different gelling systems such as physically and

chemically cross-linked gelatin networks (Yang et al., 2015), was applied to fit the data (except for the λ↓-C hydrogel with the addition of $CaCl_2$, where the fitting parameters still presented very large uncertainty values) and the obtained parameters are listed in Table 4c. The obtained power-law exponents (n) were indicative of mass fractal structures, i.e. branched network structures which, in the particular case of 2% λ↓-C + 1.5% KCl, were characteristic of randomly branched Gaussian chains. The greater exponents obtained for the high molecular weight λ-C hydrogels suggested the presence of more branched structures, which may be a direct consequence of their higher molecular weight. The Lorentz exponent (m) may be related to the local chain conformation and lower values are typically attained for more expanded polymer chains. Very similar values close to 2, which are indicative of randomly branched Gaussian polymer chains, were obtained for the different λ-C hydrogels. All these results point out towards the fact that λ-C gelation took place by means of a very distinct mechanism to that of κ-C and ι-C, forming less ordered structures. This is reasonable considering the fact that both λ-C grades were actually a mixture of different carrageenan types. The heterogeneity in the molecular structures composing these materials would then lead to the appearance of less defined scattering features.

Table 4. Parameters obtained from the fits the κ-C (a), ι-C (b) and the λ-C (c) hydrogels. Standard deviations (i.e., errors associated to the fitting results) on the last digit are shown in parentheses.

(a)

	2% κ-C + 1.5% KCl	2% κ-C + 1.5% $CaCl_2$
I_G	1236 (33)	3091 (168)
Ξ (nm)	25.1 (4)	41 (1)
IL	1314 (33)	4888 (110)
ξ (nm)	9.5 (1)	17.7 (2)

(b)

	2% ι-C + 1.5% KCl	2% ι-C + 1.5% $CaCl_2$
G_1	11068 (200)	2461 (86)
Rg1 (nm)	61.8 (3)	47.6 (9)
B1	---	3.6·10-3 (1)
P1	---	3.14 (8)
G2	132 (13)	57 (4)
Rg2 (nm)	14.4 (9)	7.3 (5)
B2	0.4 (1)	0.34 (3)
P2	1.09 (8)	1.22 (4)
I0 (cm-1)	68 (6)	---
d (nm)	84.9	---

(c)

	2% λ↑-C + 1.5% KCl	2% λ↑-C + 1.5% $CaCl_2$	2% λ↓-C + 1.5% KCl	2% λ↓-C + 1.5% $CaCl_2$
A	$1.4\cdot10^{-3}$ (1)	$2.7\cdot10^{-4}$ (6)	$4.8\cdot10^{-3}$ (1)	---
n	2.75 (1)	3.10 (4)	2.25 (3)	---
C	77 (6)	350 (61)	44 (6)	---
m	2.2 (1)	2.09 (8)	2.10 (1)	
ξL (nm)	4.0 (4)	10 (2)	3.5 (3)	---

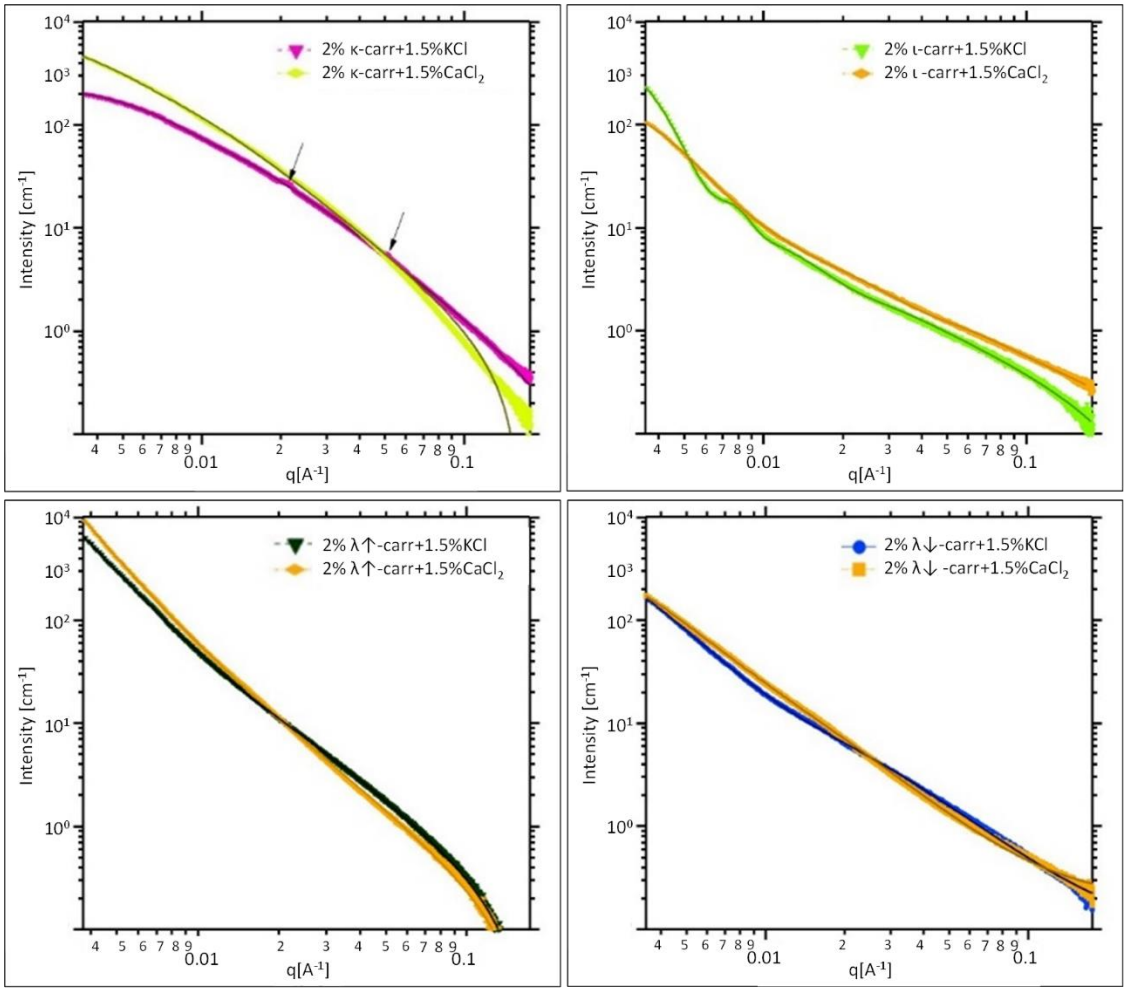

Figure 5. SAXS patterns from the different carrageenan hydrogels. Markers represent the experimental data and solid lines show the fits obtained using theoretical models**.**

Based on the characterization of the carrageenan hydrogels used in this study and according to models described in the literature for the gelation of pure carrageenans, a hypothesis for the distinct gelation mechanism of the studied commercial carrageenan grades has been developed (see Figure 6 for a graphical representation of the proposed gelation mechanisms). The κ-carrageenan found in the κ-C grade contains one sulphate group per disaccharide repeating unit, located at the C4 from the 3–linked galactose unit. The amount of sulphate groups in this type of carrageenan is low enough not to impede the association of carrageenan double helices by hydrogen bonding to form bundles, thus generating hydrogel structures. The addition of K^+

promotes a further aggregation of double helices by neutralizing the negative charges of the sulphate groups. In contrast, Ca^{2+} seems to induce weaker ionic cross-links between the sulphate groups from adjacent κ-carrageenan double helices, hence generating softer hydrogels. On the other hand, the ι-carrageenan present in the ι-C commercial grade possesses two sulphate groups per disaccharide repeating unit (one located at the C4 from the 3–linked galactose unit and another at the C-2 from the 4-linked, 3-6 anhydrogalactose). Therefore, although the ι-carrageenan chains are able to associate to a certain extent to form weak hydrogels without salt addition, less elastic and stable networks are formed (as seen from the tan δ values in Table 3) and lower temperatures are required for hydrogel formation. As opposed to κ-C, the addition of salts in the case of ι-C did not seem to mediate hydrogel formation via hydrogen bonding of carrageenan double helices, but it rather promoted gelation through ionic cross-linking and as a result, much softer hydrogels were formed. The Ca^{2+} ions are thought to form ionic cross-links between the sulphate groups of adjacent anhydrogalactose and galactose residues, whereas the K^+ ions are believed to form an ionic bond with the sulphate group from galactose residues. Subsequently, intermolecular association may take place through electrostatic forces of attraction between the sulphate groups and the cations from adjacent carrageenan double helices. Thus, Ca^{2+} ions are more efficient in promoting ι-C gelation (lower concentrations are required to neutralize the same amount of sulphate groups) but a very similar network of ionic-bonded carrageenan double helices is formed with Ca^{2+} and K^+ (producing soft hydrogels with similar strength values). In the case of the λ-C grades, the results indicated that they were composed of a mixture of the λ-, κ-, θ- and μ-C forms, thus forming very heterogeneous network structures. Due to the greater amount of sulphate groups in the λ-, θ- and μ-carrageenan grades (two or three per disaccharide unit), the association of carrageenan chains via hydrogen bonding is hindered and the addition of salts is necessary to form strong hydrogels. According to our results, the presence of K^+ is more favourable to generate stronger cross-links between the carrageenan chains in the λ-C grades (as suggested by the greater hydrogel strength values), suggesting that the gelation mechanism was mostly governed by the κ-carrageenan component in these commercial grades.

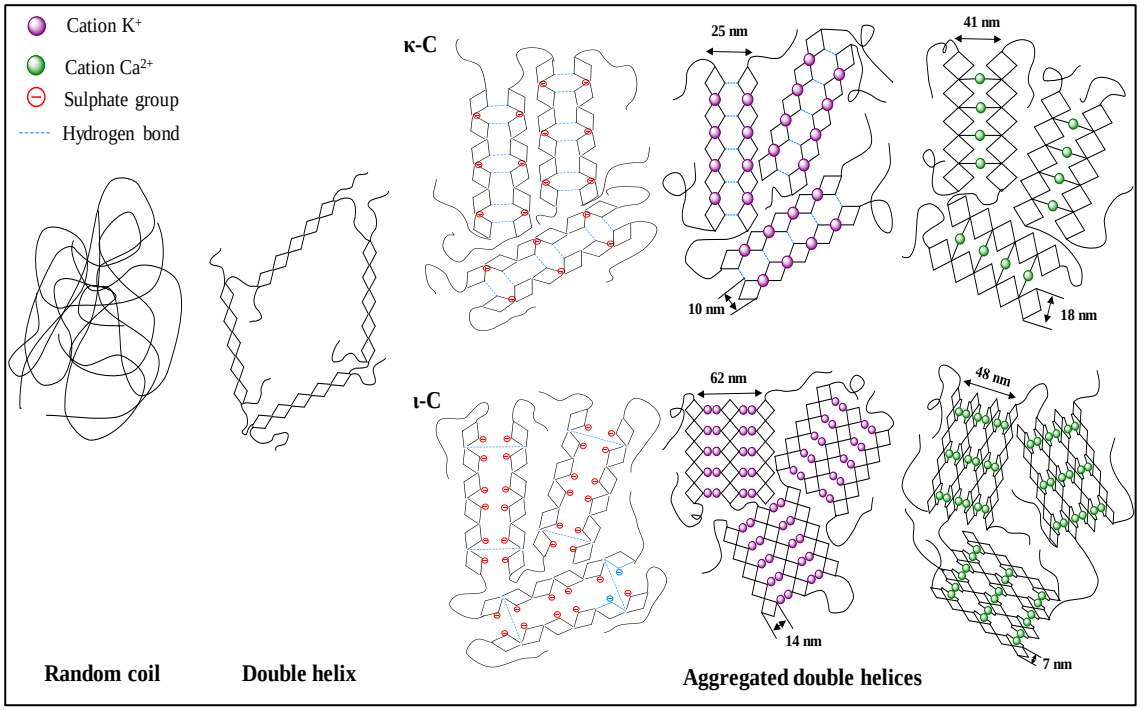

Figure 6. Proposed gelation mechanism for the κ-C and ι-C commercial grades and the effect of added salts.

5 Conclusions

Four different commercial carrageenan grades (κ-C, ι-C, λ↓-C and λ↑-C) have been used to produce hydrogels with and without the addition of salts (KCl and $CaCl_2$). The effect of carrageenan and salt concentration on the hydrogel strength were evaluated through a response surface design and the rheological behaviour and nanostructure of selected hydrogels were characterized. The results evidenced that the composition, which conditioned the amount and location of sulphate groups in the different carrageenan grades studied, had a strong impact on their gelation mechanism and on the properties of the formed hydrogels.

The lower amount of sulphate substitution in κ-carrageenan (the major component in κ-C) enabled strong association of double helices, leading to the formation of stronger hydrogel networks than the other types of carrageenan, and could be properly modelled as Gauss-Lorentz gels. The addition of K^+ resulted in the neutralization of the negative charges from sulphate groups and, thus, promoted further aggregation of the κ-carrageenan double helices

into more ordered and densely packed networks, hence increasing the hydrogel strength. In contrast, the presence of Ca^{2+} induced the formation of weaker ionic cross-links between the sulphate groups from adjacent κ-carrageenan double helices. The greater amount of sulphate groups in ι-carrageenan (the major component in ι-C) and in the mixture of carrageenans composing the λ-C grades hindered the proper association of double helices due to repulsive forces, hence making necessary the addition of salts to form hydrogels with sufficient mechanical integrity. The presence of cations produced the gelation of ι-C by the establishment of ionic cross-links between the carrageenan double helices, leading to much softer hydrogels than those from κ-C. Due to the greater ability of Ca^{2+} to form ionic cross-links with sulphate groups, these were more efficient in promoting ι-C gelation (i.e. lower concentrations were required and gelation temperatures were higher) than K^+, although similar network structures (consisting of larger but weaker aggregates than those formed in the case of κ-C) were formed in both cases, producing hydrogels with similar strength values. On the other hand, the heterogeneous composition of λ-C, which was seen to consist of a mixture of λ-, κ-, θ- and μ-carrageenans, resulted in the formation of hydrogels with irregular branched networks. In presence of K^+, stronger intermolecular cross-links were attained, as suggested by the greater hydrogel strength values. On the other hand, although lower carrageenan and salt concentrations were required to form hydrogels from λ↑-C as compared with λ↓-C, the molecular weight did not have a dramatic impact on the hydrogel strength.

These results evidence that the combination of spectroscopy, rheology and small angle scattering techniques is an efficient approach to characterize the composition and structure of commercial carrageenan grades. Understanding the distinct gelation mechanism of carrageenan hydrogels and their implications in the nanostructure of the formed hydrogels will open up the possibility of designing hydrogels with specific properties for targeted applications within the food industry and any other relevant fields.

6 Acknowledgements

Synchrotron experiments were performed at NCD beamline at ALBA Synchrotron with the collaboration of ALBA staff (2018022638 project). This work was financially supported by the grant RTI2018-094268-B-C22 (MCIU/AEI/FEDER, UE). Part of this work was supported by the

COST Action ES1408 European network for algal-bioproducts (EUALGAE). Cynthia Fontes-Candia is recipient of a pre-doctoral grant from CONACYT (MEX/Ref. 306680).

7 References

Abad, L., Okabe, S., Koizumi, S., & Shibayama, M. (2006). Small-angle neutron scattering study on irradiated kappa carrageenan. *Physica B: Condensed Matter*, *381*(1–2), 103–108.

Ako, K. (2015). Influence of elasticity on the syneresis properties of κ-carrageenan gels. *Carbohydrate Polymers*, *115*, 408–414. https://doi.org/https://doi.org/10.1016/j.carbpol.2014.08.109

Alehosseini, A., del Pulgar, E.-M. G., Gómez-Mascaraque, L. G., Martínez-Sanz, M., Fabra, M. J., Sanz, Y., Sarabi-Jamab, M., Ghorani, B., & Lopez-Rubio, A. (2018). Unpurified Gelidium-extracted carbohydrate-rich fractions improve probiotic protection during storage. *LWT*, *96*, 694–703.

Azevedo, G., Hilliou, L., Bernardo, G., Sousa-Pinto, I., Adams, R. W., Nilsson, M., & Villanueva, R. D. (2013). Tailoring kappa/iota-hybrid carrageenan from Mastocarpus stellatus with desired gel quality through pre-extraction alkali treatment. *Food Hydrocolloids*, *31*(1), 94–102.

Beaucage, G. (1995). Approximations leading to a unified exponential/power-law approach to small-angle scattering. *Journal of Applied Crystallography*, *28*(6), 717–728.

Beaucage, G. (1996). Small-angle scattering from polymeric mass fractals of arbitrary mass-fractal dimension. *Journal of Applied Crystallography*, *29*(2), 134–146.

Campo, V. L., Kawano, D. F., Braz, D., & Carvalho, I. (2009). Carrageenans : Biological properties , chemical modifications and structural analysis – A review. *Carbohydrate Polymers*, *77*(2), 167–180. https://doi.org/10.1016/j.carbpol.2009.01.020

Doyle, J. P., Giannouli, P., Rudolph, B., & Morris, E. R. (2010). Preparation, authentication, rheology and conformation of theta carrageenan. *Carbohydrate Polymers*, *80*(3), 648–654.

Evmenenko, G., Theunissen, E., Mortensen, K., & Reynaers, H. (2001). SANS study of surfactant ordering in κ-carrageenan/cetylpyridinium chloride complexes. *Polymer*, *42*(7), 2907–2913.

Falshaw, R, Bixler, H. J., & Johndro, K. (2001). Structure and performance of commercial kappa-2 carrageenan extracts: I. Structure analysis. *Food Hydrocolloids*, *15*(4–6), 441–452.

Falshaw, Ruth, Furneaux, R. H., & Stevenson, D. E. (2005). Structural analysis of carrageenans from the red alga, Callophyllis hombroniana Mont. Kütz (Kallymeniaceae, Rhodophyta). *Carbohydrate Research*, *340*(6), 1149–1158.

Fan, L., Tong, J., Tang, C., Wu, H., Peng, M., & Yi, J. (2016). Preparation and characterization of carboxymethylated carrageenan modified with collagen peptides. *International Journal of Biological Macromolecules*, *82*, 790–797.

https://doi.org/https://doi.org/10.1016/j.ijbiomac.2015.10.063

Fatin-Rouge, N., Wilkinson, K. J., & Buffle, J. (2006). Combining small angle neutron scattering (SANS) and fluorescence correlation spectroscopy (FCS) measurements to relate diffusion in agarose gels to structure. *The Journal of Physical Chemistry B*, *110*(41), 20133–20142.

Freile-Pelegrín, Y., Robledo, D., & Azamar, J. A. (2006). Carrageenan of Eucheuma isiforme (Solieriaceae, Rhodophyta) from Yucatán, Mexico. I. Effect of extraction conditions. *Botanica Marina*, *49*(1), 65–71.

Funami, T., Hiroe, M., Noda, S., Asai, I., Ikeda, S., & Nishinari, K. (2007). Influence of molecular structure imaged with atomic force microscopy on the rheological behavior of carrageenan aqueous systems in the presence or absence of cations. *Food Hydrocolloids*, *21*(4), 617–629. https://doi.org/https://doi.org/10.1016/j.foodhyd.2006.07.013

Gómez-Ordóñez, E., & Rupérez, P. (2011). FTIR-ATR spectroscopy as a tool for polysaccharide identification in edible brown and red seaweeds. *Food Hydrocolloids*, *25*(6), 1514–1520. https://doi.org/https://doi.org/10.1016/j.foodhyd.2011.02.009

Grinberg, V. Y., Grinberg, N. V, Usov, A. I., Shusharina, N. P., Khokhlov, A. R., & de Kruif, K. G. (2001). Thermodynamics of conformational ordering of ι-carrageenan in KCl solutions using high-sensitivity differential scanning calorimetry. *Biomacromolecules*, *2*(3), 864–873.

Hermansson, A.-M. (1989). Rheological and microstructural evidence for transient states during gelation of kappa-carrageenan in the presence of potassium. *Carbohydrate Polymers*, *10*(3), 163–181.

Hermansson, A., Eriksson, E., & Jordansson, E. (1991). Effects of Potassium , Sodium and Calcium on the Microstructure and Rheologicai Behaviour of Kappa-Carrageenan Gels. *Carbohydrate Polymers*, *16*, 297–320.

Hilliou, L., Larotonda, F., Abreu, P., Abreu, M. H., Sereno, A., & Gonçalves, M. (2012). The impact of seaweed life phase and postharvest storage duration on the chemical and rheological properties of hybrid carrageenans isolated from Portuguese Mastocarpus stellatus. *Carbohydrate Polymers*, *87*, 2655–2663.

Hjerde, T., Smidsrød, O., & Christensen, B. E. (1999). Analysis of the conformational properties of κ-and ι-carrageenan by size-exclusion chromatography combined with low-angle laser light scattering. *Biopolymers: Original Research on Biomolecules*, *49*(1), 71–80.

Imeson, A. P. (2000). Carrageenan. In *Handbook of hydrocolloids* (pp. 87–102). Woodhead Publishing Ltd.

Lai, V. M. F., Wong, P. A. L., & Lii, C. Y. (2000). Effects of Cation Properties on Sol-gel Transition and Gel Properties of κ-carrageenan. *Journal of Food Science*, *65*(8), 1332–1337. https://doi.org/10.1111/j.1365-2621.2000.tb10607.x

Lecacheux, D., Panaras, R., Brigand, G., & Martin, G. (1985). Molecular weight distribution of carrageenans by size exclusion chromatography and low angle laser light scattering.

Carbohydrate Polymers, *5*(6), 423–440.

Liu, J., Zhan, X., Wan, J., Wang, Y., & Wang, C. (2015). Review for carrageenan-based pharmaceutical biomaterials: favourable physical features versus adverse biological effects. *Carbohydrate Polymers*, *121*, 27–36.

Lopez-Sanchez, P., Fredriksson, N., Larsson, A., Altskär, A., & Ström, A. (2018). High sugar content impacts microstructure, mechanics and release of calcium-alginate gels. *Food Hydrocolloids*, *84*, 26–33.

MacArtain, P., Jacquier, J. C., & Dawson, K. A. (2003). Physical characteristics of calcium induced κ- carrageenan networks. *Carbohydrate Polymers*, *53*(4), 395–400. https://doi.org/https://doi.org/10.1016/S0144-8617(03)00120-6

Mangione, M. R., Giacomazza, D., Bulone, D., Martorana, V., & San Biagio, P. L. (2003). Thermoreversible gelation of κ-Carrageenan: relation between conformational transition and aggregation. *Biophysical Chemistry*, *104*(1), 95–105.

Martínez-Sanz, M., Gómez-Mascaraque, L. G., Ballester, A. R., Martínez-Abad, A., Brodkorb, A., & López-Rubio, A. (2019). Production of unpurified agar-based extracts from red seaweed Gelidium sesquipedale by means of simplified extraction protocols. *Algal Research*, *38*, 101420. https://doi.org/10.1016/j.algal.2019.101420

Michel, A. S., Mestdagh, M. M., & Axelos, M. A. V. (1997). Physico-chemical properties of carrageenan gels in presence of various cations. *International Journal of Biological Macromolecules*, *21*(1–2), 195–200.

Mohammed, Z. H., Hember, M. W. N., Richardson, R. K., & Morris, E. R. (1998). Kinetic and equilibrium processes in the formation and melting of agarose gels. *Carbohydrate Polymers*, *36*(1), 15–26.

Morris, E. R., Rees, D. A., & Robinson, G. (1980). Cation-specific aggregation of carrageenan helices: domain model of polymer gel structure. *Journal of Molecular Biology*, *138*(2), 349–362.

Peak, C. W., Wilker, J. J., & Schmidt, G. (2013). A review on tough and sticky hydrogels. *Colloid and Polymer Science*, *291*(9), 2031–2047. https://doi.org/10.1007/s00396-013-3021-y

Pereira, L., Amado, A. M., Critchley, A. T., van de Velde, F., & Ribeiro-Claro, P. J. A. (2009). Identification of selected seaweed polysaccharides (phycocolloids) by vibrational spectroscopy (FTIR-ATR and FT-Raman). *Food Hydrocolloids*, *23*(7), 1903–1909. https://doi.org/10.1016/J.FoodHyd.2008.11.014

Pereira, L., & Van de Velde, F. (2011). Portuguese carrageenophytes: carrageenan composition and geographic distribution of eight species (Gigartinales, Rhodophyta). *Carbohydrate Polymers*, *84*(1), 614–623.

Piculell, L. (1995). Gelling carrageenans. *Food Science and Technology -New York-Marcel-Dekker-*, 205.

Prado-Fernández, J., Rodríguez-Vázquez, J. A., Tojo, E., & Andrade, J. M. (2003). Quantitation of

κ-, ι- and λ-carrageenans by mid-infrared spectroscopy and PLS regression. *Analytica Chimica Acta*, *480*(1), 23–37. https://doi.org/https://doi.org/10.1016/S0003-2670(02)01592-1

Robal, M., Brenner, T., Matsukawa, S., Ogawa, H., Truus, K., Rudolph, B., & Tuvikene, R. (2017). Monocationic salts of carrageenans: Preparation and physico-chemical properties. *Food Hydrocolloids*, *63*, 656–667. https://doi.org/https://doi.org/10.1016/j.foodhyd.2016.09.032

Robinson, G., Morris, E. R., & Rees, D. A. (1980). Role of double helices in carrageenan gelation: the domain model. *Journal of the Chemical Society, Chemical Communications*, *4*, 152–153.

Rochas, C., Rinaudo, M., & Landry, S. (1989). Relation between the molecular structure and mechanical properties of carrageenan gels. *Carbohydrate Polymers*, *10*(2), 115–127.

Rochas, C., Rinaudo, M., & Landry, S. (1990). Role of the molecular weight on the mechanical properties of kappa carrageenan gels. *Carbohydrate Polymers*, *12*(3), 255–266.

Running, C. A., Falshaw, R., & Janaswamy, S. (2012). Trivalent iron induced gelation in lambda-carrageenan. *Carbohydrate Polymers*, *87*(4), 2735–2739. https://doi.org/https://doi.org/10.1016/j.carbpol.2011.11.018

Sekkal, M., & Legrand, P. (1993). A spectroscopic investigation of the carrageenans and agar in the 1500-100 cm− 1 spectral range. *Spectrochimica Acta Part A: Molecular Spectroscopy*, *49*(2), 209–221.

Shewan, H. M., & Stokes, J. R. (2013). Review of techniques to manufacture micro-hydrogel particles for the food industry and their applications. *Journal of Food Engineering*, *119*(4), 781–792. https://doi.org/https://doi.org/10.1016/j.jfoodeng.2013.06.046

Shibayama, M., Tanaka, T., & Han, C. C. (1992). Small angle neutron scattering study on poly (N-isopropyl acrylamide) gels near their volume-phase transition temperature. *The Journal of Chemical Physics*, *97*(9), 6829–6841.

Stanley, N. F. (1990). Carrageenans. In *Food gels* (pp. 79–119). Springer.

Stone, A. K., & Nickerson, M. T. (2012). Formation and functionality of whey protein isolate–(kappa-, iota-, and lambda-type) carrageenan electrostatic complexes. *Food Hydrocolloids*, *27*(2), 271–277.

Stortz, C. A., Bacon, B. E., Cherniak, R., & Cerezo, A. S. (1994). High-field NMR spectroscopy of cystocarpic and tetrasporic carrageenans from Iridaea undulosa. *Carbohydrate Research*, *261*(2), 317–326. https://doi.org/https://doi.org/10.1016/0008-6215(94)84027-X

Ström, A., Boers, H. M., Koppert, R., Melnikov, S. M., Wiseman, S., & Peters, H. P. F. (2009). Physico-chemical properties of hydrocolloids determine their appetite effects. *Gums and Stabilisers for the Food Industry*, *15*, 341.

Tako, M., Nakamura, S., & Kohda, Y. (1987). Indicative evidence for a conformational transition in ι-carrageenan. *Carbohydrate Research*, *161*(2), 247–255.

https://doi.org/https://doi.org/10.1016/S0008-6215(00)90081-8

Thrimawithana, T. R., Young, S., Dunstan, D. E., & Alany, R. G. (2010). Texture and rheological characterization of kappa and iota carrageenan in the presence of counter ions. *Carbohydrate Polymers*, *82*(1), 69–77. https://doi.org/10.1016/j.carbpol.2010.04.024

Van de Velde, F., Pereira, L., & Rollema, H. S. (2004). The revised NMR chemical shift data of carrageenans. *Carbohydrate Research*, *339*(13), 2309–2313. https://doi.org/https://doi.org/10.1016/j.carres.2004.07.015

Wang, Y., Yuan, C., Cui, B., & Liu, Y. (2018). Influence of cations on texture, compressive elastic modulus, sol-gel transition and freeze-thaw properties of kappa-carrageenan gel. *Carbohydrate Polymers*, *202*, 530–535. https://doi.org/https://doi.org/10.1016/j.carbpol.2018.08.146

Webber, V., Carvalho, S. M. de, Ogliari, P. J., Hayashi, L., & Barreto, P. L. M. (2012). Optimization of the extraction of carrageenan from Kappaphycus alvarezii using response surface methodology. *Food Science and Technology*, *32*(4), 812–818.

Yang, Z., Hemar, Y., Hilliou, L., Gilbert, E. P., McGillivray, D. J., Williams, M. A. K., & Chaieb, S. (2015). Nonlinear behavior of gelatin networks reveals a hierarchical structure. *Biomacromolecules*, *17*(2), 590–600.

Yeh, F., Sokolov, E. L., Walter, T., & Chu, B. (1998). Structure studies of poly (diallyldimethylammonium chloride-co-acrylamide) gels/sodium dodecyl sulfate complex. *Langmuir*, *14*(16), 4350–4358.

Yuguchi, Y., Thuy, T. T. T., Urakawa, H., & Kajiwara, K. (2002). Structural characteristics of carrageenan gels: temperature and concentration dependence. *Food Hydrocolloids*, *16*(6), 515–522.

Zia, K. M., Tabasum, S., Nasif, M., Sultan, N., Aslam, N., Noreen, A., & Zuber, M. (2017). A review on synthesis, properties and applications of natural polymer based carrageenan blends and composites. *International Journal of Biological Macromolecules*, *96*, 282–301. https://doi.org/https://doi.org/10.1016/j.ijbiomac.2016.11.095

8 Supplementary Material

Table S1. Cationic composition of the commercial carrageenan grades (% w/w).

Sample	K^+	Na^+	Ca^{2+}	Mg^{2+}
κ-C	7.22 ± 0.12	0.63 ± 0.01	$0.12 \pm 3.0 \cdot 10^{-3}$	$0.01 \pm 6.0 \cdot 10^{-5}$
ι-C	11.0 ± 0.14	0.73 ± 0.01	$0.06 \pm 1.0 \cdot 10^{-3}$	$0.0028 \pm 6.0 \cdot 10^{-5}$
λ↓-C	2.11 ± 0.03	5.64 ± 0.06	$0.25 \pm 2.0 \cdot 10^{-3}$	$0.11 \pm 1.0 \cdot 10^{-3}$
λ↑-C	1.83 ± 0.03	5.20 ± 0.10	$0.46 \pm 5.0 \cdot 10^{-3}$	$0.47 \pm 1.0 \cdot 10^{-3}$

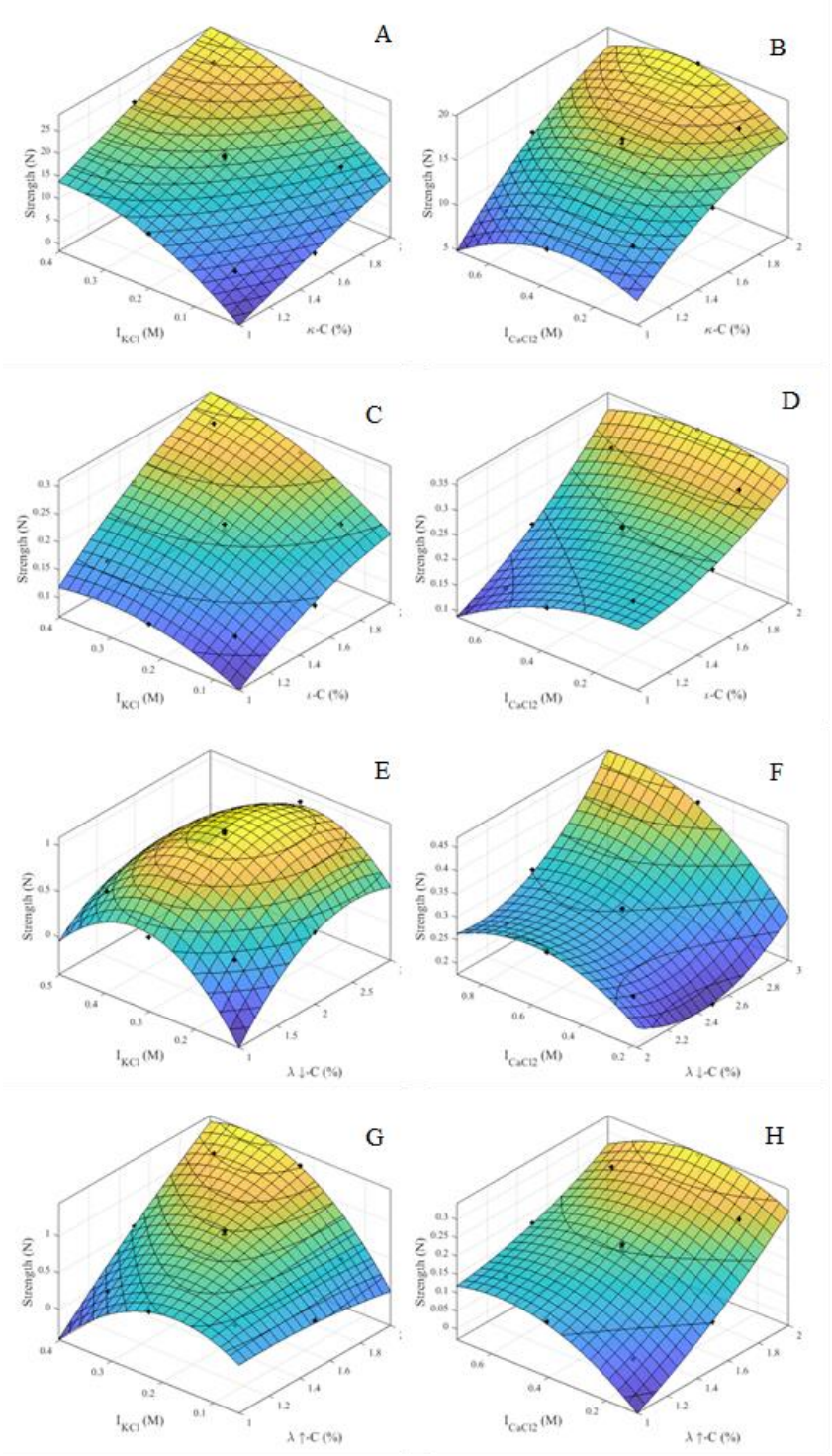

Figure S1. Response surface plots of the hydrogel strength plotted as a function of carrageenan concentration and ionic strength.

Table S2. Experimental hydrogel strength values for the κ-C formulations with the addition of KCl and $CaCl_2$

Run	% κ-C	% KCl	Strength (N)	% κ-C	% $CaCl_2$	Strength (N)
1	1.50	1.00	17.18	1.50	1.05	16.67
2	1.15	0.29	4.85	1.15	1.05	15.64
3	1.00	1.00	10.27	1.00	0.10	13.03
4	1.85	0.29	14.36	1.85	1.05	16.15
5	1.50	1.00	18.00	1.50	1.05	16.14
6	1.50	0.00	4.54	1.50	1.05	16.13
7	1.50	1.00	16.74	1.50	0.38	10.97
8	1.50	1.00	17.66	1.50	0.38	17.32
9	1.15	1.71	15.38	1.15	1.72	9.13
10	1.50	1.00	17.07	1.50	1.72	17.82
11	2.00	1.00	23.74	2.00	2.00	13.30
12	1.85	1.71	26.03	1.85	1.05	9.17
13	1.50	2.00	21.80	1.50	1.05	20.16

Table S3. Experimental hydrogel strength values for the ι-C formulations with the addition of KCl and $CaCl_2$.

Run	% ι-C	% KCl	Strength (N)	% ι-C	% CaCl2	Strength (N)
1	1.50	1.13	0.22	1.50	1.05	0.25
2	1.85	0.51	0.21	1.85	0.38	0.32
3	1.50	2.00	0.23	1.50	2.00	0.18
4	1.50	1.13	0.21	1.50	1.05	0.25
5	1.85	1.74	0.30	1.85	1.72	0.30
6	1.50	1.13	0.21	1.50	0.10	0.24
7	1.50	1.13	0.22	1.50	1.05	0.24
8	1.15	1.74	0.16	1.15	0.38	0.22
9	1.50	1.13	0.22	1.50	1.05	0.24
10	1.50	0.25	0.14	1.50	1.05	0.24
11	1.00	1.13	0.12	1.00	1.05	0.18
12	2.00	1.13	0.27	2.00	1.05	0.36
13	1.15	0.517	0.12	1.15	1.72	0.14

Table S4. Experimental hydrogel strength values (N) for the λ↑-C formulations with the addition of KCl and $CaCl_2$.

Run	% λ↑–C	% KCl	Strength (N)	% λ↑–C	% $CaCl_2$	Strength (N)
1	1.85	1.74	1.262	1.85	1.74	0.269
2	1.50	2.00	0.534	1.50	2.00	0.170
3	1.50	1.13	0.923	1.50	1.13	0.214
4	1.15	1.74	0.211	1.15	1.74	0.138
5	1.50	1.13	0.901	1.50	1.13	0.199
6	1.00	1.13	0.472	1.00	1.13	0.121
7	1.50	1.13	0.974	1.50	1.13	0.196
8	1.50	1.13	0.927	1.50	1.13	0.204
9	1.50	0.25	0.241	1.50	0.25	0.102
10	1.85	0.51	0.521	1.85	0.51	0.268
11	1.15	0.51	0.452	1.15	0.51	0.054
12	2.00	1.13	1.270	2.00	1.13	0.338
13	1.50	1.13	0.929	1.50	1.13	0.211

Table S5. Experimental hydrogel strength values (N) for the λ↓-C formulations with the addition of KCl and $CaCl_2$.

Run	% λ↓–C	% KCl	Strength (N)	% λ↓–C	% $CaCl_2$	Strength (N)
1	2.71	0.79	0.734	2.85	0.79	0.284
2	1.29	0.79	0.297	2.15	0.79	0.237
3	2.00	1.50	1.049	2.50	1.50	0.296
4	1.29	2.21	0.481	2.15	2.21	0.278
5	1.00	1.50	0.404	2.00	1.50	0.303
6	2.00	1.50	1.033	2.50	1.50	0.303
7	2.00	0.50	0.379	2.50	0.50	0.177
8	2.71	2.21	0.562	2.85	2.21	0.402
9	2.00	1.50	0.997	2.50	1.50	0.305
10	3.00	1.50	0.925	3.00	1.50	0.438
11	2.00	1.50	1.063	2.50	1.50	0.298
12	2.00	2.50	0.371	2.50	2.50	0.308
13	2.00	1.50	1.087	2.50	1.50	0.304

Table S6. Statistical parameters associated to the obtained theoretical models for the hydrogel strength obtained from the ANOVA analysis.

Source	κ-C		ι-C		λ↓-C		λ↑-C	
	KCl	$CaCl_2$	KCl	$CaCl_2$	KCl	$CaCl_2$	KCl	$CaCl_2$
Regression	«0.001	«0.001	«0.001	«0.001	«0.001	«0.001	«0.001	«0.001
Lineal	«0.001	«0.001	«0.001	«0.001	«0.001	«0.001	«0.001	«0.001
% C	«0.001	«0.001	«0.001	«0.001	«0.001	«0.001	«0.001	«0.001
% S	«0.001	0.387	«0.001	«0.001	0.993	«0.001	«0.001	«0.001
Square	«0.001	«0.001	«0.001	«0.001	«0.001	«0.001	«0.001	«0.001
%C · %C	0.004	0.001	0.003	0.001	«0.001	«0.001	0.008	0.005
% S · % S	«0.001	«0.001	«0.001	«0.001	«0.001	«0.001	«0.001	«0.001
Interaction	0.004	0.001	0.016	0.001	0.002	0.001	«0.001	«0.001
%C · % S	0.004	0.001	0.016	0.001	«0.001	0.001	0.002	«0.001
Lack of fit	0.813	0.465	0.574	0.275	0.290	0.102	0.595	0.434
R^2 (%)	99.1	99.3	99.1	98.1	99.7	99.3	99.1	99.4

Table S7. Experimental hydrogel strength values (N) for the λ↓-C formulations with the addition of KCl and $CaCl_2$.

Sample	Experimental Strength (N)
2%κ-C+1.5%KCl	26.3 ± 1.1
2%κ-C+1.5%$CaCl_2$	25.5 ± 1.2
2%ι+1.5%KCl	0.31 ± 0.01
2%ι+1.5%$CaCl_2$	0.34 ± 0.06
2%λ↓+1.5%KCl	1.2 ± 0.01
2%λ↓+1.5% $CaCl_2$	0.30 ± 0.02
2%λ↑+1.5%KCl	1.1 ± 0.04
2%λ↑+1.5% $CaCl_2$	0.34 ± 0.01

3.1.2

DEVELOPMENT OF POLYSACCHARIDE-CASEIN GEL-LIKE STRUCTURES RESISTANT TO *IN VITRO* GASTRIC DIGESTION

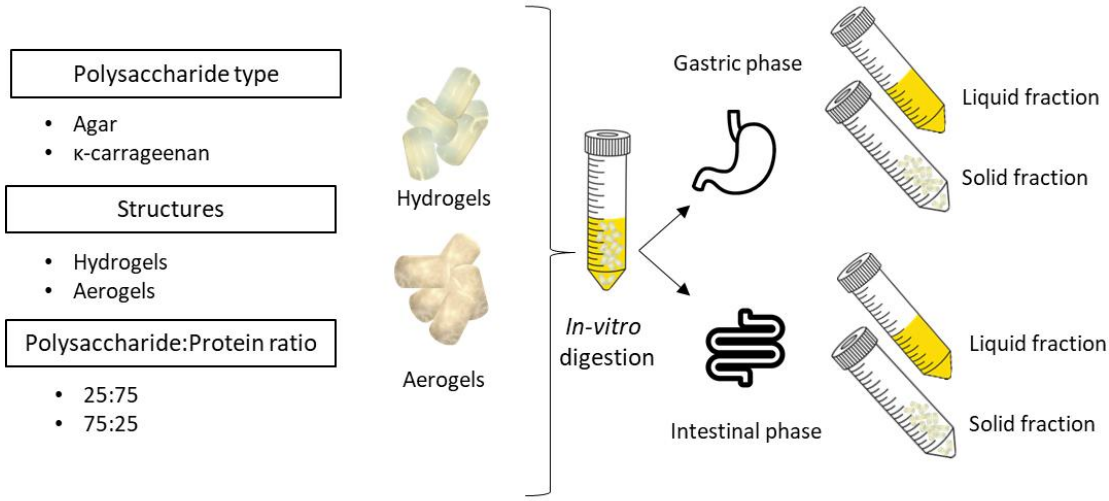

This section is an adapted version of the following submitted research article:

Fontes-Candia, C., Jiménez-Barrios, P., Miralles, B., Recio, I., López-Rubio, A., & Martínez-Sanz, M. (2021). Development of polysaccharide-casein gel-like structures resistant to *in vitro* gastric digestion. Food Hydrocolloids (accepted)

1 Abstract

Controlling protein digestion is a promising strategy to modulate hormonal responses involved in satiety and appetite regulation. In this context, polysaccharide-casein gel-like structures have been developed and subjected to in-vitro gastrointestinal digestions to evaluate their potential for delaying casein hydrolysis. The effect of the polysaccharide type (agar vs. κ-carrageenan), the polysaccharide:casein ratio and the physical state of the structures (hydrogels vs. aerogels) on the protection ability was investigated. The microstructure evolution of the materials upon the digestions was studied and the molecular weight distribution and peptidomic profile of the digestion products were also determined.

During the gastric phase most of the developed structures exerted a protective effect and intact casein clusters were even detected in some of the formulations. In contrast, during the intestinal phase most of the casein was released and hydrolysed to a certain extent. In general, the hydrogels showed a greater protective effect than the aerogels, due to a limited diffusion of the protein towards the liquid medium. Moreover, a higher polysaccharide:protein ratio produced stronger gel networks which provided greater protection. In particular, agar-based and κ-carrageenan hydrogels with 25% polysaccharide and agar-based aerogels with 75% polysaccharide would be the most optimum for delaying casein digestion, since they were able to preserve intact casein after the gastric phase while promoting the release of peptides during the intestinal phase.

2 Introduction

During the gastrointestinal digestion process, food undergoes physical, chemical and biochemical changes that promote the release of nutrients, which will be further used by the organism. Proteins are known to be extensively hydrolysed throughout the digestive tract by the gastrointestinal environment, leading to the release of numerous peptides and free amino acids. In the stomach, proteins are digested by pepsin, while in the small intestine they are hydrolysed by the action of several pancreatic proteases. Amongst milk proteins, globular and compact proteins like β-lactoglobulin are resistant to the action of pepsin, while other proteins with a looser structure like caseins are hydrolysed into smaller polypeptides by the action of this enzyme (Apong, 2019). The micellar structure of casein is readily disassembled upon gastric

digestion, followed by clotting, and producing a complex mixture of peptides and free amino acids (Miralles et al., 2021). Protein digestibility does not only determine the bioavailability of essential units with nutritional value, but may also cause changes along the gastrointestinal tract, such as metabolic and immune responses, epithelial and microbial changes (Dallas et al., 2017). In fact, some peptides generated upon protein digestion are able to interact with different receptors expressed on the surface of enteroendocrine cells in the gut, which in turn, secrete hormones controlling the digestive process and regulating food intake (Caron et al., 2016). In this context, protein digestion could be controlled throughout technological treatments, such as heat treatments or cross-linking, with the aim of causing different metabolic responses. For instance, casein cross-linking has been shown to induce a more sustained release of hormones such as cholecystokinin (CCK) and a stronger feeling of fullness than control casein or whey, suggesting that food structure can modulate postprandial responses (Juvonen et al., 2011). As an alternative, the encapsulation of proteins using gastric resistant matrices is a promising approach to generate protein-rich products with the potential to induce a higher release of anorexigenic hormones or to protect protein compounds to be delivered in distal intestinal regions. Although methods such as atomization (Putney, 1998) and electrohydrodynamic processing (Xiaoqiang Li et al., 2010; Xie & Wang, 2007) have been used for the encapsulation and protection of proteins, these technological processes may require denaturation of the proteins to get them fully solubilized or induce denaturation upon processing and thus, other methods such as gelation may be preferred for food-related applications. In this sense, exploiting the ability of proteins to form complexes with polysaccharides is an efficient strategy to produce hybrid gels that may exert a protective effect on the proteins (Alavi et al., 2018).

Many works have reported the formation of protein-polysaccharide hybrid gel networks where the protein has been denatured to induce its capacity to form gels (de Jong et al., 2009; Xianghong Li et al., 2008; Zhang et al., 2016, 2017), while fewer works have focused on the incorporation of native proteins within the network of a gelling polysaccharide. Alginate and chitosan are the most widely used polysaccharides to encapsulate proteins or peptides through gelation and to delivery systems (Gombotz & Wee, 2012; Ozel et al., 2020; Zhang et al., 2016).

However, chitosan-based hydrogels are pH-dependent and swell at acidic pH, which could lead to the undesired release of protein in the stomach (Yuan et al., 2018). Sulphated polysaccharides such as agar and κ-carrageenan are able to form hydrogels with a varied range of mechanical and structural properties (Fontes-Candia, Ström, Gómez-Mascaraque, et al., 2020; Martínez-Sanz et al., 2020), being an alternative to design encapsulation matrices oriented to protect protein structures during gastrointestinal conditions. Furthermore, these gels can be subjected to drying processes, yielding porous structures known as aerogels (Agostinho et al., 2020; Manzocco et al., 2017), with potential as controlled delivery systems.

In terms of protein digestibility, interactions between proteins and polysaccharides have been studied as the latter are well known to impart different viscoelastic properties which have an impact on the digestion process. Moreover, the physical structure of the materials also will influence the protein digestion. Markussen et al. described the influence of different hydrocolloids such as alginate, pectin and guar gum on the digestibility of milk proteins, concluding that the presence of polysaccharides has a significant impact on gastric emptying and protein digestion kinetics (Markussen et al., 2021). Furthermore, the electrostatic complexation of proteins to polysaccharides may limit their susceptibility to the hydrolytic action of digestive enzymes (Mouécoucou et al., 2004). Recent works have reported on the complexation of soy, pea and whey proteins with k-carrageenan (Ozel et al., 2020), and whey protein isolate with alginate (Zhang et al., 2017), resulting in a higher resistance to gastric conditions in comparison with control proteins, which might be useful to modulate hormonal responses and appetite. Another important aspect to consider is that the incorporation of these protein-polysaccharide complexes into different types of food matrices is expected to have a strong impact on their digestibility and, thus, this should be studied in the future.

Based on this, we aimed to develop hybrid polysaccharide-casein gel-like structures capable of shifting protein digestion towards the intestine. Casein was chosen as a model protein due to its high susceptibility to hydrolysis upon gastric digestion. The influence of the polysaccharide type (agar vs. κ-carrageenan) and the physical state of the gel-like structures (hydrated hydrogels vs. freeze-dried aerogels) on the ability to protect casein upon *in vitro* gastric digestion were evaluated and the generated digestion products were characterized in terms of

microstructure, molecular weight distribution and peptidomic analyses. Understanding the digestion mechanism on the developed structures will open up the possibility of designing novel dietary products to modulate postprandial response and satiety.

3 Materials and methods

3.1 Materials

Commercial κ-carrageenan (Ceamgel 90-093) and agar (PRONAGAR), in the form of powders, were kindly donated by CEAMSA (Pontevedra, Spain) and Hispanagar (Burgos, Spain), respectively. The commercial κ-carrageenan grade was composed of 92% κ-carrageenan and 8% ι-carrageenan (Fontes-Candia, Ström, Gómez-Mascaraque, et al., 2020). The agar content in the commercial agar was 80% (Martínez-Sanz et al., 2020). Casein powder in the form of micellar casein (with a protein content of 78.4%) was supplied by Ingredia (Arras, France). KCl was purchased from Sigma-Aldrich (Spain).

3.2 Preparation of polysaccharide-casein gel-like structures

Polysaccharide-casein gel-like structures were produced by using κ-carrageenan and agar as the gelling matrices (coded as KC and A, respectively). After gelation of the polysaccharides, the materials were used in their hydrated state, i.e., hydrogels (coded as HG) and after being subjected to a freeze-drying process to remove water and obtain porous dry materials known as aerogels (coded as AG). Firstly, polysaccharide and casein solutions in water were prepared separately. To obtain hydrogels with good mechanical integrity, the concentration of the polysaccharide and casein solutions was fixed at 2% (w/v), based on previous experiments (Fontes-Candia, Ström, López-Sánchez, et al., 2020; Martínez-Sanz et al., 2020). The casein and polysaccharide powders were dispersed in hot water (at a temperature of 40 °C for the casein and 90 °C for the polysaccharides) for 30 min. For the κ-carrageenan samples, KCl (0.25% (w/v) with respect to the carrageenan solution) was then added to the hot solution, which was gently stirred until the salt was completely dissolved. The required volume of casein solution was added to the polysaccharide solution and the samples were homogenized by further stirring. The polysaccharide:casein ratio was set at 75:25 or 25:75, w/w. It should be noted that the 75:25 ratio corresponded to the maximum casein content which could be incorporated into the

hydrogels without compromising their mechanical integrity. 0.4 mL of the polysaccharide-casein blends were transferred to a cylindrical silicon mould (7 mm diameter, 10 mm height) and were cooled down to room temperature and subsequently stored at 4 °C overnight. The hydrogels were stored in the fridge for a maximum of 48 h prior to the *in-vitro* digestions. For the preparation of the polysaccharide-casein aerogels (AG), the prepared hydrogel samples were frozen at -80 °C and subsequently, freeze-dried using a Genesis 35-EL freeze-dryer (Virtis, Spain). The produced aerogels were stored at 0% RH. Table 1 summarizes the different formulations prepared and their corresponding sample codes.

Table 1. Composition of polysaccharide-casein gel-like structures.

Sample code	Polysaccharide type	Physical state	Polysaccharide (% w/w)	Casein (%w/w)
HG-A25	Agar	Hydrogel	25	75
HG-A75	Agar	Hydrogel	75	25
AG-A25	Agar	Aerogel	25	75
AG-A75	Agar	Aerogel	75	25
HG-KC25	κ-carrageenan	Hydrogel	25	75
HG-KC75	κ-carrageenan	Hydrogel	75	25
AG-KC25	κ-carrageenan	Aerogel	25	75
AG-KC75	κ-carrageenan	Aerogel	75	25

3.3 *In vitro* simulated gastrointestinal digestions

The prepared hydrogel and aerogel samples were digested according to the INFOGEST *in-vitro* gastrointestinal digestion protocol (Brodkorb et al., 2019) with minor modifications. Briefly, the required amount of sample to provide 75 mg of casein was added to a polypropylene tube, 5 mL of human salivary fluid were incorporated, and the sample was incubated for 5 min. Subsequently, 5 mL of simulated gastric fluid (SGF) (pH=3) containing pepsin from porcine gastric mucosa (final pepsin concentration 2000 U/mL of gastric digest, Sigma-Aldrich, St Louis, MO, USA) were added. Gastric digestion was stopped at 120 min by adjusting the pH to 7 with 1 M NaOH. The intestinal phase was conducted by mixing the end point from the gastric phase

with 10 mL of simulated intestinal fluid (SIF) (pH=7) containing pancreatin from porcine pancreas (100 U trypsin activity per mL of final mixture, Sigma-Aldrich) and porcine bile extract (Sigma-Aldrich). Since the digests will be tested in cell lines in future works, the bile salt concentration was reduced to 2.5 mM, given the cytotoxic effects of 10 mM bile salts in the STC-1 cell line reported by (Santos-Hernández et al., 2018). The intestinal digestion was stopped after 120 min by heating the sample at 85 °C for 15 min. In most of the cases, the gastric and intestinal digests could be separated into two phases: a solid fraction consisting of the non-digested material and the liquid fraction containing the digested soluble compounds. These two phases were separately characterized for each formulation after each digestion step, giving rise to four different samples: gastric solid (GS), gastric liquid (GL), intestinal solid (IS) and intestinal liquid (IL). After separating the two phases, the samples were subjected to snap freezing in liquid nitrogen, freeze-dried and stored at −20 °C until further analyses. Micellar casein (coded as Cas) was also subjected to the same digestion protocol and its digestion products were analysed. Finally, to evaluate the effect of the physical structures formed upon gelation, control samples were prepared by physically blending the casein with the polysaccharides prior to the digestion (i.e., without subjecting the polysaccharides to the gelation process). The polysaccharide:protein ratios were the same used for the hydrogels and aerogels, i.e., 75:25 and 25:75. These control samples were coded as C-A75 and C-A25 in the case of the agar formulations and C-KC75 and C-KC25 for the κ-carrageenan formulations. For each specific formulation the digestions were performed in triplicate by using individual tubes per time point (gastric and intestinal).

The nitrogen content in the freeze-dried digests was determined by elemental analysis using the Dumas method in a LECO CHNS-932 (Thermo Fisher, USA) analyser. Further analyses were performed on a protein basis according to the results.

3.4 Scanning electron microscopy (SEM)

Aerogel samples were coated with a gold-palladium mixture under vacuum and their morphology was studied using a Hitachi microscope (Hitachi S-4800) at an accelerating voltage of 10 kV and a working distance of 8–16 mm.

3.5 Confocal laser scanning microscopy (CLSM)

CLSM was used to visualize the microstructure of the polysaccharide-casein hydrogels and aerogels before and after being subjected to gastrointestinal digestion. Imaging was performed using a Confocal Microscope Leica TCS SP5 (Leica Microsystems, Germany) equipped with the LAS-AF software. Thick sections were carefully cut from solid samples with the help of a scalpel. Then, a sufficient amount of Fast Green solution (0.1% wt. in water) was added to completely soak the sample and stain the protein. After that, the sample was placed onto a microscopy glass slide and covered with a glass cover slip. The light source used was a HeNe laser with an emission wavelength of 647 nm. A lens with a magnification of 20 and a numerical aperture (NA) of 0.7 was used throughout the study. Images were processed using the Fiji software.

3.6 Sorption capacity of aerogels

The capacity of the aerogels to sorb SGF was tested by soaking the samples previously weighed into 15 mL of SGF in sealed containers. The samples were periodically taken out of the liquid and weighed using an analytical balance (Mettler-Toledo, Ms105du, Switzerland, d=0.01 mg) after removing the excess liquid. Measurements were taken until the samples were equilibrated and the total weight gain was calculated.

3.7 Gel strength

Gel strength values were determined from penetration assays using a texture analyser (Stable Micro Systems model TA-XT2, Surrey, UK) equipped with a cylindrical aluminium plunger (3.6 cm diameter) and a load cell of 30N. The assays were carried out at room temperature (20–25 °C). Gel disks were compressed to 80 % of the original height, using a crosshead speed of 0.1 mm/s. All measurements were performed, at least, in triplicate.

3.8 Sodium Dodecyl Sulphate-Polyacrylamide Gel Electrophoresis (SDS-PAGE)

SDS-PAGE was performed as previously described by (Santos-Hernández et al., 2018) with minor modifications. Gastric and intestinal digests were dissolved in sample buffer which contained Tris-HCl (0.05M, pH 6.8, SDS (1.6% w:v), glycerol (8% v:v), β-mercaptoethanol (2% v:v) and bromophenol blue indicator (0.002% w:v) at a protein concentration of 1.5 mg/mL and 2.0 mg/mL, respectively. The samples were heated at 95 ºC for 5 min and kept warm until they

were loaded on the 12% Bis-Trispolyacrilamide gels (Criterion XT, Bio-Rad, Richmond, CA, USA). Electrophoretic separations were carried out at 150 V using XT-MES as running buffer (Bio-Rad), in the Criterion cell (Bio-Rad). The gels were stained with Coomassie Blue (Instant Blue, Expedeon, Swavesey, UK) and images were taken with a Molecular Imager VersaDoc™ MP 5000 system (Bio-Rad, Hercules, CA, USA).

3.9 Molecular weight distribution of peptides by MALDI-TOF/TOF

Intestinal digests were reconstituted at 0.1 mg of protein/mL in 33% acetonitrile with 0.1% trifluoroacetic acid prior to being spotted into a MALDI target plate with a 2,5-dihydroxybenzoic acid matrix. Analyses were performed on an Autoflex SpeedTM (Bruker Daltonic, Bremen, Germany). Ions were detected in positive linear mode at a mass range of *m*/*z* 5–20 kDa for proteins and in reflectron mode at a mass range of *m*/*z* 500–3000 Da for peptides and were collected from the sum of 1,000 on average lasers shots. Protein Calibration Standard I and Peptide Calibration Standard, Bruker Daltonics were employed for external calibration of spectra. The monoisotopic peaks were generated using FlexAnalysis 3.3 software and were represented in a molecular weight distribution range.

3.10 Peptide identification by HPLC-tandem mass spectrometry (HPLC-MS/MS) analysis

The identification of resistant peptides to intestinal digestion was performed by HPLC-tandem mass spectrometry (HPLC-MS/MS) according (Santos-Hernández et al., 2018). Freeze-dried intestinal and gastric digests were reconstituted in solvent A (water:formic acid, 100:0.1, v:v); prior to analysis, fractions were centrifuged at 11,000 × *g* for 10 min. The spectra were recorded over the mass/charge (*m/z*) ranges of 100–600, 100–1700, and 100–2000, selecting 500, 750, and 1200 and as target mass, respectively. A homemade database of bovine casein protein was used for peptide sequencing in MASCOT v2.4 software (Matrix Science). Biotools version 3.2 was used for interpreting the matched MS/MS spectra.

3.11 Statistics

All data have been represented as the average ± standard deviation. Different letters show significant differences both in tables and graphs ($p \leq 0.05$). Analysis of variance (ANOVA)

followed by a Tukey-test were used to determine significant differences between the formulation using the statistical software IBM SPSS (v.24) (IBM corp., USA).

4 Results and discussions

4.1 Structural behaviour of the polysaccharide-casein gel-like structures upon gastrointestinal digestion

While the gastric and intestinal digests from the casein and the control polysaccharide-casein blends were homogeneous, the digests from the gel-like structures were heterogeneous, presenting two different phases which were separated and analysed individually: a solid fraction (presumably containing non-digested material) and a liquid fraction composed of the digested soluble compounds. The presence of the solid phase was not surprising, since the polysaccharide gel-like structures were expected to be resistant to the digestion conditions (McClements, 2017). As an example, Figure 1 shows the visual appearance of the gel-like structures with a polysaccharide:protein ratio of 75:25 in their initial state and the solid phases obtained after the gastric (coded as GS) and intestinal (coded as IS) digestions. As observed, the hydrogel structure for both polysaccharides remained apparently intact after the gastric and intestinal digestions. A slight change in the colouration from the hydrogels, which turned from whitish to yellowish, was noted after the intestinal digestion. This suggests that the hydrogels were able to retain a certain fraction of the bile salts (responsible for that yellowish coloration) present in the intestinal fluid within their structure. Moreover, a change in the transparency of the gels was noted after the intestinal phase, which may be ascribed to the disruption of the micellar casein structure upon the action of the pancreatic enzymes (Huppertz et al., 2008; Ozel et al., 2020). In the case of the aerogels, the structure was substantially different depending on the polysaccharide. While the agar aerogels showed a fluffier appearance, the κ-carrageenan aerogels were clearly shrunk forming more collapsed and denser structures, especially in the case of aerogels with the greatest polysaccharide ratio. The greater susceptibility of agar aerogels to rehydration was also observed in pure polysaccharide aerogels which were rehydrated in SGF (cf. Figure S1). Interestingly, all the aerogels were highly re-hydrated during the digestions, allowing the diffusion of the gastric and intestinal fluids into the aerogel structure and producing solid fractions with a similar consistency to that from the hydrogels.

This is not unexpected, since previous studies have demonstrated the great sorption capacity of polysaccharide-based aerogels (Benito-González et al., 2020; Fontes-Candia et al., 2019). In fact, sorption experiments showed that the aerogels were able to sorb relatively high amounts of liquid when soaked in SGF (cf. Figure S2), reaching their maximum sorption values after approximately 60 min, with >30 g SGF/g aerogel for AG-A75, ~25 g SGF/g aerogel for AG-KC25, ~23 g SGF/g aerogel for AG-A25 and ~15 g SGF/g aerogel for AG-KC75. The sorption capacity of the aerogels is expected to be highly relevant, since a limited sorption of the SGF would impede a proper diffusion of the digestive enzymes into the aerogels through the liquid media. While in the case of κ-carrageenan an increase in the polysaccharide content reduced the sorption capacity of the aerogels due to the formation of very compacted and shrunk structures, the opposite was noted in the case of the agar aerogels, with the AG-A75 presenting the greatest SGF sorption capacity of all the samples. In fact, due to its high sorption capacity, when AG-A75 was incubated in the SGF it was capable of retaining the whole volume of liquid within its structure and thus, only a solid phase, corresponding to the re-hydrated aerogel, was obtained after the gastric digestion. This can also be linked to the morphology of the aerogels, which was characterized by SEM and representative images are shown in Figure S3. As observed, in the case of agar an increase in the polysaccharide ratio led to a more open porous structure. However, in the case of κ-carrageenan, the shrinkage of the aerogels observed when increasing the polysaccharide content was also reflected in the microstructure, noting a more heterogeneous porous structure where some of the pores were disrupted. Previous studies have demonstrated that more porous polysaccharide-based aerogels are able to sorb greater amounts of liquid than those presenting a more compacted structure (Benito-González et al., 2020; Fontes-Candia et al., 2019). This may explain the greater capacity of AG-A75 to sorb and retain SGF within its structure.

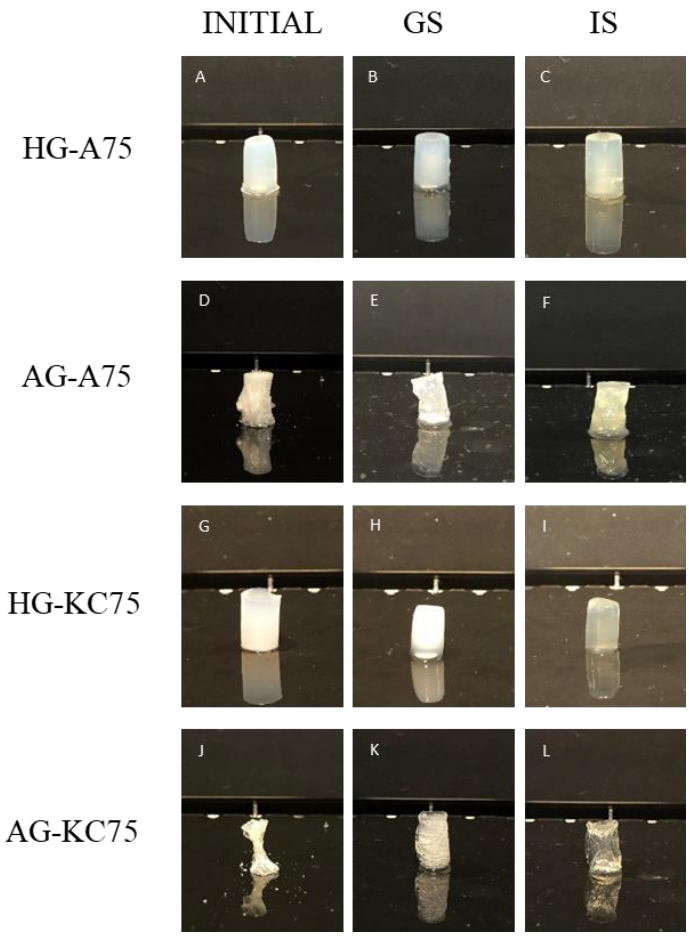

Figure 1. Visual appearance of the initial polysaccharide-casein gel formulations with a polysaccharide:protein ratio of 75:25, and the corresponding gastric and intestinal solid phases.

The solid and liquid fractions obtained after the gastric and intestinal digestion of all the samples were characterized by means of elemental analysis to determine their protein content and the obtained results, together with the corresponding dry weight fractions, are summarized in Table S1. The estimated dry weight fractions for the liquid and solid phases obtained from the gel-like structures evidence that during the gastric phase all the samples were able to sorb part of the SGF, leading to solid weight fractions higher than the theoretical values expected if no sorption had taken place (60% w/w in the formulations with a polysaccharide:protein ratio of 75:25 and 33% w/w in the formulations with a polysaccharide:protein ratio of 25:75). In contrast, during the intestinal phase the sorption of the SIF seemed to be limited, significantly

increasing the weight fraction in the liquid phase. Interestingly, while the solid weight fractions for the gel-like structures with a polysaccharide:protein ratio of 75:25 were generally higher than the theoretical value (i.e., 43% w/w), the opposite trend was observed for the formulations with a polysaccharide:protein ratio of 25:75, with solid weight fractions lower than expected (i.e., 20% w/w). This indicates that the structural integrity of the gel-like structures with lower polysaccharide content was partially lost during the intestinal digestion, which is reasonable since the polysaccharide is the main structuring component in the developed gel-like structures.

The protein distribution in the solid and liquid phases, after the gastric and intestinal digestions of the gel-like structures, were determined and the results are displayed in Figure 2. According to the results, the hydrogels from both polysaccharides behaved similarly during the gastric phase, with at least half of the total protein content remaining in the solid fraction. The hydrogels with a polysaccharide:protein ratio of 75:25 presented greater protein content in the solid fraction than the 25:75 hydrogels which could be ascribed to a greater diffusion of the casein towards the liquid medium in the hydrogels with the lower structuring polysaccharide content. This effect was also observed in the case of the aerogels. On the other hand, in general, the protein content in the solid fraction from the aerogels after the gastric phase was similar or lower than that from the corresponding hydrogels (except for the AG-A75 in which there was only one solid phase containing all the protein), suggesting that the physical state of the matrix had a strong effect on the release of the casein from the gel-like structures.

After the intestinal phase, the protein content in the liquid fraction increased in all the samples, especially in the gel-like structures with a polysaccharide:protein ratio of 25:75. This, together with the calculated weight fractions, suggests that a greater amount of protein was released during the intestinal phase for these materials as compared to the 75:25 formulations. These results could be ascribed to the fact that a lower concentration of gelling polysaccharides generally leads to the formation of weaker gel structures (Fontes-Candia, Ström, Gómez-Mascaraque, et al., 2020). Indeed, as shown in Table S2, the estimated gel strength values were significantly lower (6-7-fold) when reducing the polysaccharide content from 75% to 25%,

regardless of the type of polysaccharide. Thus, the gel-like structures with a polysaccharide:protein ratio of 25:75 are expected to promote a greater release of the casein and be more susceptible to disintegration upon the gastrointestinal digestion conditions. In fact, Koutina et al. reported that at low alginate:protein ratios, there was not sufficient alginate to create a shielding effect able to delay or even prevent the digestion of the protein, while at high alginate:protein ratios whey proteins were protected from pepsin digestion (Koutina et al., 2018).

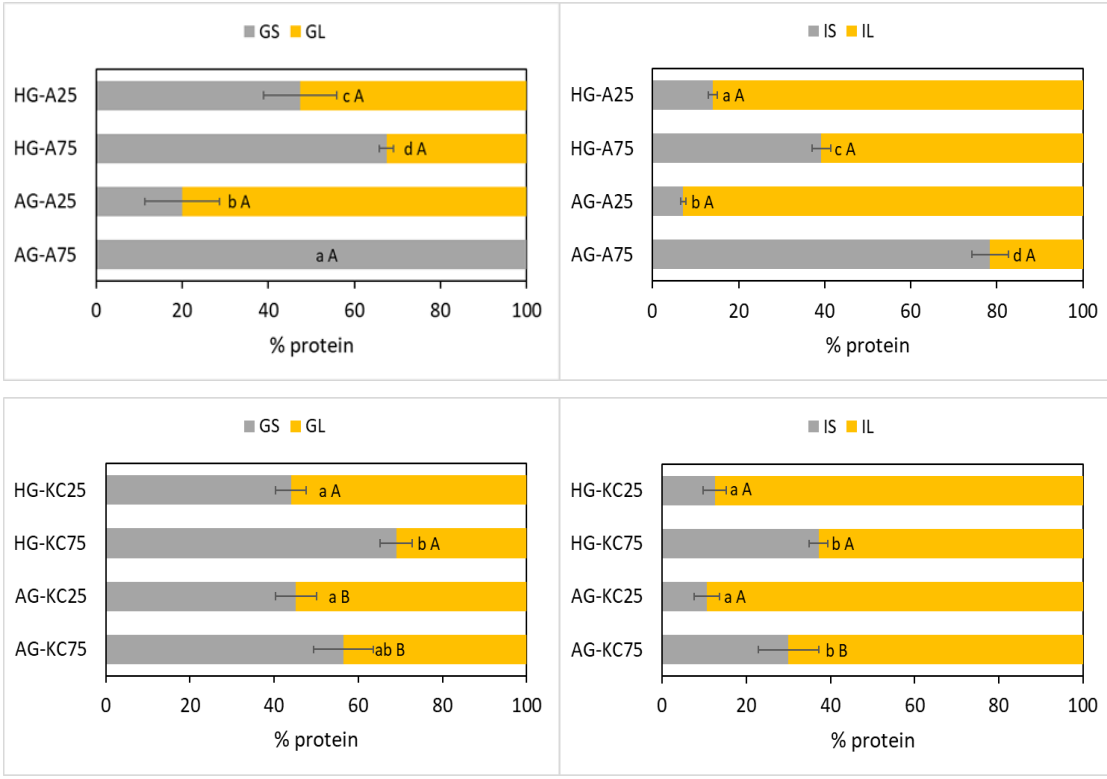

Figure 2. Protein content distribution in the solid (S) and liquid (L) fractions after the gastric (G) and intestinal (I) digestion phases for the agar (top) and κ-carrageenan (bottom) gel-like structures. Different lowercase letters (a, b, c, d) indicate statistically meaningful differences ($p \leq 0.05$) between the protein content in the liquid fraction from each graph (i.e., samples with the same polysaccharide type and at the same digestive stage). Different capital letters (A, B, C, D) indicate statistically meaningful differences ($p \leq 0.05$) between the protein content in the liquid fraction from agar and κ-carrageenan formulations (for samples with the same physical state, polysacharide:protein ratio and digestive stage).

To investigate the evolution of the microstructure during the gastrointestinal digestions, the polysaccharide-casein gel-like structures, as well as the control samples, and the digested materials obtained after the gastric and intestinal phases were examined by means of CLSM, using a specific staining agent for the protein, and representative images are shown in Figure 3. As observed, the control casein showed a well-defined structure of spherically-shaped particles (cf. Figure S4) with heterogeneous size distribution (average diameter of ca. 30.3 ± 24.6 μm). Such particles correspond to aggregated casein, i.e. casein clusters, which are known to be formed in commercial caseinate powders as a result of ionic interactions (Jarunglumlert et al., 2015). After the gastric digestion, these characteristic structures were almost completely disrupted, with the remaining protein forming heterogeneous aggregates with a relatively large size. After the intestinal phase, the casein seemed to be completely digested and only very small structures (ca. 5.8 ± 1.9 μm) could be visualized, which most likely corresponded to aggregates of the digestive enzymes (cf. Figure S4). Surprisingly, the presence of a small fraction of polysaccharide (i.e., polysaccharide:protein ratio of 25:75) had a significant impact on the microstructure of the digested samples, giving rise to completely different microstructures depending on the added polysaccharide. While in the presence of agar the digested protein was detected as a diffused network of small particles both after the gastric and intestinal digestions, the addition of κ-carrageenan led to the formation of protein aggregates similar to those observed in the control casein after the gastric digestion, but larger protein fragments were detected after the intestinal digestion. This suggests that the establishment of polysaccharide-casein interactions may have an effect on the digestion of the protein and the nature of these interactions is dependent on the type of polysaccharide (Markussen et al., 2021). In particular, it seems that the negative charges provided by the sulphate groups in the agar promoted the formation of polysaccharide-protein complexes at the acidic conditions of the gastric digestion phase, while in the case of the κ-carrageenan, the inclusion of K^+ ions (added to stabilize the gel networks) precluded from this effect and instead, protein and polysaccharide phases separated.

With respect to the polysaccharide-casein gel-like structures, the microstructure of the digested samples was seen to be different depending on the physical state of the matrix and the gelling

polysaccharide. Figure 3A compiles the images corresponding to the agar-based gel-like structures and the solid fractions obtained after the gastric and intestinal digestions. The intact casein clusters could be clearly visualized in the HG-A25 hydrogel; however, in the case of HG-A75 and of the aerogels, the protein did not seem to be properly stained (although in some cases the clusters could be visualized in the images as solid non-stained particles). The reason for this distinct staining of the protein in the samples is unknown and could be due to diffusion effects or to a lower amount of reactive functional groups in some of the samples due to the formation of protein-polysaccharide complexes. After the gastric phase, some intact casein clusters could be detected in the solid fraction from HG-A25 and AG-A75, while smaller protein fragments were visualized in HG-A75. In line with the protein distribution results, CLSM images show that a significant amount of casein remains in the solid fraction. These results are indicative of a protective effect of these structures during the gastric digestion, limiting the disruption of the casein aggregates as it occurred in the non-complexed casein. After the intestinal digestion, casein clusters were not detected, suggesting that the protein remaining in the solid fraction had been extensively digested; however, larger structures were observed in HG-A75 and AG-A75. This might be due to a lower extent of digestion in the remaining casein or to the establishment of interactions between the digested casein and the agar.

The κ-carrageenan gel-like structures and the solid fractions from their digests were also analysed and representative images are shown in Figure 3B**.** Similarly to the agar-based structures, casein aggregates were clearly visualized in HG-KC25, while the strongly compacted structure of the other samples impeded a proper staining and visualization of the casein. Examination of the solid fractions obtained after the gastric digestions suggested that a greater proportion of protein was released towards the liquid medium in the case of the aerogels, which is in agreement with the protein distribution results (cf. Figure 2). Intact casein clusters were observed in the solid fraction from HG-KC75 and a few smaller fragments were detected in AG-KC25 and AG-KC75. Interestingly, the structure of casein aggregates could be unequivocally seen in the solid fraction from HG-KC25 but the staining agent did not seem to penetrate towards the interior of the clusters and the surface regions appear with a green coloration instead. This might be attributed to strong polysaccharide-protein interactions impeding a

proper penetration of the staining agent. After the intestinal phase, few clusters could be still detected in the solid from HG-KC75, indicating that the strong hydrogel network structure formed in this case (Table S2) limited the release of the casein towards the liquid phase. Smaller particles were detected in the solids from HG-KC25, AG-KC25 and AG-KC75, similarly to what was observed in the intestinal solids from the agar-based gel-like structures.

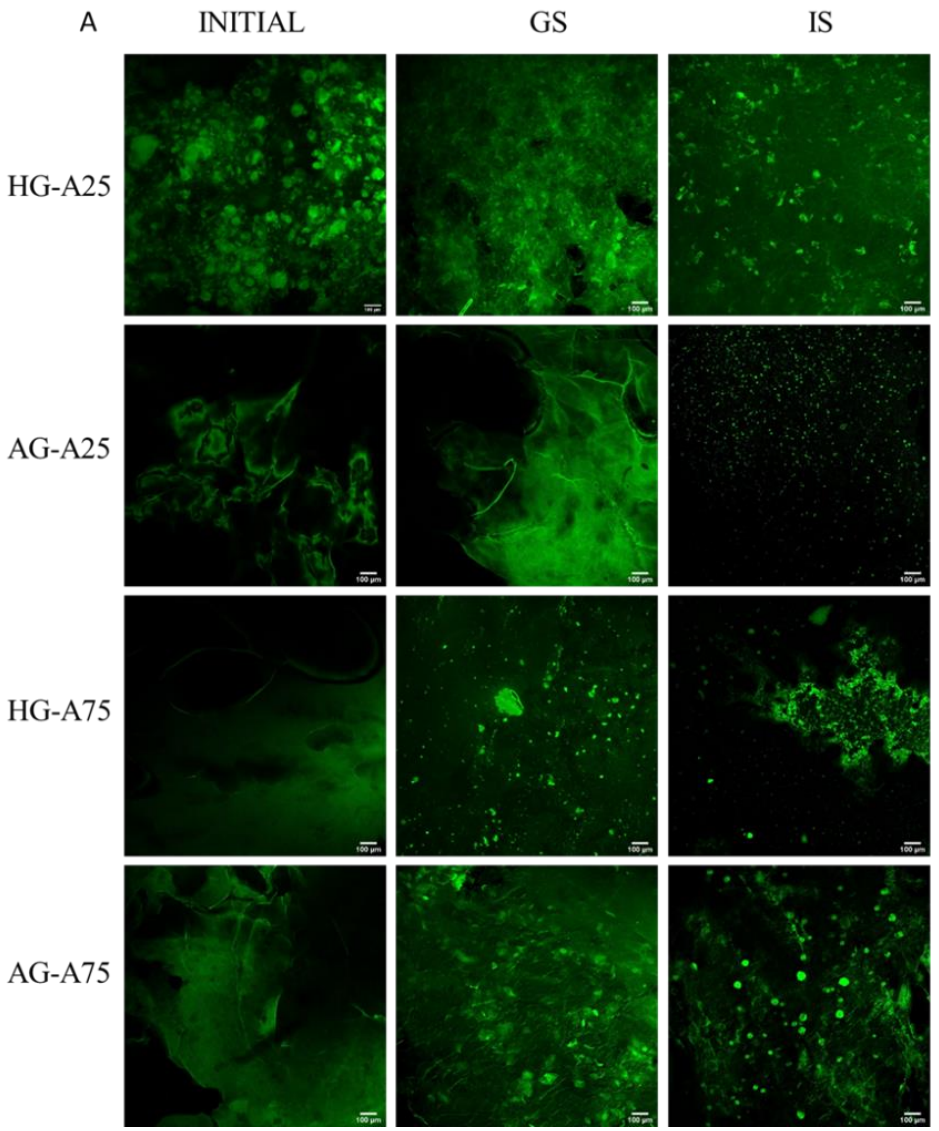

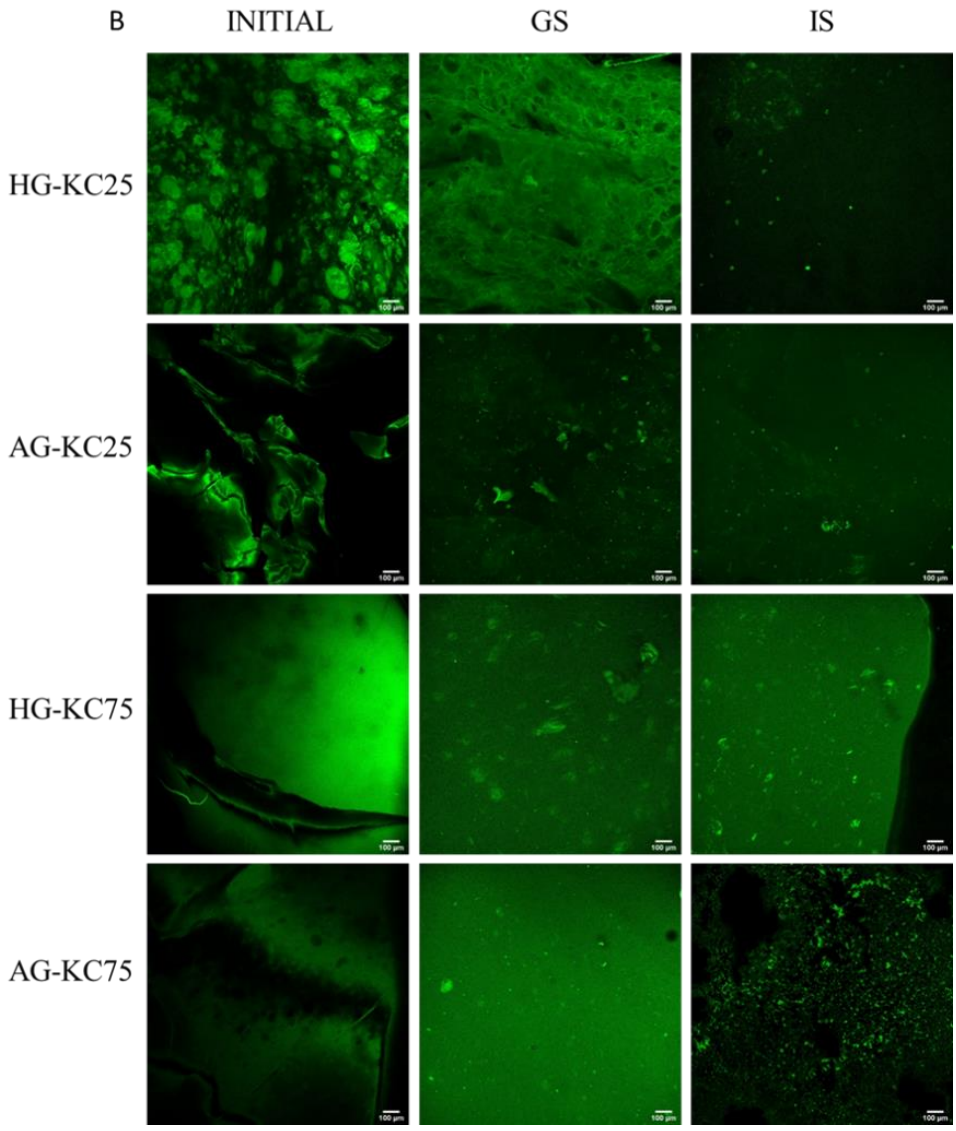

Figure 3. Confocal laser microscopy images of the initial polysaccharide-casein gel-like structures and their corresponding solid fractions generated after the gastric (GS) and intestinal (IS) digestion phases. The images shown in (A) correspond to the agar-based formulations and the images in (B) correspond to the κ-carrageenan-based formulations.

4.2 Protein degradation upon gastrointestinal *in vitro* digestion

Casein degradation during simulated gastrointestinal digestion was followed by studying the molecular weight (MW) distribution of proteins and peptides above 10 kDa through SDS-PAGE.

Figures 4A and 4B show the obtained protein profiles after the gastric and intestinal digestions. The bands corresponding to the control casein were observed between 25 and 37 kDa, which correspond to the α_{s1}-casein, α_{s2}-casein, β-casein and κ-casein (Egger et al., 2016). A band was also observed around 18 kDa, which corresponds to the residual serum protein β-lactoglobulin (Li et al., 2020) As expected, after the gastric digestion the casein characteristic bands were absent in the non-complexed protein and instead the presence of β-lactoglobulin and peptides with MW < 10 kDa was noted. After the subsequent intestinal digestion only the bands corresponding to the added pancreatic enzymes (porcine pancreatic lipase (50 kDa), trypsin (23.3 kDa), chymotrypsin (25.5-29.10 kDa) and elastase (25.9 kDa) could be detected (Sanchón et al., 2018), suggesting that the protein had been digested into small peptide fragments. The casein degradation observed after the gastric phase is in agreement with other works (Egger et al., 2016; Sanchón et al., 2018) and it is explained by the flexible and open structure of casein, leading to a higher sensitivity to proteolysis (Li et al., 2020).

After the gastric digestion, the casein characteristic bands were clearly observed in the solid fractions from the hydrogels (HG-A25 and HG-A75) and less evidently in the aerogel AG-A75. In agreement with CLSM, this confirms the presence of non-digested casein which is retained within the structure of these materials. It should be noted that in the case of AG-A75 the bands were less clearly discerned and the whole well was stained. This can be attributed to interference of the polysaccharide due to casein-polysaccharide interactions being established. Sample handling was indeed more complex due to the higher viscosity of this material. After the intestinal phase, the casein bands were absent in all the samples; however, peptides with MW < 10 kDa were observed in most of them, appearing this region more intensely stained in C-A75, the liquid from HG-A25, HG-A75 and AG-A75, as well as the solid phase from AG-A75. This suggests a lower degree of casein hydrolysis during the intestinal digestion in these samples.

The SDS-PAGE profile of the digests from the κ-carrageenan gel-like structures are shown in Figure 4B. As observed, after the gastric digestion the characteristic bands of intact casein were present in the solid fraction from the hydrogels (HG-KC25 and HG-KC75), as well as the liquid from HG-KC75. Once again, handling some of these samples was extremely complex due to their

high viscosity and, in some cases such as for the AG-KC25 sample, polysaccharide interference impeded a proper visualization of the electrophoretic bands. After the intestinal digestion, all the samples showed a very similar profile to that from the non-complexed casein, suggesting that the κ-carrageenan structures did not exert a significant protective effect against the effect of the pancreatin. It should be noted that although intact casein clusters were detected in the CLSM images from the intestinal solid from HG-KC75, no signs of protein were seen in the corresponding well. This may be explained by the remaining clusters being strongly interacting with the polysaccharide network, hence being separated upon sample preparation and not able to migrate into the electrophoresis gel. Thus, it should be taken into consideration that the SDS-PAGE results are not conclusive since (i) higher polysaccharide contents in some of the samples could hinder the migration of the protein through the gel and (ii) polysaccharide-protein complexes may have not been properly detected due to polysaccharide interference. A possible strategy to avoid this and improve the accuracy of the SDS-PAGE results would be the use of specific enzymes to hydrolyse and separate the polysaccharides, hence allowing a proper identification of the whole protein fraction remaining in the samples.

These results, together with CLSM, suggest that some of the developed gel-like structures exerted a strong protective effect during the gastric digestion, being able to retain a fraction of non-digested casein clusters in the solid phase. In general, the hydrogels limited to a greater extent the release of casein towards the liquid medium and showed a greater protective effect than the aerogels. Despite the high sorption capacity of AG-A75, this specific structure also resulted in a notable protective capacity. Moreover, the polysaccharide:protein ratio seems to be highly relevant, with higher ratios limiting the digestion of casein even during the intestinal phase.

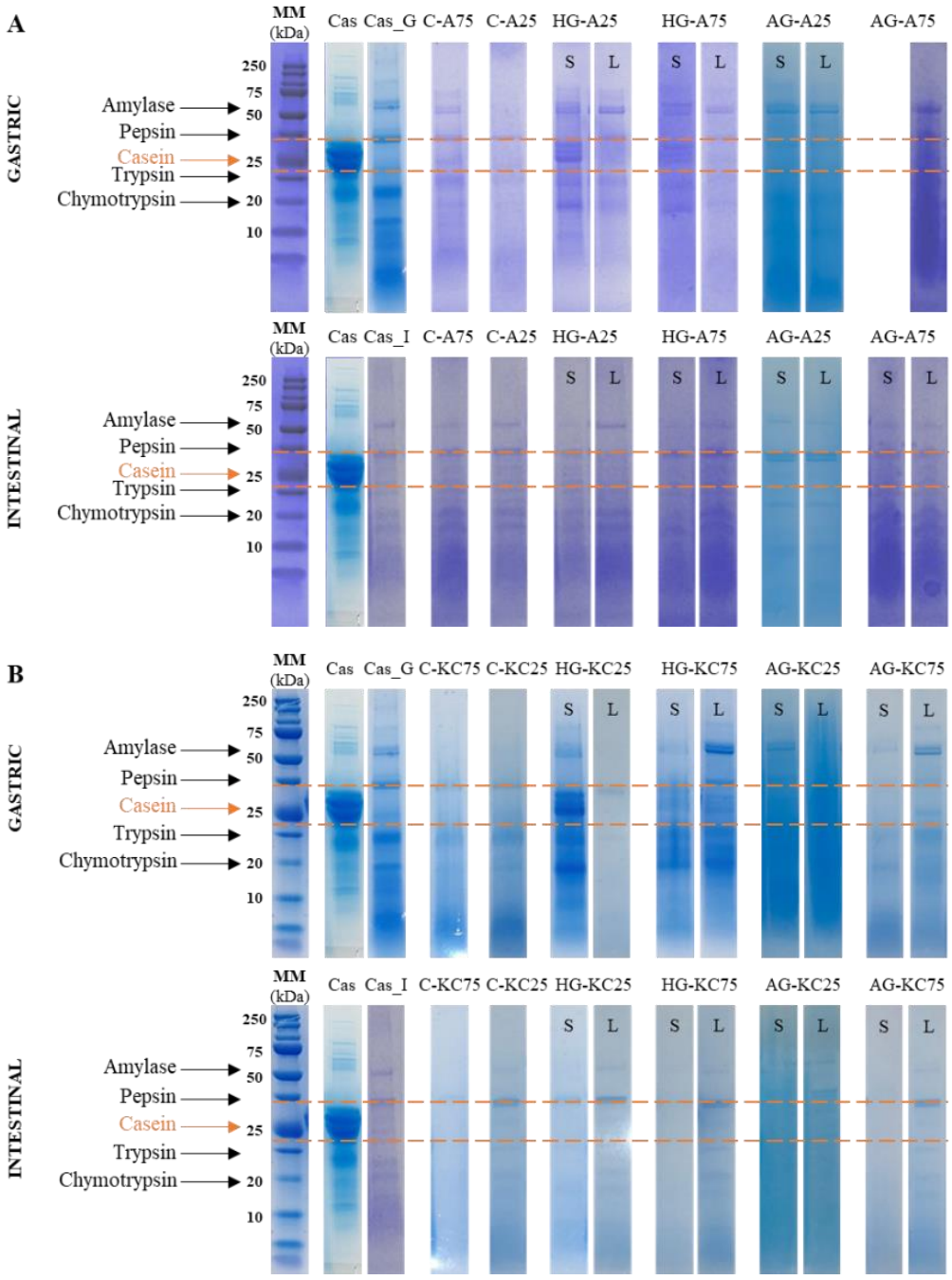

Figure 4. SDS-PAGE protein profiles of casein after gastric and intestinal digestion of agar (A) and κ-carrageenan (B) gel-like structures. MW: molecular weight marker; S: solid phase; L: liquid phase.

In order to evaluate the MW distribution of the intestinal digestion-derived peptides from the polysaccharide-casein gel-like structures, the samples were characterized by MALDI-TOF and the results, expressed as the percentage of peptides within a given MW range, are shown in Figure 5. As observed, in most of the samples the majority of the peptides detected were within the low MW range (0.5-1 kDa), while less than 30% of the peptides showed MW>4 KDa. Interestingly, the MW distribution of the peptides detected in the gastrointestinal digests from the polysaccharide-casein gel-like structures varied depending on the type of polysaccharide. In particular, digests from κ-carrageenan presented a greater percentage of peptides within the range of 0.5-1 kDa than those from the non-complexed casein and from the agar samples. On the other hand, species larger than 18 kDa, that is whole proteins, were found in the κ-carrageenan digests, while proteins within this MW range could not be detected in the agar samples, except in AG-A25. This might be indicative of the presence of a small fraction of casein being strongly bound to κ-carrageenan, hence being less susceptible to the hydrolytic effect of pepsin and pancreatic enzymes. For both polysaccharides, the MW distribution of the peptides was dependent on the polysaccharide:protein ratio and the physical state of the gel-like structures. Thus, while a greater percentage of peptides with MW>2 kDa was observed in the aerogels with higher polysaccharide content (75:25 ratio), the opposite effect was noted in the hydrogels. Overall, the agar-based gel-like structures seemed to provide a greater release of peptides within the range of MW>2 kDa towards the liquid media.

Linking these results with CLSM, it seems that the strong network originated in the hydrogels with the higher polysaccharide:protein ratio (75:25), especially in the case of κ-carrageenan, provided a great protection against the digestion of casein, with larger protein fragments remaining in the solid fraction even after the intestinal phase. In that case, reducing the polysaccharide:protein ratio to 25:75 seemed to be beneficial to promote the release of casein during the intestinal phase towards the liquid medium and provide a greater relative amount of peptides with MW>2 kDa. On the other hand, the porous structure of the aerogels seemed to provide a greater release of the casein towards the liquid medium, limiting the protective effect of these type of structures. Thus, increasing the polysaccharide:protein ratio to 75:25 would be positive in that case to generate stronger and more compact structures. The stronger

networks originated in the case of κ-carrageenan are due to the gelation mechanism induced by the presence of added cations (K^+) which lead to the formation of strong ionic interactions, as opposed to the agar networks, which are solely held by means of hydrogen bonding (Fontes-Candia et al., 2021). Upon freeze-drying, the κ-carrageenan networks are strongly collapsed, forming very compact aerogels which would be less suitable for a sustained release of the casein than the more porous structure of the agar-based aerogels (cf. Figure S3).

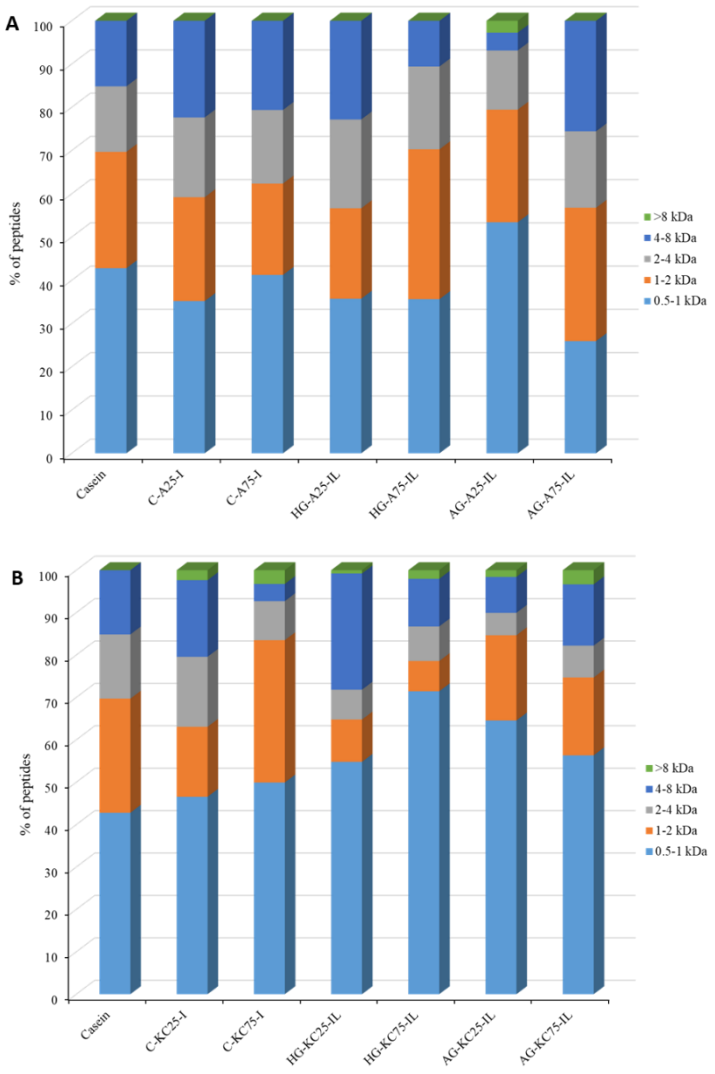

Figure 5. Molecular weight distribution expressed as the relative fraction of casein peptides detected in the intestinal phase (I) of the control samples and the liquid intestinal fractions (IL) from the agar (A) and κ-carrageenan (B) gel-like structures in comparison to casein and control.

4.3 Peptidomic characterization of intestinal *in vitro* digests

Digested casein and the liquid fractions from the gel-like structures with the highest protein content were analysed by HPLC-MS/MS after the gastrointestinal digestion. All the peptides identified for each sample were simultaneously compared and the results are represented in a Venn diagram (cf. Figure 6). As observed, the amount of peptides detected in the polysaccharide:casein hydrogels at the end of the intestinal digestion was greater than in the control casein, which may be due to a certain degree of protection of the hydrogel structures against the hydrolytic enzymes. Furthermore, the peptide sequences detected in the digests from the hydrogels were significantly different to those observed in the control casein, since only a small overlapping region of the total number of peptides was noted. The longer peptide sequences detected in the hydrogel samples suggest that the microstructure of these materials seems to be optimum to delay casein digestion during the gastric phase, while allowing the release and hydrolysis of casein during the intestinal phase. Contrarily, for the aerogel structures the amount of detected peptides was lower than the control casein. This could be related to the greater release of protein which took place in these samples during the gastric phase, leading to a greater casein hydrolysis. When evaluating the obtained results, the limitations of the HPLC-MS/MS analyses should be taken into consideration. Firstly, all those compounds which are not completely soluble in the solvent (water:formic acid) are removed during sample preparation; this means that the protein bound to polysaccharides is discarded. In this regard, the use of specific enzymes to hydrolyse the polysaccharide fraction, prior to the analyses, could be useful. Additionally, the instrumental conditions favour the detection of peptides with MW between 0.5 and 3 kDa, although a few peptides with longer sizes could be identified depending on their ionization capacity. Thus, long peptide fragments are not expected to be detected by HPLC-MS/MS since they may not be properly solubilized or ionized. Most of the identified peptides corresponded to sequences from β-casein and α_{s1}-casein, with minor amounts of peptides corresponding to α_{s2}-casein. The peptide patterns, color-coded to represent the abundance of amino acids identified along the protein sequence for the β-, and α_{s1}-casein are represented in Figure S5. The patterns for the control casein at the end of the intestinal digestion are similar to previously reported data (Ana-Isabel Mulet-Cabero et al.,

2020; Bohn et al., 2017; Egger et al., 2019) and confirm that this protein fraction undergoes a high degree of degradation during digestion. A greater amount of peptides within the region ^{62}FPGPI^{66} and ^{150}PLPPT^{154} from β-casein were observed for all the samples, while the region ^{73}NIPPL^{77} also presented higher abundance of peptides for the control casein and HG-A25. Interestingly, a greater amount of peptides were detected within different regions in the intestinal liquid from each particular gel-like structure. For instance, in the case of HG-KC25 the ^{120}TESQSLTLTDVEN^{132} and ^{160}QSVLS^{164} regions appeared more intense than in the control casein, while the ^{33}FQSEEQQQTEDELQDKIHP^{51} region was more intense in AG-A25. In the case of the α_{s1}-casein, the ^{65}ISSS^{68} and the C-terminal region ^{182}IPNPI^{187} were consistently detected in all the samples. Notably, peptide fragments from the region ^{65}ISSSEEIVPNSVEQKHIQKEDV^{86} were highly abundant in the intestinal liquid from AG-A25, while peptides within the region ^{50}EDQAMEDIKQMEAESIS^{66} were more abundant in HG-KC25. Overall, the results confirm the protective effect of both hydrogels, limiting the hydrolysis of casein and promoting the release of longer soluble peptide sequences. This was especially noted in the case of HG-KC25, which may be explained by the greater proportion of peptides with lower MW in this sample, as evidenced by the MALDI-TOF results. The peptides with higher MW present in the intestinal liquid from HG-KC25 may have not been detected by HPLC-MS/MS due to the already mentioned limitations of this technique. It should be noted that in the particular case of AG-A25, despite the greater release of casein during the gastric phase, leading to greater casein hydrolysis, a small proportion of casein may have still remained tightly bound to the polysaccharide, being hydrolysed during the intestinal phase and giving rise to longer peptides within specific regions of the protein sequence.

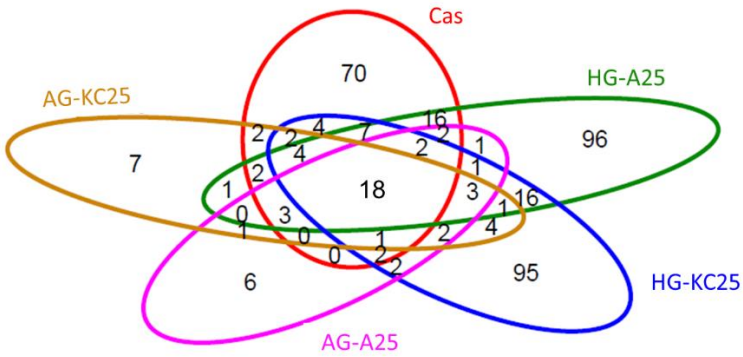

Figure 6. Venn diagrams of the peptide sequences identified in the intestinal digests from selected polysaccharide-protein gel-like structures and the control casein.

5 Conclusions

Polysaccharide-casein gel-like structures (hydrogels and aerogels) were able to affect the hydrolysis of casein upon *in-vitro* gastrointestinal digestions, being this effect dependent on the polysaccharide type, the polysaccharide:casein ratio and the physical state of the structures. Although the mere presence of the sulphated polysaccharides seemed to produce a slight protective effect against the hydrolysis of casein during the gastric phase, this effect was maximized by the development of gel-like structures.

During the gastric phase all the developed structures kept their physical integrity and the aerogels were able to sorb SGF to rehydrate. Non-digested casein, in the form of clusters, was seen to remain in the solid fraction from most of the samples after the gastric phase, while smaller particles were observed in the solids obtained at the end of the intestinal digestion. In general, the hydrogels limited to a greater extent the release of casein towards the liquid medium and showed a greater protective effect than the aerogels, except for AG-A75. Moreover, lower polysaccharide concentration yielded softer gels with less physical integrity and more prone to release the protein.

HG-A25, AG-A75 and HG-KC25 were determined as the most optimal structures for the intended application, since they were able to preserve intact casein after the gastric phase while promoting the release of peptides with greater molecular weights during the intestinal phase. These results evidence the potential of polysaccharide-protein gel-like structures to produce

satiating dietary products and demonstrate the relevance of their structural properties on their behavior upon digestion.

6 Acknowledgements

The projects RTI2018-094268-B-C22 and RTI2018-094408-J-I00 were funded by MCIN/AEI/10.13039/501100011033 and by "ERDF A way of making Europe". This work has also received financial support from project PID2019-107663RB-I00 from the Spanish Ministry of Science and Innovation (MICINN). Cynthia Fontes-Candia is recipient of a pre-doctoral grant from CONACYT (MEX/Ref. 306680).

7 References

Agostinho, D. A. S., Paninho, A. I., Cordeiro, T., Nunes, A. V. M., Fonseca, I. M., Pereira, C., Matias, A., & Ventura, M. G. (2020). Properties of κ-carrageenan aerogels prepared by using different dissolution media and its application as drug delivery systems. *Materials Chemistry and Physics*, *253*, 123290. https://doi.org/10.1016/J.MATCHEMPHYS.2020.123290

Alavi, F., Emam-Djomeh, Z., Yarmand, M. S., Salami, M., Momen, S., & Moosavi-Movahedi, A. A. (2018). Cold gelation of curcumin loaded whey protein aggregates mixed with k-carrageenan: Impact of gel microstructure on the gastrointestinal fate of curcumin. *Food Hydrocolloids*, *85*, 267–280. https://doi.org/10.1016/j.foodhyd.2018.07.012

Ana-Isabel Mulet-Cabero, Lotti Egger, Reto Portmann, Olivia Ménard, Sébastien Marze, Mans Minekus, Feunteun, S. L., Anwesha Sarkar, M.-L. Grundy, M., Frédéric Carrière, Matt Golding, Didier Dupont, Isidra Recio, André Brodkorb, & Alan Mackie. (2020). A standardised semi-dynamic in vitro digestion method suitable for food – an international consensus. *Food & Function*, *11*(2), 1702–1720. https://doi.org/10.1039/C9FO01293A

Apong, P. E. (2019). Nutrition and Dietary Recommendations for Bodybuilders. In *Nutrition and enhanced sports performance* (pp. 737–750). Elsevier.

Benito-González, I., López-Rubio, A., Gómez-Mascaraque, L. G., & Martínez-Sanz, M. (2020). PLA coating improves the performance of renewable adsorbent pads based on cellulosic aerogels from aquatic waste biomass. *Chemical Engineering Journal*, 124607.

Bohn, T., Carriere, F., Day, L., Deglaire, A., Egger, L., Freitas, D., Golding, M., Feunteun, S. Le, Macierzanka, A., Menard, O., Miralles, B., Moscovici, A., Portmann, R., Recio, I., Rémond, D., Santé-Lhoutelier, V., Wooster, T. J., Lesmes, U., Mackie, A. R., & Dupont, D. (2017). Correlation between in vitro and in vivo data on food digestion. What can we predict with static in vitro digestion models? *Https://Doi.Org/10.1080/10408398.2017.1315362*, *58*(13), 2239–2261. https://doi.org/10.1080/10408398.2017.1315362

Brodkorb, A., Egger, L., Alminger, M., Alvito, P., Assunção, R., Ballance, S., Bohn, T., Bourlieu-Lacanal, C., Boutrou, R., Carrière, F., Clemente, A., Corredig, M., Dupont, D., Dufour, C., Edwards, C., Golding, M., Karakaya, S., Kirkhus, B., Le Feunteun, S., … Recio, I. (2019). INFOGEST static in vitro simulation of gastrointestinal food digestion. *Nature Protocols*, *14*(4), 991–1014. https://doi.org/10.1038/s41596-018-0119-1

Caron, J., Cudennec, B., Domenger, D., Belguesmia, Y., Flahaut, C., Kouach, M., Lesage, J., Goossens, J. F., Dhulster, P., & Ravallec, R. (2016). Simulated GI digestion of dietary protein: Release of new bioactive peptides involved in gut hormone secretion. *Food Research International*, *89*, 382–390. https://doi.org/10.1016/J.FOODRES.2016.08.033

Dallas, D. C., Sanctuary, M. R., Qu, Y., Khajavi, S. H., Van Zandt, A. E., Dyandra, M., Frese, S. A., Barile, D., & German, J. B. (2017). Personalizing protein nourishment. *Critical Reviews in Food Science and Nutrition*, *57*(15), 3313–3331.

de Jong, S., Klok, H. J., & van de Velde, F. (2009). The mechanism behind microstructure formation in mixed whey protein–polysaccharide cold-set gels. *Food Hydrocolloids*, *23*(3), 755–764. https://doi.org/10.1016/J.FOODHYD.2008.03.017

Egger, L., Ménard, O., Baumann, C., Duerr, D., Schlegel, P., Stoll, P., Vergères, G., Dupont, D., & Portmann, R. (2019). Digestion of milk proteins: Comparing static and dynamic in vitro digestion systems with in vivo data. *Food Research International*, *118*, 32–39. https://doi.org/10.1016/J.FOODRES.2017.12.049

Egger, L., Ménard, O., Delgado-Andrade, C., Alvito, P., Assunção, R., Balance, S., Barberá, R., Brodkorb, A., Cattenoz, T., Clemente, A., Comi, I., Dupont, D., Garcia-Llatas, G., Lagarda, M. J., Le Feunteun, S., JanssenDuijghuijsen, L., Karakaya, S., Lesmes, U., Mackie, A. R., … Portmann, R. (2016). The harmonized INFOGEST in vitro digestion method: From knowledge to action. *Food Research International*, *88*, 217–225. https://doi.org/10.1016/j.foodres.2015.12.006

Fontes-Candia, C., Erboz, E., Martínez-Abad, A., López-Rubio, A., & Martínez-Sanz, M. (2019). Superabsorbent food packaging bioactive cellulose-based aerogels from Arundo donax waste biomass. *Food Hydrocolloids*, *96*, 151–160.

Fontes-Candia, C., Lopez-Sanchez, P., Ström, A., Martínez, J. C., Salvador, A., Sanz, T., Trefna, H. D., López-Rubio, A., & Martínez-Sanz, M. (2021). Maximizing the oil content in polysaccharide-based emulsion gels for the development of tissue mimicking phantoms. *Carbohydrate Polymers*, *256*, 117496. https://doi.org/https://doi.org/10.1016/j.carbpol.2020.117496

Fontes-Candia, C., Ström, A., Gómez-Mascaraque, L. G., López-Rubio, A., & Martínez-Sanz, M. (2020). Understanding nanostructural differences in hydrogels from commercial carrageenans: Combined small angle X-ray scattering and rheological studies. *Algal Research*, *47*, 101882. https://doi.org/https://doi.org/10.1016/j.algal.2020.101882

Fontes-Candia, C., Ström, A., Lopez-Sanchez, P., López-Rubio, A., & Martínez-Sanz, M. (2020).

Rheological and structural characterization of carrageenan emulsion gels. *Algal Research*, *47*, 101873. https://doi.org/https://doi.org/10.1016/j.algal.2020.101873

Gombotz, W. R., & Wee, S. F. (2012). Protein release from alginate matrices. *Advanced Drug Delivery Reviews*, *64*(SUPPL.), 194–205. https://doi.org/10.1016/J.ADDR.2012.09.007

Huppertz, T., Vaia, B., & Smiddy, M. A. (2008). Reformation of casein particles from alkaline-disrupted casein micelles. *Journal of Dairy Research*, *75*(1), 44–47. https://doi.org/10.1017/S0022029907002956

Jarunglumlert, T., Nakagawa, K., & Adachi, S. (2015). Influence of aggregate structure of casein on the encapsulation efficiency of β-carotene entrapped via hydrophobic interaction. *Food Structure*, *5*, 42–50. https://doi.org/10.1016/J.FOOSTR.2015.05.001

Juvonen, K. R., Karhunen, L. J., Vuori, E., Lille, M. E., Karhu, T., Jurado-Acosta, A., Laaksonen, D. E., Mykkänen, H. M., Niskanen, L. K., Poutanen, K. S., & Herzig, K.-H. (2011). Structure modification of a milk protein-based model food affects postprandial intestinal peptide release and fullness in healthy young men. *British Journal of Nutrition*, *106*(12), 1890–1898. https://doi.org/DOI: 10.1017/S0007114511002522

Koutina, G., Ray, C. A., Lametsch, R., & Ipsen, R. (2018). The effect of protein-to-alginate ratio on in vitro gastric digestion of nanoparticulated whey protein. *International Dairy Journal*, *77*, 10–18. https://doi.org/10.1016/J.IDAIRYJ.2017.09.001

Li, S., Hu, Q., Chen, C., Liu, J., He, G., Li, L., Wu, J., & Ren, D. (2020). Formation of bioactive peptides during simulated gastrointestinal digestion is affected by αs1-casein polymorphism in buffalo milk. *Food Chemistry*, *313*, 126159.

Li, Xianghong, Hua, Y., Qiu, A., Yang, C., & Cui, S. (2008). Phase behavior and microstructure of preheated soy proteins and κ-carrageenan mixtures. *Food Hydrocolloids*, *22*(5), 845–853. https://doi.org/10.1016/J.FOODHYD.2007.04.008

Li, Xiaoqiang, Su, Y., Liu, S., Tan, L., Mo, X., & Ramakrishna, S. (2010). Encapsulation of proteins in poly(l-lactide-co-caprolactone) fibers by emulsion electrospinning. *Colloids and Surfaces B: Biointerfaces*, *75*(2), 418–424. https://doi.org/10.1016/j.colsurfb.2009.09.014

Manzocco, L., Valoppi, F., Calligaris, S., Andreatta, F., Spilimbergo, S., & Nicoli, M. C. (2017). Exploitation of κ-carrageenan aerogels as template for edible oleogel preparation. *Food Hydrocolloids*, *71*, 68–75. https://doi.org/https://doi.org/10.1016/j.foodhyd.2017.04.021

Markussen, J. Ø., Madsen, F., Young, J. F., & Corredig, M. (2021). A semi dynamic in vitro digestion study of milk protein concentrate dispersions structured with different polysaccharides. *Current Research in Food Science*, *4*, 250–261. https://doi.org/10.1016/J.CRFS.2021.03.012

Martínez-Sanz, M., Ström, A., Lopez-Sanchez, P., Knutsen, S. H., Ballance, S., Zobel, H. K., Sokolova, A., Gilbert, E. P., & López-Rubio, A. (2020). Advanced structural characterisation of agar-based hydrogels: Rheological and small angle scattering studies. *Carbohydrate Polymers*, *236*, 115655. https://doi.org/https://doi.org/10.1016/j.carbpol.2019.115655

McClements, D. J. (2017). Recent progress in hydrogel delivery systems for improving nutraceutical bioavailability. *Food Hydrocolloids*, *68*, 238–245. https://doi.org/10.1016/J.FOODHYD.2016.05.037

Miralles, B., Sanchón, J., Sánchez-Rivera, L., Martínez-Maqueda, D., Le Gouar, Y., Dupont, D., Amigo, L., & Recio, I. (2021). Digestion of micellar casein in duodenum cannulated pigs. Correlation between in vitro simulated gastric digestion and in vivo data. *Food Chemistry*, *343*, 128424. https://doi.org/10.1016/j.foodchem.2020.128424

Mouécoucou, J., Villaume, C., Sanchez, C., & Méjean, L. (2004). β-Lactoglobulin/polysaccharide interactions during in vitro gastric and pancreatic hydrolysis assessed in dialysis bags of different molecular weight cut-offs. *Biochimica et Biophysica Acta (BBA) - General Subjects*, *1670*(2), 105–112. https://doi.org/10.1016/J.BBAGEN.2003.10.017

Ozel, B., Zhang, Z., He, L., & McClements, D. J. (2020). Digestion of animal- and plant-based proteins encapsulated in κ-carrageenan/protein beads under simulated gastrointestinal conditions. *Food Research International*, *137*, 109662. https://doi.org/https://doi.org/10.1016/j.foodres.2020.109662

Putney, S. D. (1998). Encapsulation of proteins for improved delivery. *Current Opinion in Chemical Biology*, *2*(4), 548–552. https://doi.org/10.1016/S1367-5931(98)80133-6

Sanchón, J., Fernández-Tomé, S., Miralles, B., Hernández-Ledesma, B., Tomé, D., Gaudichon, C., & Recio, I. (2018). Protein degradation and peptide release from milk proteins in human jejunum. Comparison with in vitro gastrointestinal simulation. *Food Chemistry*, *239*, 486–494. https://doi.org/10.1016/j.foodchem.2017.06.134

Santos-Hernández, M., Tomé, D., Gaudichon, C., & Recio, I. (2018). Stimulation of CCK and GLP-1 secretion and expression in STC-1 cells by human jejunal contents and in vitro gastrointestinal digests from casein and whey proteins. *Food and Function*, *9*(9), 4702–4713. https://doi.org/10.1039/c8fo01059e

Xie, J., & Wang, C.-H. (2007). Encapsulation of proteins in biodegradable polymeric microparticles using electrospray in the Taylor cone-jet mode. *Biotechnology and Bioengineering*, *97*(5), 1278–1290. https://doi.org/10.1002/BIT.21334

Yuan, D., Jacquier, J. C., & O'Riordan, E. D. (2018). Entrapment of proteins and peptides in chitosan-polyphosphoric acid hydrogel beads: A new approach to achieve both high entrapment efficiency and controlled in vitro release. *Food Chemistry*, *239*, 1200–1209. https://doi.org/10.1016/J.FOODCHEM.2017.07.021

Zhang, Z., Zhang, R., & McClements, D. J. (2017). Control of protein digestion under simulated gastrointestinal conditions using biopolymer microgels. *Food Research International*, *100*, 86–94. https://doi.org/10.1016/J.FOODRES.2017.08.037

Zhang, Z., Zhang, R., Zou, L., & McClements, D. J. (2016). Protein encapsulation in alginate hydrogel beads: Effect of pH on microgel stability, protein retention and protein release. *Food Hydrocolloids*, *58*, 308–315. https://doi.org/10.1016/J.FOODHYD.2016.03.015

8 Supplementary Material

Table S1. Weight fraction, protein content determined by elemental analysis and calculated protein fraction for the solid and liquid fractions from the non-encapsulated casein, the polysaccharide-casein controls and the different polysaccharide-casein gel-like structures after the gastric and intestinal digestion phases.

Sample	Phase	Weight fraction (w/w %)	Protein (w/w %)	Protein fraction (w/w %)
Casein	G	100	53.19 ± 0.78	100
	I	100	52.61 ± 0.32	100
C-A25	G	100	53.91 ± 3.83	100
	I	100	52.22 ± 5.80	100
C-A75	G	100	28.00 ± 2.86	100
	I	100	42.39 ± 6.34	100
HG-A25	GS	53.41 ± 8.70	41.80 ± 3.02	47.38 ± 8.50
	GL	46.59 ± 8.70	53.44 ± 3.01	52.62 ± 8.50
	IS	17.26 ± 1.80	42.44 ± 3.72	13.95 ± 1.02
	IL	82.74 ± 1.80	54.42 ± 2.84	86.05 ± 1.02
HG-A75	GS	84.30 ± 0.21	17.62 ± 0.83	67.44 ± 1.57
	GL	15.70 ± 0.21	46.53 ± 2.05	32.56 ± 1.57
	IS	52.96 ± 0.44	28.38 ± 1.802	39.19 ± 2.16
	IL	47.04 ± 0.44	50.76 ± 4.27	60.81 ± 2.16
AG-A25	GS	32.70 ± 5.06	29.93 ± 6.56	20.00 ± 8.62
	GL	67.30 ± 5.06	59.67 ± 1.98	80.00 ± 8.62
	IS	10.73 ± 0.69	30.14 ± 1.52	7.15 ± 0.62
	IL	89.27 ± 0.69	47.12 ± 1.94	92.85 ± 0.62
AG-A75	G	100	21.29 ± 2.32	100
	IS	83.99 ± 0.01	39.31 ± 1.54	78.38 ± 4.26
	IL	16.01 ± 0.01	48.54 ± 2.67	21.62 ± 4.26

Sample	Phase	Weight fraction (w/w %)	Protein (w/w %)	Protein fraction (w/w %)
C- KC25	G	100	46.69 ± 1.42	100
	I	100	41.52 ± 1.22	100
C- KC75	G	100	24.79 ± 1.02	100
	I	100	39.52 ± 3.37	100
HG-KC25	GS	40.46 ± 6.19	48.67 ± 3.96	44.02 ± 3.66
	GL	59.54 ± 6.19	42.29 ± 6.50	55.98 ± 3.66
	IS	14.33 ± 2.16	37.11 ± 0.78	12.50 ± 2.73
	IL	85.67 ± 2.16	43.52 ± 1.19	87.50 ± 2.73
HG-KC75	GS	83.74 ± 1.29	14.61 ± 1.72	69.01 ± 3.85
	GL	16.26 ± 1.29	33.51 ± 1.72	30.99 ± 3.85
	IS	51.13 ± 1.43	24.68 ± 1.48	37.19 ± 2.20
	IL	48.87 ± 1.43	43.59 ± 1.52	62.81 ± 2.20
AG-KC25	GS	51.46 ± 4.50	44.07 ± 1.16	45.19 ± 4.91
	GL	60.23 ± 4.50	56.60 ± 1.65	54.81 ± 4.91
	IS	13.11 ± 2.93	36.58 ± 2.53	10.61 ± 3.02
	IL	86.89 ± 2.93	46.89 ± 1.51	89.39 ± 3.02
AG-KC75	GS	74.90 ± 5.90	17.41 ± 1.89	56.50 ± 7.12
	GL	25.10 ± 5.90	40.57 ± 4.99	43.50 ± 7.12
	IS	42.41 ± 5.25	25.89 ± 3.81	30.02 ± 7.11
	IL	57.59 ± 5.25	44.54 ± 2.07	69.97 ± 7.11

GS: gastric solid; GL: gastric liquid; IS: intestinal solid; IL: intestinal liquid; G: one-phase homogeneous gastric digest; I: one-phase homogeneous intestinal digest.

Table S2. Gel strength values of agar and κ-carrageenan hydrogels.

Sample	Gel strength (N)
HG-A25	$0.59^{b} \pm 0.06$
HG-A75	$4.32^{a} \pm 0.20$
HG-KC25	$0.79^{b} \pm 0.06$
HG-KC75	$4.54^{a} \pm 0.61$

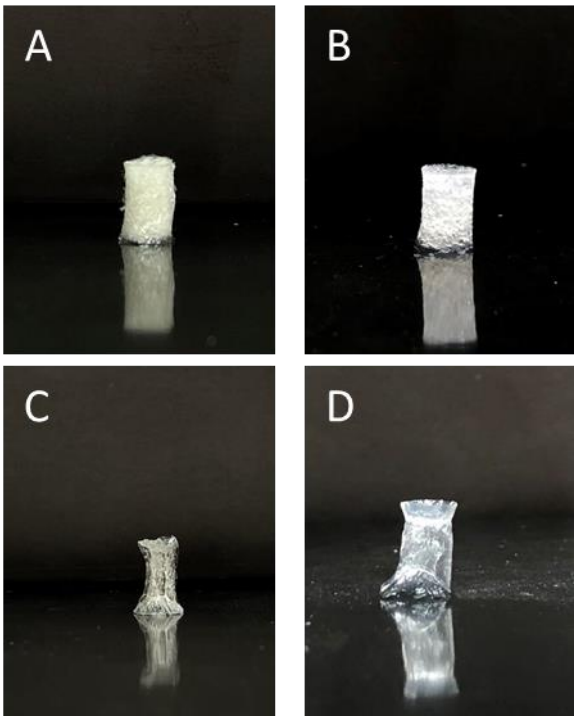

Figure S1. Visual appearance of the pure polysaccharide aerogels from agar (A) and κ-carrageenan (C) and the corresponding solid phases obtained after rehydration in SGF (agar (B), κ-carrageenan (D)).

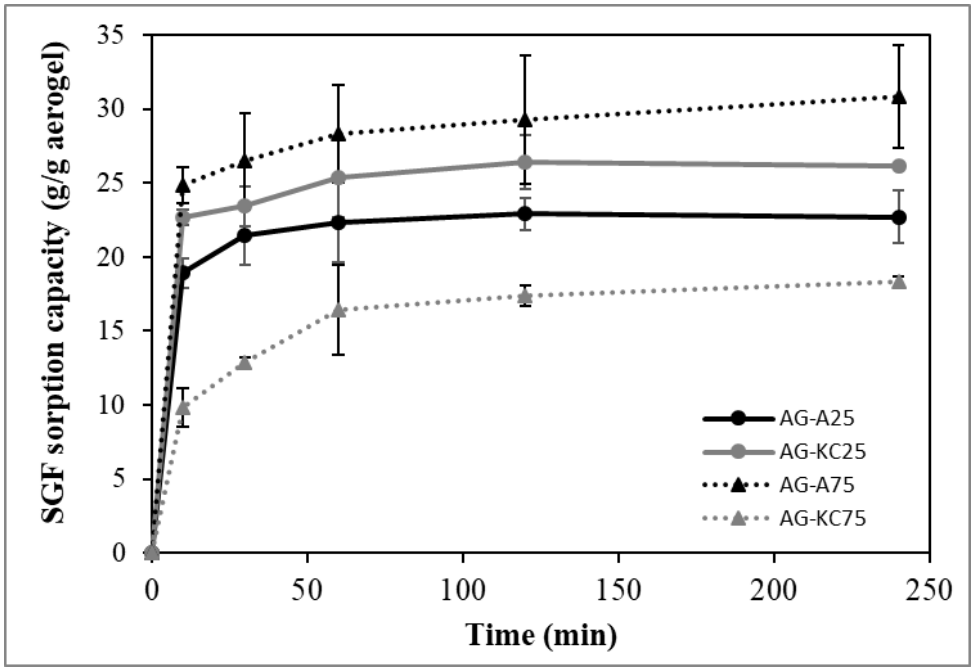

Figure S2. SGF sorption kinetics of the polysaccharide-casein aerogels.

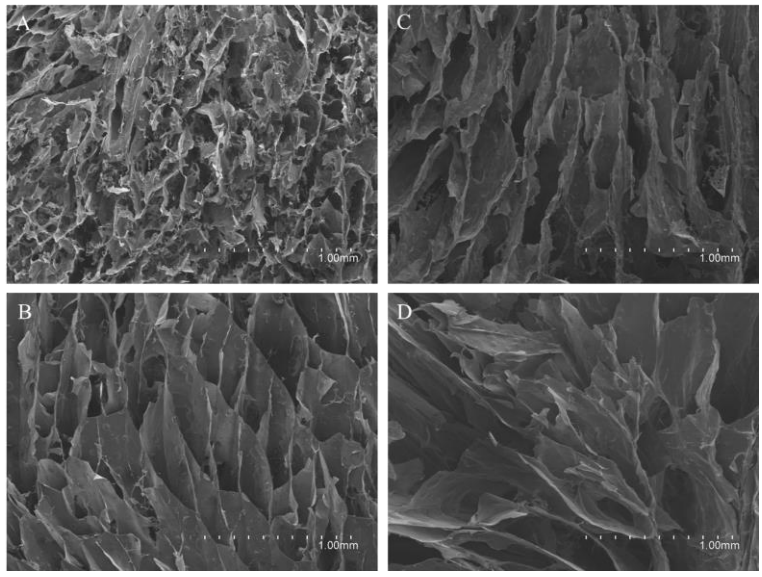

Figure S3. SEM micrographs of the surface from the polysaccharide-casein aerogels. (A) AG-A25, (B) AG-A75, (C) AG-KC25 and (D) AG-KC75.

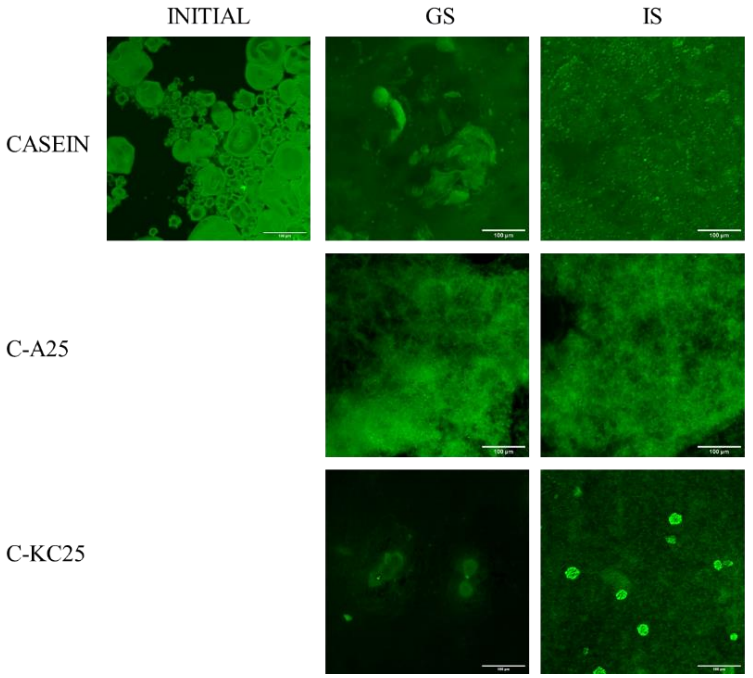

Figure S4. Confocal laser microscopy images of the non-encapsulated casein and the control polysaccharide-casein blends with a polysaccharide:protein ratio of 25:75 after the gastric and intestinal digestions.

Figure S5. Peptide patterns from β-casein, α_{s1}-casein identified in the liquid phase from the intestinal digests of control casein and the polysaccharide-protein gel-like structures with a polysaccharide:protein ratio of 25:75. The colour coding ranges from red (representing the highest number of identified amino acids within a peptide of the corresponding protein) to yellow and green (representing the intermediate to lowest numbers of identified amino acids). White regions represent amino acids without identification within any peptide.

CHAPTER 2

CELLULOSIC AEROGELS AS ADSORBENT PACKAGING STRUCTURES

3.2.1 Superabsorbent food packaging bioactive cellulose-based aerogels from *Arundo donax* waste biomass

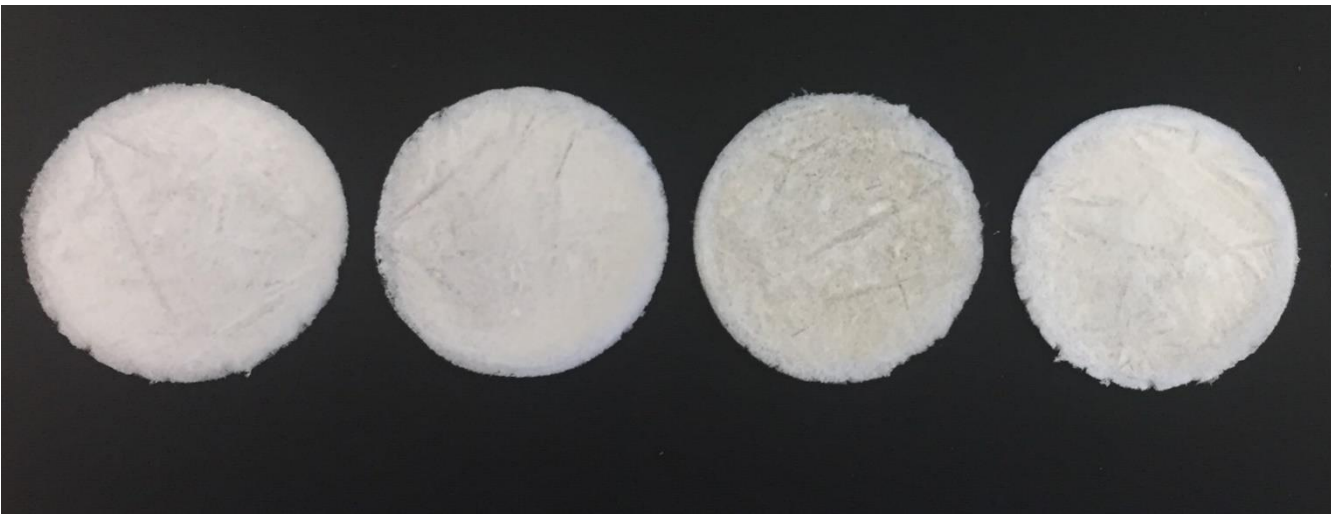

INTRODUCTION TO CHAPTER 2

The recent concerns associated to the massive use of conventional petroleum-based plastics are motivating the search for more sustainable bio-based materials in the food packaging area. Furthermore, current trends in the sector are moving towards the development of packaging structures able to extend the shelf-life of food products and provide added functionalities. One example of packaging structures which are typically used to maintain the quality of fresh food products are the absorption pads, which are manufactured using synthetic polymers. In this chapter, we developed highly porous aerogels by valorizing the waste biomass from *Arundo donax*, an invasive aquatic plant. To do so, a sequential extraction protocol was applied to stems and leaves to generate cellulosic fractions with different purification degrees. Additionally, the water-soluble fraction was utilized to generate bioactive extracts. The obtained cellulosic fractions and the aqueous extracts were then combined to develop superabsorbent bioactive aerogels. The properties of these materials were characterized and finally, their potential as absorbent pads for meat quality preservation were evaluated.

3.2.1

SUPERABSORBENT FOOD PACKAGING BIOACTIVE CELLULOSE-BASED AEROGELS FROM *Arundo donax* WASTE BIOMASS

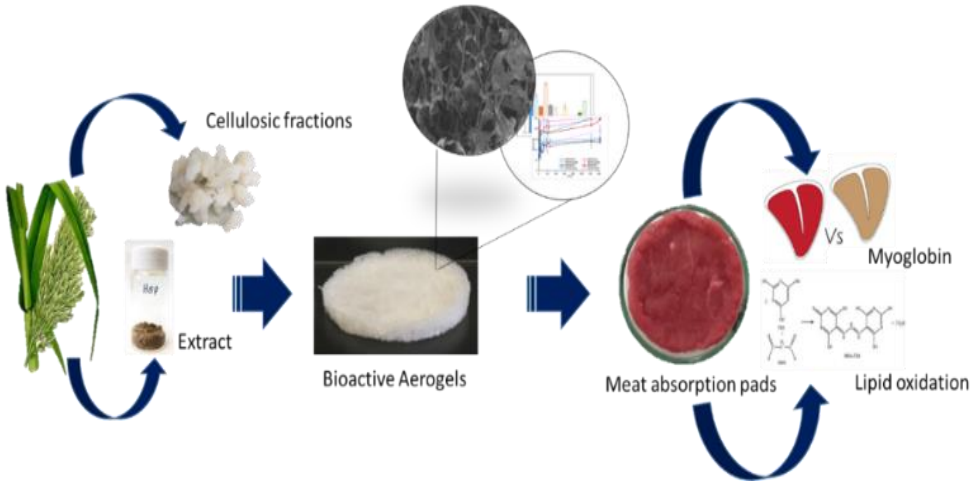

This section is an adapted version of the following published research article:

Fontes-Candia, C., Erboz, E., Martínez-Abad, A., López-Rubio, A., & Martínez-Sanz, M. (2019). Superabsorbent food packaging bioactive cellulose-based aerogels from *Arundo donax* waste biomass. Food Hydrocolloids, 96, 151-160

---

1 Abstract

Arundo donax waste biomass has been valorized for the extraction of cellulosic fractions with different purification degrees, as well as aqueous bioactive extracts, which were then combined to develop superabsorbent bioactive aerogels. All the developed aerogels presented excellent water and oil sorption capacities; however, the presence of hemicelluloses yielded more porous and hydrophilic aerogels, capable of absorbing more water. With regards to the aqueous extracts, the hot water treatment (HW) of *A. donax* stems promoted the extraction of polysaccharides and polyphenols, producing the extract (S-HW) with the highest antioxidant capacity. This extract was then incorporated into the aerogels produced from the less purified stem fractions (F2A and F3A), which were chosen due to their good water sorption capacity, higher antioxidant potential and lower production costs and environmental impact. The hybrid aerogels showed a great potential to be used as bioactive pads for food packaging. In particular, the F2A+S-HW aerogel would be the most optimum choice since it provides a complete release of the extract in hydrophilic media, as demonstrated by *in vitro* release and β-carotene bleaching inhibition studies, and it is able to reduce the colour loss and lipid oxidation in red meat upon refrigerated storage to a greater extent.

2 Introduction

In the context of the extremely demanding market within the food industry, packaging plays a crucial role, not only protecting the product from the external environment and maintaining food quality to extend products' shelf life, but also being able to provide added functionalities, such as the incorporation of health-beneficial compounds (e.g. antioxidants) which can improve the nutritional value of the packaged product. Accordingly, strategies based on the controlled release of bioactive compounds from the package towards the food product, are being extensively investigated. For instance, some studies have reported on the incorporation of bioactive extracts into packaging films to preserve meat quality and organoleptic properties(Barbosa-Pereira et al., 2014; Bolumar et al., 2011; Camo et al., 2011; Jofré et al., 2008; Lorenzo et al., 2014), demonstrating that the processes of lipid oxidation and colour loss upon storage could be reduced through the antioxidant activity of the incorporated extracts.

In the particular case of meat packaging, absorption pads are commonly used as moisture control elements, which absorb the excess liquids released by meat upon storage. These pads are typically made of a non-permeable/non-stick synthetic polymer, such as polyethylene and a hydrophilic non-woven bottom layer filled with active substances which prevent bacterial growth, such as citric acid and sodium bicarbonate (McMillin, 2017). Given the severe environmental issues associated to the production and use of synthetic plastics, current trends in the food packaging sector are clearly moving towards the utilization of more sustainable bio-based and renewable materials, i.e. biopolymers. Polysaccharides and, in particular, lignocellulosic materials, have already demonstrated their great potential to develop high performance bio-based packaging structures (Benito-González et al., 2018; Martínez-Sanz et al., 2018; Rampazzo et al., 2017; Satyanarayana et al., 2009). Lignocellulosic materials can be extracted from multiple sources such as terrestrial and aquatic plants, seaweeds and agriculture and forestry-derived waste by-products (Djalal Trache et al., 2017). However, the extraction from waste or underutilized resources that do not compete with the food chain is particularly interesting and in line with the principles of circular economy. For instance, lignocellulosic fractions have been extracted from waste biomass derived from the aquatic plant *Posidonia oceanica* (Benito-González et al., 2018) and the aquatic invasive species *Arundo donax* (Martínez-Sanz et al., 2018).

In addition to other polysaccharides, cellulosic materials have been used to produce aerogel structures, which are extremely light, highly porous materials, with low density, large surface area and high water sorption capacity (Henschen et al., 2016; Wang et al., 2016). Due to their large inner surface areas and high surface-to-volume ratios, these aerogels may be suitable for the development of controlled release systems. In fact, cellulose aerogels from different vegetal and bacterial sources have already demonstrated their potential as templates for the incorporation and sustained release of drugs (Haimer et al., 2010; Valo et al., 2013), although their application in the food area has not been evaluated yet. One of the issues associated to the production of cellulose aerogels is that they are typically obtained by means of a complex synthesis method involving multiple steps: (i) dissolution of cellulose through the disruption of its crystalline structure, (ii) gelation, (iii) cellulose regeneration, (iv) solvent exchange and (v) a

final drying step such as freeze-drying or supercritical drying (Gavillon & Budtova, 2007; Innerlohinger et al., 2006). Such process presents two main drawbacks: the high production costs and the unsuitability of the produced aerogels for food-grade applications due to the use of organic solvents.

In this work, the possibility of producing cellulose-based aerogels using a simple freeze-drying method from aqueous suspensions of cellulosic fractions from *A. donax* waste biomass with different purification degrees has been explored. To further valorize this waste biomass, aqueous extracts were produced by simple heating and ultrasound protocols and their composition and antioxidant capacity was evaluated. Finally, the most active extract was incorporated into selected aerogels to investigate the extract release and the antioxidant capacity of the hybrid structures, as well as to evaluate them as bioactive superabsorbent pads to preserve the quality of packaged red meat by reducing colour loss and lipid oxidation processes.

3 Materials and methods

3.1 Materials

Arundo donax (*A. donax*) was collected from a freshwater environment in Buñol, Valencia (Spain) in September 2017. The leaves were separated from the stems and the material was washed vigorously with water, ground with an electric blender and stored at 4 °C until use.

Gallic acid (97.5-102.5%), hydrochloric acid (37%), sulphuric acid (≥97.5%), potassium sulphate, potassium persulphate (≥99%), potassium chloride (99%), phosphate buffered saline tablets, ABTS (≥98%) and 6-hydroxy-2,5,7,8- tetramethyl chroman-2-carboxylic acid (97%), β- carotene (≥97%), linoleic acid (≥99%), Tween® 40, 2-Thiobarbituric acid (98%), ethylenediaminetetraacetic acid disodium salt dehydrate (98.5-101.5%), propyl gallate, were obtained from Sigma-Aldrich (Spain). Sodium chlorite 80% was obtained from Acros organics (Spain). The Folin-Ciocalteau reagent, modified Lowry reagent and bovine serum albumin were obtained from the “modified Lowry protein assay kit” purchased from Thermo Fisher scientific (Spain).

3.2 Preparation of holocellulosic fractions

A purification procedure previously reported (Martínez-Sanz et al., 2018) for the extraction of holocellulosic fractions from *A. donax* leaves and stems was applied, generating six different fractions labelled as F2, F3, F2A, F3A, F2L and F3L.

Briefly, the stem biomass was subjected to a Soxhlet treatment, followed by a de-lignification step with $NaClO_2$, obtaining F2. After that, the hemicelluloses were removed by means of alkali treatment with KOH, yielding F3. The same process, but omitting the initial Soxhlet treatment, was carried out to produce the fractions labelled as F2A and F3A (obtained from the stem biomass) and F2L and F3L (obtained from the leaf biomass). The obtained fractions were stored in the fridge as partially hydrated materials until use.

3.3 Production of water-soluble extracts from *Arundo donax*

Water-soluble extracts were generated from *A. donax* leaves and stems, using two different methods: (i) Hot water extraction (HW) and (ii) ultrasound-assisted extraction (US).

For the hot water extraction, 10 g of leaf or stem biomass (dry weight basis) were added to 200 mL of distilled water and mixed in a blender until a paste was obtained. The material was then heated up to 90 ºC and kept at a constant temperature and under stirring for 1 h. After that, the material was centrifuged at 12500 rpm and 15ºC for 20 min. The supernatant was separated, placed in an ice bath and the required volume of ethanol (75% with regards to the volume of aqueous supernatant v/v) was slowly added. The material was kept stirring in the ice bath overnight and after that, centrifuged again (12500 rpm, 15ºC, 20 min). The precipitate was collected, re-suspended in distilled water and freeze-dried. The obtained powder extracts were labelled as S-HW (stem biomass) and L-HW (leaf biomass).

For the ultrasound-assisted extraction, 10 g of leaf or stem biomass (dry weight basis) were added to 200 mL of distilled water, mixed in a blender and subjected to an ultrasound treatment with a probe UP-400S (Hielcher GmbH, Germany) operating at a maximum power of 400W and a constant frequency of 24 kHz for 30min. After that, the material was centrifuged (12500 rpm, 15ºC, 20 min) and processed following the same procedure described for the hot water extraction. The obtained powder extracts were labelled as S-US (stem biomass) and L-US (leaf biomass). All the extracts were stored at 0% RH until further use.

3.4 Preparation of aerogels

Pure cellulosic aerogels were prepared by adding 0.075 g of the different fractions (dry weight) to 15 mL of distilled water and dispersing them by ultra-turrax homogenization until obtaining homogeneous suspensions. These were then poured into Petri dishes (diameter of 6 cm), frozen at -80 °C and subsequently, freeze-dried using a Genesis 35-EL freeze-dryer (Virtis). For the production of bioactive aerogels, 0.015 g of water-soluble extract (ca. 17 wt.-% with regards to the total solids content) were dispersed together with the corresponding lignocellulosic fraction. In order to assess the effect of the material porosity the same formulations used to produce the bioactive aerogels were utilized to generate films by a vacuum filtration method, as previously described (Martínez-Sanz et al., 2018). The produced aerogels and films were stored at 0% RH.

3.5 Density of aerogels

Aerogel densities were determined by measuring the weight and volume of each individual aerogel. The weight of each aerogel was measured by an analytical balance (Precisa Gravimetrics AG SERIES 320XB, Dietikon, Switzerland) and the dimensions were measured by a digital caliper at three different positions.

3.6 Scanning electron microscopy (SEM)

Aerogel samples were coated with a gold-palladium mixture under vacuum and their morphology was studied using a Hitachi microscope (Hitachi S-4800) at an accelerating voltage of 10kV and a working distance of 8-16 mm.

3.7 Water vapour sorption

The water vapour sorption capacity of the aerogels was evaluated by registering the weight gain, using an analytical balance, when placing the samples in a cabinet equilibrated at 25 ºC and 100 % RH. Square samples with a total surface area of 6.25 cm^2 were cut from the aerogels and their initial weight was registered. The assays were carried out at least in triplicate.

3.8 Water and oil sorption and desorption

Square specimens with a total surface area of 1 cm^2 were cut, weighed and immersed in sealed containers containing 15 mL of distilled water or soybean oil. The samples were periodically taken out of the liquid and weighed after removing the liquid excess. Measurements were taken until the samples were equilibrated and the total weight gain was calculated. After equilibration, the samples were removed from the liquid, placed on top of absorbent paper and left drying at ambient conditions. The weight was registered periodically, until it was constant. The water and oil retention was calculated from the difference between the weight after drying and the initial weight of the samples, before soaking them in the liquids.

3.9 Determination of extract composition

The total phenolic compounds in the water-soluble extracts from *A. donax* were estimated by the Folin-Ciocalteau colorimetric assay (Singleton et al., 1999) and the results were expressed as mg gallic acid (GA)/g extract. The total protein content was measured following the Lowry method (Lowry et al., 1951) and the results were expressed as mg bovine serum albumin (BSA)/g extract. The total carbohydrate content was determined after sulphuric acid hydrolysis, following the method described in (Martínez-Abad et al., 2018). A detailed description of these protocols can be found elsewhere (Martínez-Sanz et al., 2019). All the determinations were carried out in triplicate.

3.10 ABTS Assay

The radical cation scavenging activity of the different lignocellulosic fractions and the water-soluble extracts was determined according to (Re et al., 1999). Briefly, 0.192 g of ABTS were dissolved in 50 mL of PBS at pH = 7.4 and mixed with 0.033 g of potassium persulfate overnight in the dark to yield the $ABTS^{\cdot+}$ radical cation. Prior to use in the assay, the $ABTS^{\cdot+}$ was diluted with PBS for an initial absorbance of ~0.700 ± 0.02 (1:50 ratio) at 734 nm, at room temperature. Free radical scavenging activity was assessed by mixing 1.0 mL diluted $ABTS^{\cdot+}$ with 10 µL of aqueous suspensions of the samples (5 mg/mL) and monitoring the change in absorbance at 0, 1, 5, 10 min and 24 h. A calibration curve was developed by using 6-Hydroxy-2,5,7,8-

tetramethylchromane-2-carboxylic acid (Trolox). The antioxidant capacity of test extracts was expressed as mg Trolox equivalents (TE)/g extract. All determinations were carried in triplicate.

3.11 β-Carotene-linoleic acid assay

The antioxidant capacity of the extracts and the generated aerogels was evaluated by the β-carotene-linoleic acid assay, according to (Martins et al., 2013), with minor modifications. In brief, 2 mg of β-carotene was dissolved in 10 mL of chloroform. 2 mL of this solution were placed on a rotary evaporator and the chloroform was evaporated. Then, 50 µL of linoleic acid and 400 mg of Tween 40 were added and the content of the flask was mixed with stirring. After that, 100 mL of aerated distilled water was transferred to the flask and stirred vigorously. 0.5 mL of ethanolic solutions of the extracts (0.5- 5 mg/mL), BHT (0.5 mg/mL), or 0.5 mL of ethanol as a control were transferred to test tubes and then 5 mL of the β-carotene emulsion were added. For testing the bioactive aerogels, 25 mg of sample was transferred to the tubes and 5 mL of the β-carotene emulsion were added. The samples were incubated in a water bath at 50 °C for 120 min. The absorbance of each sample at 470 nm was measured every 15 minutes using a spectrophotometer. The determinations were carried out in duplicate.

3.12 *In vitro* release assays

In vitro release assays were carried out for the bioactive aerogels and films using water and ethanol as the release media. 10 mg of the films and aerogels were soaked in 2 mL of ethanol or water at room temperature. At appropriate time intervals, the concentration of the extract in the release media was estimated by measuring the absorbance of the supernatant at a wavelength of 271 nm using a NanoDrop ND1000 spectrophotometer (Thermo Fisher Scientific, USA), until equilibrium was reached.

A calibration curve was previously built by recording the whole spectra of the extract diluted in water and ethanol at concentrations ranging from 0.1 mg/mL to 0.5 mg/mL. The obtained data were used to determine the total amount of the extract released from the samples at each time point, taking into account that the maximum concentration of extract, if 100% release occurred, was 0.85 mg/mL ($\frac{10\ mg\ aerogel/film}{2\ mL\ H2O/etOH} \cdot \frac{17\ mg\ extract}{100\ mg\ aerogel/film}$). Three independent replicates of each sample were analyzed.

3.13 Evaluation of the antioxidant effect of bioactive aerogels on red meat

Bioactive aerogels containing the S-HW extract (F2A + S-HW and F3A + S-HW) and the respective control samples (F2A and F3A) were tested as absorption pads for the preservation of red meat. The aerogels were placed covering the bottom surface of glass Petri dishes (diameter=6 cm) and portions of ca. 12 g of minced beef meat were placed on top of the aerogels. The samples were then sealed with plastic wrap film and stored in the fridge at 4 °C for 10 days. Control samples were prepared by using commercial meat pads and blank samples were prepared by adding the same amount of meat to Petri dishes with no pads.

3.13.1 Determination of oxymyoglobin and metmyoglobin

The ability of the aerogels to prevent the colour loss in the red meat after storage was evaluated through the determination of the oxymyoglobin and metmyoglobin content proportions in the raw red meat and in the samples after refrigerated storage for 10 days by following the procedure described by Carlez et al. (Carlez et al., 1995). Briefly, two grams of minced meat samples were homogenized with 20 mL of 0.04 mol/L potassium phosphate buffer (pH=6.8). The homogenized samples were kept in an ice bath for 1 h and after that, they were centrifuged at 4200 rpm and 10 °C for 30 minutes. The supernatant was then filtered using 0.45 µm pore size filters (Nylon, OlimPeak) and the volume of the filtrate was adjusted to 25 mL with the same phosphate buffer. The absorbance of the supernatant was measured at 525, 545, 565 and 572 nm in a spectrophotometer. The concentrations of oxymyoglobin and metmyoglobin were calculated using the following equations:

$$\%\, MbO2 = (0.882\, R\_1 - 1.267\, R\_2 - 0.809\, R\_3 + 0.361) \times 100 \quad (1)$$

$$\%\, MetMb = (-2.541\, R1 + 0.777\, R_2 + 0.800\, R_3 + 1.098) \times 100 \quad (2)$$

Where R1, R2, R3 are the absorbance ratios A^{572}/A^{525}, A^{565}/A^{525}, A^{545}/A^{525}, respectively. All the determinations were done in triplicate.

3.13.2 Measurement of lipid oxidation

The degree of lipid oxidation in the red meat samples after 10 days of storage was also measured by following the 2-thiobarbituric acid (TBA) distillation method (Tang et al., 2001).

10.0 g of meat were homogenised with 30 mL of water. The sample was then transferred to a distillation flask with 65 mL of water and the pH was adjusted to 1.5 with HCl 4N. Ethanolic propyl gallate (10%, 1mL), 10% EDTA (disodium salt, 1 mL), and a drop of antifoaming agent were added. The flask was connected to a Soxhlet apparatus and the mixture was boiled until 50 mL of distillate was collected. In a screw capped test tube, 5 mL of the distillate was reacted with 5 mL of TBA reagent (0.02 M TBA in 90% acetic acid) in a boiling water bath for 35 min. A control made up of 5 mL distilled water and 5 mL of TBA reagent was also boiled for 35 min. The tubes were cooled to room temperature and the absorbance was measured at 535 nm in a spectrophotometer. The TBA reactive substances (TBARS) were calculated by multiplying the absorbance readings by a factor of 7.8 and expressed as mg malondialdehyde (MDA)/Kg meat. The inhibition of lipid oxidation was calculated as follows:

$$Inhibition\ (\%) = \frac{(TBARS_{Blank} - TBARS_{Day\ 0}) - (TBARS_{Pad} - TBARS_{Day\ 0})}{(TBARS_{Blank} - TBARS_{Day\ 0})} \times 100 \quad (3)$$

Where $TBARS_{Day\ 0}$ refers to the TBARS in the raw minced meat and $TBARS_{Blank}$ and $TBARS_{Pad}$ correspond to the TBARS in the meat samples after 10 days of refrigerated storage (blank sample and samples with the commercial or the cellulosic aerogel pads, respectively). These determinations were carried out in triplicate.

3.14 Statistics

All data have been represented as the average ± standard deviation. Different letters show significant differences both in tables and graphs ($p \leq 0.05$). Analysis of variance (ANOVA) followed by a Tukey-test were used when comparing more than two data sets.

4 Results and discussions

4.1 Characterization of cellulosic aerogels

Aquatic biomass from the invasive species *A. donax* was valorized for the extraction of different holocellulosic fractions, as described in a previous work (Martínez-Sanz et al., 2018). These fractions were previously used to produce films by a simple vacuum filtration method and their properties were seen to be significantly different depending on the source (stems vs. leaves) and the extraction protocol (Martínez-Sanz et al., 2018). In this work, the extracted fractions were dispersed in water and subsequently freeze-dried to generate aerogel structures. As

shown in Figure 1A, the obtained aerogels consisted of whitish sponge-like materials, with a soft consistency but good mechanical integrity (see also Figure S1). The aerogels obtained from the leaf fractions (F2L and F3L) were more heterogeneous than the homologous aerogels obtained from the stem fractions (F2A and F3A). In particular, the F2L aerogel presented a very soft consistency and poor integrity. It was also observed that the more purified cellulose aerogels presented a whiter coloration than the less purified ones. Specifically, the presence of hemicelluloses and lipids in the F2A and F2L aerogels conferred them a brownish hue.

The morphology of the aerogels was characterized by SEM and representative images are shown in Figure 1B. As observed, in general the aerogels presented an open porous network structure. It appears that those aerogels composed of fractions where the hemicelluloses had been removed (i.e. F3, F3A and F3L) presented a more compacted structure with less pores than their analogous aerogels containing hemicelluloses. Comparing the aerogels obtained from fractions extracted with (F2 and F3) and without (F2A and F3A) the Soxhlet treatment, it seems that the presence of lipidic impurities also promoted the formation of slightly more porous structures. Moreover, it should be noted that the aerogels obtained from leaf biomass fractions (F2L and F3L) presented a more heterogeneous structure, especially F2L, where large fibrillar aggregates were also detected. This can be attributed to the presence of higher amounts of impurities such as minerals and proteins in the leaf biomass (Martínez-Sanz et al., 2018), suggesting that stem fractions are more suitable for the production of aerogels. Thus, it seems that a higher degree of cellulose purity led to the formation of more homogenous and continuous structures, while the presence of other components resulted in the formation of more porous structures.

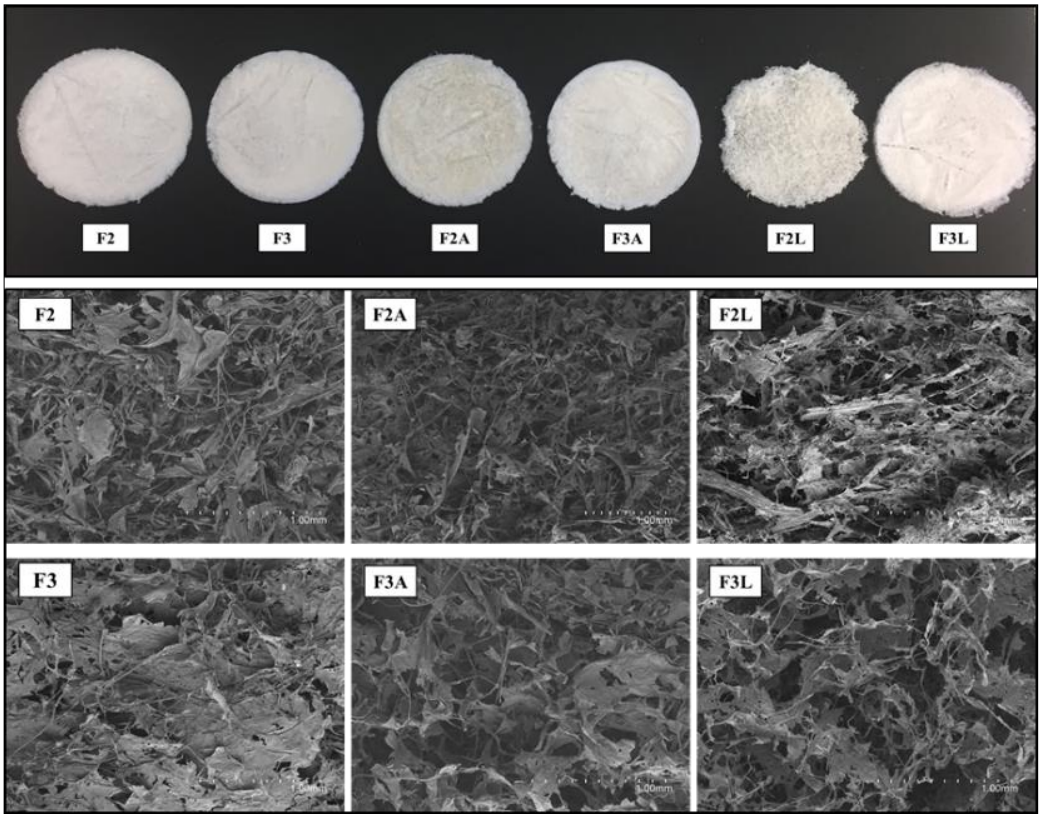

Figure 1. (A) Visual appearance and (B) SEM micrographs of the surface from the *A. donax* cellulosic aerogels.

The density of the aerogels was estimated and the results are summarized in Table 1. Although the differences were not statistically significant, the more purified cellulose aerogels seemed to present greater density values than the aerogels containing hemicelluloses, supporting the porosity differences observed by SEM. The F2L aerogel presented an anomalously high density, which may be the result of its more heterogeneous structure. On the other hand, the F2A aerogel was the most lightweight material, corresponding with its more open porous structure (cf. Figure 1A). The densities of most aerogels were significantly lower than those previously reported for aerogels prepared by solvent exchange and supercritical CO_2 drying of cellulose solutions in NMMO (ca. 50 mg/cm^3) (Innerlohinger et al., 2006) and cellulose nanowhiskers aqueous suspensions (78 mg/cm^3) (Heath & Thielemans, 2010), having the same cellulose concentration used in this work (i.e. 0.5 wt.-%) and similar to aerogels produced by supercritical CO_2 drying of regenerated tunicate cellulose (10 mg/cm^3) (Cai et al., 2008). In contrast, lower

density values (down to 6-8 mg/cm^3) have been reported for optimized aerogels produced by means of freeze-drying of aqueous suspensions of rice straw cellulose nanofibrils produced by coupled TEMPO-oxidation and mechanical blending (Jiang & Hsieh, 2014b, 2014a).

The highly porous structure of cellulose aerogels offers a great advantage for the development of superabsorbent materials and/or matrices for the selective release of bioactive components in different media. The differences in composition and structure of the developed aerogels are expected to affect their behaviour when exposed to different media, which will ultimately determine their suitability to be used as template for the sorption and/or release of bioactive extracts. The water vapour sorption capacity of the aerogels was evaluated gravimetrically by exposing the samples to 100% RH conditions and the results are summarized in Table 1. As observed, the presence of hemicelluloses in the aerogels clearly had a significant impact, leading to increased water sorption capacity. This might be attributed to (i) the more hydrophilic character of hemicelluloses, provided by the greater amount of free hydroxyl groups in their structure and to their amorphous structure, as opposed to cellulose, which presents a more crystalline structure, with greater degree of self-association (Benito-González et al., 2018) and (ii) the more porous aerogel structure induced by the presence of hemicelluloses. The same trend has been previously reported for films produced from the cellulosic fractions extracted from *A. donax*, although the absolute water uptake values obtained for the films (0.06-0.1 g/g film for the films containing hemicelluloses and 0.02-0.05 g/g film for the purified cellulose films) (Martínez-Sanz et al., 2018) were significantly lower than those estimated for the aerogels, hence evidencing the great impact of the porosity on the sorption capacity. It is also worth noting that the presence of minor amounts of lipidic impurities in the aerogels obtained from fractions without the Soxhlet treatment did not have an impact on the water vapour sorption.

Table 1. Density and water vapour sorption of the cellulosic aerogels.

Sample	Density (mg/cm^3)	Water vapour sorption (g/g aerogel)
F2	12.84 ± 0.29^{ab}	0.91 ± 0.02^{b}
F3	13.77 ± 0.53^{ab}	0.39 ± 0.04^{c}
F2A	10.21 ± 0.10^{b}	0.83 ±0.02^{b}
F3A	14.39 ± 0.04^{ab}	0.41 ± 0.02^{c}
F2L	25.55 ± 0.57^{a}	1.09 ± 0.01^{a}
F3L	12.55 ± 0.08^{ab}	0.52 ± 0.05^{c}

Values with different letters are significantly different ($p \leq 0.05$).

Further to the behaviour of the aerogels when exposed to high relative humidity, which could take place, for instance, upon storage of foodstuffs at ambient conditions, their capacity to absorb and retain hydrophilic and hydrophobic media was also evaluated through immersion in water and soybean oil and subsequent drying at ambient conditions. All the aerogels were able to maintain their integrity, even after soaking them for 24h in both media. Figure S2 shows the sorption/desorption kinetics and Figure 2 displays the sorption equilibrium values (after immersion in the liquid media and after subsequent drying). As observed, both water and oil were quickly absorbed into the aerogels, reaching equilibrium values approximately after 24h. When drying the samples at ambient conditions, water was quickly released from the aerogels, producing a steep weight decrease within the first 30 min and reaching the equilibrium after ca. 2 h. In contrast, the drying process took place more slowly in the case of oil, which was expected due to its higher viscosity (ca. 0.041 Pa·s at 20ºC (Diamante & Lan, 2014) versus 0.001 Pa·s for water) and evaporation temperature. A sharper weight loss occurred during the first 3 h, reaching the equilibrium after ca. 7-8 h. A significant amount of both water and oil was released from the aerogels upon drying and, thus, the retention values were much lower than the sorption capacities, indicating that a significant amount of the absorbed liquids was not strongly interacting with the aerogel matrix materials. It should be noted that the lowest water and oil sorption capacity values corresponded to the F2L aerogel, which can be related to its heterogeneous structure.

For the water sorption/desorption process, the aerogels containing hemicelluloses showed a faster sorption/desorption kinetics than their more purified counterparts, which can be attributed to their more porous structure. Furthermore, the water sorption equilibrium values were greater for the hemicellulose-containing aerogels. This can be ascribed to the greater compatibility of the more hydrophilic hemicelluloses with water, as compared with the cellulose hydrogels, where less amount of free hydroxyl groups may be available on the surface of the pore walls due to strong self-association. In fact, (Chen et al., 2011) reported that aerogels with higher cellulose contents lead to the formation of stronger hydrogen bonding networks, resulting in a decreased water uptake. It should also be noted that the aerogels obtained from fractions without the Soxhlet treatment, containing hydrophobic lipidic impurities, showed lower water and oil sorption capacities than their purified counterparts. These results suggest that although the water sorption/desorption process was mostly a physical phenomenon, the affinity and interactions established between the components in the aerogels and the water played also an important role. This can be explained by the existence of two different adsorbed water domains, as previously reported for silica aerogels: (i) one fraction of bound water interacting with the aerogel components through hydrogen bonding and (ii) one fraction of bulk water which is physically adsorbed within the aerogel pores (Da Silva et al., 1992).

In the case of the soybean oil, the opposite trend was observed for the sorption process, i.e. the more purified cellulose-based aerogels presented faster kinetics and reached greater oil sorption equilibrium values. In particular, the purest cellulose aerogel, i.e. F3, presented the greatest oil sorption capacity. This seems to confirm the more hydrophobic behaviour of the cellulose-based aerogels due to the strong cellulose self-association, facilitating the oil sorption process. However, although the more purified aerogels seemed to show a faster oil desorption process, no significant differences were encountered between the oil retention values for all the samples. The soybean oil retention values were greater than those for water for all the samples, which is explained by the stronger effect of capillary forces in the case of the more viscous oil, a fraction of which remained adhered to the pore walls and trapped within the macropores (Hu et al., 2014). The same effect has been previously observed for oils with different viscosities (Feng et al., 2015; Nguyen et al., 2013).

The values previously reported in the literature for the sorption of liquids of cellulose-based aerogels evidence the excellent capacity of the *A. donax* aerogels to absorb liquid media, without the need of any physical or chemical modification. A lower water sorption capacity of 19.8 g water/g aerogel has been previously reported for aerogels from native recycled cellulose (Nguyen et al., 2014). Only modified cellulose aerogels have been shown to present greater water sorption capacities. For instance, water sorption values of 104-210 g water/g aerogel have been reported for aerogels from TEMPO-oxidated and defibrillated cellulose nanofibers (Jiang & Hsieh, 2014b, 2014a). It should be noted that these aerogels possessed a less dense structure than the ones developed in this work, confirming the relevance of the porosity for the liquid sorption capacity of the aerogels. Salam *et al.,* obtained hemicellulose aerogels incorporating carboxylic groups from a reaction with citric acid followed by cross-linking with chitosan, increasing the water sorption capacity up to 100 g water/g sample (Salam et al., 2011). With regards to the oil sorption capacity, lower values of 18-20 g crude oil/g aerogel were reported for methyltrimethoxysilane-coated cellulose aerogels (Nguyen et al., 2013) and a similar value of 62.6 g motor oil/g aerogel was obtained for cross-linked and hydrophobized 0.5 wt.-% cellulose aerogels (measured at 25 ºC) (Feng et al., 2015). The authors reported a maximum sorption capacity of 95 g motor oil/g aerogel, which could be achieved by lowering the cellulose concentration down to 0.25 wt.-% and producing less dense and more porous structures. Lower sorption capacities for different oils and organic solvents have also been reported for nanocellulose aerogels chemically modified to increase their hydrophobicity (Mulyadi et al., 2016; Phanthong et al., 2018).

The overall objective of this work was to generate bioactive aerogel structures by utilizing the waste biomass from *A. donax*. Since some of the components remaining in the less purified extracts, such as polyphenols, proteins and lipids may present antioxidant properties, the different cellulosic fractions, prior to the preparation of the aerogels, were characterized by means of the ABTS assay. From the results compiled in Table S1, it is clear that (i) the stem fractions presented higher antioxidant capacity than the leaf fractions and (ii) the components remaining in the less purified fractions conferred them greater antioxidant capacity. These

results show the potential of the less purified aerogels to be used as bioactive food packaging structures.

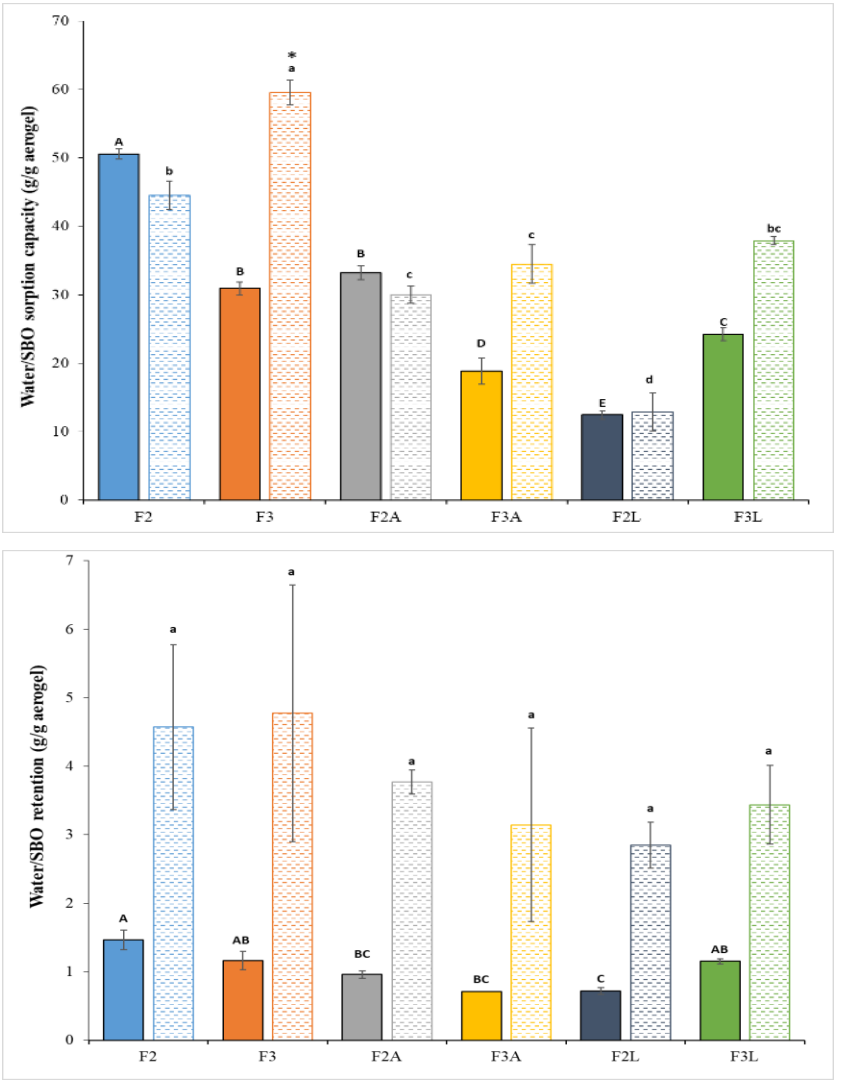

Figure 2. (A) Water and soybean oil sorption capacity and (B) water/oil retention capacity of the *A. donax* cellulosic aerogels after drying at ambient conditions. Solid bars represent the water sorption/retention values and patterned bars represent the soybean oil sorption/retention values. Bars with different letters are significantly different ($p \leq 0.05$). * Indicates significant differences ($p \leq 0.05$) for the same sample when soaked in water and oil.

4.2 Production and characterization of water-soluble extracts from *A. donax*

Aquatic plants and seaweeds are known to contain bioactive components such as polyphenols and sulphated polysaccharides that possess bioactive functionalities. Thus, the biomass from *A. donax* (stems and leaves) was also utilized to produce water-soluble extracts and their composition and antioxidant capacity were evaluated. To generate the extracts, two different protocols based on hot-water and ultrasound treatments were explored. The composition of the four different extracts was determined and the results are compiled in Table 2. As observed from this table, while polysaccharides were the main component in the stem extracts, similar amounts of proteins and polysaccharides were detected in the leaf extracts. It should be noted that, in general, the hot water treatment promoted the extraction of polysaccharides and polyphenols.

The antioxidant capacity the extracts was measured by using the ABTS and β-carotene bleaching assays. The first method is based on the scavenging capacity of the tested extract against the ABTS radical, converting it into a colourless product. On the other hand, the second protocol quantifies the ability of the extract to prevent the β-carotene degradation when subjected to high temperatures. The results listed in Table 2 evidence that the S-HW extract presented the highest antioxidant capacity according to the ABTS assay, which can be related to the higher content of polysaccharides and polyphenols in this extract. To the best of our knowledge, no previous data on the antioxidant capacity of aqueous *A. donax* extracts are available. In general, organic solvents are preferred to produce plant extracts with antioxidant capacity, since bioactive compounds such as non-glycosilated flavonoids, phospholipids, carotenoids and chlorophyll analogues, are known to be more soluble in these solvents. However, other bioactive compounds such as sulphated polysaccharides and glycosylated polyphenols present a more hydrophilic character. In fact, lower antioxidant capacity values of ca. 70 μmol TE/g extract have been reported for the acetone extracts from *A. donax* leaves (Piluzza & Bullitta, 2011), which can be directly related to their lower polyphenol content (ca. 21 mg GA/g extract) (Piluzza & Bullitta, 2011). The aqueous *A. donax* extracts presented greater phenolic contents than those previously reported in the literature for the methanolic extracts from a range of aquatic plants (1.6-21.6 mg GA/g extract) (Dellai et al., 2013; Kannan et al., 2013). Thus, the

results seem to point out that *A. donax,* in particular the stem fraction, is rich in polysaccharides and polyphenols which confer the aqueous extracts a relatively high antioxidant capacity.

With regards to the capacity of the extracts to inhibit the β-carotene bleaching, Figure S2 shows the effect of the extracts when tested at three different concentrations, while the values compiled in Table 2 correspond to the highest concentration of 5 mg/mL. From Figure S3, increasing the extract concentration seemed to slightly improve the inhibition capacity, although the effect was not significant due to the large standard deviation values. It should be highlighted that the extracts presented similar antioxidant activities to that of a commercial synthetic antioxidant such as BHT. No significant differences amongst the extracts were found at a concentration of 5 mg/mL, although the S-HW extract showed the highest percentage of inhibition. To the best of our knowledge, the capacity of *A. donax* extracts to inhibit the β-carotene bleaching has not been reported in the literature, although data for other plant extracts can be found in the literature. For instance, the aqueous extract from *Tossa jute* leaves has been reported to present ca. 70.8% inhibition when tested at 0.5 mg/mL (Ben Yakoub et al., 2018) and the ethanolic extracts from *Osmundaria obtusiloba* and *Pterocladiella capillacea* have shown 90% and 45% inhibition, respectively, when tested at a concentration of 1 mg/mL (De Alencar et al., 2016). Thus, although no reference values could be found in the literature for a fair comparison, the β-carotene bleaching results, together with the ABTS assay, seem to evidence the high antioxidant capacity of the aqueous *A. donax* extracts.

Table 2. Composition and antioxidant activity of *A. donax* water-soluble extracts.

	Polysaccharides (mg/g sample)	Proteins (mg BSA/g extract)	Polyphenols (mg GA/g sample)	TEAC (μmol TE/g sample)(*)	β-Carotene bleaching inhibition (%) (†)
S-HW	432.3 ± 84.6^{a}	150.0 ± 2.1^{a}	52.3 ± 0.9^{a}	143.7 ± 17.2^{a}	93.3 ± 0.7^{a}
L-HW	170.1 ± 51.2^{b}	143.7 ± 0.7^{a}	43.7 ± 3.4^{ab}	86. ± 7.2^{b}	86.9 ± 14.9^{a}
S-US	224.4 ± 16.4^{b}	149.3 ± 11.0^{a}	35.4 ± 5.4^{b}	97.1 ± 11.9^{b}	84.76 ± 12.32^{a}
L-US	117.1 ± 28.8^{b}	148.5 ± 8.5^{a}	35.2 ± 1.0^{b}	79.6 ± 5.3^{b}	60.80 ± 16.05^{a}

Values with different letters are significantly different ($p \leq 0.05$).

(*) TEAC values were calculated after 10 minutes.

(†) Calculated for the extracts at a concentration of 5 mg/mL.

4.3 Production of bioactive aerogels

Highly porous, superabsorbent aerogels and bioactive extracts from *A. donax* biomass were generated by green processes. Subsequently, these two components were combined to develop bioactive aerogels for food packaging applications. The F2A and F3A aerogels were selected as the matrices for several reasons: (i) these fractions were produced by a more cost-effective and greener process in which the use of organic solvents was avoided, (ii) they showed greater inherent antioxidant capacity and (iii) the produced aerogels showed excellent water and oil sorption capacities (although lower than the more purified F2 and F3 aerogels) and, thus, they were good candidates for the incorporation and release of bioactive extracts. The S-HW extract was selected due to its higher antioxidant capacity and it was incorporated into the F2A and F3A aerogels at a concentration of 17 wt.-%, which was the maximum concentration allowing to preserve the integrity of the aerogels.

In order to evaluate the release of the bioactive extract from the F2A and F3A aerogels when exposed to different liquid media, *in vitro* release studies were carried out in ethanol and water. Additionally, to assess the impact of the material porosity in the release behaviour, F2A and F3A films, presenting a much more compact structure (Martínez-Sanz et al., 2018), were also prepared by incorporating the same amount of extract. The results from the release studies, shown in Figure 3, indicate that, in general, the less purified F2A fraction provided greater extract release than the F3A fraction, both in films and aerogels. When water was selected as the release medium, a steeper release took place in the aerogels during the first 25 minutes, but after that both aerogels and films showed a much slower release, reaching the equilibrium after ca. 3-4 h (ca. 100% release for the F2A aerogel, 84% for the F3A aerogel, 86% for the F2A film and 56% for the F3A film). The greater release values in the aerogels may be directly linked to their morphology, i.e. their porous structure facilitated the diffusion of water inwards and outwards the aerogel structure and as a consequence, promoted the quick release of the hydrophilic extract. In contrast, the compact structure of the films hindered the accessibility of water, releasing mostly the extract present on the surface of the films during the beginning of the experiment. Furthermore, stronger matrix-extract interactions seem to have been developed in the case of the films, hence leading to lower amounts of extract released after

reaching the equilibrium. Moreover, in agreement with the water swelling experiments (cf. Figures 2A and 2B), the F2A aerogel seemed to promote water diffusion to a greater extent, thus increasing the amount of hydrophilic extract released to the liquid medium. Bacterial cellulose aerogels loaded with L-ascorbic acid and dexpanthenol, prepared by antisolvent precipitation with supercritical CO_2, showed similar release profiles, achieving 100% release of the bioactives after ca. 2-3 h and the authors claimed that the release process was purely diffusion driven (Haimer et al., 2010). On the other hand, (Valo et al., 2013) observed that the release of a drug incorporated into nanocellulose aerogels obtained from different sources was not only dependent on the structure but was also strongly affected by the interactions between the drug nanoparticles and the cellulose matrix, reaching equilibrium release values of ca. 40-60% for those cellulose aerogels where stronger interactions with the drug were established.

The use of a less polar solvent such as ethanol reduced the amount of released extract in the case of the aerogels. Interestingly, in that case very similar or even lower release values were obtained for the aerogels (ca. 62% for the F3A aerogel and 77% for the F2A aerogel) as compared with the films (ca. 60% for the F3A film and 99% for the F2A film). This might be due to a reduced diffusion of ethanol through the aerogel pores due to the lower affinity of this solvent with the cellulosic components. These results seem to indicate that while the release of the extract took place mostly at the surface level in the case of the films, a liquid medium diffusion-induced release mechanism took place in the case of the aerogels. Thus, the aerogels offer a clear advantage for their application as bioactive food packaging structures, since they are expected to release large amounts of extract when placed in contact with high moisture content foodstuffs.

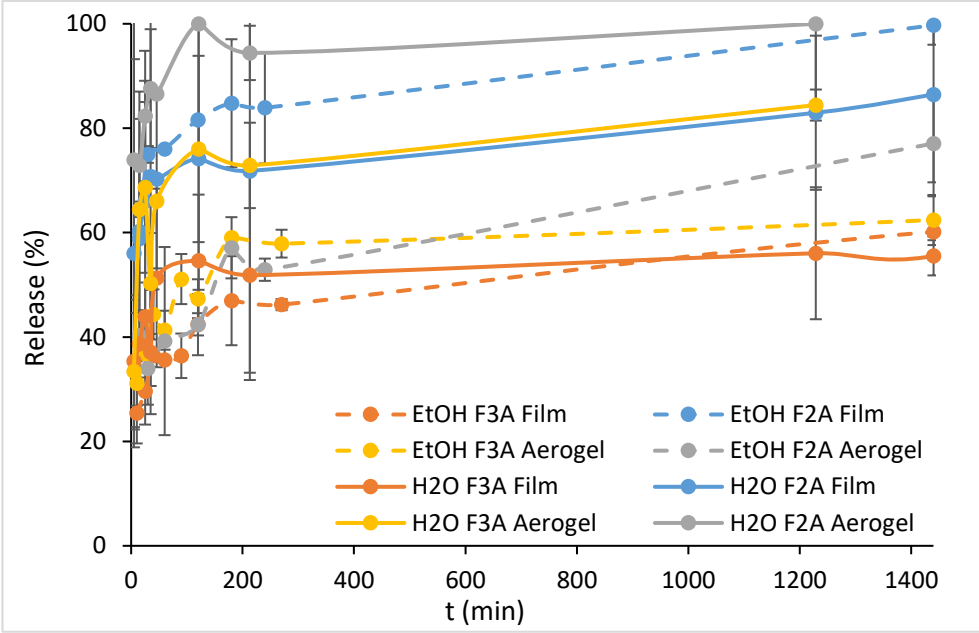

Figure 3. Release profiles of S-HW extract from *A. donax* aerogels and films in ethanol and water.

The high release of the bioactive S-HW extract when the aerogels were subjected to high moisture conditions, together with the inherent antioxidant effect of the F2A and F3A fractions, were expected to confer the hybrid aerogels antioxidant capacity. To confirm this and to compare the performance of aerogels and films, the β-carotene bleaching assay was carried out by soaking film and aerogel samples in the β-carotene emulsion. Since the cellulosic fractions were previously observed to present antioxidant potential, the pure films and aerogels with no added extract were firstly tested. As observed in Table 3, the aerogels, in particular the F2A aerogel, were able to reduce the degradation of β-carotene, while the films did not show a significant effect. This confirms that (i) the F2A fraction presented greater antioxidant capacity due to the presence of impurities like phenolic compounds and (ii) the release of bioactive components into aqueous media is favoured in the porous aerogels as compared to the compact-structured films. The β-carotene bleaching inhibition of the hybrid aerogels and films, containing the S-HW extract was then evaluated and the difference between the obtained inhibition values and those corresponding to the pure aerogels and films was calculated to

evaluate the effect of the incorporated extract. On the other hand, the inhibition of the pure extract at the same concentration present in the films and aerogels (i.e. 0.84 mg/mL) was estimated as 58.8 ± 0.9 %. The results, gathered in Table 3, show that the hybrid F2A aerogel provided the greatest inhibition capacity. Interestingly, no significant differences were found between the analogous aerogels and films when removing the contribution from the matrices (see third column in Table 2), suggesting that the extract was released to the same extent in both types of structures when heating up to 50ºC for 120 min. Furthermore, and in agreement with the *in vitro* release experiments, the results indicate that stronger matrix-extract interactions must have been established in the case of the F3A aerogel/film, limiting the release. Overall, the hybrid F2A aerogel presented the highest inhibition percentage, thus being the most promising material for the development of antioxidant food packaging structures.

Table 3. Antioxidant capacity of *A. donax* aerogels and films, measured from the β-carotene bleaching assay.

	β-Carotene bleaching inhibition (%)		
Sample	Aerogel/Film	Aerogel/Film + S-HW	(Aerogel/Film +S-HW) – Aerogel/Film
Aerogel F2A	32.8 ± 8.8^{a}	90.1 ± 2.8^{a}	57.3 ± 2.9^{a}
Aerogel F3A	19.3 ± 0.7^{ab}	57.7 ± 0.06^{b}	38.4 ± 0.1^{b}
Film F2A	5.6 ± 3.2^{b}	58.9 ± 4.4^{b}	53.3 ± 4.4^{ab}
Film F3A	5.7 ± 1.5^{b}	42.5 ± 6.1^{b}	36.8 ± 6.1^{b}

Values with different letters are significantly different ($p \leq 0.05$).

4.4 Evaluation of the antioxidant effect of bioactive aerogels on red meat

As a final proof of concept, the hybrid and the pure cellulosic aerogels were tested as absorption pads to inhibit lipid oxidation and colour loss during storage of minced red meat. Meat discoloration is attributed to the process of oxymyoglobin oxidation, giving rise to the formation of metmyoglobin. The proportion of these two myoglobin forms was determined in the raw minced meat and in the samples after storage for 10 days. The visual appearance of representative meat samples after storage is shown in Figure 4A and the estimated myoglobin

contents are shown in Figure 4B. It is observed that at day 0 (i.e. fresh meat) the oxymyoglobin content was higher than metmyoglobin, as expected. After storage, a colour loss, indicated by the lower oxymyoglobin content and the higher metmyoglobin content, took place in all the samples. Interestingly, and as supported by Figure 4A, the samples stored with aerogel pads presented higher oxymyoglobin and lower metmyoglobin content than the control sample prepared using commercial pads, highlighting the potential of these materials to limit the oxidation processes giving rise to meat discoloration upon storage. In particular, the F2A+S-HW aerogel showed the strongest effect, which may be attributed to the antioxidant capacity of its components (both the extract and the F2A fraction). To the best of our knowledge, no previous works have reported on the utilization of aerogel structures or cellulose-based materials as antioxidant food packaging structures. As a reference, 60% of metmyoglobin was detected in foal meat after storage for 10 days in modified atmosphere using bioactive films containing oregano extract (Lorenzo et al., 2014), which is higher than the value estimated for the meat stored in contact with the F2A+S-HW aerogel (ca. 46% metmyoglobin).

The ability of the developed aerogels to prevent lipid oxidation in red meat was also evaluated by calculating the TBARS content in the raw minced meat and in the samples after storage and estimating the percentage of lipid oxidation inhibition with regards to a blank sample (i.e. meat stored without any pad). Although, as seen from the results summarized in Table 4, due to the large standard deviation values arising from the large inherent variability of the meat samples, no significant differences were found between samples, the meat stored in contact with the F2A+S-HW aerogel showed the lowest TBARS content and the highest lipid oxidation inhibition. To the best of our knowledge no previous works have reported on the potential of highly porous cellulose-based aerogels as bioactive food packaging structures. The most typical approach reported in the literature to prevent lipid oxidation in meat consists on the utilization of natural extracts. For instance, active packaging films containing 2% of oregano essential oil or 1% of green tea extract were utilized to store foal steaks, although no significant effect in the TBARS content was detected after 10 days of storage (Lorenzo et al., 2014). In another work, meat steaks were packaged in polystyrene trays and sprayed with oregano extract. The addition of 0.5% of oregano extract showed a high inhibitory effect on lipid oxidation, reaching a maximum

value of 2 mg malonaldehyde/Kg meat after 28 days of storage (Camo et al., 2011). These results, together with the results from the meat colour evaluation and the antioxidant capacity of the aerogels, evidence the antioxidant potential of the F2A+S-HW aerogel, which could be used as bioactive pads in high moisture fresh packaged foods such as red meat.

Table 4. 2-thiobarbituric acid reactive substances (TBARS) and estimated lipid oxidation inhibition in the raw minced red meat (day 0) and in the meat after 10 days of storage.

	TBARS (mg malonaldehyde/ Kg meat)	Lipid oxidation Inhibition (%)
Day 0	0.53 ± 0.15^{b}	---
Control	6.37 ± 1.68^{a}	2.2
F2A	4.36 ± 1.25^{ab}	35.9
F2A+S-HW	4.04 ± 2.34^{ab}	41.3
F3A	4.84 ± 0.89^{ab}	27.9
F3A+S-HW	$4.57. \pm 1.50^{ab}$	32.3

Values with different letters are significantly different ($p \leq 0.05$).

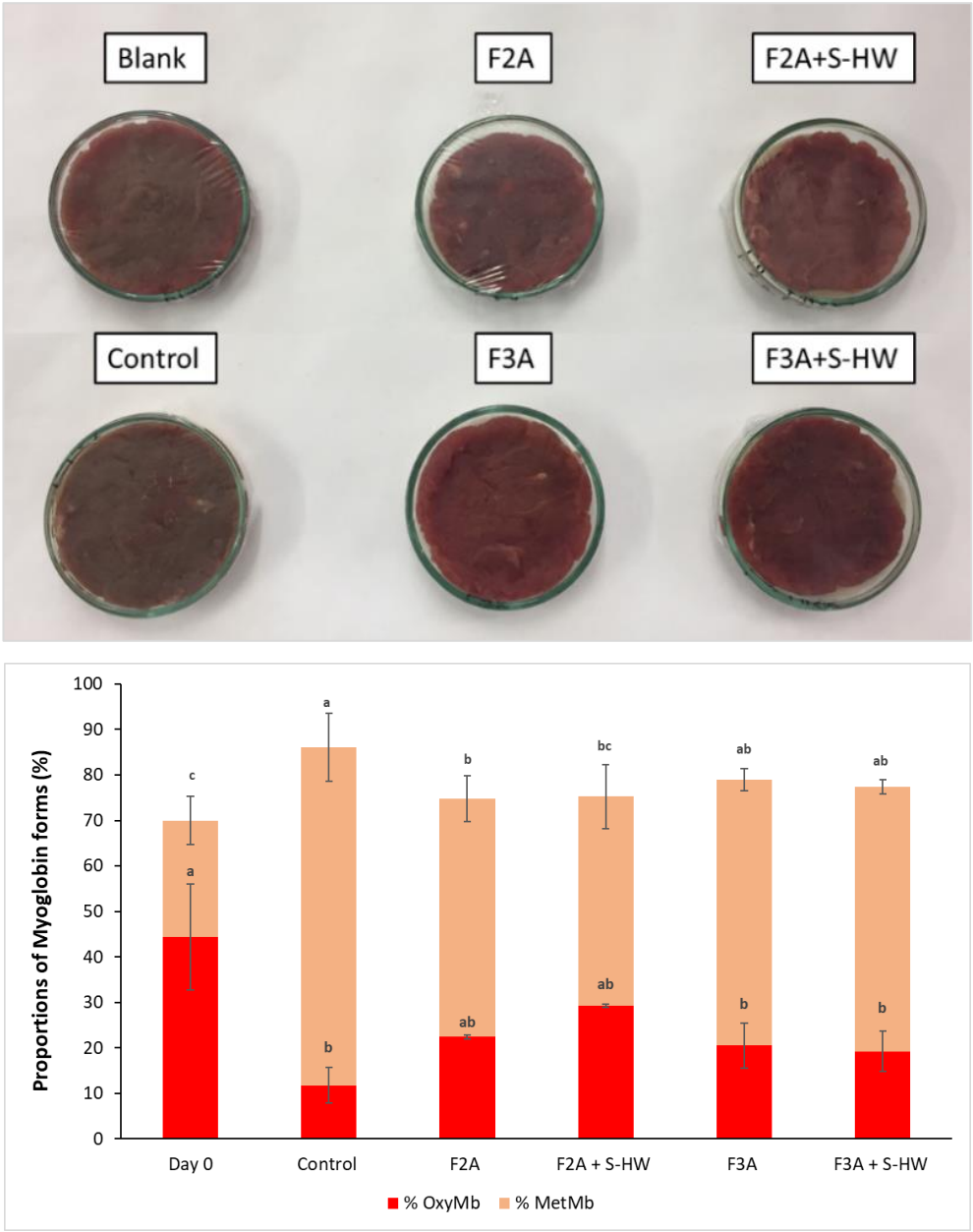

Figure 4. (A) Visual appearance of the meat samples after storage for 10 days. (B) Proportions of oxymyoglobin (%OxyMb) and metmyoglobin (%MetMb) in the raw minced red meat (day 0) and in the meat after 10 days of storage. Bars with different letters are significantly different ($p \leq 0.05$).

5 Conclusions

Highly porous bio-based bioactive aerogels have been produced by valorizing the lignocellulosic waste biomass from *A. donax* biomass. Cellulosic aerogels were produced by a simple freeze-drying method from aqueous suspensions of the fractions extracted from *A. donax* stems and leaves. All the developed aerogels presented an excellent water and oil sorption capacity, comparable to those previously reported for chemically modified nanocellulose aerogels. The presence of hemicelluloses in the F2 and F2A aerogels conferred them a less dense, more porous structure, as well as a more hydrophilic character, promoting water sorption through diffusion and water-hemicelluloses interactions.

Additionally, aqueous extracts with high antioxidant capacities were generated by subjecting the *A. donax* biomass to simple heating and ultrasound methods. The higher polysaccharide and polyphenol content in the stems extract generated by heating (S-HW) conferred it the highest antioxidant capacity. This extract was incorporated into the F2A and F3A aerogels, which were selected due to their good water sorption capacity, their inherent antioxidant potential and their greater suitability from an economical and environmental perspective.

The release of the extract from the hybrid aerogels towards liquid media was mostly a diffusion-driven process, which was strongly promoted by the highly porous structure of the aerogels. In particular, the more porous structure and the greater water affinity of the F2A aerogel led to a complete release of the extract in water after 2-4 h. This, together with the inherent antioxidant capacity of the F2A fraction, resulted in a high inhibitory effect on the β-carotene bleaching upon heating. Furthermore, all the tested aerogels showed promising results to be used as bioactive food packaging pads, as they were able to reduce the colour loss and lipid oxidation in red meat upon refrigerated storage, being the hybrid F2A+ S-HW aerogel the most active.

6 Acknowledgements

Marta Martinez-Sanz is recipient of a Juan de la Cierva (IJCI-2015-23389) contract from the Spanish Ministry of Economy, Industry and Competitiveness. Cynthia Fontes-Candia is recipient of a pre-doctoral grant from CONACYT (MEX/Ref. 306680).

7 References

Barbosa-Pereira, L., Aurrekoetxea, G. P., Angulo, I., Paseiro-Losada, P., & Cruz, J. M. (2014). Development of new active packaging films coated with natural phenolic compounds to improve the oxidative stability of beef. *Meat Science*, *97*(2), 249–254. https://doi.org/https://doi.org/10.1016/j.meatsci.2014.02.006

Ben Yakoub, A. R., Abdehedi, O., Jridi, M., Elfalleh, W., Nasri, M., & Ferchichi, A. (2018). Flavonoids, phenols, antioxidant, and antimicrobial activities in various extracts from Tossa jute leave (Corchorus olitorus L.). *Industrial Crops and Products*, *118*(March), 206–213. https://doi.org/10.1016/j.indcrop.2018.03.047

Benito-González, I., López-Rubio, A., & Martínez-Sanz, M. (2018). Potential of lignocellulosic fractions from Posidonia oceanica to improve barrier and mechanical properties of bio-based packaging materials. *International Journal of Biological Macromolecules*, *118*, 542–551. https://doi.org/https://doi.org/10.1016/j.ijbiomac.2018.06.052

Bolumar, T., Andersen, M. L., & Orlien, V. (2011). Antioxidant active packaging for chicken meat processed by high pressure treatment. *Food Chemistry*, *129*(4), 1406–1412. https://doi.org/https://doi.org/10.1016/j.foodchem.2011.05.082

Cai, J., Kimura, S., Wada, M., Kuga, S., & Zhang, L. (2008). Cellulose aerogels from aqueous alkali hydroxide–urea solution. *ChemSusChem: Chemistry & Sustainability Energy & Materials*, *1*(1-2), 149–154.

Camo, J., Lorés, A., Djenane, D., Beltrán, J. A., & Roncalés, P. (2011). Display life of beef packaged with an antioxidant active film as a function of the concentration of oregano extract. *Meat Science*, *88*(1), 174–178. https://doi.org/https://doi.org/10.1016/j.meatsci.2010.12.019

Carlez, A., Veciana-Nogues, T., & Cheftel, J. C. (1995). Changes in Color and Myoglobin of Minced Beef Meat Due to High-Pressure Processing. *Food Science and Technology-Lebensmittel-Wissenschaft & Technologie*, *28*(5), 528–538. https://doi.org/http://dx.doi.org/10.1006/fstl.1995.0088

Chen, W., Yu, H., Li, Q., Liu, Y., & Li, J. (2011). Ultralight and highly flexible aerogels with long cellulose I nanofibers. *Soft Matter*, *7*(21), 10360. https://doi.org/10.1039/c1sm06179h

Da Silva, A., Donoso, P., & Aegerter, M. A. (1992). Properties of water adsorbed in porous silica aerogels. *Journal of Non-Crystalline Solids*, *145*, 168–174.

De Alencar, D. B., de Carvalho, F. C. T., Rebouças, R. H., dos Santos, D. R., dos Santos Pires-Cavalcante, K. M., de Lima, R. L., Baracho, B. M., Bezerra, R. M., Viana, F. A., dos Fernandes Vieira, R. H. S., Sampaio, A. H., de Sousa, O. V., & Saker-Sampaio, S. (2016). Bioactive extracts of red seaweeds Pterocladiella capillacea and Osmundaria obtusiloba (Floridophyceae: Rhodophyta) with antioxidant and bacterial agglutination potential. *Asian Pacific Journal of Tropical Medicine*, *9*(4), 372–379. https://doi.org/https://doi.org/10.1016/j.apjtm.2016.03.015

Dellai, A., Laajili, S., Morvan, V. Le, Robert, J., & Bouraoui, A. (2013). Antiproliferative activity

and phenolics of the Mediterranean seaweed Laurencia obusta. *Industrial Crops and Products*, *47*, 252–255. https://doi.org/https://doi.org/10.1016/j.indcrop.2013.03.014

Diamante, L. M., & Lan, T. (2014). Absolute viscosities of vegetable oils at different temperatures and shear rate range of 64.5 to 4835 s− 1. *Journal of Food Processing*, *2014*.

Djalal Trache, Hazwan Hussin, M., Mohamad Haafiz, M. K., & Kumar Thakur, V. (2017). Recent progress in cellulose nanocrystals: sources and production. *Nanoscale*, *9*(5), 1763–1786. https://doi.org/10.1039/C6NR09494E

Feng, J., Nguyen, S. T., Fan, Z., & Duong, H. M. (2015). Advanced fabrication and oil absorption properties of super-hydrophobic recycled cellulose aerogels. *Chemical Engineering Journal*, *270*, 168–175.

Gavillon, R., & Budtova, T. (2007). Aerocellulose: New Highly Porous Cellulose Prepared from Cellulose−NaOH Aqueous Solutions. *Biomacromolecules*, *9*(1), 269–277. https://doi.org/10.1021/BM700972K

Haimer, E., Wendland, M., Schlufter, K., Frankenfeld, K., Miethe, P., Potthast, A., Rosenau, T., & Liebner, F. (2010). Loading of bacterial cellulose aerogels with bioactive compounds by antisolvent precipitation with supercritical carbon dioxide. *Macromolecular Symposia*, *294*(2), 64–74. https://doi.org/10.1002/MASY.201000008

Heath, L., & Thielemans, W. (2010). Cellulose nanowhisker aerogels. *Green Chemistry*, *12*(8), 1448–1453.

Henschen, J., Illergård, J., Larsson, P. A., Ek, M., & Wågberg, L. (2016). Contact-active antibacterial aerogels from cellulose nanofibrils. *Colloids and Surfaces B: Biointerfaces*, *146*, 415–422.

Hu, H., Zhao, Z., Gogotsi, Y., & Qiu, J. (2014). Compressible carbon nanotube–graphene hybrid aerogels with superhydrophobicity and superoleophilicity for oil sorption. *Environmental Science & Technology Letters*, *1*(3), 214–220.

Innerlohinger, J., Weber, H. K., & Kraft, G. (2006). Aerocellulose: aerogels and aerogel-like materials made from cellulose. *Macromolecular Symposia*, *244*(1), 126–135.

Jiang, F., & Hsieh, Y.-L. (2014a). Amphiphilic superabsorbent cellulose nanofibril aerogels. *Journal of Materials Chemistry A*, *2*(18), 6337–6342.

Jiang, F., & Hsieh, Y.-L. (2014b). Super water absorbing and shape memory nanocellulose aerogels from TEMPO-oxidized cellulose nanofibrils via cyclic freezing–thawing. *Journal of Materials Chemistry A*, *2*(2), 350–359.

Jofré, A., Aymerich, T., & Garriga, M. (2008). Assessment of the effectiveness of antimicrobial packaging combined with high pressure to control Salmonella sp. in cooked ham. *Food Control*, *19*(6), 634–638. https://doi.org/https://doi.org/10.1016/j.foodcont.2007.06.007

Kannan, R. R. R., Arumugam, R., Thangaradjou, T., & Anantharaman, P. (2013). Phytochemical constituents, antioxidant properties and p-coumaric acid analysis in some seagrasses. *Food Research International*, *54*(1), 1229–1236.

https://doi.org/https://doi.org/10.1016/j.foodres.2013.01.027

Lorenzo, J. M., Batlle, R., & Gómez, M. (2014). Extension of the shelf-life of foal meat with two antioxidant active packaging systems. *LWT - Food Science and Technology*, *59*(1), 181–188. https://doi.org/https://doi.org/10.1016/j.lwt.2014.04.061

Lowry, O. H., Rosebrough, N. J., Farr, A. L., & Randall, R. J. (1951). Protein measurement with the Folin phenol reagent. *Journal of Biological Chemistry*, *193*(1), 265–275.

Martínez-Abad, A., Giummarella, N., Lawoko, M., & Vilaplana, F. (2018). Differences in extractability under subcritical water reveal interconnected hemicellulose and lignin recalcitrance in birch hardwoods. *Green Chemistry*, *20*(11), 2534–2546. https://doi.org/10.1039/C8GC00385H

Martínez-Sanz, M., Erboz, E., Fontes, C., & López-Rubio, A. (2018). Valorization of Arundo donax for the production of high performance lignocellulosic films. *Carbohydrate Polymers*, *199*, 276–285. https://doi.org/https://doi.org/10.1016/j.carbpol.2018.07.029

Martínez-Sanz, M., Gómez-Mascaraque, L. G., Ballester, A. R., Martínez-Abad, A., Brodkorb, A., & López-Rubio, A. (2019). Production of unpurified agar-based extracts from red seaweed Gelidium sesquipedale by means of simplified extraction protocols. *Algal Research*, *38*, 101420. https://doi.org/10.1016/j.algal.2019.101420

Martins, C. D. L., Ramlov, F., Nocchi Carneiro, N. P., Gestinari, L. M., dos Santos, B. F., Bento, L. M., Lhullier, C., Gouvea, L., Bastos, E., Horta, P. A., & Soares, A. R. (2013). Antioxidant properties and total phenolic contents of some tropical seaweeds of the Brazilian coast. *Journal of Applied Phycology*, *25*(4), 1179–1187. https://doi.org/10.1007/s10811-012-9918-x

McMillin, K. W. (2017). Advancements in meat packaging. *Meat Science*, *132*, 153–162.

Mulyadi, A., Zhang, Z., & Deng, Y. (2016). Fluorine-Free Oil Absorbents Made from Cellulose Nanofibril Aerogels. *ACS Applied Materials and Interfaces*, *8*(4), 2732–2740. https://doi.org/10.1021/acsami.5b10985

Nguyen, S. T., Feng, J., Le, N. T., Le, A. T. T., Hoang, N., Tan, V. B. C., & Duong, H. M. (2013). Cellulose aerogel from paper waste for crude oil spill cleaning. *Industrial & Engineering Chemistry Research*, *52*(51), 18386–18391.

Nguyen, S. T., Feng, J., Ng, S. K., Wong, J. P. W., Tan, V. B. C., & Duong, H. M. (2014). Advanced thermal insulation and absorption properties of recycled cellulose aerogels. *Colloids and Surfaces A: Physicochemical and Engineering Aspects*, *445*, 128–134. https://doi.org/10.1016/j.colsurfa.2014.01.015

Phanthong, P., Reubroycharoen, P., Kongparakul, S., Samart, C., Wang, Z., Hao, X., Abudula, A., & Guan, G. (2018). Fabrication and evaluation of nanocellulose sponge for oil/water separation. *Carbohydrate Polymers*, *190*, 184–189. https://doi.org/10.1016/j.carbpol.2018.02.066

Piluzza, G., & Bullitta, S. (2011). Correlations between phenolic content and antioxidant

properties in twenty-four plant species of traditional ethnoveterinary use in the Mediterranean area. *Pharmaceutical Biology*, *49*(3), 240–247.

Rampazzo, R., Alkan, D., Gazzotti, S., Ortenzi, M. A., Piva, G., & Piergiovanni, L. (2017). Cellulose Nanocrystals from Lignocellulosic Raw Materials, for Oxygen Barrier Coatings on Food Packaging Films. *Packaging Technology and Science*, *30*(10), 645–661. https://doi.org/10.1002/PTS.2308

Re, R., Pellegrini, N., Proteggente, A., Pannala, A., Yang, M., & Rice-Evans, C. (1999). Antioxidant activity applying an improved ABTS radical cation decolorization assay. *Free Radical Biology and Medicine*, *26*(9–10), 1231–1237.

Salam, A., Venditti, R. A., Pawlak, J. J., & El-Tahlawy, K. (2011). Crosslinked hemicellulose citrate-chitosan aerogel foams. *Carbohydrate Polymers*, *84*(4), 1221–1229. https://doi.org/10.1016/j.carbpol.2011.01.008

Satyanarayana, K. G., Arizaga, G. G. C., & Wypych, F. (2009). Biodegradable composites based on lignocellulosic fibers-An overview. *Progress in Polymer Science (Oxford)*, *34*(9), 982–1021.

Singleton, V. L., Orthofer, R., & Lamuela-Raventós, R. M. (1999). Analysis of total phenols and other oxidation substrates and antioxidants by means of folin-ciocalteu reagent. *Methods in Enzymology*, *299*, 152–178.

Tang, S., Kerry, J. P., Sheehan, D., Buckley, D. J., & Morrissey, P. A. (2001). Antioxidative effect of added tea catechins on susceptibility of cooked red meat, poultry and fish patties to lipid oxidation. *Food Research International*, *34*(8), 651–657. https://doi.org/10.1016/S0963-9969(00)00190-3

Valo, H., Arola, S., Laaksonen, P., Torkkeli, M., Peltonen, L., Linder, M. B., Serimaa, R., Kuga, S., Hirvonen, J., & Laaksonen, T. (2013). Drug release from nanoparticles embedded in four different nanofibrillar cellulose aerogels. *European Journal of Pharmaceutical Sciences*, *50*(1), 69–77.

Wang, X., Zhang, Y., Jiang, H., Song, Y., Zhou, Z., & Zhao, H. (2016). Fabrication and characterization of nano-cellulose aerogels via supercritical CO2 drying technology. *Materials Letters*, *183*, 179–182.

8 Supplementary Material

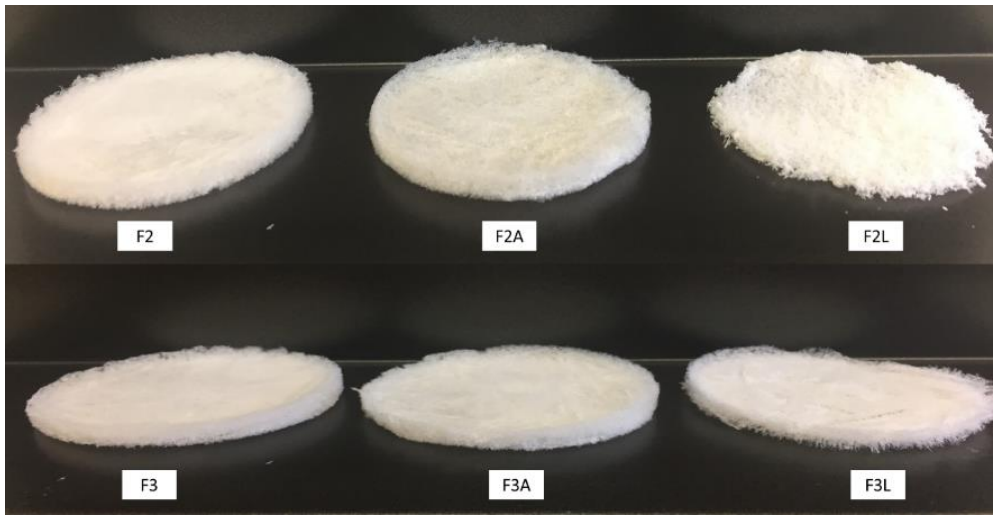

Figure S1. Visual appearance of *A. donax* cellulosic aerogels.

Table S1. Antioxidant activity of *A. donax* cellulosic fractions.

Sample	TEAC (µmol TE/g sample) (*)
F2	89.8 ± 8.4 [ab]
F3	52.8 ± 8.2 [c]
F2A	94.4 ± 14.7 [a]
F3A	89.4 ± 0.4 [ab]
F2L	60.9 ± 1.4 [b]
F3L	16.0 ± 4.8 [d]

Values with different letters are significantly different ($p \leq 0.05$).

(*) TEAC values were calculated after 24 hours.

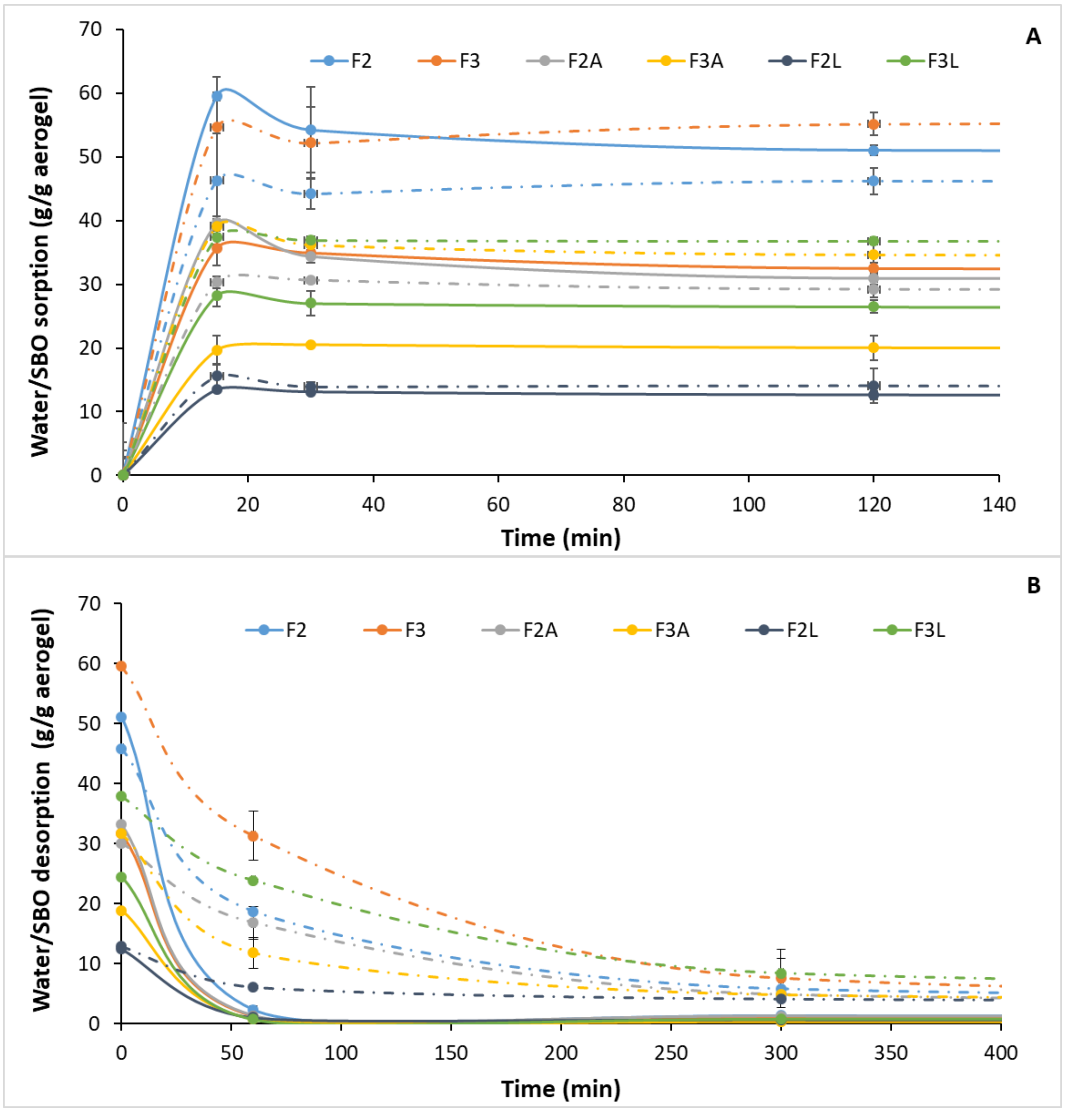

Figure S2. (A) Water and soybean oil sorption kinetics and (B) release kinetics and of the *A. donax* cellulosic aerogels. Solid lines represent the water sorption/desorption and dotted lines represent the soybean oil sorption/desorption.

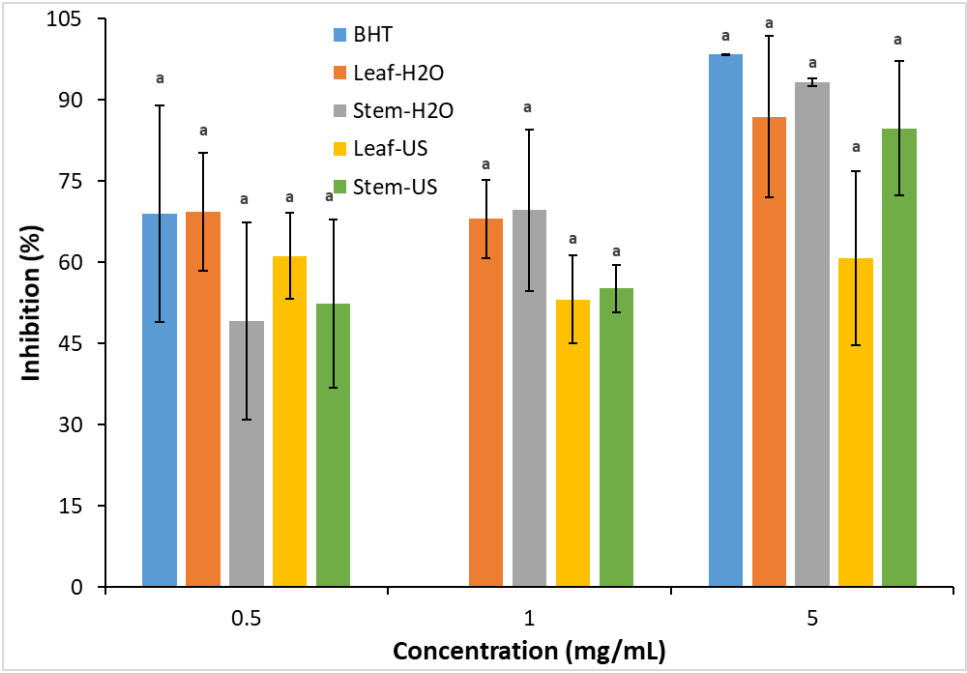

Figure S3. β-carotene bleaching inhibition capacity of the water-soluble extracts from *A. donax* tested at different concentrations. Bars with different letters are significantly different ($p \leq 0.05$).

CHAPTER 3

STRUCTURE, PROPERTIES AND APPLICATIONS OF EMULSION GELS BASED ON SULPHATED POLYSACCHARIDES

INTRODUCTION TO CHAPTER 3

Emulsion-gels are soft-solid materials composed of a three-dimensional network structure formed by a continuous phase consisting of a gel matrix and a dispersed phase consisting of an emulsion. These materials have a wide range of applications within the pharmaceutical and food industry sectors. In particular, they present a great potential within the food industry as functional additives to modify food texture, as templates for the controlled release of bioactive compounds and as ingredients for solid fat replacement.

In the first work of this chapter, we aimed to understand how the gelation mechanism of sulphated polysaccharides such as carrageenans is affected by the incorporation of an oil phase and how the formulations can be optimized to produce emulsion-gels with specific textural properties. Thus, emulsion-gels were produced using three different commercial carrageenan grades (κ-C, ι-C and λ-C) and the effect of the carrageenan type and concentration, salt content and oil:water ratio on the emulsion-gel strength was evaluated through a response surface methodology. Moreover, the rheological properties and the micro- and nanostructure from the stronger emulsion-gel formulations were investigated and compared to their analogous hydrogel formulations by using advanced scattering techniques in combination with confocal microscopy.

After assessing the parameters affecting the properties of the emulsion-gels, the following works were focused on the application of these systems for different purposes.

Firstly, in the second work from this chapter, agar and κ-carrageenan emulsion-gels and oil filled aerogels were produced and their use as curcumin carriers was evaluated. The structure and mechanical properties of the initial gel-like structures were characterized and their behaviour upon simulated *in vitro* digestions was investigated through nanostructural characterization of the digestion products by means of advanced scattering techniques.

Finally, in the last work in this chapter, the application of agar and κ-carrageenan emulsion-gels as tissue mimicking phantoms was investigated. The effects of the polysaccharide matrix, the

oil content and the presence of surfactants on the micro-/nanostructure, rheology, and mechanical and dielectric properties were studied to understand how these parameters could be modified in order to produce tissue mimicking phantoms with varying mechanical and dielectric properties.

3.3.1

RHEOLOGICAL AND STRUCTURAL CHARACTERIZATION OF CARRAGEENAN EMULSION-GELS

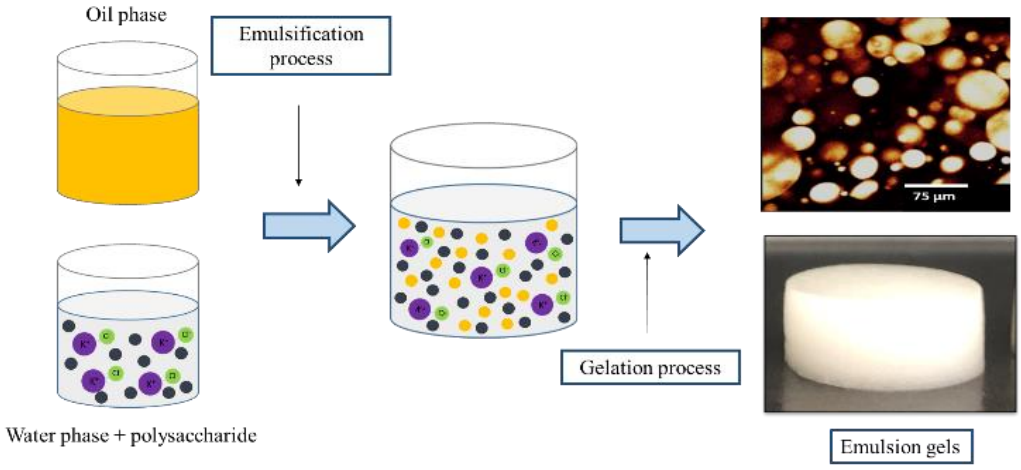

This section is an adapted version of the following published research article:

Fontes-Candia, C., Ström, A., Lopez-Sanchez, P., López-Rubio, A., & Martínez-Sanz, M. (2020). Rheological and structural characterization of carrageenan emulsion-gels. Algal Research, 47, 101873.

1 Abstract

Carrageenan emulsion-gels containing sunflower oil were prepared using three different commercial carrageenan grades (κ-C, ι-C and λ-C). The effect of the carrageenan and salt content, as well as the oil:water ratio, on the emulsion-gel strength was evaluated through a response surface methodology. Moreover, the rheological properties and the micro- and nanostructure from the stronger emulsion-gel formulations were investigated and compared to their analogous hydrogel formulations. Interestingly, emulsion-gels formed stronger and more thermally stable networks than the hydrogels, being this effect more evident in ι-C and λ-C. The results indicate that this was mainly due to a polysaccharide concentration effect, as no evidence of interactions between the carrageenan and the oil phase was found. Consequently, the rheological behaviour of the emulsion-gels was mostly determined by the type of carrageenan. The association of carrageenan molecular chains was favoured in κ-C and λ-C (due to the presence of κ-carrageenan in the latter) and promoted by the addition of KCl. In contrast, a lower degree of chain association, mostly driven by ionic cross-linking, took place in ι-C. These results evidence the relevance of the gelation mechanism on the properties of emulsion-gels and provide the basis for the design of these systems for targeted applications within the food industry.

2 Introduction

Emulsion-gels are soft-solid materials composed of a three-dimensional network structure formed by a continuous phase consisting of a gel matrix and a dispersed phase consisting of an emulsion (Feng et al., 2019). These materials present a great potential within the food industry as functional ingredients to modify food texture (Devezeaux de Lavergne et al., 2016; Matsumura et al., 1993), for solid fat replacement (Giarnetti et al., 2015; Poyato et al., 2014) or even as templates for the controlled release of bioactive compounds (Thakur et al., 2012). Fats play a very important role in food processing; however, solid fats contain high amounts of saturated fatty acids which have been associated with several health conditions such as obesity, cancer and cardiovascular diseases (Tavernier et al., 2017). Consequently, the food industry is actively looking for alternative ingredients to replace, at least partially, saturated and trans fats in products such as dairy and processed meats, while preserving their original organoleptic

attributes as much as possible to ensure consumers' acceptance. A plausible approach consists in the replacement of solid fats with emulsion-gels where an oil is incorporated into the dispersed phase. However, mimicking the rheological and textural properties of solid fats using emulsion-gels is not trivial and many factors such as the physicochemical properties of the gelling matrix, the interactions between matrix and oil phase, oil droplet size, volume fraction and distribution, etc., have an impact on the textural and rheological properties of the product (Oliver et al., 2015; Sala et al., 2007, 2008). Depending on the interactions between the gel and the emulsified phase, the oil droplets can be classified as active (bound to the gel matrix) or inactive (unbound) fillers (Geremias-Andrade et al., 2016). Active fillers can increase or decrease the stiffness of the gel depending on the ratio between the modulus of the oil droplets and that of the gel matrix, whereas inactive fillers are thought to cause a reduction on the gel stiffness (Dickinson & Chen, 1999). Therefore, the properties of emulsion-gels can be optimized by means of an adequate selection of the gelling matrices and fillers and a rational structural design of the produced materials.

Ethyl cellulose has been widely used as solid fat replacement in meat and bakery products (Stortz et al., 2012; Zetzl et al., 2012), since it can be directly dispersed in edible oils. However, the high temperatures required for its processing promote the oxidation of the oil phase. The use of synthetic polymers such a polyvinylalcohol and polysiloxanes as oil structuring agents has also been reported, but due to their synthetic nature, these compounds are not accepted as edible matrices (Siraj et al., 2015). As an alternative, natural compounds such as proteins (Derkach et al., 2015; Koo et al., 2019; Sala, Van Vliet, Stuart, Van Aken, et al., 2009; Tavernier et al., 2017) and polysaccharides (Iqbal et al., 2019; Koç et al., 2019; Lorenzo et al., 2013; Patel et al., 2014; Tan et al., 2018) are being studied as gelling agents for food-grade emulsions gels. Sulphated polysaccharides are particularly interesting due to their excellent gelling capacities. Carrageenans are sulphated polysaccharides obtained from red seaweeds and are widely used within the food industry as gelling, thickening and stabilising agents (Zia et al., 2017). Depending on the amount and distribution of sulphate groups (SO_3^-) carrageenans can be classified into different groups. The k-, ι and λ-carrageenan (containing one, two and three sulphate groups per disaccharide unit, respectively) are the most commonly used in the food industry, since they

are considered as generally recognized as safe (GRAS) (Necas & Bartosikova, 2013). Although carrageenans are not directly dispersible in oils, it is possible to obtain stable emulsion-gels by combining a carrageenan solution with a proportion of oil by a simple emulsification process (Iqbal et al., 2019; Paglarini et al., 2018; Perrechil & Cunha, 2013). However, a detailed structural characterization of carrageenan emulsion-gels is not available to date and the underlying gelation mechanism is not completely understood. A recent work (Fontes-Candia et al., 2020) demonstrated that the gelation mechanism and type of gel networks originated by different commercial carrageenan grades are significantly different and can be further altered by the inclusion of cations. Specially, the addition of K^+ was seen to induce the formation of stronger κ-C and λ-C hydrogels. On the other hand, although Ca^{2+} promoted more efficiently the formation of ι-C hydrogels than K^+ (requiring lower salt concentrations), the hydrogel strength was not significantly affected by the type of salt, suggesting that similar supramolecular structures may have been formed.

Accordingly, the utilization of these different carrageenan grades to produce emulsion-gels is expected to provide materials with distinct structure and rheological behaviour. The presence of oil may also have a different impact depending on the type of carrageenan used. A previous study found that ι-carrageenan was more effective than κ- and λ-carrageenan at creating highly charged interfacial membranes to stabilize soybean oil emulsions, which was attributed to its most densely charged helical structure (Wu et al., 2011).

In this context, the objective of the present work was to investigate the nanostructure, rheological and textural properties of emulsion-gels prepared using three different commercial carrageenan grades. The influence of the concentration of the commercial carrageenan and salt, as well as the oil:water ratio (OWR) in the obtained emulsion-gels were evaluated through a response surface design and the optimal formulations in terms of gel strength were determined. Moreover, the rheological properties and the nanostructure of the optimal emulsion-gels were evaluated to determine the impact of the different carrageenan grades. These results provide the basis for the formulation of emulsion-gels with target properties for their application in the food industry.

3 Materials and methods

3.1 Materials

Different commercial carrageenan grades, in the form of powders were kindly donated by CEAMSA (Pontevedra, Spain): κ-carrageenan (extracted from *Euchema cottonii*), composed by 92% κ-carrageenan and 8% ι-carrageenan; ι-carrageenan (extracted from *Euchema spinosum*), composed by 82% ι-carrageenan and 18% floridean starch; and λ-carrageenan (high viscosity grade) (extracted from *Gigartina pistillata*), composed by 29% λ-carrageenan, 27% κ-carrageenan, 2% μ-carrageenan, 20% θ-carrageenan and 19% starch (Fontes-Candia et al., 2020). KCl was obtained from Sigma-Aldrich (Spain) and sunflower oil was purchased in a local market (Valencia, Spain). The commercial carrageenan powders were dried in an oven at 60 ºC overnight and then stored in a 0%RH cabinet until further use.

3.2 Preparation of carrageenan emulsion-gels

Emulsion-gels were produced from κ-carrageenan (κ-C), ι-carrageenan (ι-C) and λ-carrageenan (λ-C), with the addition of salt (KCl). The range of carrageenan and salt concentration, as well as the oil:water volume ratio (OWR) (cf. Table 1) were established by preliminary experiments and a central composite design was carried out for each carrageenan type. The required amount of carrageenan powder was dispersed in hot water (90°C) for 30min. After that, the required volume of oil was added and the samples were homogenized with an Ultraturrax for 2 min, producing an emulsion. The salt was then added to the emulsion, which was gently stirred until the salt was completely dissolved. Aliquots of the prepared emulsions were directly transferred to quartz capillaries for SAXS analyses or to the rheometer plate. For the penetration tests, the hot emulsions were transferred to cylindrical containers (30 mm diameter, 40 mm height) and were cooled down to room temperature and subsequently stored at 4 °C for 24 h prior to the analyses.

For selected formulations, the corresponding hydrogel systems (the same formulations but without the addition of oil) were also prepared and subjected to rheological and small angle scattering characterization.

3.3 Emulsion-gel strength

The emulsion-gel strength values were determined from penetration assays using a texture analyser (Stable Micro Systems model TA-XT2, Surrey, UK) equipped with a cylindrical Teflon probe (1 cm diameter). The assays were carried out at room temperature (20–25 °C) and consisted in one penetration cycle at a penetration rate of 1 mm/s, to a depth of 5 mm. All measurements were performed, at least, in triplicate.

3.4 Experimental design

A statistical central composite design was carried out to evaluate the influence of the carrageenan concentration (C), salt concentration (KCl) and oil:water volume ratio (OWR) in the emulsion-gel strength (GS). The considered ranges for each variable in this model are shown in Table 1 and were established based on preliminary experiments, ensuring that emulsion-gels with good homogeneity and sufficient mechanical integrity to be manipulated could be obtained. According to the central composite design, 15 runs for each carrageenan type were carried out. The matrix designs and the graphical analysis were performed using IBM SPSS Statistic software (v.24) (IBM corp., USA) and Matlab (Mathworks, Inc., USA), respectively.

The response values were predicted by the quadratic polynomial equation as follows:

$$\gamma = \beta 0 + \sum_{i=1}^{k} \beta_i + \sum_{i=1}^{k} \beta_{ii} {X_i}^2 + \sum_{i \neq j}^{k} \beta_{ij} X_i X_j \quad (1)$$

were γ correspond to the predicted response: β0, βi, βii and βij were the constant regression coefficients of the model; Xi and Xj represent the independent variables. The results obtained were analyzed by ANOVA to investigate the significance and fitness of the model, as well as the effect of significant individual terms and the interactions on the responses. The optimization of the response was obtained using a response surface methodology.

Table 1. Minimum and maximum levels considered in the statistical central composite design for commercial carrageenan (C) and added salt concentration (S) expressed in % m/v, and the oil:water volume ratio (OWR).

Sample	Level	C (%)	S (%)	OWR
κ-C	Min	0.50	0.25	0.00
	Max	2.00	1.25	1.25
ι-C	Min	1.00	0.30	0.00
	Max	2.00	0.50	0.80
λ-C	Min	1.00	0.30	0.00
	Max	1.50	0.50	0.80

3.5 Oscillatory rheological measurements

The rheological measurements were performed on DHR-3 rheometer from TA instruments (USA) using a cone-plate geometry with an angle of 1°, a diameter of 40 mm and 26 µm of gap. Temperature was controlled using a Peltier plate. The cone was equipped with a solvent trap and an evaporation blocker from TA Instruments. In addition, the edge of the sample was covered with a layer of paraffin oil. Freshly prepared hot emulsions were loaded onto the rheometer, which plate was pre-heated to 80 °C. After an equilibration time of 5 minutes, a cooling step from 80 to 20 °C was performed at a constant rate of 1 °C/min and with a constant strain of 1% (selected from the linear viscoelastic region) and a frequency of 6.28 rad/s. The samples were then kept at 20 ºC during 10 min. Finally, a heating step from 20 ºC to 85 ºC was carried out at a rate of 1 ºC/min, 1% strain and a fixed frequency of 6.28 rad/s. Frequency sweeps were also performed at different selected temperatures. The samples, initially equilibrated at 85 ºC, were cooled down to the desired temperature at a rate of 1 ºC/min and frequency sweeps within the range of 0.05-100 rad/s were carried out, at 1% strain amplitude. Additionally, to determine the linear visco-elastic region, strain amplitude sweeps were performed at 20 ºC by applying a constant frequency of 6.28 rad/s and varying the strain amplitude within the range of 0.01-100% (see Figure S1).

3.6 Fourier transform infrared spectroscopy (FT-IR)

FT-IR spectra from the raw oil and the commercial carrageenan powders, the emulsion-gel samples and the corresponding hydrogels were recorded in attenuated total reflectance (ATR) mode in a controlled chamber at 21°C and CO_2 using a Thermo Nicolet Nexus (GMI, USA) equipment. The spectra were taken at 4 cm^{-1} resolution in a wavelength range between 650-4000 cm^{-1} and averaging a minimum of 32 scans.

3.7 Confocal Laser Scanning microscopy

Confocal scanning laser microscopy (CSLM) was used to visualize the microstructure of the emulsion-gels and to determine oil droplet size distribution. Imaging was performed using a Leica TCS SP2 (Leica Microsystems, Germany). From each emulsion-gel two thick sections (ca. 500µm thickness) were carefully cut with the help of a scalpel and placed onto a glass slide with the cross section facing upwards. One drop of Nile Red (0.2% wt. in acetone), which is able to stain fat, was added on top of the sample and covered with a glass cover slip. The light source used was an argon laser with an emission wavelength of 488 nm. An oil immersion objective with a magnification of 40 and a numerical aperture (NA) of 0.50 was used throughout the study. A total of six images were taken for each sample. Oil droplet size was determined by image analysis using the ImageJ software. Measurements were performed from at least 120 droplets on 5 different images and mean and standard deviation values were calculated.

3.8 Small angle X-ray scattering (SAXS)

SAXS experiments were carried out in the Non Crystalline Diffraction beamline, BL-11, at ALBA synchrotron light source (www.albasynchrotron.es). Aliquots of selected emulsions and their corresponding hydrogel systems (i.e., the same formulations but without the addition of oil) were placed in sealed 2 mm quartz capillaries (Hilgenburg Gmbh, Germany) and were left to cool down at 25 ºC for 24 h to form emulsion-gels prior to the experiments. The energy of the incident photons was 12.4 KeV or equivalently a wavelength, λ, of 1 Å. The SAXS diffraction patterns were collected by means of a photon counting detector, Pilatus 1M, with an active area of 168.7x 179.4 mm^2, an effective pixel size of 172 x 172 μm^2 and a dynamic range of 20 bits. The sample-to-detector distance was set to 6425 mm, resulting in a q range with a

maximum value of q = 0.23 $Å^{-1}$. An exposure time of 0.5 seconds was selected based on preliminary trials. The data reduction was treated by pyFAI python code (ESRF) (Kieffer & Wright, 2013), modified by ALBA beamline staff, to do on-line azimuthal integrations from a previously calibrated file. The calibration files were created from a silver behenate (AgBh) standard. The intensity profiles were then represented as a function of q using the IRENA macro suite (Ilavsky & Jemian, 2009) within the Igor software package (Wavemetrics, Lake Oswego, Oregon). A scattering background (corresponding to a quartz capillary filled with distilled water) was subtracted from all the samples.

Different models were used to fit the experimental data, depending on the type of gel structure formed. The scattering patterns from the pure carrageenan hydrogels (with no added salt) were properly described by a mathematical function consisting of a power-law term plus one Gaussian peak:

$$I(q) = \frac{A}{q^n} + I_0 \cdot \exp\left[-\frac{1}{2}\cdot\left(\frac{q-q_0}{B}\right)^2\right] + bkg \qquad (2)$$

The first term in equation (2) corresponds to the power-law function (where A is a prefactor and n is the power-law exponent) to account for the underlying diffuse scattering, the second term corresponds to the Gaussian function (where q_0 is the peak position, I_0 is the intensity of the peak and B is the standard deviation of the peak position) and the fourth term accounts for the incoherent background.

The scattering patterns from the carrageenan hydrogels and emulsion-gels (with added salt) were significantly different and could not be described by the same function. In the case of κ-C, a Gauss-Lorentz Gel model was required to fit the experimental data from the gels. This model, described by the scattering function (3), calculates the scattering from a gel structure (typically physical networks) (Evmenenko et al., 2001; Shibayama et al., 1992; Yeh et al., 1998) as the sum of a low-q exponential decay plus a Lorentzian at higher q-values:

$$< I(q) = I_G(0) \cdot \exp\left[-\frac{q^2\Xi^2}{2}\right] + I_L(0)/(1+q^2\xi^2) + bkg \qquad (3)$$

where $I_L(0)$ and $I_G(0)$ are, respectively, the linear coefficients of the Lorentzian and Gaussian terms, Ξ is the characteristic mean size of the static heterogeneities in the system under study

and ξ is the correlation length of polymer–polymer interactions between the fluctuating chains of polymer.

The ι-C and λ-C gels could be properly fitted using a correlation length model. This model contains a first term, described by a power-law function, which accounts for the scattering from large clusters in the low q region and a second term, consisting of a Lorentzian function, which describes scattering from polymer chains in the high q region:

$$I(q) = \frac{A}{q^n} + \frac{C}{1+(q\xi_L)^m} + bkg \quad (4)$$

where n is the power-law exponent, A is the power-law coefficient, m is the Lorentzian exponent, C is the Lorentzian coefficient and ξ_L is the correlation length for the polymer chains (which gives an indication of the gel's mesh size).

4 Results and discussions

4.1 Optimization of emulsion-gels

Three types of commercial carrageenans (κ-C, ι-C, λ-C) were used to produce emulsion-gels in presence of salt. The effect of the carrageenan type and concentration (C), the salt concentration (S) and the oil:water volume ratio (OWR) on the emulsion-gels' strength were evaluated through a central composite design. The measured emulsion-gel strength (GS) values for each type of carrageenan are compiled in Tables S.1, S2 and S3 (in the Supplementary Material). The results obtained for each type of carrageenan were properly fitted using quadratic models (R^2 >0.97) (cf. Table S4 for the associated statistical parameters), described by the following equations:

$$GS_{\kappa-C} = -21.44 + 18.37 \cdot C + 55.06 \cdot S + 12.44 \cdot OWR - 5.72 \cdot C^2 - 48.96 \cdot S^2 - 8.78 \cdot OWR^2 - 3.9 \cdot CS - 2.75 \cdot COWR + 0.74 \cdot SOWR \quad (5)$$

$$GS_{\iota-C} = 0.34 - 0.15 \cdot C - 1.27 \cdot S + 0.13 \cdot OWR + 0.12 \cdot C^2 + 2.01 \cdot S^2 - 0.20 \cdot OWR^2 - 0.16 \cdot CS - 0.04 \cdot COWR + 0.30 \cdot SOWR \quad (6)$$

$$GS_{\lambda-C} = -0.38 + 0.57 \cdot C + 0.71 \cdot S + 0.44 \cdot OWR - 0.21 \cdot C^2 - 0.58 \cdot S^2 - 0.30 \cdot OWR^2 - 0.01 \cdot CS + 0.03 \cdot COWR - 0.32 \cdot SOWR \quad (7)$$

To investigate the effect of the studied parameters (commercial carrageenan concentration, salt concentration and OWR) on the emulsion-gel strength, the response surface plots were also obtained for each type of carrageenan (cf. Figures 1, 2 and 3). In general, the results showed that the κ-C emulsion-gels were the strongest compared with those obtained from ι-C and λ-C. This was already anticipated since the lower amount of sulphate substitution in κ-carrageenan (the main component in the κ-C grade) is known to facilitate the formation of stronger hydrogen-bonded gel networks (Fontes-Candia et al., 2020). For the κ-C emulsion-gels, the statistical analysis showed that the linear term of OWR, all the quadratic terms and the interaction between κ-C and OWR presented significant effect on the gel strength ($P<0.05$). The obtained response surface plots, shown in Figure 1, illustrate that the highest gel strength values were obtained within the middle range of all the studied variables. This is in contrast with what has been previously reported for κ-C hydrogels, where higher strength values were obtained when increasing the κ-C and KCl concentrations (Fontes-Candia et al., 2020). Whereas the creation of stronger carrageenan networks is favourable for the development of hydrogels, these strong interactions between the polysaccharide chains may not be completely desirable in the emulsion-gels since it could impede a proper dispersion of the oil droplets within the polysaccharide matrix. According to eq.5, the highest gel strength (8.42 N) would be obtained for a formulation of 1.3% κ-C + 0.5% KCl and 0.5 OWR.

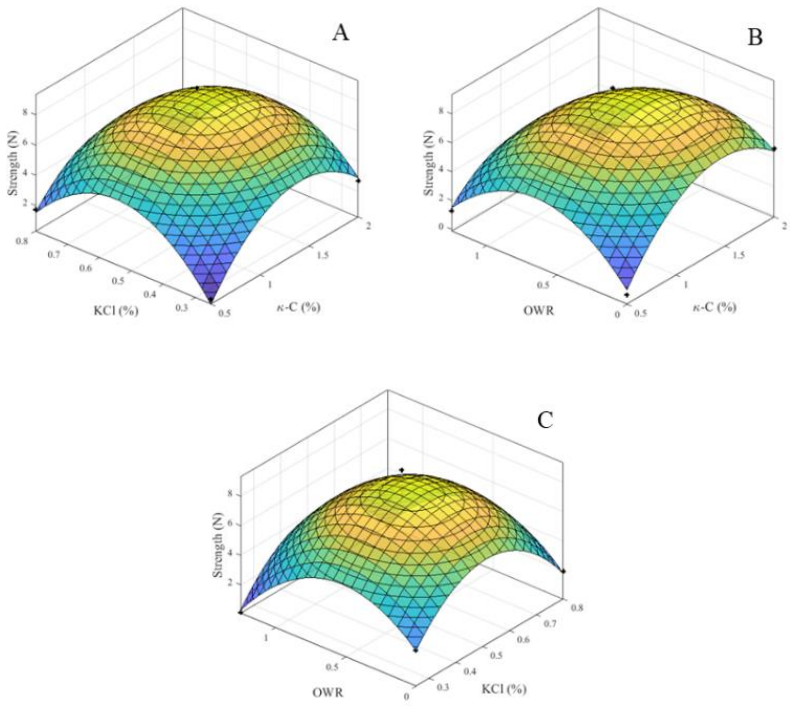

Figure 1. Response surface plots of the emulsion-gel strength for κ-C. Effect of (A) κ-C and KCl concentration (OWR fixed at central point), (B) κ-C concentration and OWR (KCl concentration fixed at central point) and (C) KCl concentration and OWR (κ-C concentration fixed at central point).

For the ι-C emulsion-gels, the linear terms of ι-C and KCl concentration, as well as the quadratic terms of ι-C and OWR, showed a significant effect on the gel strength ($P<0.05$). In particular, as shown in Figures 2A and 2B, the ι-C content had the strongest effect on the emulsion-gel strength, with the greatest strength values corresponding to the highest ι-C contents. Similarly, as deduced from Figure 2C, greater salt contents favoured the formation of stronger emulsion-gels. The maximum hydrogel strength (0.30 N), calculated from eq.6, corresponded to a formulation of 2.0% ι-C + 0.5% KCl and 0.5 OWR. The same behaviour has been reported for ι-C hydrogels, where the maximum ι-C and KCl concentrations produced the strongest hydrogel (Fontes-Candia et al., 2020). The reduced strength of ι-C emulsion-gels as compared with κ-C can be attributed to the electrostatic repulsive forces exerted by the greater amount of sulphate groups in the ι-carrageenan chains (the main component in the ι-C grade), hence producing

weaker interactions between the polysaccharide chains. Moreover, although these repulsive forces can be counteracted with the addition of salts, weaker networks held by ionic cross-linking have described in the case of ι-C (Fontes-Candia et al., 2020).

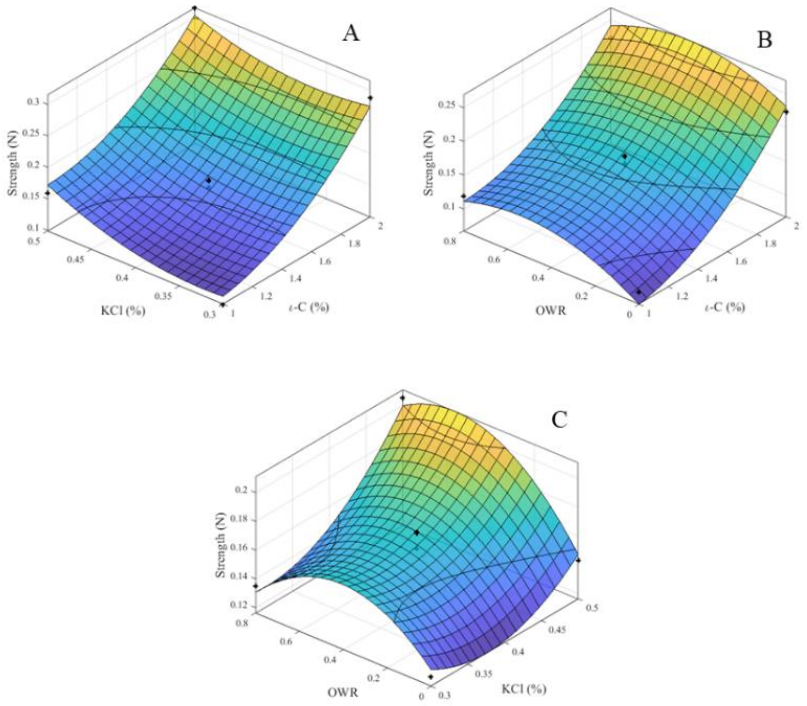

Figure 2. Response surface plots of the emulsion-gel strength for ι-C. Effect of (A) ι-C and KCl concentration (OWR fixed at central point), (B) ι-C concentration and OWR (KCl concentration fixed at central point) and (C) KCl concentration and OWR (ι-C concentration fixed at central point).

The emulsion-gels obtained from λ-C presented similar strength values to those from ι-C. Even though λ-carrageenan is thought to be a non-gelling polysaccharide, the presence of 27% κ-carrageenan in the λ-C grade seemed to be sufficient to guarantee its gelation capacity. The statistical analysis showed that the linear terms of the λ-C concentration, the OWR, the interaction between the KCl concentration and the OWR, and all the quadratic terms presented a significant effect in the gel strength. Figure 3 shows that greater gel strength values could be attained by increasing the λ-C concentration and the OWR. The formulation consisting of 1.4 % λ-C + 0.4% KCl and 0.6 OWR was the optimal in terms of gel strength (0.28 N), according to eq.7.

This formulation is very similar to the κ-C optimum, although the strength was significantly greater in κ-C as compared with λ-C; thus, it seems that the behaviour of the λ-C grade was mostly governed by the small fraction of κ-carrageenan.

The three formulations corresponding to the maximum gel strength (calculated from the theoretical models) for each type of carrageenan were prepared and their strength values were measured. Table 2 shows the emulsion-gel strength values predicted by the models and their corresponding experimental results, demonstrating the accuracy of the models to predict the behaviour of the carrageenan emulsion-gels. As deduced from the results, the carrageenan concentration needed to obtain the maximum strength was higher in the case of ι-C, which can be related to the inherent weaker intermolecular interactions of the ι-carrageenan present in this commercial grade. As previously described (Fontes-Candia et al., 2020), while κ-carrageenan chains seem to be able to associate by hydrogen bonding, the greater amount of sulphate groups in ι-carrageenan prevents the formation of strong intermolecular association. The addition of salts is therefore required in ι-C, promoting the gelation through ionic cross-linking. On the other hand, the salt concentration and OWR needed to form stronger emulsion-gels where very similar for the three carrageenan grades. The optimum salt content was intermediate for the strong κ-C emulsion-gels (to facilitate a proper dispersion of the oil droplets within the strongly bound aqueous carrageenan phase), while greater concentrations were required for the ι-C and λ-C grades (to promote intermolecular chain association). With regards to the OWR, an increase up to intermediate oil contents enhanced the emulsion-gel strength values. Further increasing the amount of oil reduced the integrity of the materials leading to softer gels. This may be attributed to an excessive proportion of oil limiting the cross-linking between the carrageenan chains (Feng et al., 2019).

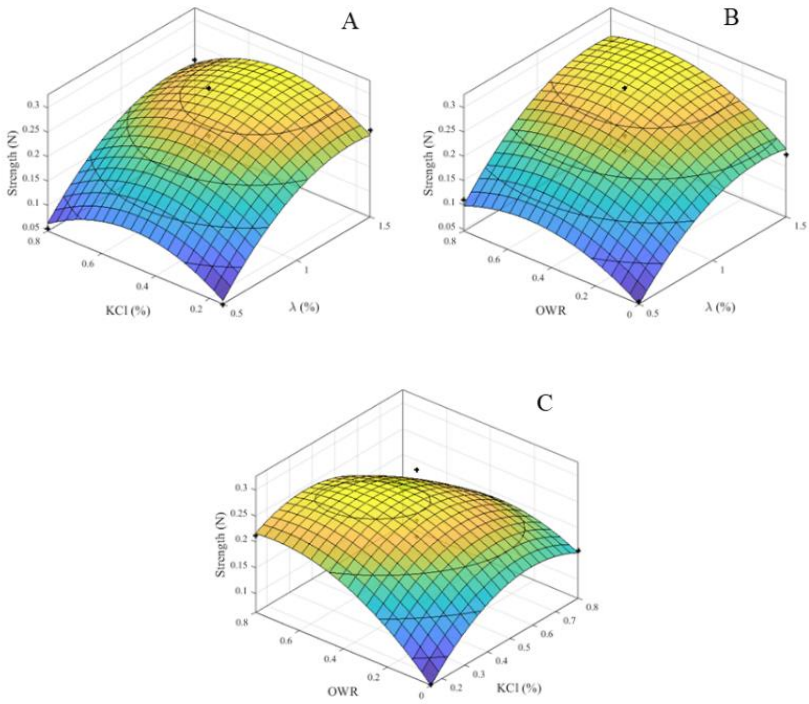

Figure 3. Response surface plot of the emulsion-gel strength for λ-C. Effect of (A) λ-C and KCl concentration (OWR fixed at central point), (B) λ-C concentration and OWR (KCl concentration fixed at central point) and (C) KCl concentration and OWR (λ -C concentration fixed at central point).

Table 2. Model-predicted and experimental strength values for the optimum emulsion-gel formulations, being C (%) the carrageenan concentration, S (%) the salt concentration, OWR oil:water volume ratio and GS (N) the theoretical emulsion-gel strength. Data shown as mean +/-SD, n=3.

Sample	C (%)	S (%)	OWR	GS (N)	Experimental strength (N)
κ-C	1.33	0.51	0.50	8.42	7.92 ± 0.30
ι-C	2.00	0.50	0.50	0.30	0.28 ± 0.05
λ-C	1.37	0.41	0.58	0.28	0.27 ± 0.01

4.2 Rheological characterization of optimum formulations

The rheological behaviour of the optimum formulations providing the highest emulsion-gel strength values for the κ-C, ι-C and λ-C grades was evaluated by means of oscillatory rheological measurements. Temperature and frequency sweeps were carried out to investigate the gelation mechanism of the three produced emulsion-gel systems. Their respective hydrogel systems (i.e., the same formulations with no added oil) were also characterized to evaluate the effect of the incorporated oil on the rheological properties of the structured systems. The elastic (G') and viscous moduli (G'') were firstly recorded during cooling and heating ramps and representative results are illustrated in Figure 4. As observed, all the samples presented a clear sol-gel transition, showing an initial stage at which G' and G'' remained almost constant, followed by a sharp increase in both moduli producing the cross-over between G' and G'' (here defined as the gelling point) and a final step where both moduli reached a plateau or continued increasing slowly. The corresponding gelling temperatures (T_{gel}), as well as the G' and G'' values of the emulsion-gels and the control hydrogels at 20 ºC were determined and the results are summarized in Table 3. In general, the emulsion-gel samples presented the same (κ-C) or even higher (ι-C and λ-C) T_{gel} than the corresponding hydrogels, indicating that the carrageenan coil-helix transition, responsible for the gelation, was somehow facilitated in the case of the emulsions**.** Similarly, (Patel & Dewettinck, 2015) reported a higher gelling temperature (T_{gel} ~35 °C) for an emulsion-gel prepared from a mixture of locus bean gum and carrageenan as compared with the hydrogel from the same mixture (T_{gel} ~13 °C). Moreover, the G' values at 20 °C were higher for the emulsion-gels than for the control hydrogels (ca. 2-fold increase), suggesting the formation of a stronger gel network in the former ones. This is in agreement with the results from the optimization, where it was observed that maximum gel strength values were attained at intermediate OWR values (cf. Table 2). Several authors have also reported higher G' and G'' values for emulsion-gels containing κ-C as compared with the corresponding aqueous solutions (Iqbal et al., 2019; Patel & Dewettinck, 2015). This observation has been consistently attributed to systems where the oil droplets acted as active fillers (Boutin et al., 2007; Line et al., 2005; Rosa et al., 2006), i.e. the droplets were somehow interacting with the gel matrix and thus, contributed to gel strength. However, it should be mentioned that no

direct evidence for the interaction between the matrix and the filler was provided in these studies. On the contrary, a negative effect has been observed in systems where no interactions exist between the filler and the gel matrix (Sala et al., 2007; Van Vliet, 1988). Thus, one possible explanation for the increased strength of the emulsion-gels would be the existence of interactions between the oil phase and the carrageenan-rich aqueous phase. Another possible explanation is simply that the carrageenan concentration in the aqueous phase of an emulsion-gel is greater than that of the corresponding hydrogel formulation. At higher carrageenan concentrations stronger and more stable hydrogels (with higher T_{gel} and T_m) are formed (Fontes-Candia et al., 2020; Kara et al., 2003). In other words, the emulsion-gels would consist of more concentrated and stronger carrageenan hydrogel networks containing homogeneously distributed oil droplets. To investigate the possible interactions established between the carrageenans and the oil phase, FT-IR spectra of the emulsion-gels and the corresponding hydrogels were recorded and the bands characteristic from the sunflower oil were compared in the raw oil and the emulsion-gel to identify band shifts indicative of oil-carrageenan interactions. Figure S2 shows, as an example, the spectra obtained for the ι-C gels. As observed, the spectra from the ι-C hydrogel corresponded mainly to that of water (due to the high hydration level in the sample), while the ι-C emulsion-gel showed several bands attributed to the presence of the sunflower oil, being the most intense ones those located at ca. 3010 cm^{-1}, 2960 cm^{-1}, 1740 cm^{-1}, 1460 cm^{-1}, 1380 cm^{-1} and 1160 cm^{-1}. The position of these bands was not shifted with regards to the raw sunflower oil, hence supporting the fact that no interactions were being established between the carrageenan and the oil phase. Assuming that the commercial carrageenans were only dispersed within the aqueous phase, the commercial carrageenan concentrations in the aqueous phase would be 1.94% for the κ-C emulsion-gel, 2.99% for ι-C and 2.17% for λ-C. Interestingly, the increase in the G' values of the emulsion-gels with respect to their corresponding hydrogels is very well correlated to the increase in the real concentration of the commercial carrageenans within the aqueous phase in the emulsion-gels with respect to their concentrations in the hydrogels. This supports the fact that the changes observed in the properties of the emulsion-gels with regards to the hydrogels are due to a polysaccharide concentration effect.

When comparing the three different emulsion-gels, the T_{gel} values were very similar for κ-C and ι-C, whereas λ-C presented a significantly lower T_{gel}. This could be explained by the heterogeneous composition of the λ-C grade, mostly composed of non-gelling carrageenans and containing only a small fraction of gelling κ-carrageenan. The high fraction of non-gelling carrageenans obstructs the formation of helical strands, hindering the gelation process and therefore, lower temperatures are required for the formation of gel networks. As expected, the κ-C emulsion formed stronger gels (with a strength value very similar to that previously reported for other κ-C emulsion systems (Iqbal et al., 2019)) than the ι-C and λ-C, as deduced by the higher G' values of the former. This can be explained by the lower sulphate substitution in κ-carrageenan, which facilitates the association of the carrageenan double helices due to reduced electrostatic repulsive forces (Fontes-Candia et al., 2020). Furthermore, the addition of KCl is known to promote the intermolecular association of κ-carrageenan double helices by hydrogen bonding through neutralization of the negative charges from sulphate groups (Fontes-Candia et al., 2020; Wang et al., 2018), giving rise to the formation of very strong gel networks.

After equilibration at 20 °C to set the formed gels, the samples were heated up to 85°C. A decrease in G' and G'' was observed when increasing the temperature, followed by the cross-over between G' and G'' indicating the gel-sol transition, i.e., the disruption of the carrageenan double helices. The melting temperatures (T_m) of the ι-C and λ-C emulsion-gels were higher than those from the corresponding hydrogel formulations, once again indicating that stronger networks were created in the case of the emulsion-gels. Interestingly, the κ-C and λ-C gels presented large hysteresis, i.e., a marked difference was observed between the cooling and heating behaviour, being T_m higher than T_{gel}. This phenomenon has been previously observed for carrageenan and agar gels and was ascribed to the formation of larger aggregates of polysaccharide helices (Makshakova et al., 2019; Mangione et al., 2003). The formation of these aggregates originates strong gel networks, which are more thermally stable and thus, higher temperatures are required to disrupt the carrageenan helical aggregates upon heating. In contrast, the ι-C gels did not present thermal hysteresis, suggesting that a distinct type of gel structures were formed (Brenner et al., 2014; Zia et al., 2017). In fact, it has been demonstrated

that gelation of ι-C with the addition of salts occurs mostly through ionic cross-linking, leading to the formation of much weaker gel structures (Fontes-Candia et al., 2020).

Table 3. Rheological properties of carrageenan optimal emulsion-gels. Gelation temperature (T_{gel}), melting temperature (T_m) and elastic modulus ($G'_{20°C}$) and viscous modulus ($G''_{20°C}$) at 20°C.

Samples	T_{gel} (ºC)	G' (kPa)	G'' (kPa)	T_m (°C)
κ-C hydrogel	62	12.5	0.60	79
κ-C emulsion-gel	61	25.0	1.40	76
ι-C hydrogel	48	0.50	0.02	49
ι-C emulsion-gel	61	1.0	0.03	61
λ-C hydrogel	46	0.8	0.100	61
λ-C emulsion-gel	53	1.7	0.100	72

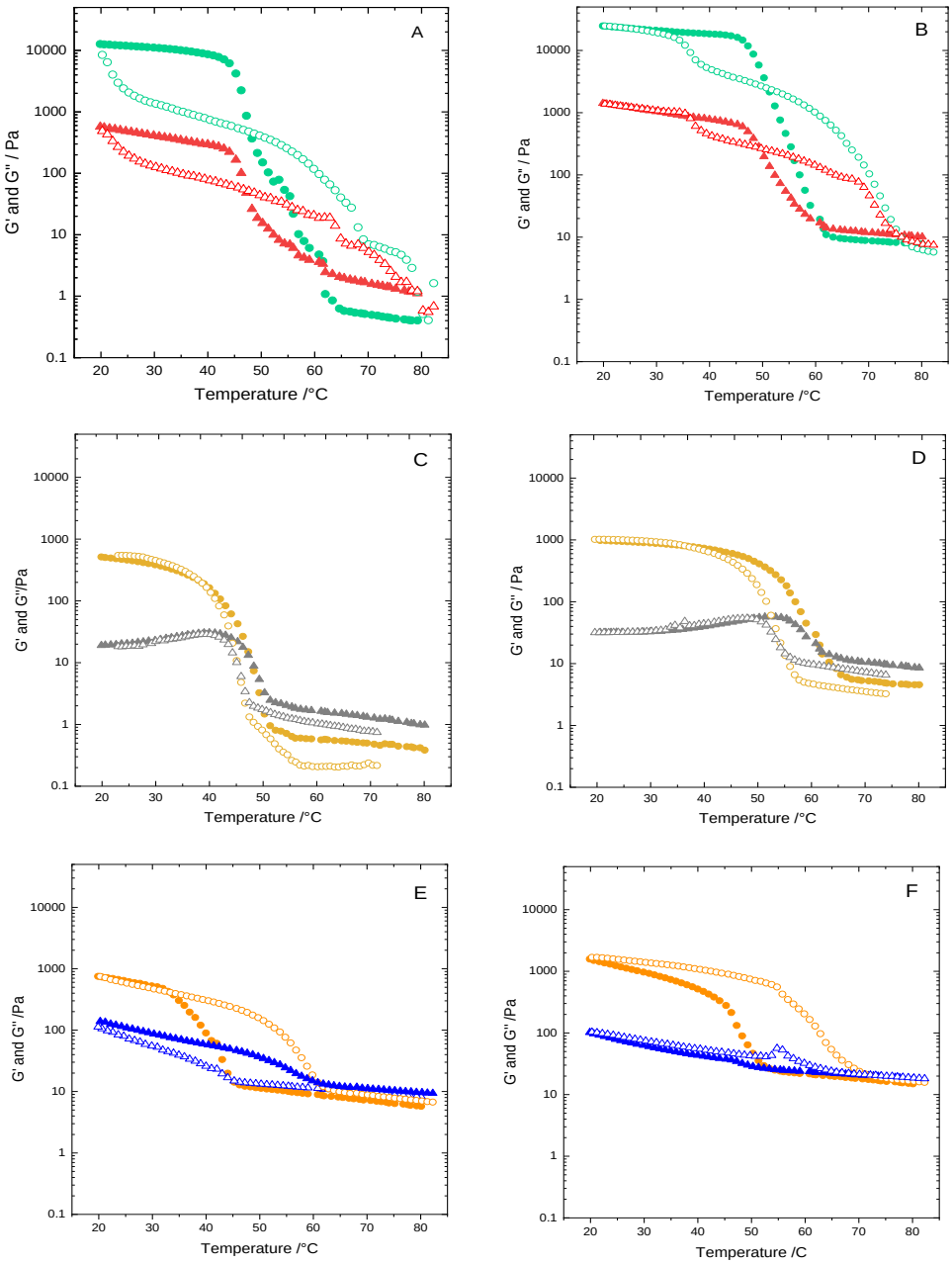

Figure 4. Temperature dependence of G' and G'' moduli of carrageenan emulsion-gels during cooling (solid markers) and heating (open markers) ramps. (A) κ-C hydrogel; (B) κ-C emulsion-gel; (C) ι-C hydrogel; (D) ι-C emulsion-gel; (E) λ-C hydrogel and (F) λ-C emulsion-gel.

All the emulsion-gels were subjected to frequency sweeps at 70 and 20 °C and the frequency dependence of G' and G'' was determined at a fixed strain of 1%. As shown in Figure 5, all the emulsion-gels presented a solid-like behaviour (G' > G'') at 20 °C, which was frequency independent. Similar results were reported by (Soukoulis et al., 2017) for κ-C emulsions using KCl (G~10 kPa) at 25 °C. At a higher temperature of 70°C (before the gelling transition of the three carrageenan grades) all the emulsion systems presented a frequency dependent behaviour. While G' was higher than G'' at low frequencies, a cross-over point was observed when further increasing the frequency indicating a fluid-like behaviour.

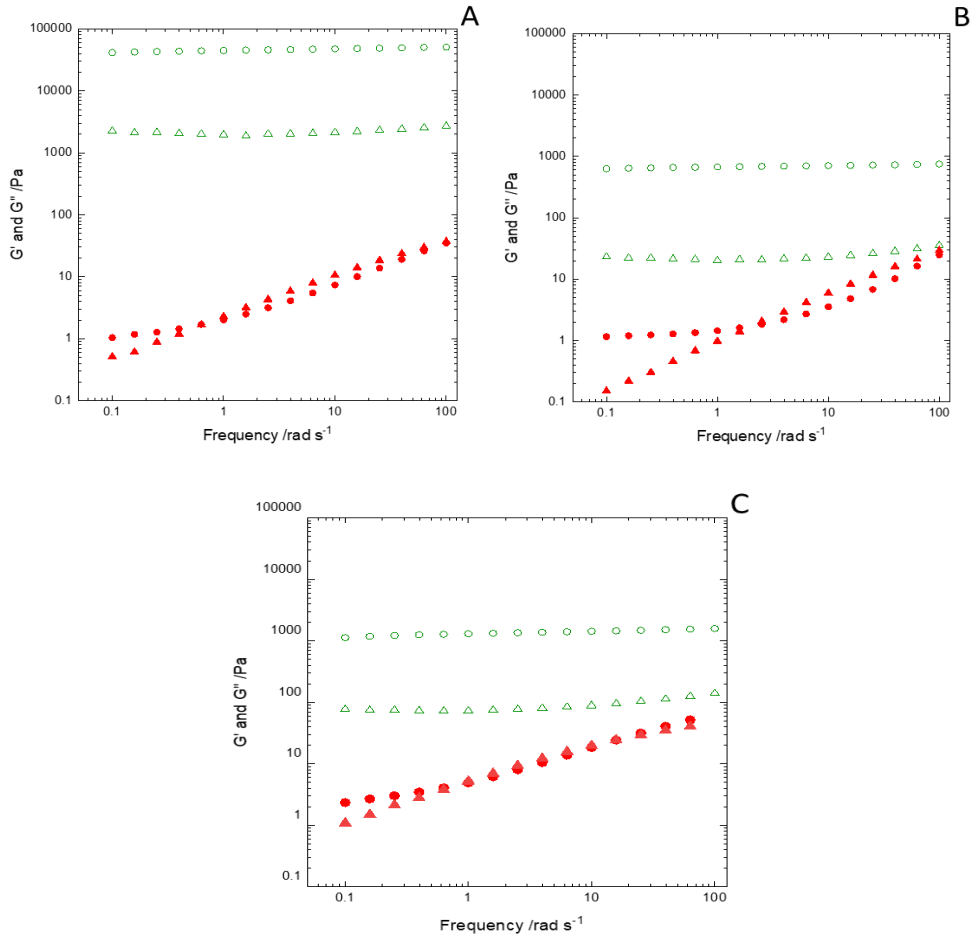

Figure 5. G' and G'' as a function of frequency for the optimal emulsion-gels, measured at temperature of 70 °C (solid markers) and 20 °C (open markers). (A) κ-C emulsion-gel; (B) ι-C emulsion-gel; (C) λ-C emulsion-gel.

4.3 Micro and nanostructural characterization of optimum formulations

As shown in Figure 6, the optimized κ-C, ι-C and λ-C emulsion-gels and the corresponding hydrogel formulations presented a good integrity and homogeneity. The microstructure of the emulsion-gels was further investigated by means of confocal microscopy by staining the sunflower oil with Nile red. Representative confocal images (cf. Figures 6G-I) show the distribution of the oil droplets within the carrageen matrix and evidence a great heterogeneity of droplet sizes. Looking at the average droplet sizes (35.8 ± 21.1 μm for κ-C, 21.9 ± 16.4 μm for ι-C and 27.6 ± 18.1 μm for λ-C), it seems that κ-C contained a greater population of large droplets; however, due to the large standard deviation values, the differences between samples were not statistically significant. Previous studies have reported that oil coalescence, induced by the addition of KCl, took place in κ-carrageenan emulsion-filled gels, giving rise to oil droplets much larger than those occurring in the original emulsions (Sala, Van Vliet, Stuart, Van Aken, et al., 2009; Sala, Van Vliet, Stuart, Van de Velde, et al., 2009). In addition, Wu et al., (2021) reported that oil body emulsions stabilized with ι-carrageenan presented a more stable structure (less coalescence took place) than those stabilized with κ- and λ-carrageenan and ascribed such behaviour to the higher charge density of the ι-carrageenan helical structures, forming more charged interfacial membranes and thus reducing the aggregation of oil droplets (Wu et al., 2011). This, together with the inherent difficulty of dispersing the oil into the more viscous κ-C solutions during the homogenization step to prepare the emulsions, may explain the larger average droplet size in the κ-C emulsion-gel.

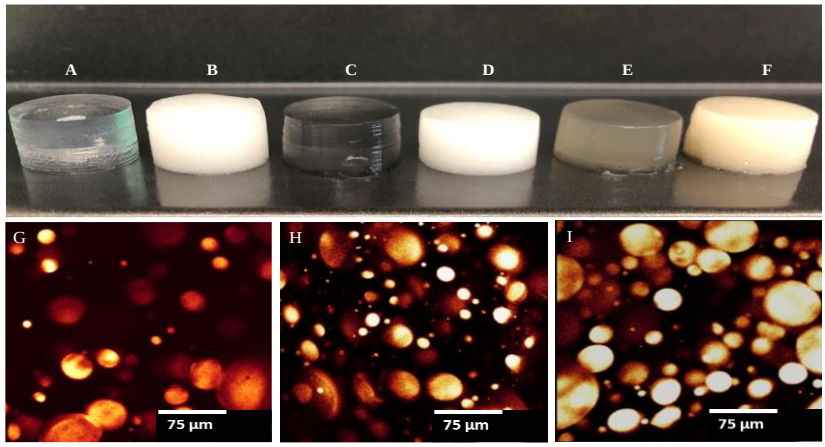

Figure 6. Visual appearance of κ-C hydrogel (A) and emulsion-gel (B); ι-C hydrogel (C) and emulsion-gel (D); λ-C hydrogel (E) and emulsion-gel (F). Confocal microscopy images of (G) κ-C, (H) ι-C and (I) λ-C emulsion-gel samples.

The nanostructure of the stronger emulsion-gels was also investigated by means of SAXS experiments. To understand the structural changes induced by the presence of the oil and by the addition of KCl, the same formulations used for the emulsion-gels were also used to produce hydrogels with and without the addition of the salt and the obtained materials were characterized. The experimental scattering curves, shown in Figure 7, evidenced clear structural differences between the carrageenan grades. Interestingly, while a scattering peak was clearly detected in the pure carrageenan hydrogels, such feature was absent when KCl was incorporated into the formulations. Comparable correlation peaks have been detected in the SAXS patterns from κ-carrageenan solutions and gels and were ascribed to the existence of bundles of parallel carrageenan double helices (Turquois et al., 1995). To extract more information from the SAXS results, a mathematical function consisting of a power-law term plus a Gaussian peak was applied to fit the experimental data from the pure carrageenan hydrogels. The obtained fitting parameters, gathered in Table 4a, indicate structural differences between the different carrageenan grades. The power-law exponents from κ-C and ι-C are characteristic of non-aggregated polymeric chains, whereas the exponent for the λ-C hydrogel is indicative of a clustered network. This may be a consequence of the more heterogeneous composition of λ-C, giving rise to more randomly distributed structures within the corresponding size range (>60 nm). On the other hand, the characteristic size of the aggregates of double helices decreased

from ca. 15 nm for κ-C, to 12 nm for λ-C and 9 nm for ι-C. The formation of larger aggregates in κ-C is most likely related to the lower amount of sulphate groups in κ-carrageenan, enabling a greater degree of intermolecular chain association.

The gel systems produced with the addition of KCl showed distinct scattering patterns, where the Gaussian peak was not visible or replaced by very broad shoulder-like features. Thus, the power-law plus Gaussian peak model was not suitable for these data. According to previous works (Evmenenko et al., 2001; Fontes-Candia et al., 2020), a Gauss-Lorentz gel model is appropriate to fit the scattering data from carrageenan hydrogels. In the present work, the Gauss-Lorentz gel model was suitable for the κ-C gels, but it was not able to provide satisfactory fits for the ι-C and λ-C gels. The obtained fitting parameters for the κ-C hydrogel and emulsion-gel (cf. Table 4b) evidence that the structure of both systems was very similar at the nanoscale level. The Gaussian parameter (Ξ), i.e., the mean size of the static heterogeneities in the system, was close to the value previously reported for other κ-C hydrogels (25 nm for hydrogels consisting of 2% κ-C + 1.5% KCl) (Fontes-Candia et al., 2020). This parameter is related to the existence of aggregates of carrageenan helices, formed as a consequence of the addition of salt through neutralization of the electrostatic repulsions for the carrageenan sulphate groups. The appearance of a small peak located at 0.021 $Å^{-1}$ in the κ-C hydrogel (indicative of the existence of well-ordered structures with real distances of ca. 29 nm), suggests that these aggregates were arranged forming well-ordered structures. The Lorentzian parameter (ξ) corresponds to the correlation length for the polymer chains and can be associated to the size of the carrageenan double helices. The obtained value for the κ-C hydrogel and emulsion-gel (ca. 7 nm) is within the range of values previously reported in the literature (Abad et al., 2006; Fontes-Candia et al., 2020).

A simpler correlation length model was used to fit the data from the ι-C and λ-C gels. The obtained power-law exponents were indicative of surface fractal structures, i.e., rough or smooth surfaces. The ι-C and λ-C hydrogels presented exponents of 2.9 and 2.8, respectively, but the value increased up to 4 in the case of the ι-C emulsion-gel. A power-law exponent of 4 corresponds to smooth surfaces and might indicate that at the corresponding size range, only the structure of carrageenan bundles is observed. This suggests that a structure of more

compacted carrageenan bundles was attained in the case of ι-C when the oil was incorporated into the system. As previously commented, the higher concentration of the carrageenan in the aqueous phase in the emulsion-gels was responsible for the formation of stronger gel networks. The Lorentz exponent (m) is related to the local chain conformation. Values close to 2, characteristic from randomly branched Gaussian polymer chains, were obtained for the λ-C gels. On the other hand, the ι-C gels presented values closer to 1, indicative of rigid rods. The associated correlation lengths were also greater for the λ-C gels. These results suggest that larger helical structures were formed in the case of λ-C, whereas smaller and more rigid structures (which could be modelled as rigid rods) were attained for ι-C. This would explain the decreased mechanical integrity (lower G') and thermal stability (lower T_m) of the λ-C emulsion-gels, as indicated by the rheological characterization. Another important implication from the fitting results is that the scattering patterns were more strongly dominated by the power-law behaviour in the case of the λ-C gels as opposed to the ι-C gels (as indicated by the lower power-law coefficients of the latter), i.e., the contribution of the larger scale structure was more prominent in the λ-C gels. Overall, it seems that the presence of a small amount of κ-carrageenan in the λ-C grade facilitated the association of polysaccharide chains.

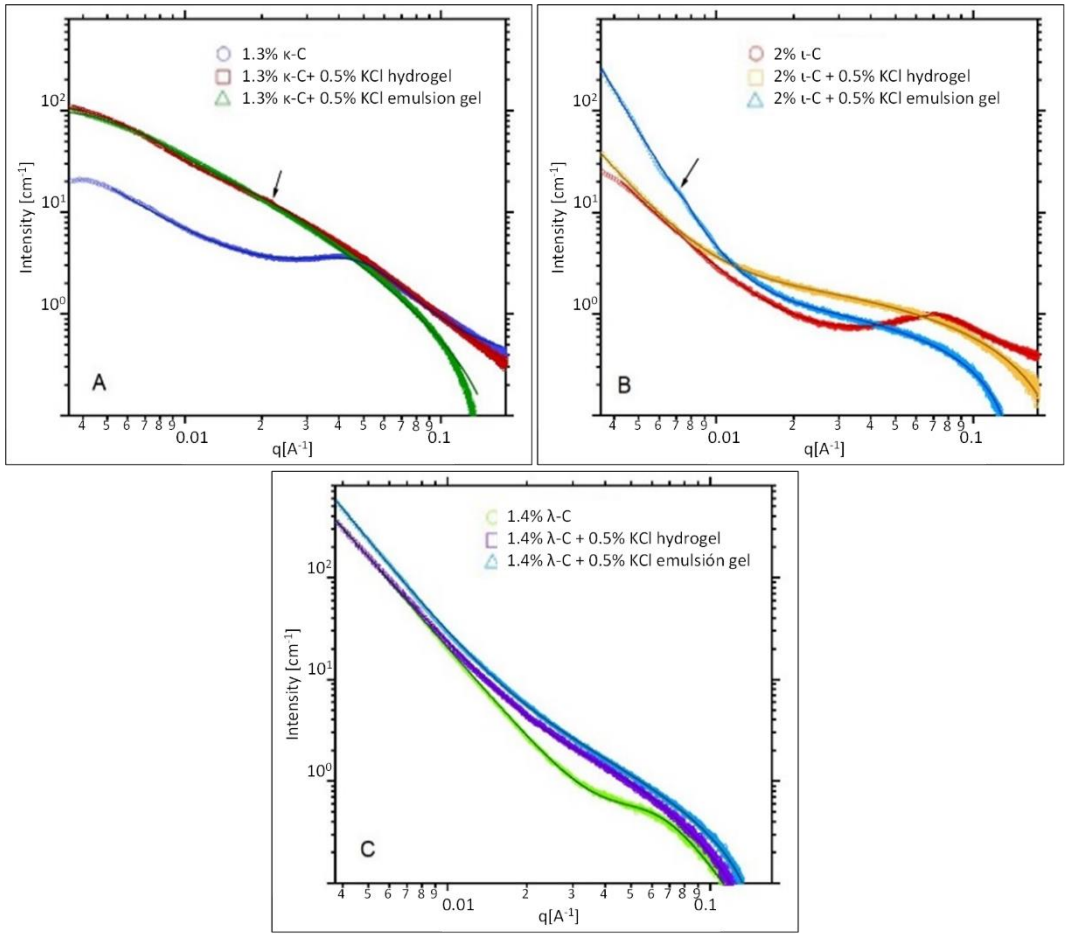

Figure 7. SAXS patterns from the different carrageenan emulsion-gels and their corresponding hydrogel systems. (A) κ-C, (B) ι-C and (C) λ-C. Markers represent the experimental data and solid lines show the fits obtained using theoretical models.

Table 4. Parameters obtained from the fits of (a) the pure carrageenan hydrogels (b) the κ-C hydrogel and emulsion-gel and (c) the ι-C and λ-C hydrogels and emulsion-gels.

(a)

Samples	A	n	I_0	d (nm)
1.3% κ-C	$2.9 \cdot 10^{-2}$	1.6	27.1	15.2
2.0% ι-C	$4.3 \cdot 10^{-4}$	2.4	6.0	8.9
1.4% λ-C	$2.5 \cdot 10^{-4}$	3.0	4.4	11.8

(b)

Samples	I_G	Ξ (nm)	I_L	ξ (nm)
1.3% κ-C + 0.5% KCl hydrogel	1006	23.6	373	6.5
1.3% κ-C + 0.5% KCl emulsion-gel	750	22.3	450	7.3

(c)

Samples	A	*n*	C	*m*	ξ (nm)
2.0% ι-C + 0.5% KCl hydrogel	$3 \cdot 10^{-5}$	2.92	28	1.1	1.3
1.3% ι-C + 0.5% KCl emulsion-gel	$1 \cdot 10^{-7}$	4.00	17	1.5	1.6
1.4% κ-C + 0.4% KCl hydrogel	$5 \cdot 10^{-4}$	2.84	16	2.5	2.0
1.4% κ-C + 0.4% KCl emulsion-gel	$1 \cdot 10^{-4}$	3.14	42	1.9	3.6

5 Conclusions

Emulsion-gels consisting of a gelling carrageenan matrix and a dispersed sunflower oil phase were produced. Three different commercial carrageenan grades (κ-C, ι-C, λ-C) were used as the gelling matrix and the effect of carrageenan and salt concentration, as well as the OWR, on the emulsion-gel strength were evaluated through a response surface design. The results indicate that the strongest emulsion-gels were obtained with κ-C due to the lower amount of sulphate groups in the κ-carrageenan composing this grade, which enabled the formation of stronger hydrogen-bonded gel networks.

The rheological behaviour and micro-/nano-structure of the optimum emulsion-gel formulations were also characterized and compared to their respective hydrogel formulations. In general, the emulsion-gels formed stronger (greater G' values) and more thermally stable (higher T_{gel} and T_m) networks than the hydrogels, being this effect more evident in ι-C and λ-C. However, no evidence of interactions between the carrageenans and the oil phase was found and the different rheological behaviour of the emulsion-gels was merely induced by a greater carrageenan concentration in the aqueous phase. The rheological behaviour and structure of the emulsion-gels were mostly governed by the type of carrageenans composing each commercial grade. The lower amount of sulphate groups in κ-carrageenan enabled a greater degree of intermolecular chain association in κ-C gels, forming larger bundles of double helices.

Despite the non-gelling capacity of λ-carrageenan, the presence of κ-carrageenan in the λ-C grade enabled the association of carrageenan chains into double helices and bundles, although weaker networks than those found in κ-C were formed. In contrast, a lower degree of chain association took place in ι-C, where ionic cross-linking was the main mechanism driving the intermolecular interactions.

These results provide the basis for a rational design of carrageenan emulsion-gels and demonstrate that the rheological and mechanical behaviour of these materials is governed by the nanostructure and intermolecular associations. This opens up the possibility of using these emulsion-gel systems in diverse applications within the food industry, such as fat replacement ingredients and encapsulation systems for the controlled release of bioactive compounds.

6 Acknowledgements

Synchrotron experiments were performed at NCD beamline at ALBA Synchrotron with the collaboration of ALBA staff (2018022638 project). This work was financially supported by the grant RTI2018-094268-B-C22 (MCIU/AEI/FEDER, UE). Part of this work was supported by the COST Action ES1408 European network for algal-bioproducts (EUALGAE). Cynthia Fontes-Candia is recipient of a pre-doctoral grant from CONACYT (MEX/Ref. 306680).

7 References

Abad, L., Okabe, S., Koizumi, S., & Shibayama, M. (2006). Small-angle neutron scattering study on irradiated kappa carrageenan. *Physica B: Condensed Matter*, *381*(1–2), 103–108.

Boutin, C., Giroux, H. J., Paquin, P., & Britten, M. (2007). Characterization and acid-induced gelation of butter oil emulsions produced from heated whey protein dispersions. *International Dairy Journal*, *17*(6), 696–703.

Brenner, T., Tuvikene, R., Parker, A., Matsukawa, S., & Nishinari, K. (2014). Rheology and structure of mixed kappa-carrageenan/iota-carrageenan gels. *Food Hydrocolloids*, *39*, 272–279. https://doi.org/https://doi.org/10.1016/j.foodhyd.2014.01.024

Derkach, S., Zhabyko, I., Voron'ko, N., Maklakova, A., & Dyakina, T. (2015). Stability and the rheological properties of concentrated emulsions containing gelatin–κ-carrageenan polyelectrolyte complexes. *Colloids and Surfaces A: Physicochemical and Engineering Aspects*, *483*, 216–223. https://doi.org/https://doi.org/10.1016/j.colsurfa.2015.04.007

Devezeaux de Lavergne, M., Strijbosch, V. M. G., Van den Broek, A. W. M., Van de Velde, F., & Stieger, M. (2016). Uncoupling the Impact of Fracture Properties and Composition on

Sensory Perception of Emulsion-Filled Gels. *Journal of Texture Studies*, *47*(2), 92–111.

Dickinson, E., & Chen, J. (1999). Heat-set whey protein emulsion gels: role of active and inactive filler particles. *Journal of Dispersion Science and Technology*, *20*(1–2), 197–213. https://doi.org/10.1080/01932699908943787

Evmenenko, G., Theunissen, E., Mortensen, K., & Reynaers, H. (2001). SANS study of surfactant ordering in κ-carrageenan/cetylpyridinium chloride complexes. *Polymer*, *42*(7), 2907–2913.

Feng, L., Jia, X., Zhu, Q., Liu, Y., Li, J., & Yin, L. (2019). Investigation of the mechanical, rheological and microstructural properties of sugar beet pectin /soy protein isolate-based emulsion-filled gels. *Food Hydrocolloids*, *89*, 813–820. https://doi.org/https://doi.org/10.1016/j.foodhyd.2018.11.039

Fontes-Candia, C., Ström, A., Gómez-Mascaraque, L. G., López-Rubio, A., & Martínez-Sanz, M. (2020). Understanding nanostructural differences in hydrogels from commercial carrageenans: Combined small angle X-ray scattering and rheological studies. *Algal Research*, *47*, 101882. https://doi.org/https://doi.org/10.1016/j.algal.2020.101882

Geremias-Andrade, M. I., Souki, P. B. G. N., Moraes, C. F. I., & Pinho, C. S. (2016). Rheology of Emulsion-Filled Gels Applied to the Development of Food Materials. In *Gels* (Vol. 2, Issue 3). https://doi.org/10.3390/gels2030022

Giarnetti, M., Paradiso, V. M., Caponio, F., Summo, C., & Pasqualone, A. (2015). Fat replacement in shortbread cookies using an emulsion filled gel based on inulin and extra virgin olive oil. *LWT-Food Science and Technology*, *63*(1), 339–345.

Iqbal, S., Xu, Z., Huang, H., & Chen, X. D. (2019). Structuring of water-in-oil emulsions using controlled aggregation of polysaccharide in aqueous phases. *Journal of Food Engineering*, *258*, 34–44. https://doi.org/https://doi.org/10.1016/j.jfoodeng.2019.04.008

Kara, S., Tamerler, C., Bermek, H., & Pekcan, Ö. (2003). Cation effects on sol–gel and gel–sol phase transitions of κ-carrageenan–water system. *International Journal of Biological Macromolecules*, *31*(4), 177–185. https://doi.org/https://doi.org/10.1016/S0141-8130(02)00080-6

Koç, H., Drake, M., Vinyard, C. J., Essick, G., van de Velde, F., & Foegeding, E. A. (2019). Emulsion filled polysaccharide gels: Filler particle effects on material properties, oral processing, and sensory texture. *Food HydrocolloidsKoç, H., Drake, M., Vinyard, C. J., Essick, G., van de Velde, F., & Foegeding, E. A. (2019). Emulsion Filled Polysaccharide Gels: Filler Particle Effects on Material Properties, Oral Processing, and Sensory Texture. Food Hydrocolloids, 9*, *94*, 311–325. https://doi.org/https://doi.org/10.1016/j.foodhyd.2019.03.018

Koo, C. K. W., Chung, C., Fu, J.-T. R., Sher, A., Rousset, P., & McClements, D. J. (2019). Impact of sodium caseinate, soy lecithin and carrageenan on functionality of oil-in-water emulsions. *Food Research International*, *123*, 779–789. https://doi.org/https://doi.org/10.1016/j.foodres.2019.05.043

Line, V. L. S., Remondetto, G. E., & Subirade, M. (2005). Cold gelation of β-lactoglobulin oil-in-water emulsions. *Food Hydrocolloids*, *19*(2), 269–278.

Lorenzo, G., Zaritzky, N., & Califano, A. (2013). Rheological analysis of emulsion-filled gels based on high acyl gellan gum. *Food Hydrocolloids*, *30*(2), 672–680. https://doi.org/https://doi.org/10.1016/j.foodhyd.2012.08.014

Makshakova, O. N., Faizullin, D. A., & Zuev, Y. F. (2019). Interplay between secondary structure and ion binding upon thermoreversible gelation of κ-carrageenan. *Carbohydrate Polymers*, 115342. https://doi.org/https://doi.org/10.1016/j.carbpol.2019.115342

Mangione, M. R., Giacomazza, D., Bulone, D., Martorana, V., & San Biagio, P. L. (2003). Thermoreversible gelation of κ-Carrageenan: relation between conformational transition and aggregation. *Biophysical Chemistry*, *104*(1), 95–105.

Matsumura, Y., Kang, I.-J., Sakamoto, H., Motoki, M., & Mori, T. (1993). Filler effects of oil droplets on the viscoelastic properties of emulsion gels. *Food Hydrocolloids*, *7*(3), 227–240.

Necas, J., & Bartosikova, L. (2013). Carrageenan: a review. *Veterinarni Medicina*, *58*(4), 187–205.

Oliver, L., Scholten, E., & van Aken, G. A. (2015). Effect of fat hardness on large deformation rheology of emulsion-filled gels. *Food Hydrocolloids*, *43*, 299–310.

Paglarini, C. de S., Furtado, G. de F., Biachi, J. P., Vidal, V. A. S., Martini, S., Forte, M. B. S., Cunha, R. L., & Pollonio, M. A. R. (2018). Functional emulsion gels with potential application in meat products. *Journal of Food Engineering*, *222*, 29–37. https://doi.org/https://doi.org/10.1016/j.jfoodeng.2017.10.026

Patel, A. R., Cludts, N., Sintang, M. D. Bin, Lesaffer, A., & Dewettinck, K. (2014). Edible oleogels based on water soluble food polymers: preparation, characterization and potential application. *Food & Function*, *5*(11), 2833–2841.

Patel, A. R., & Dewettinck, K. (2015). Comparative evaluation of structured oil systems: Shellac oleogel, HPMC oleogel, and HIPE gel. *European Journal of Lipid Science and Technology*, *117*(11), 1772–1781.

Perrechil, F. A., & Cunha, R. L. (2013). Stabilization of multilayered emulsions by sodium caseinate and κ-carrageenan. *Food Hydrocolloids*, *30*(2), 606–613. https://doi.org/https://doi.org/10.1016/j.foodhyd.2012.08.006

Poyato, C., Ansorena, D., Berasategi, I., Navarro-Blasco, Í., & Astiasarán, I. (2014). Optimization of a gelled emulsion intended to supply ω-3 fatty acids into meat products by means of response surface methodology. *Meat Science*, *98*(4), 615–621.

Rosa, P., Sala, G., Van Vliet, T. O. N., & Van De Velde, F. (2006). Cold gelation of whey protein emulsions. *Journal of Texture Studies*, *37*(5), 516–537.

Sala, G., de Wijk, R. A., van de Velde, F., & van Aken, G. A. (2008). Matrix properties affect the sensory perception of emulsion-filled gels. *Food Hydrocolloids*, *22*(3), 353–363.

Sala, G., Van Aken, G. A., Stuart, M. A. C., & Van De Velde, F. (2007). Effect of droplet-matrix interactions on large deformation properties of emulsion-filled gels. *Journal of Texture Studies*, *38*(4), 511–535.

Sala, G., Van Vliet, T., Stuart, M. A. C., Van Aken, G. A., & Van de Velde, F. (2009). Deformation and fracture of emulsion-filled gels: effect of oil content and deformation speed. *Food Hydrocolloids*, *23*(5), 1381–1393.

Sala, G., Van Vliet, T., Stuart, M. C., Van de Velde, F., & Van Aken, G. A. (2009). Deformation and fracture of emulsion-filled gels: Effect of gelling agent concentration and oil droplet size. *Food Hydrocolloids*, *23*(7), 1853–1863.

Shibayama, M., Tanaka, T., & Han, C. C. (1992). Small angle neutron scattering study on poly (N-isopropyl acrylamide) gels near their volume-phase transition temperature. *The Journal of Chemical Physics*, *97*(9), 6829–6841.

Siraj, N., Shabbir, M. A., Ahmad, T., Sajjad, A., Khan, M. R., Khan, M. I., Butt, M. S., Siraj, N., Shabbir, M. A., Ahmad, T., Sajjad, A., Siraj, N., Shabbir, M. A., Ahmad, T., & Sajjad, A. (2015). Organogelators as a Saturated Fat Replacer for Structuring Edible Oils Organogelators as a Saturated Fat Replacer for Structuring Edible Oils. *International Journal of Food Properties*, *18*(9), 1973–1989. https://doi.org/10.1080/10942912.2014.951891

Soukoulis, C., Tsevdou, M., Andre, C. M., Cambier, S., Yonekura, L., Taoukis, P. S., & Hoffmann, L. (2017). Modulation of chemical stability and in vitro bioaccessibility of beta-carotene loaded in kappa-carrageenan oil-in-gel emulsions. *Food Chemistry*, *220*, 208–218. https://doi.org/https://doi.org/10.1016/j.foodchem.2016.09.175

Stortz, T. A., Zetzl, A. K., Barbut, S., Cattaruzza, A., & Marangoni, A. G. (2012). Edible oleogels in food products to help maximize health benefits and improve nutritional profiles. *Lipid Technology*, *24*(7), 151–154.

Tan, T. B., Nakajima, M., & Tan, C. P. (2018). Effect of polysaccharide emulsifiers on the fabrication of monodisperse oil-in-water emulsions using the microchannel emulsification method. *Journal of Food Engineering*, *238*, 188–194. https://doi.org/https://doi.org/10.1016/j.jfoodeng.2018.06.026

Tavernier, I., Patel, A. R., Meeren, P. Van Der, & Dewettinck, K. (2017). Emulsion-templated liquid oil structuring with soy protein and soy protein : k -carrageenan complexes. *Food Hydrocolloids*, *65*, 107–120. https://doi.org/10.1016/j.foodhyd.2016.11.008

Thakur, G., Naqvi, M. A., Rousseau, D., Pal, K., Mitra, A., & Basak, A. (2012). Gelatin-based emulsion gels for diffusion-controlled release applications. *Journal of Biomaterials Science, Polymer Edition*, *23*(5), 645–661.

Turquois, T., Rochas, C., Taravel, F., Doublier, J. L., & Axelos, M. (1995). Small-angle x-ray scattering of κ-carrageenan based systems: Sols, gels, and blends with carob galactomannan. *Biopolymers: Original Research on Biomolecules*, *36*(5), 559–567.

Van Vliet, T. (1988). Rheological properties of filled gels. Influence of filler matrix interaction. *Colloid and Polymer Science*, *266*(6), 518–524.

Wang, Y., Yuan, C., Cui, B., & Liu, Y. (2018). Influence of cations on texture, compressive elastic modulus, sol-gel transition and freeze-thaw properties of kappa-carrageenan gel. *Carbohydrate Polymers*, *202*, 530–535. https://doi.org/https://doi.org/10.1016/j.carbpol.2018.08.146

Wu, N., Yang, X., Teng, Z., Yin, S., Zhu, J., & Qi, J. (2011). Stabilization of soybean oil body

emulsions using κ, ι, λ-carrageenan at different pH values. *Food Research International*, *44*(4), 1059–1068. https://doi.org/https://doi.org/10.1016/j.foodres.2011.03.019

Yeh, F., Sokolov, E. L., Walter, T., & Chu, B. (1998). Structure studies of poly (diallyldimethylammonium chloride-co-acrylamide) gels/sodium dodecyl sulfate complex. *Langmuir*, *14*(16), 4350–4358.

Zetzl, A. K., Marangoni, A. G., & Barbut, S. (2012). Mechanical properties of ethylcellulose oleogels and their potential for saturated fat reduction in frankfurters. *Food & Function*, *3*(3), 327–337.

Zia, K. M., Tabasum, S., Nasif, M., Sultan, N., Aslam, N., Noreen, A., & Zuber, M. (2017). A review on synthesis, properties and applications of natural polymer based carrageenan blends and composites. *International Journal of Biological Macromolecules*, *96*, 282–301. https://doi.org/https://doi.org/10.1016/j.ijbiomac.2016.11.095

8 Supplementary Material

Table S1. Experimental emulsion-gel strength values for the κ-C formulations.

Run	C	S	OWR	GS (N)
1	0.80	0.62	52.6	0.51
2	0.52	0.00	54.5	0.53
3	0.52	0.62	774.2	7.59
4	0.52	0.62	819.7	8.03
5	0.25	1.25	13.8	0.13
6	0.52	1.25	20.4	0.20
7	0.52	0.62	949.9	9.31
8	0.25	0.62	65.3	0.64
9	0.25	0.62	273.3	2.68
10	0.80	0.00	200.0	1.96
11	0.52	1.25	131.2	1.28
12	0.80	0.62	173.8	1.70
13	0.25	0.00	256.5	2.51
14	0.80	1.25	9.7	0.09
15	0.52	0.00	470.3	4.61

Table S2. Experimental emulsion-gel strength values for the ι-C formulations.

Run	C	S	OWR	GS (N)
1	2.0	0.40	0.00	0.22
2	1.0	0.30	0.40	0.09
3	1.0	0.40	0.00	0.08
4	1.5	0.30	0.80	0.13
5	1.5	0.30	0.00	0.12
6	1.5	0.50	0.80	0.20
7	1.5	0.40	0.40	0.16
8	2.0	0.40	0.80	0.22
9	1.5	0.40	0.40	0.16
10	2.0	0.30	0.40	0.28
11	1.0	0.50	0.40	0.15
12	1.0	0.40	0.80	0.11
13	1.5	0.40	0.40	0.15
14	1.5	0.50	0.00	0.14
15	2.0	0.50	0.40	0.31

Table S3. Experimental emulsion-gel strength values for the λ-C formulations.

Run	C	S	OWR	GS (N)
1	1.0	0.80	0.80	0.13
2	1.5	0.48	0.00	0.17
3	1.0	0.48	0.40	0.27
4	0.5	0.80	0.40	0.05
5	1.0	0.48	0.40	0.26
6	1.0	0.48	0.40	0.23
7	0.5	0.15	0.40	0.05
8	1.0	0.15	0.00	0.07
9	1.0	0.80	0.00	0.16
10	1.5	0.48	0.80	0.26
11	1.5	0.15	0.40	0.22
12	1.5	0.80	0.40	0.22
13	0.5	0.48	0.80	0.11
14	1.0	0.15	0.80	0.21
15	0.5	0.48	0.00	0.05

Table S4. Statistical parameters associated to the obtained theoretical models for the emulsion-gel strength obtained from the ANOVA analysis.

Source	κ-C	ι-C	λ-C
Regression	0.001	0.002	0.001
Lineal	0.027	0.505	«0.001
% C	0.099	0.310	«0.001
% S	0.412	0.219	0.888
OWR	0.009	0.835	0.003
Square	«0.001	0.015	0.001
%-C * %-C	«0.001	0.020	0.002
% S * % S	«0.001	0.084	0.001
OWR * OWR	«0.001	0.018	0.003
Interaction	0.031	0.404	0.025
% C * % S	0.061	0.406	0.771
% C * OWR	0.012	0.406	0.453
% S * OWR	0.717	0.226	0.005
Lack of fit	0.845	0.078	0.735
R^2 (%)	98.36	97.35	98.29

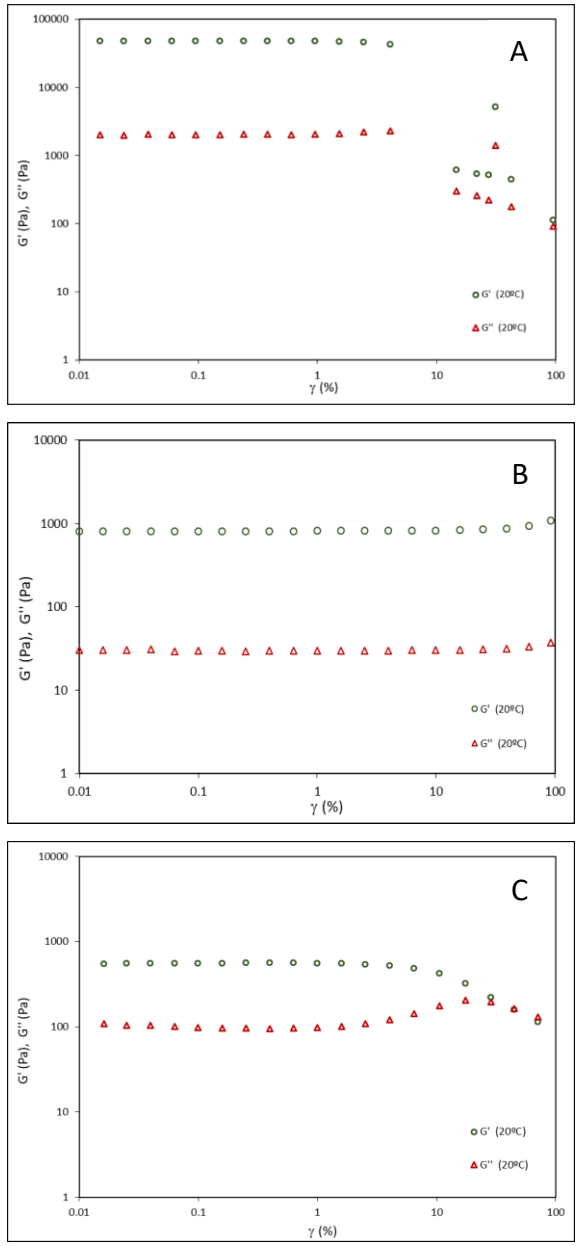

Figure S1. G' and G'' as a function of strain amplitude for the optimal emulsion-gels, measured at temperature of 20 °C. (A) κ-C emulsion-gel; (B) ι-C emulsion-gel; (C) λ-C emulsion-gel.

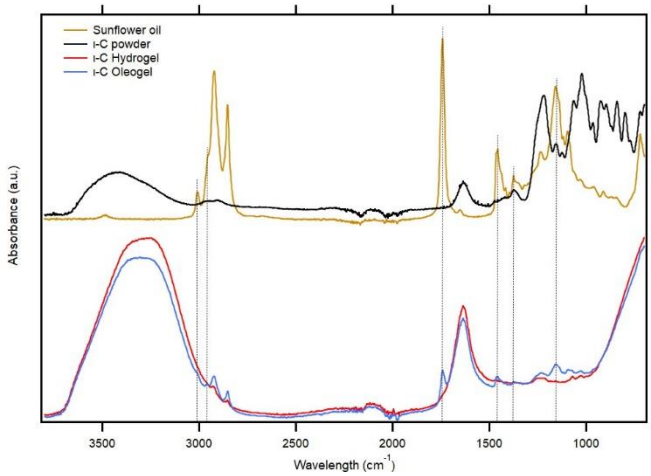

Figure S2. FT-IR spectra from the raw sunflower oil, the ι-C commercial powder and the ι-C hydrogel and emulsion-gel. Spectra have been offset for clarity.

3.3.2

EMULSION-GELS AND OIL-FILLED AEROGELS AS CURCUMIN CARRIERS: NANOSTRUCTURAL CHARACTERIZATION OF GASTROINTESTINAL DIGESTION PRODUCTS

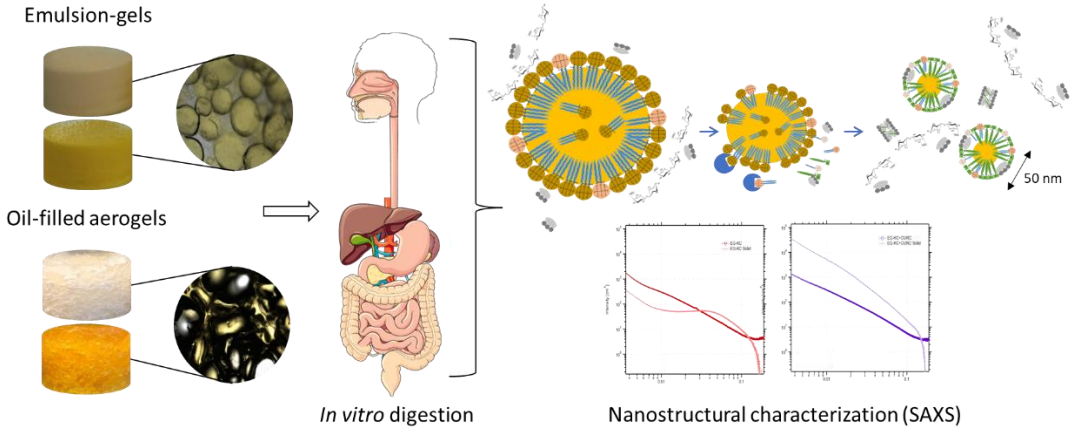

Fontes-Candia, C., Martínez, J.C., López-Rubio, A., Salvia-Trujillo, L., Martín-Belloso, O., Martínez-Sanz, M. (2021). Emulsion-gels and oil-filled aerogels as curcumin carriers: nanostructural characterization of gastrointestinal digestion products. Food Hydrocolloids (submitted)

1 Abstract

Agar and κ-carrageenan emulsion-gels and oil-filled aerogels were produced and investigated as curcumin carriers. The structure and mechanical properties of the gel-like structures were characterized, as well as their structural changes upon *in vitro* gastrointestinal digestion. Agar emulsion-gels presented a more rigid behaviour with smaller and more homogeneously distributed oil droplets than those from κ-carrageenan. Furthermore, agar emulsion-gels collapsed during freeze-drying process and only κ-carrageenan was capable to produce oil-filled aerogels.

After simulated gastrointestinal digestion bile salt lamellae/micelles (5 nm) and larger vesicles of partially digested oil (20-50 nm) were the predominant structures produced, being their proportion dependent of the polysaccharide type and the physical state of the gel network. Interestingly, the presence of curcumin induced the formation of larger vesicles and limited the formation of mixed bile salt lamellae/micelles.

These results evidence the high relevance of the microstructure and mechanical behavior of oil-filled gel-like structures upon gastrointestinal digestion, since the formation of different structures in the digestion products are expected to affect the intestinal transport and adsorption of the generated compounds.

2 Introduction

Emulsion-gels are soft solid materials formed by a matrix of a polymeric or biopolymeric hydrogel into which oil droplets have been incorporated. The 3D gel network enclosing the fat droplets can be produced using food-grade proteins or polysaccharides, with the properties of the emulsion-gel being strongly affected by the chosen matrix and its gelling behaviour (Li et al., 2020). The use of polysaccharides as matrices has been demonstrated to increase the thickness of the interfacial layer and the viscosity of the aqueous phase, thus improving the emulsion stability. These emulsion-gel systems exhibit a great potential application for the improvement of thermodynamic stability, texture modification, and encapsulation of both lipophilic and hydrophilic components (Li et al., 2020). In particular, the interest of these gelling structures for the encapsulation of lipophilic compounds with health-promoting properties has been growing over the last few years.

Curcumin is a natural flavonoid obtained from *Curcuma longa L.*, which is known to be an effective bioactive compound to prevent several diseases like cancer, obesity, infectious diseases, and cardiovascular illnesses (Hewlings & Kalman, 2017). Moreover, other beneficial health attributes have been ascribed to curcumin, related to reduced inflammatory conditions, metabolic syndrome and pain, while it has also shown benefits in the management of inflammatory and degenerative eye conditions (Cas & Ghidoni, 2019). Given this broad spectrum of bioactive properties, its incorporation within food matrices as a natural flavouring additive, yellow colorant and preservative is of great interest for the food industry (María Artiga-Artigas et al., 2018). However, its poor aqueous solubility, reduced bioavailability and high light sensitivity, are the main drawbacks that limit its application in food formulations. These limitations can be overcome by encapsulation within lipid-based matrices that can efficiently enhance its stability and bioavailability (Geremias-Andrade et al., 2017). Consequently, many efforts have been made to optimize the encapsulation of curcumin through various biological assemblies such as micelles, mixed micelles, vesicles, proteins and polysaccharides (Hosseini-Zare et al., 2021; Mandal et al., 2013). Emulsion-gels may represent a promising alternative for the encapsulation of curcumin; as previously commented, they constitute solid carriers that can be used as encapsulation systems for lipophilic bioactives, which are dispersed within the oil phase and structured within the gelling matrix (Geremias-Andrade et al., 2017; Mao et al., 2020). However, the bioaccessibility of the emulsified oil and of the incorporated hydrophobic bioactives has been scarcely studied and it is expected to be highly dependent on the gastrointestinal fate of the emulsion system. Several works have reported that polysaccharides may impact lipid digestion through various physical mechanisms: (i) they may adsorb to the surfaces of lipid droplets and form protective coatings inhibiting the lipase access to the lipid phase; (ii) they may alter the colloidal interactions between the lipid droplets, which alters their aggregation state and, thus, the surface area of lipids exposed to lipase; (iii) they may bind components present in the gastrointestinal fluids (such as bile salts, fatty acids, phospholipids, calcium ions, or digestive enzymes) that normally play a critical role in lipid digestion; (iv) they may alter the mass transport of digestive components due to their ability to increase the viscosity or form hydrogel networks (Chang & McClements, 2016).

Therefore, the ability and mechanisms of a given polysaccharide to impact lipid digestion and, consequently, the bioaccessibility of the incorporated bioactive compounds, depend on its structure, composition and physicochemical properties (Espinal-Ruiz et al., 2014). One way of modifying lipid hydrolysis rates, which could thus impact the bioaccessibility of lipid-soluble molecules, is through oil structuring techniques (Okuro et al., 2020).

Our recent works have demonstrated the suitability of κ-carrageenan and agar to produce emulsion-gels whose properties can be tuned depending on the requirements by adjusting the formulations (Fontes-Candia et al., 2021; Fontes-Candia, Ström, Lopez-Sanchez, et al., 2020). Furthermore, recent works have reported that aerogels produced by drying polysaccharide- or protein-based emulsion-gels are able to retain oil within their structure (Manzocco et al., 2017; Patel et al., 2014; Plazzotta et al., 2019; Tavernier et al., 2017), thus representing an interesting alternative type of materials (to which we will refer to as oil-filled aerogels) with potential for the encapsulation of lipophilic bioactives. It is hypothesized that the differences in the initial structure and properties of the emulsion-gels and oil-filled aerogels formed using different polysaccharides would alter their behaviour during gastrointestinal digestion, due to different susceptibility to enzyme penetration and/or stability to mechanical forces or pH changes, hence yielding different digestion products.

Therefore, the aim of this study was to incorporate curcumin into the oil phase of gel-like structures and to evaluate the influence of the polysaccharide type (agar or κ-carrageenan) and the physical state (emulsion-gels or oil-filled aerogels), as well as the presence or absence of curcumin in the oil phase, under simulated gastrointestinal conditions. The structure and mechanical properties of the developed materials were investigated as the basis for understanding their structural behaviour during the subsequent *in vitro* digestion experiments. While the effect of the different developed structures on the lipolysis process will be evaluated in a separate work, in this study we focused on characterizing the structure of the materials at the end of each digestion phase at the nanoscale level by means of small angle X-ray scattering (SAXS) to understand the structural changes taking place upon the digestion process.

3 Materials and methods

3.1 Materials

Commercial κ-carrageenan (Ceamgel 90-093) and agar (PRONAGAR) grades, in the form of powders, were kindly donated by CEAMSA (Pontevedra, Spain) and Hispanagar (Burgos, Spain), respectively. The commercial κ-carrageenan grade was composed of 92% κ-carrageenan and 8% ι-carrageenan (Fontes-Candia, Ström, Gómez-Mascaraque, et al., 2020). The agar content in the commercial agar was 80% (Martínez-Sanz et al., 2020). Curcumin and KCl were obtained from Sigma-Aldrich (Spain). Sunflower oil, kindly provided by Borges Pont, S.A. (Lleida, Spain), was used as the lipid phase. Polysorbate 80 (Tween 80), digestive enzymes (pepsin and pancreatin from porcine pancreas) and bovine bile were purchased from Sigma-Aldrich, Inc. (St Louis, MO, USA). The ultrapure water used to prepare all solutions of this study was obtained using a Milli-Q filtration system (18.2 mΩ, Merck Millipore, Madrid, Spain).

3.2 Preparation of emulsion-gels and oil-filled aerogels

Emulsion-gels (EG) were produced by using κ-carrageenan (KC) and agar (AG) as the gelling matrices, following the method previously described in (Fontes-Candia et al., 2021). The polysaccharide concentrations were fixed at 1.3% (w/v) for κ-carrageenan and 1.6% (w/v) for agar, based on previous experiments (Fontes-Candia, Ström, Lopez-Sanchez, et al., 2020; Martínez-Sanz et al., 2020). The polysaccharide powder was firstly dispersed in hot water (90°C) for 30 min. For the κ-carrageenan samples, KCl (0.5%; w/v) was then added to the hot solution, which was gently stirred until the salt was completely dissolved. After that, the oil was added and the samples were homogenized using an Ultraturrax for 2 min, producing emulsions. The oil volume fraction was fixed at 50% (v/v), which was the maximum amount which could be incorporated into both polysaccharides. Additionally, emulsion-gels incorporating curcumin into the oil phase were also prepared. The curcumin powder (0.1% (w/v) with respect to the total volume) was dispersed in the oil phase. Then, the oil phase was added to the formulations as described above to form the emulsions. The hot emulsions were transferred to cylindrical molds (20 mm diameter, 10 mm height) and were cooled down to room temperature and subsequently stored at 4 °C for 24 h prior to the analyses. Samples were coded as EG-KC (without curcumin) and EG-KC+CURC (containing curcumin in the oil phase) in the case of the

κ-carrageenan emulsion-gels and EG-AG (without curcumin) and EG-AG+CURC (containing curcumin in the oil phase) in the case of the agar emulsion-gels.

For the preparation of the κ-carrageenan oil-filled aerogels (OAG), the emulsion-gel samples were frozen at -80°C and subsequently, freeze-dried using a Genesis 35-EL freeze-dryer (Virtis, Spain). The same protocol was applied to the agar emulsion-gels, but in that case, the oil leaked from the aerogels and therefore, the materials could not be further used in this study. The produced aerogels, coded as OAG-KC (without curcumin) and OAG-KC+CURC (containing curcumin in the oil phase), were stored at 0% RH.

3.3 Textural analysis

The textural analysis of emulsion-gels and oil-filled aerogels was measured in terms of the uniaxial compression and the texture profile analysis.

3.4 Uniaxial compression

Uniaxial compression tests were performed using a texture analyzer (Stable Micro Systems model TA-XT2, Surrey, UK) equipped with a cylindrical aluminum plunger (3.6 cm diameter) and a load cell of 30 N. Gel disk specimens were compressed to 90% of the original height, using a crosshead speed of 0.1 mm/s. Force (N) and distance (mm) were converted to true stress (σ_T) and true strain (ε_T) using Eqs. (1) and (2). Compression moduli were calculated from the slopes of the initial linear zone of the true stress vs. true strain curves. All the measurements were performed, at least, in triplicate.

$$\sigma_T = \frac{F(t)\ (h_0\ -\ \Delta \mathrm{h(t)}}{\pi r^2 h_0} \tag{1}$$

$$\varepsilon_T = \ln \frac{h_0}{h_0 - \Delta h(t)} \tag{2}$$

3.5 Texture Profile Analysis (TPA)

Textural properties of the emulsion-gels were measured using a texture analyzer (Stable Micro Systems model TA-XT2) equipped with a cylindrical aluminum plunger (3.6 cm diameter) and a load cell of 30 N. Gel disk specimens were subjected to a two-cycle compression in each compression cycle the sample was compressed at 50% of deformation ratio at pre-test speed, test speed and post-test speed of 1 mm/s. Tiger force was 5 g, tiger distance of 2 mm and time

interval of two bites was set at 50 s. at least three independent measurements were obtained for each formulation. TPA curves were used to calculate the mechanical parameters of the emulsion-gels.

3.6 Optical microscopy

Optical microscopy was used to visualize the microstructure of the emulsion-gels and the oil-filled aerogels to determine oil droplet size distribution. Digital images were taken using an Eclipse 90i microscope (Nikon Corporation, Japan) equipped with a 5-megapixels cooled digital color microphotography camera Nikon Digital Slight DS-Mc. From each sample, two thick sections (ca. 1-2 mm thickness) were carefully cut with the help of a scalpel and placed onto a glass slide. Oil droplet size was determined by image analysis using the ImageJ software. Measurements were performed from at least 50 droplets on three different images and mean and standard deviation values were calculated.

3.7 Oil binding capacity (OBC)

The oil binding capacity was evaluated using the method described by (Palla et al., 2017). Emulsion-gels previously gelled in 1.5 mL tubes were centrifuged at 9000 rpm for 15 min at room temperature using a microcentrifuge (5424 R, Eppendorf, Hamburg, Germany). For the oil-filled aerogels, 1 g of each sample were placed in a 1.5 mL tube and the same protocol was followed. The OBC was expressed as function of the percentage of oil released from the sample after centrifugation. Three replicates of each sample were analyzed.

3.8 *In vitro* gastrointestinal digestion of emulsion-gels and oil-filled aerogels

The obtained emulsion-gels and oil-filled aerogels were subjected to *in vitro* gastrointestinal digestions. Additionally, plain and curcumin-loaded nanoemulsions (NE) were used as control samples where no gelling matrix was present. The formation of curcumin-loaded NE was performed as described by Artiga-Artigas et al., (2017) with minor modifications. Briefly, NE were prepared using sunflower oil as the lipid phase, whereas curcumin-loaded NE contained sunflower oil enriched with 0.1% (w/v) curcumin as the lipid phase. Coarse emulsions were obtained by mixing 0.5 % (w/w) of Tween 80, 5% (w/w) of the lipid phase and 94.5 % (w/w) of Milli-Q water using an Ultra-Turrax (IKA, Staufen, Germany) at 9500 rpm for 3 min. Then, the

coarse emulsions were passed through a microfluidizer (MP-110 Microfluidics, MA, USA) at 100 MPa for 5 cycles to obtain NE.

The *in vitro* gastrointestinal digestions of NE, emulsion-gels and oil-filled aerogels were performed according to the INFOGEST standardized method (Brodkorb et al., 2019), consisting on a gastric and small intestinal phase. Firstly, a simulated gastric fluid (SGF) solution was prepared to perform the gastric digestion phase. The SGF contained a mixture of electrolytes [0.5 M KCl, 0.5 M KH_2PO_4, 1 M NaCl, 2 M NaCl, 0.15 M $MgCl_2(H_2O)$, 0.5 M $(NH_4)_2CO_3$] dissolved in Milli-Q water. The amount of initial material introduced in the gastric phase was calculated individually for each type of sample according to their known lipid concentration to provide 0.25 g of oil. For this, 5 mL of the nanoemulsions were diluted to a final volume of 20 mL using Milli-Q water. Then, 0.4 mL of 1 M HCl, 1.39 mL of Milli-Q water, 10 µL of $CaCl_2$ and 18.2 mL of SGF containing pepsin (8.8 mg/mL) were added to the 20 mL of the diluted NE. The mixture was incubated under subdued light conditions for 2 h at 37 °C and continuous agitation using an orbital shaker working at 100 rpm. For the digestion of solid systems, 0.5 g of emulsion-gels or 0.26 g of oil-filled aerogels were mixed with 21.39 mL of Milli-Q water, 0.4 mL 1 M HCl, 10 µL of $CaCl_2$ and 18.2 mL of SGF containing pepsin (8.8 mg/mL). The gastric phase incubation time and conditions were performed as previously described for liquid systems. It should be noted that while the NE samples were composed of a homogeneous liquid at the end of the gastric phase, all the emulsion-gel samples could be separated into a solid fraction (composed of the gel-like structure) and a liquid fraction. The oil-filled aerogels presented poorer mechanical integrity and their structure was disrupted upon the gastric phase, yielding a liquid phase with solid particles in suspension.

Subsequently, a 30 mL-aliquot of the liquid phase was placed in a water bath at 37 °C to perform the intestinal digestion phase. In the case of the emulsion-gels, the solid fraction remaining after the gastric phase was also added together with the 30 mL aliquot of liquid. Then, to simulate the small intestinal conditions, 3.5 mL of bile salts (54 mg/mL) and 1.5 mL of intestinal salts (10 mM of $CaCl_2$ and 160 mM of NaCl) were added to the chyme, and the pH was adjusted to 7.0. Subsequently, 2.5 mL of pancreatin (215 mg/mL) solution was added to the chyme to start the lipid hydrolysis. Finally, immediately after the intestinal digestion, the digested

samples were transferred into glass tubes and heat-shocked at 85 °C for 3 min and placed in an iced-water bath to stop the lipolysis reaction. Similarly to what was observed after the gastric phase, after completing the intestinal digestion of the emulsion-gels two phases could be identified: a solid phase and a liquid phase. These two phases were manually separated and analyzed independently.

3.9 Small angle X-ray scattering (SAXS)

SAXS experiments were carried out in the Non-Crystalline Diffraction beamline, BL-11, at ALBA synchrotron light source (www.albasynchrotron.es). The polysaccharide emulsion-gels, and oil-filled aerogels were analysed at room temperature (25 ºC). Disk-like specimens were directly exposed to the X-ray beam with no container. The solid phase (samples coded as "solid") and the liquid phase (samples coded as "digesta") from the digestion products obtained after the intestinal digestion phase were also characterised. Furthermore, an aliquot of the liquid fraction was centrifuged at 6000 rpm for 20 min at 25 °C (AVANTI J-25, Beckman Instruments Inc., Fullerton, CA, USA) to obtain the supernatant, corresponding to the micellar fraction (samples coded as "micellar"), which was also analysed separately. These samples were placed into sealed 1.5 mm quartz capillaries (Hilgenberg GmbH, Germany). The energy of the incident photons was 12.4 KeV or equivalently a wavelength, λ, of 1 Å. The SAXS diffraction patterns were collected by means of a photon counting detector, Pilatus 1M, with an active area of 168.7 x 179.4 mm^2, an effective pixel size of 172 x 172 μm^2 and a dynamic range of 20 bits. The sample-to-detector distance was set to 7570 mm, resulting in a q range with a maximum value of q = 0.19 $Å^{-1}$. An exposure time of 10 s was selected based on preliminary trials. The data reduction was treated by pyFAI python code (ESRF) (Kieffer & Wright, 2013), modified by ALBA beamline staff, to do on-line azimuthal integrations from a previously calibrated file. The calibration files were created from a silver behenate (AgBh) standard. The intensity profiles were then represented as a function of q using the IRENA macro suite (Ilavsky & Jemian, 2009) within the Igor software package (Wavemetrics, Lake Oswego, Oregon).

The scattering patterns from the polysaccharide gels were properly described using a two-level unified model:

$$I(q) = \sum_{i=1}^{N} G_i \exp\left(-q^2 \cdot \frac{R_{g,i}^2}{3}\right) + \frac{B_i\left[\mathrm{erf}(qR_{g,i}/\sqrt{6})\right]^{3P_i}}{q^{P_i}} + bkg \quad (3)$$

The unified model considers that, for each individual level, the scattering intensity is the sum of a Guinier term and a power-law function (Beaucage, 1995). $G_i = c_i V_i \Delta SLD_i{}^2$ is the exponential prefactor (where V_i is the volume of the particle and ΔSLD_i is the scattering length density (SLD) contrast existing between the ith structural feature and the surrounding solvent), $R_{g,i}$ is the radius of gyration describing the average size of the ith level structural feature and B_i is a q-independent prefactor specific to the type of power-law scattering with power-law exponent, P_i.

The SAXS patterns from the digesta samples were fitted adding an additional term to equation (3), consisting of a Lorentzian peak:

$$I(q) = \sum_{i=1}^{N} G_i \exp\left(-q^2 \cdot \frac{R_{g,i}^2}{3}\right) + \frac{B_i\left[\mathrm{erf}(qR_{g,i}/\sqrt{6})\right]^{3P_i}}{q^{P_i}} + \frac{I_0}{1 + \left((q - q_0)/B\right)^2} + bkg \quad (4)$$

The obtained values from the fitting coefficients are those that minimize the value of Chi-squared, which is defined as:

$$\chi^2 = \sum \left(\frac{y - y_i}{\sigma_i}\right)^2 \quad (5)$$

where y is a fitted value for a given point, y_i is the measured data value for the point and σ_i is an estimate of the standard deviation for y_i. The curve fitting operation is carried out iteratively and for each iteration, the fitting coefficients are refined to minimizeχ^2.

3.10 Statistical analysis

An analysis of variance was carried out on the data obtained for the characterization of the gel-like oil-filled structures and the Tukey test was used to determine significant differences between the treatments ($p \leq 0.05$) with a 95% confidence interval using the statistical software IBM SPSS (v.24) (IBM corp., USA).

4 Results and discussions

4.1 Characterization of the gel-like oil-filled structures

The microstructure and mechanical properties of the developed emulsion-gels and oil-filled aerogels with and without curcumin were evaluated as the basis to understand their behaviour during the subsequent *in vitro* digestion experiments. The morphology of the oil-filled materials was studied by means of optical microscopy and representative images are shown in Figure 1, together with pictures demonstrating the macroscopic appearance of the samples. As observed, at the macroscopic level, the agar emulsion-gels presented a more opaque appearance, which is typically associated to the formation of emulsions with smaller droplet size (McClements & Rao, 2011). In fact, at the microscopic level, the κ-carrageenan samples presented a much more heterogeneous distribution of oil droplets with larger diameters of ca. 243 μm (cf. Table 1) as compared to the agar emulsion-gels, in which the oil was dispersed more homogeneously and forming smaller droplets of ca. 12 μm. This was ascribed to the high emulsifying properties of agar (Z. Wang et al., 2013). Moreover, the inherent difficulty of dispersing the oil in the κ-carrageenan samples, has been recently reported (Fontes-Candia et al., 2021). This is due to the fact that κ-carrageenan formulations start to form gels at higher temperatures than agar, becoming much more viscous during the oil dispersion phase. Although the oil phase could be identified in the κ-carrageenan oil-filled aerogels, no defined oil droplets were detected. It should be noted that while the κ-carrageenan formulations were able to preserve their physical integrity after the freeze-drying process, that was not the case for the agar formulations; in that case the polysaccharide matrix collapsed upon drying and the oil droplets seemed to coalesce and leaked out of the aerogel structure. As expected, all the materials acquired a yellow coloration with the incorporation of curcumin. The incorporation of the bioactive did not seem to affect the distribution of the oil within the materials and, as deduced from Table 1, the oil droplet size was not significantly affected. The microscopy images also show that, as expected, the curcumin was preferentially distributed within the oil phase (as suggested by the yellow colour).

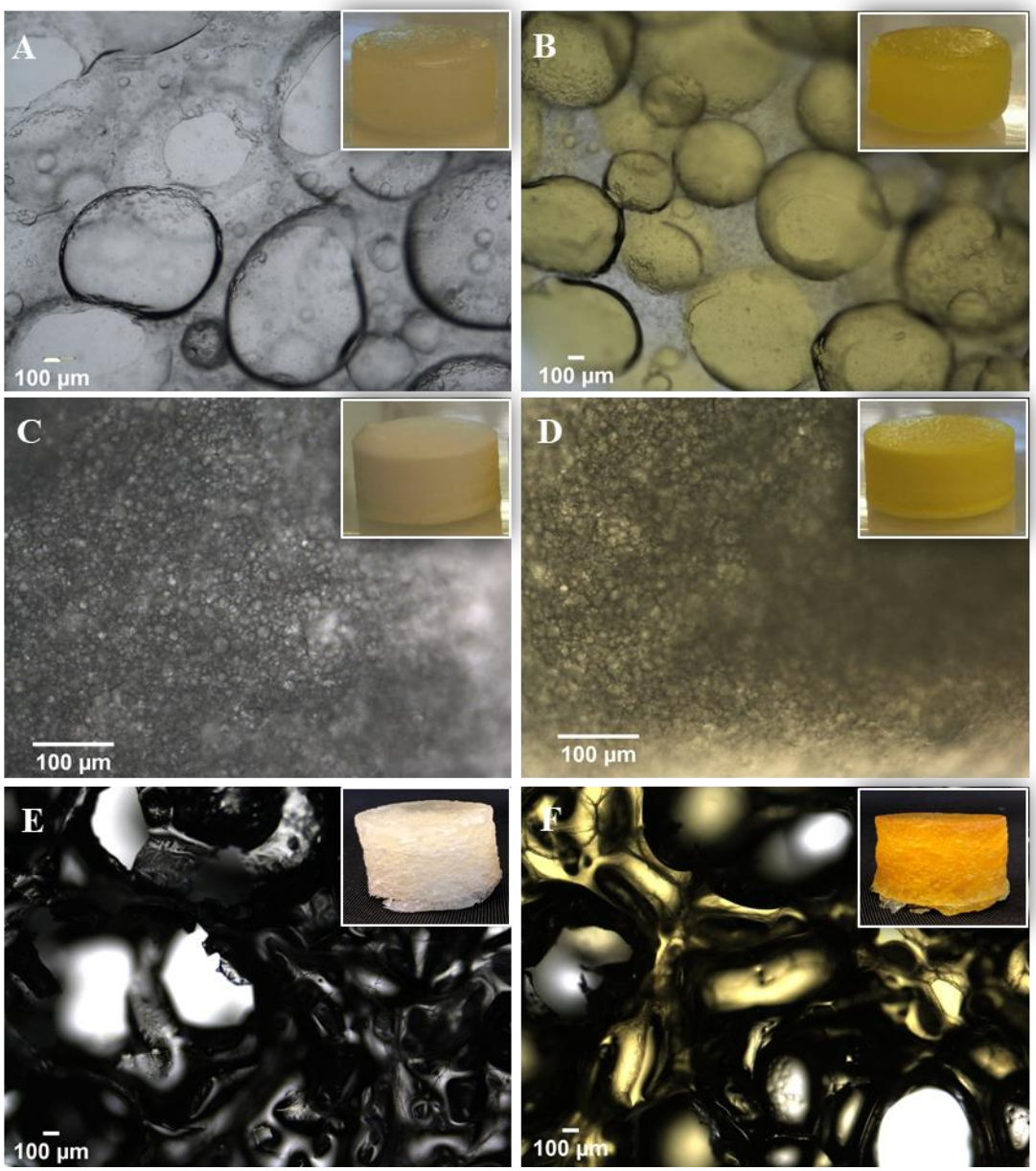

Figure 1. Optical microscopy images and visual appearance of κ-carrageenan (A, B) and agar (C, D) emulsion-gels and κ-carrageenan oil-filled aerogels (E-F). Samples on the left and right correspond to the oil-filled structures without and with curcumin, respectively.

To characterize their mechanical behaviour, κ-carrageenan and agar emulsion-gels, as well as the κ-carrageenan oil-filled aerogels, were subjected to compression tests and the results are summarized in Table 1. The Young's modulus (E) and the maximum stress (σ_{max}) were estimated from the corresponding stress-strain curves (cf. Figure 2). As observed, the agar emulsion-gels presented a well-defined fracture at strains within the range of 25-35% and their Young's modulus ranged between 60-70 kPa. In contrast, the κ-carrageenan emulsion-gels presented a less rigid behaviour within the linear elastic region, but withstood higher maximum stresses and the samples did not show a clear fracture upon compression. A similar behaviour has been previously reported for these types of structures, with agar emulsion-gels showing a more rigid behaviour than carrageenan-locust bean gum samples (Koç et al., 2019). This might be related to the nature of interactions holding together the polysaccharide gel networks. In the case of agar, the gel network was mainly held by hydrogen bonds, while in the case of κ-carrageenan, ionic interactions were responsible for the association of the polysaccharide chains. In fact, previous work (Fontes-Candia et al., 2021) demonstrated that κ-carrageenan emulsion-gels present network structures where the carrageenan double helices aggregated forming larger but less densely packed bundles than in the agar emulsion-gels. For the κ-carrageenan oil-filled aerogels, the modulus increased seven-fold as compared to the corresponding emulsion-gels, which is due to the formation of more compacted structures upon removal of water by freeze-drying. The absence of water is expected to promote the formation of stronger interactions between the carrageenan chains, as has been previously reported for other polysaccharides such as cellulose and chitosan (Benito-González et al., 2020; Takeshita & Yoda, 2015). It should be noted that, unlike the emulsion-gels, the aerogels did not recover their shape after compression and were incapable of retaining the oil inside the matrix. The incorporation of curcumin into the oil phase did not have a significant effect on the mechanical compression behaviour of any of the samples.

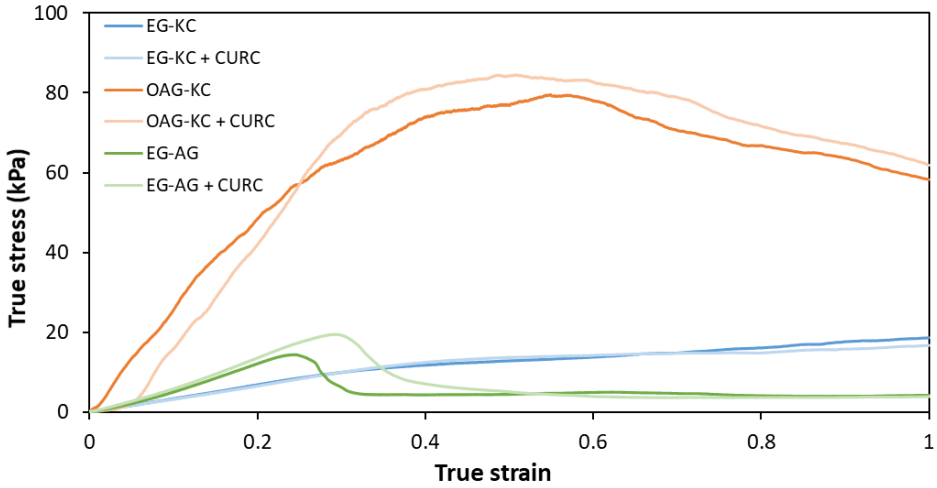

Figure 2. Representative compressive true stress-true strain curves for the agar and κ-carrageenan emulsion-gels and the κ-carrageenan oil-filled aerogels.

TPA analyses were also carried out on the emulsion-gels, and the most relevant parameters are compiled in Table 1. The hardness, which is related to the gel strength, was higher in the κ-carrageenan samples. The differences between the compression moduli and the hardness behaviour were related to the low compression rates used for the compression test. For a low compression rate, the sample has a chance to relax within the timescale of the compression and this relaxation occurs at the same time as the chains in the gel are being pulled out of their sites. On the other hand, at a high compression rate, there is no time for the relaxation and the gel network reaches quickly to a point of fracture propagation and thereafter collapse (Nordqvist & Vilgis, 2011). The cohesiveness values were also higher for the κ-carrageenan emulsion-gels. This parameter is representative of the ability of the gels to resist external damage while maintaining their integrity, thus being indicative of the internal bonding strength. In line with the compression tests, these results evidence that the agar formed gel networks showing a more rigid behaviour when subjected to forces within the linear elastic region, but the ionic interactions holding together the κ-carrageenan provided more resistant structures, which were able to withstand greater stress values. Again, the incorporation of curcumin did not seem to have a strong effect on the mechanical behaviour of the samples.

Table 1. Oil droplet size, oil-binding capacity (OBC) and mechanical properties of the gel-like oil-filled structures prepared without or with curcumin.

Sample	Oil droplet size (μm)	OBC (%)	σ_{max} (kPa)	E (kPa)	Hardness (N)	Cohesiveness
EG-KC	243 ± 258^{a}	88.7 ± 2.1^{b}	---	34.4 ± 1.1^{b}	16.4 ± 0.4^{a}	0.40 ± 0.02^{a}
EG-KC + CURC	349 ± 265^{a}	87.7 ± 2.2^{b}	---	34.3 ± 2.3^{b}	16.3 ± 0.5^{a}	0.37 ± 0.01^{a}
EG-AG	11.7 ± 4.4^{b}	98.4 ± 0.17^{a}	13.6 ± 1.3^{b}	61.0 ± 4.0^{b}	12.4 ± 1.1^{b}	0.16 ± 0.02^{b}
EG-AG + CURC	10.9 ± 2.8^{b}	98.2 ± 0.10^{a}	18.1 ± 2.9^{b}	68.8 ± 7.1^{b}	14.9 ± 0.7^{a}	0.13 ± 0.03^{b}
OAG-KC	---	4.1 ± 0.52^{c}	79.5 ± 0.6^{a}	269.3 ± 42.3^{a}	---	---
OAG-KC + CURC	---	3.2 ± 0.54^{c}	80.5 ± 13.8^{a}	267.3 ± 100^{a}	---	---

Values within the same column with different letters are significantly different ($p \leq 0.05$).

The oil binding capacity (OBC) was also evaluated to determine the capacity of the developed materials to retain the oil phase within their structure and the values are also compiled in Table 1. As observed, the emulsion-gels showed a high oil binding capacity, with values of 88-89% for the κ-carrageenan emulsion-gels and ~98% for the agar emulsion-gels. The higher oil binding capacity of the agar emulsion-gels may be related to their structure, where smaller oil droplets were homogeneously distributed within the polysaccharide matrix, as opposed to the very large oil droplets contained within the κ-carrageenan emulsion-gels. Indeed, it has been reported that smaller oil droplets provide more stable emulsions (Meng et al., 2018). In contrast, the oil binding capacity of the aerogels was very low, suggesting the lack of chemical interactions between the oil phase and the carrageenan structure. It seems that the oil droplets were physically entrapped within the pores of the carrageenan aerogels, leaking from the material when subjected to external forces.

4.2 Nanostructural characterization of the digestion products

Emulsion-gels and oil-filled aerogels were subjected to *in vitro* gastrointestinal digestions to assess the effect of the different structures on the digestion of the lipid phase and the effect of the curcumin when it was incorporated into the oil. Nanoemulsions (NE) were used as control samples where no structuring gelling polysaccharide was present. The structural evolution of the gel-like oil-filled structures, as well as the control nanoemulsions, upon the simulated *in*

vitro gastrointestinal digestions was studied at the nanoscale level by analysing the digestion products through synchrotron SAXS experiments. Firstly, the structure of the native gel-like oil-filled structures was characterized and the obtained SAXS patterns are shown in Figure 3. The initial κ-carrageenan and agar emulsion-gels showed scattering patterns similar to those previously reported for analogous samples (Fontes-Candia et al., 2021), with the agar samples presenting greater scattering intensity due to the presence of more densely packed networks. The data were fitted using a two-level Beaucage model and the main fitting parameters obtained are summarized in Table S1. While Rg_1 is related to the bundles of carrageenan/agar double helices, Rg_2 is associated with the thickness of the polysaccharide double helices. In agreement with previous work (Fontes-Candia et al., 2021), the power-law exponents P_1 for the κ-carrageenan emulsion-gels (1.7-2.0) indicated the presence of rigid swollen linear chains, with carrageenan double helices of ca. 8-9 nm. On the other hand, the agar emulsion-gels presented power-law exponents of 2.5-2.7, characteristic from mass fractal structures (i.e. branched network structures) and agar double helices of 8 nm. The different conformation of agar and κ-carrageenan at the nanostructural level is again related to the different nature of the interactions holding together the polysaccharide gel network. It should be noted that the κ-carrageenan emulsion-gel showed two small peaks located at 0.027 $Å^{-1}$ and 0.058 $Å^{-1}$, indicative of the existence of well-ordered structures with real distances of ca. 23 nm and 11 nm (cf. arrows in Figure 3). These peaks have been previously associated to the formation of carrageenan bundles with an ordered periodical structure due to the ionic cross-links formed between the carrageenan sulphate groups and the K^+ ions added to induce gelation (Fontes-Candia et al., 2021; Fontes-Candia, Ström, Lopez-Sanchez, et al., 2020). Surprisingly, these small peaks were not visible in the emulsion-gel containing curcumin, suggesting that there might be a certain degree of interaction between the K^+ ions and the curcumin, in line with previous studies (Mandal et al., 2013). After subjecting the κ-carrageenan emulsion-gels to the freeze-drying process, the oil-filled aerogels presented greater power-law exponents, which may be due to an increased interfacial scattering contrast generated when replacing water with air. Furthermore, smaller thicknesses were estimated for the carrageenan double helices, which may be a consequence of the shrinking of the polysaccharide structure when removing water.

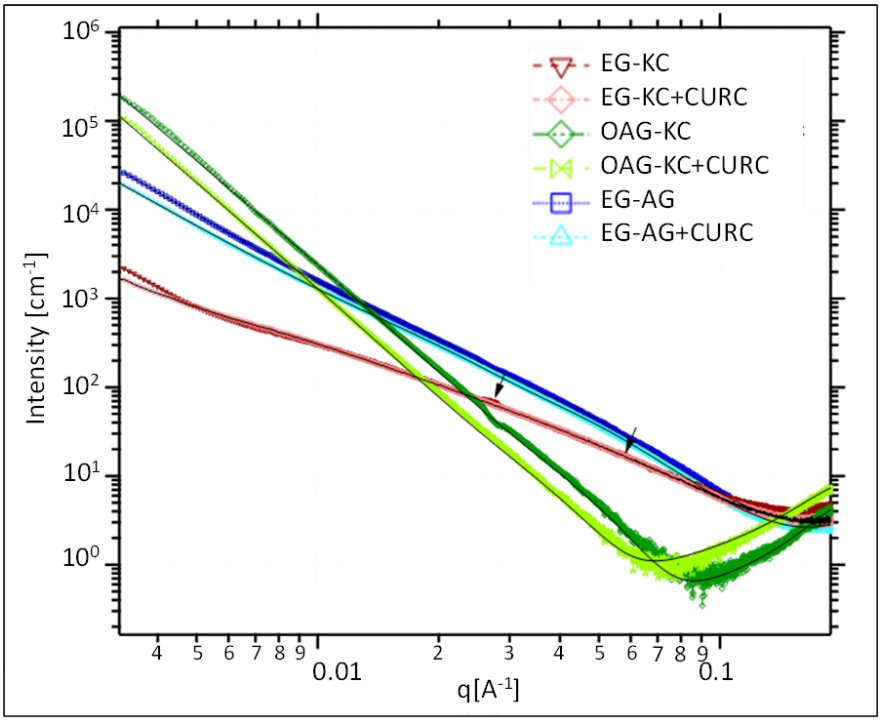

Figure 3. SAXS patterns from the agar and κ-carrageenan gel-like oil-filled structures. Markers represent the experimental data and solid lines show the fits obtained using theoretical models. Arrows point out to small peaks related to structural features in EG-KC.

As shown in Figure 4A, the scattering patterns from the initial nanoemulsions were characterized by the appearance of multiple scattering features. The data were fitted within the medium-low q region ($q<0.02$ Å^{-1}) using a three-level Beaucage model, with characteristic radii of gyration of 4.7 nm and 2.8 nm for the plain nanoemulsion and 3.8 nm and 3.1 nm for the nanoemulsion loaded with curcumin. Within the high q range ($q>0.02$ Å^{-1}), the data could be fitted using a two-level model, with radii of gyration of ca. 35 nm for the plain nanoemulsion and 26 nm and 23 nm for the nanoemulsion with curcumin. Previous works have reported on larger droplet sizes of ca. 260 nm for similar nanoemulsion systems (M. Artiga-Artigas et al., 2017). In fact, particle size analyses of the nanoemulsions prepared in this work suggested average droplet sizes of ca. 581 ± 153 nm for the plain NE and 419 ± 6 nm for the NE containing curcumin. However, it should be considered that the laser diffraction technique used for the particle size analyses is suitable to determine sizes within the range of 100 nm to 1000 µm.

Thus, the scattering features might be associated to populations of smaller oil droplets, which were not detected by laser diffraction. While the radii of gyration associated to the structures in the lower q range may be related to the overall size of the droplets, the radii of gyration corresponding to the higher q range may be associated with the thickness of the layer of the surfactant coating the oil droplets, observed due to the scattering length density contrast generated between the surfactant and the oil and water phases (L. Wang et al., 2008). An important observation is that the addition of curcumin resulted in smaller oil droplet sizes, which could be related to a reduced surface tension effect, allowing a more efficient emulsification in the formulation with curcumin.

The different fractions constituting the digestion products after the complete gastrointestinal digestions were also analysed by SAXS. Figures 4B-E show the scattering patterns from the solid fractions obtained after digestion as compared to the initial gel-like structures. It should be noted that while in the case of the emulsion-gels, a solid fraction of non-digested material could be separated from the liquid digesta that was not the case for the κ-carrageenan oil-filled aerogels, where the aerogel structure was disrupted upon the digestion process, although some polysaccharide particles could be still detected in the liquid digesta. This is not surprising, since the microstructural and mechanical characterization of the initial samples pointed out towards the oil being only physically entrapped in these materials, thus expecting a high release of the oil towards the liquid medium, leaving the poorly interconnected network of the polysaccharide. Furthermore, some works have reported on the poor mechanical integrity of aerogels from hydrophilic polysaccharides when soaked in liquid media (Benito-González et al., 2020). This indicates a greater resistance of the polysaccharide network formed in the case of the emulsion-gels as compared to the oil-filled aerogels. Interestingly, the SAXS patterns from the remaining solid fractions were very different to those from the corresponding initial gel-like structures, which was not unexpected since the structure of the materials must have been strongly modified with the release of the oil phase upon the digestion process. In general, the scattering intensity of the remaining solids was higher than that of the initial oil-filled structures, which may be due to an increased scattering length density contrast when the oil phase was removed from the structures. Particularly interesting was the scattering pattern from the solid

corresponding to the κ-carrageenan emulsion-gel, which is similar to those previously shown for different oil-in-water emulsions and associated to droplet surface structural features (Bastien Marze et al., 2015). This suggests the presence of partially digested emulsified oil structures retained within the κ-carrageenan gel network, but only when curcumin was not added into the oil phase. Interactions between bile salts and polysaccharides have been reported to hinder lipid digestion due to a limited adhesion of bile salts to the oil droplets, thus hampering the access of intestinal lipase (Klinkesorn & McClements, 2010; Pilosof, 2017). According to this, our hypothesis is that electrostatic complexes of bile salts and κ-carrageenan were formed, limiting the oil droplet digestibility. The presence of curcumin impeded the formation of these κ-carrageenan-bile salt complexes, most likely due to the capacity of curcumin to interact with bile salts (Mandal et al., 2013; Patra et al., 2013).

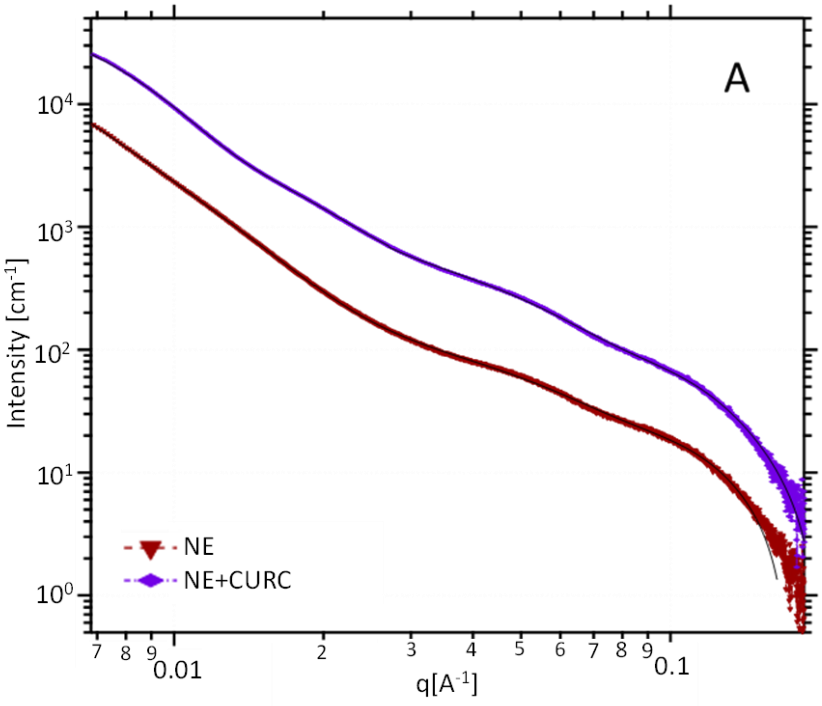

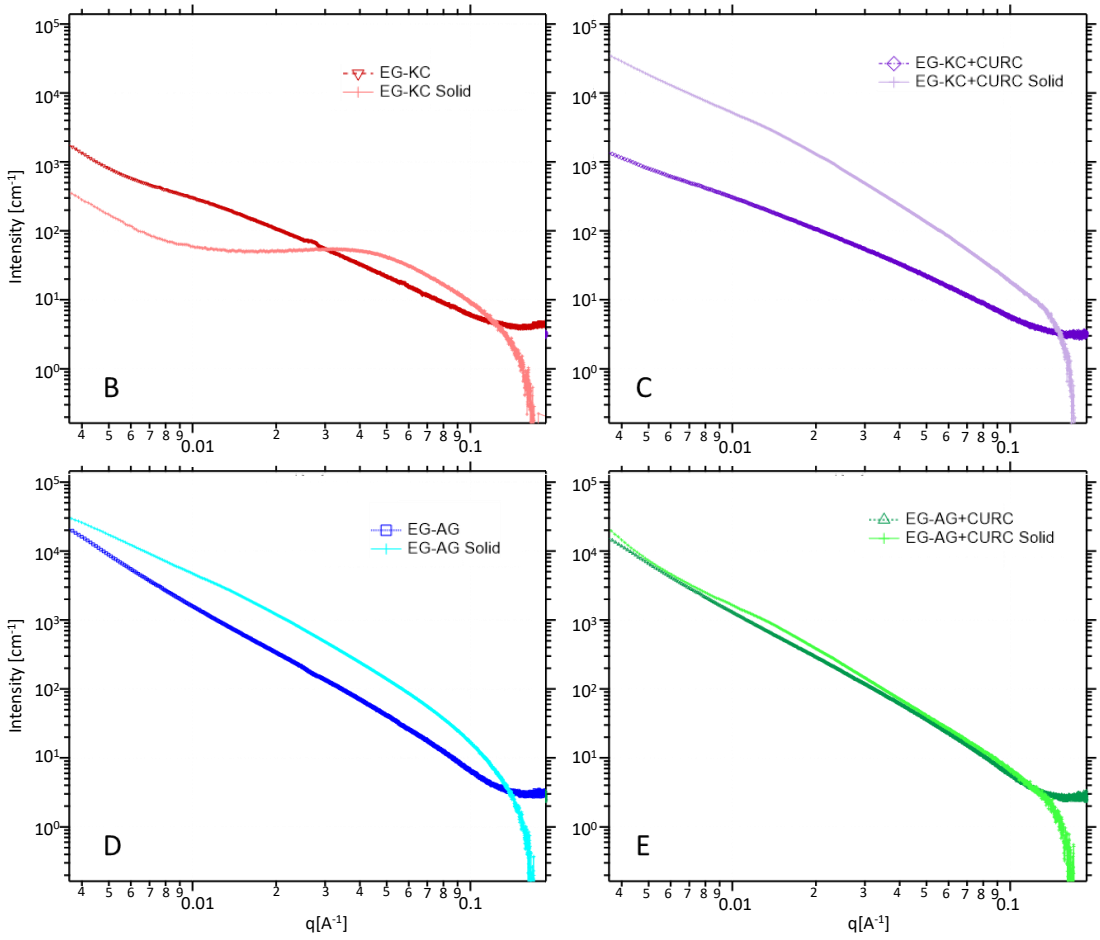

Figure 4. SAXS patterns from the initial nanoemulsions. Markers represent the experimental data and solid lines show the fits obtained using theoretical models. (B-E) Comparison of the SAXS patterns from the initial emulsion-gels and the solid fractions remaining after the *in vitro* gastrointestinal digestions**.**

The SAXS patterns from the liquid digesta are shown in Figure 5. The experimental data were fitted using a two-level Beaucage function plus a Lorentzian peak, to account for a scattering peak appearing within the high q range. As shown in Table 2, the real distances associated to this scattering peak were within the range of 4.7-5.1 nm for all the samples. It should be noted that the medium used for the *in vitro* digestions (containing salts, digestive enzymes and bile salts) showed a sharp peak at 0.133 $Å^{-1}$ (corresponding to a real distance of 4.7 nm) (cf. Figure S1). Several works indicated that bile salts are in the form of lamellar (more specifically, vesicles)

or micellar structures when dissolved in aqueous media above certain concentrations (Lopez-Pena et al., 2019; Mandal et al., 2013). Thus, the sharp peak detected in the digestion medium is expected to arise from the presence of ordered bile salt structures. Furthermore, it has been reported that the lipid digestion products (i.e. free fatty acids, medium chain triglycerides and phospholipids) are able to interact with these bile salt lamellae/micelles, forming different types of micellar structures (Macierzanka et al., 2019). Thus, the scattering peaks observed in the digesta samples may arise from the presence of mixed lamellae/micelles of ca. 5 nm composed by bile salts and digestion products. In fact, previous works have reported similar values for the estimated diameter of mixed micelles composed of bile salts and lipid digestion products (Marze et al., 2012; Salentinig et al., 2014). This peak was sharper and more intense in the nanoemulsion and the κ-carrageenan emulsion-gel without curcumin (cf. Table 2). The greater abundance of this type of structures in the nanoemulsion may be due to a higher degree of lipid hydrolysis in this sample due to the lack of a polysaccharide gelling agent hindering the accessibility of intestinal lipase towards the surface of the oil droplets (see Figure 7 for a schematic representation). A greater digestion extent of the oil is expected to produce a greater release of free fatty acids, which may be interacting with free bile salt lamellae/micelles. In the case of the κ-carrageenan emulsion-gel, the abundance of this type of structures is not likely to be linked to a higher extent of lipolysis, since some partially digested oil was seen to remain in the solid phase from the digested sample (cf. Figure 4). In turn, it may be possible that the strong gelling structure in this material limited the diffusion of bile salts towards the oil droplets entrapped within the gel, thus reducing the extent of lipolysis and also producing a greater amount of free bile salt lamellae/micelles in the liquid medium, as represented in Figure 7. Moreover, the larger oil droplet size found in these emulsion-gels was also expected to limit the degree of lipolysis (Salvia-Trujillo et al., 2017). In general, the peak became less defined in the samples containing curcumin, which may be indicative of the curcumin interfering with the formation of these mixed bile salt-digestion products lamellae/micelles. In the case of the κ-carrageenan oil-filled aerogel, the scattering peak was fainter than that of the corresponding emulsion-gel, and it became a broad shoulder in the oil-filled aerogel with curcumin, suggesting the presence of micelles with a more heterogeneous size distribution. The less intense

scattering features associated to the formation of lamellae/micelles in the case of the oil-filled aerogels can be explained by the lower integrity of these materials when subjected to the gastrointestinal digestions, with the aerogel polysaccharide structure being completely disrupted to form suspended particles. These polysaccharide particles may be responsible for de-stabilizing the structures formed by the bile salts and the digestion products (Klinkesorn & McClements, 2010; Pilosof, 2017). With regards to the estimated radii of gyration, while Rg_2 corresponds to smaller dimensions of ca. 2-5 nm, Rg_1 is indicative of the existence of larger structures of ca. 20-50 nm. Marze et al. reported similar dimensions for the scattering features appearing at the intermediate scattering vector (q) region in the SAXS patterns from digested oil emulsions, which were attributed to vesicles (Bastien Marze et al., 2015). The products generated upon gastrointestinal digestion of oils are, in fact, complex mixtures of colloid particles such as micelles, multi- and uni-lamellar vesicles, bilayer fragments, and calcium soaps (Ahmed et al., 2012; Fatouros et al., 2007; Sabet et al., 2021; Tran et al., 2017). Figure 7 shows a graphical representation of the structures formed upon digestion of the different samples, as deduced from the SAXS results. The digesta samples were composed of mixtures of different structures, amongst which small mixed micelles and larger vesicles were the most abundant. The larger vesicles may be formed by a core of partially digested oil or other lipophilic compounds and stabilized by adsorbed bile salts and digestion products. The lower abundance of small mixed bile salt micelles in the samples containing curcumin could be explained by the fact that the curcumin released from the oil phase upon digestion may be preferentially located in the inner region of vesicles protected by bile salts and digestion products, similarly to the model proposed for the digestion of carotenoids incorporated into emulsified lipid droplets (Cervantes-Paz et al., 2017).

Table 2. Parameters obtained from the fits of (a) the pure carrageenan hydrogels (b) the κ-C hydrogel and emulsion-gel and (c) the ι-C and λ-C hydrogels and emulsion-gels.

Samples	A	n	I_0	d (nm)
NE	25	2.1	4.9	0.017
NE + CURC	20	2.5	4.7	0.041
EG-KC	26	2.4	4.8	0.009
EG-KC + CURC	23	5.1	5.1	0.021
EG-AG	23	2.2	4.9	0.024
EG-AG + CURC	31	2.9	4.7	0.033
OAG-KC	48	4.9	5.1	0.023
OAG-KC + CURC	27	3.7	---	---

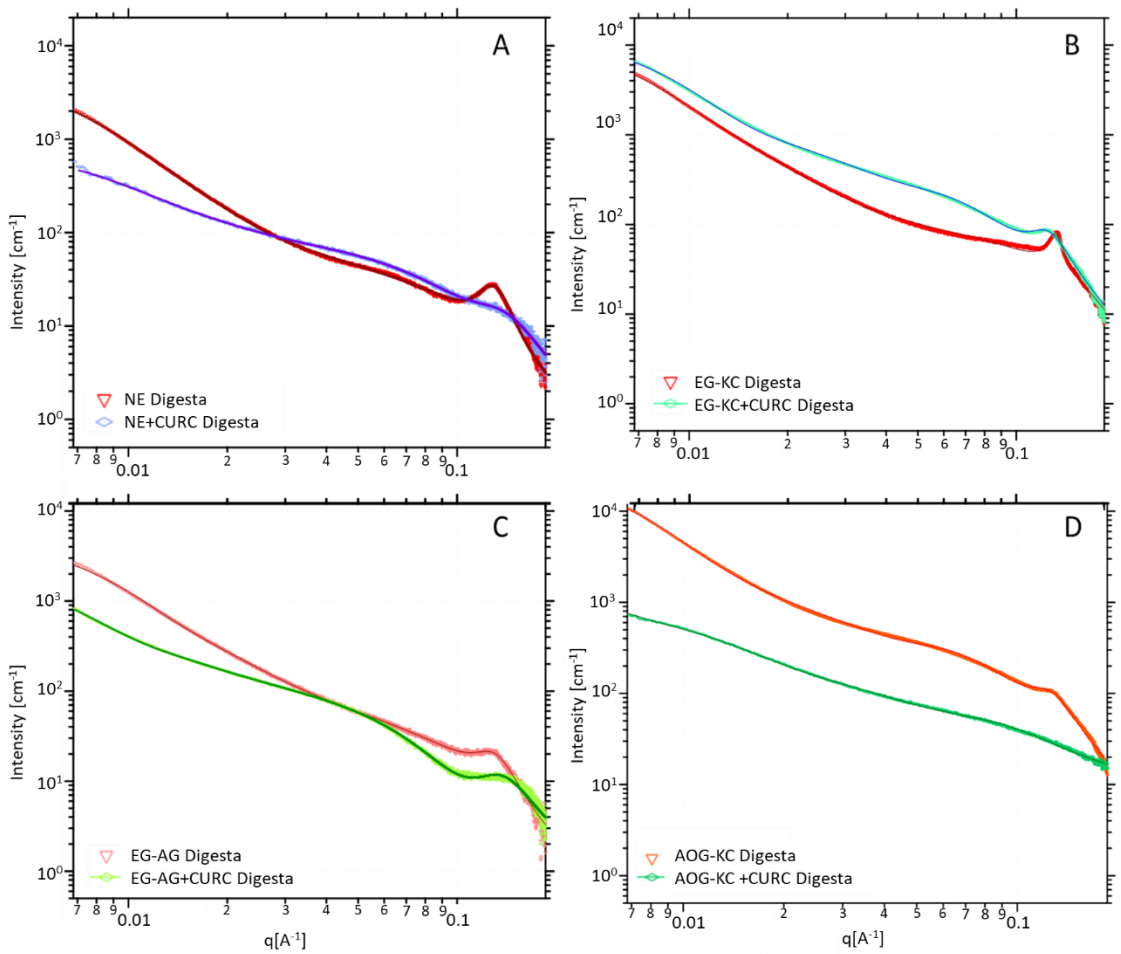

Figure 5. SAXS patterns from the liquid fraction (digesta) obtained after the gastrointestinal digestion for the nanoemulsions (A), κ-carrageenan emulsion-gels (B), agar emulsion-gels (C)

and κ-carrageenan oil-filled aerogels (D). Markers represent the experimental data and solid lines show the fits obtained using theoretical models.

The micellar phase, where the curcumin was expected to be found after digestion, was separated from the digesta by centrifugation and then analysed by SAXS. In most of the cases, this micellar phase separated into two different phases upon storage for a few hours: an aqueous phase that remained at the bottom (AQ) and an upper oily phase (OIL); consequently, these two phases were analysed separately, and the results are shown in Figure 6. As observed, in most cases, the high-q scattering peak associated to the presence of mixed bile salt lamellae/micelles was absent in the scattering patterns from the aqueous phase and only the scattering features attributed to the presence of larger vesicles were observed. On the other hand, the scattering curves corresponding to the oily phase presented less defined scattering features and were more similar to that of partially digested emulsified oil (cf. Figure 4B). This phase separation may have occurred due to the de-stabilization of micelles and/or vesicles and subsequent coalescence, induced by the freeze-thawing process to which the samples were subjected upon storage before analysis. Interestingly, the κ-carrageenan emulsion-gel showed a homogeneous micellar phase which did not separate into two phases and the corresponding scattering pattern was very similar to that obtained for the digesta (i.e., the whole liquid phase before centrifugation), being characterized by the appearance of a scattering peak characteristic from bile salt lamellae/micelles. This supports our previous hypothesis of more abundant and monodisperse mixed bile salt micelles, with greater stability, in the case of the κ-carrageenan emulsion-gel.

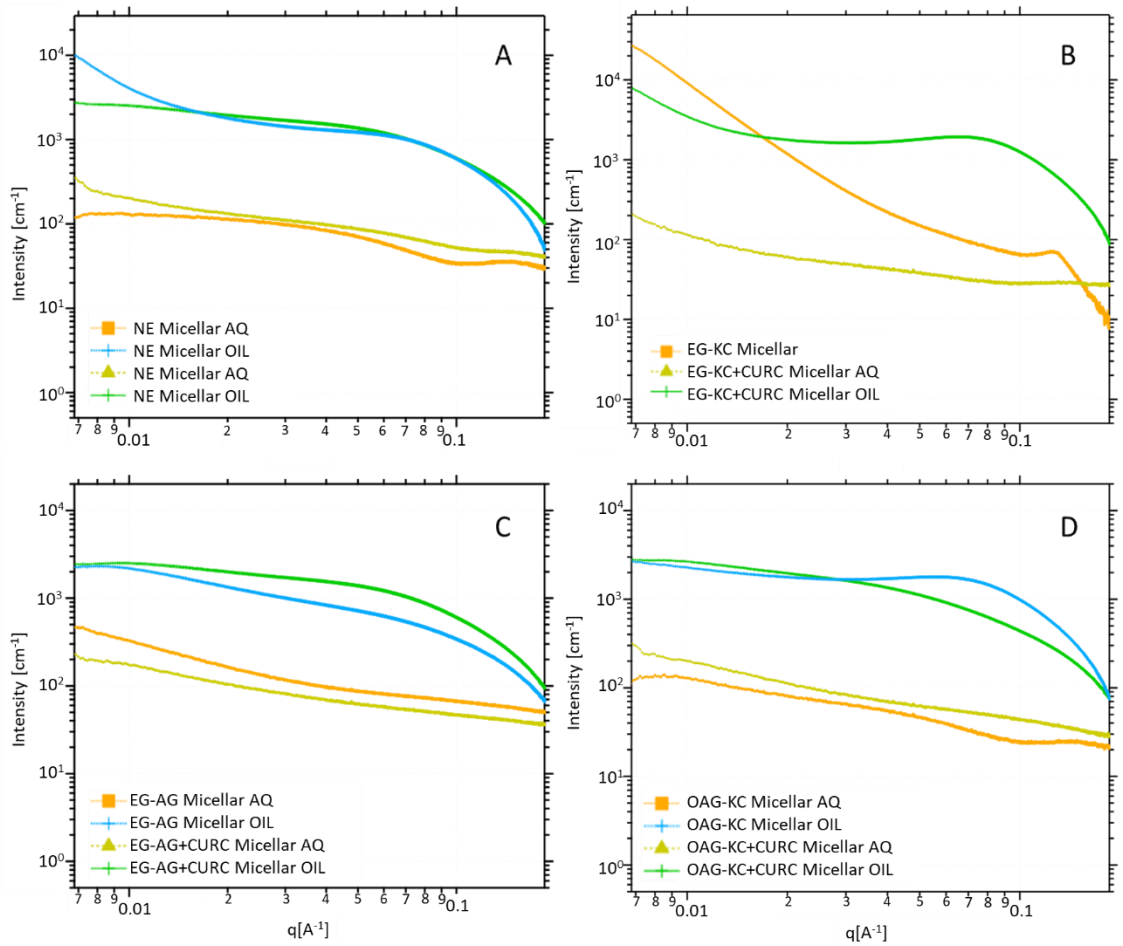

Figure 6. SAXS patterns from the micellar phase obtained after the gastrointestinal digestion for the nanoemulsions (A), κ-carrageenan emulsion-gels (B), agar emulsion-gels (C) and κ-carrageenan oil-filled aerogels (D). Where applicable, "AQ" corresponds to the aqueous phase, while "OIL" corresponds to the oily phase.

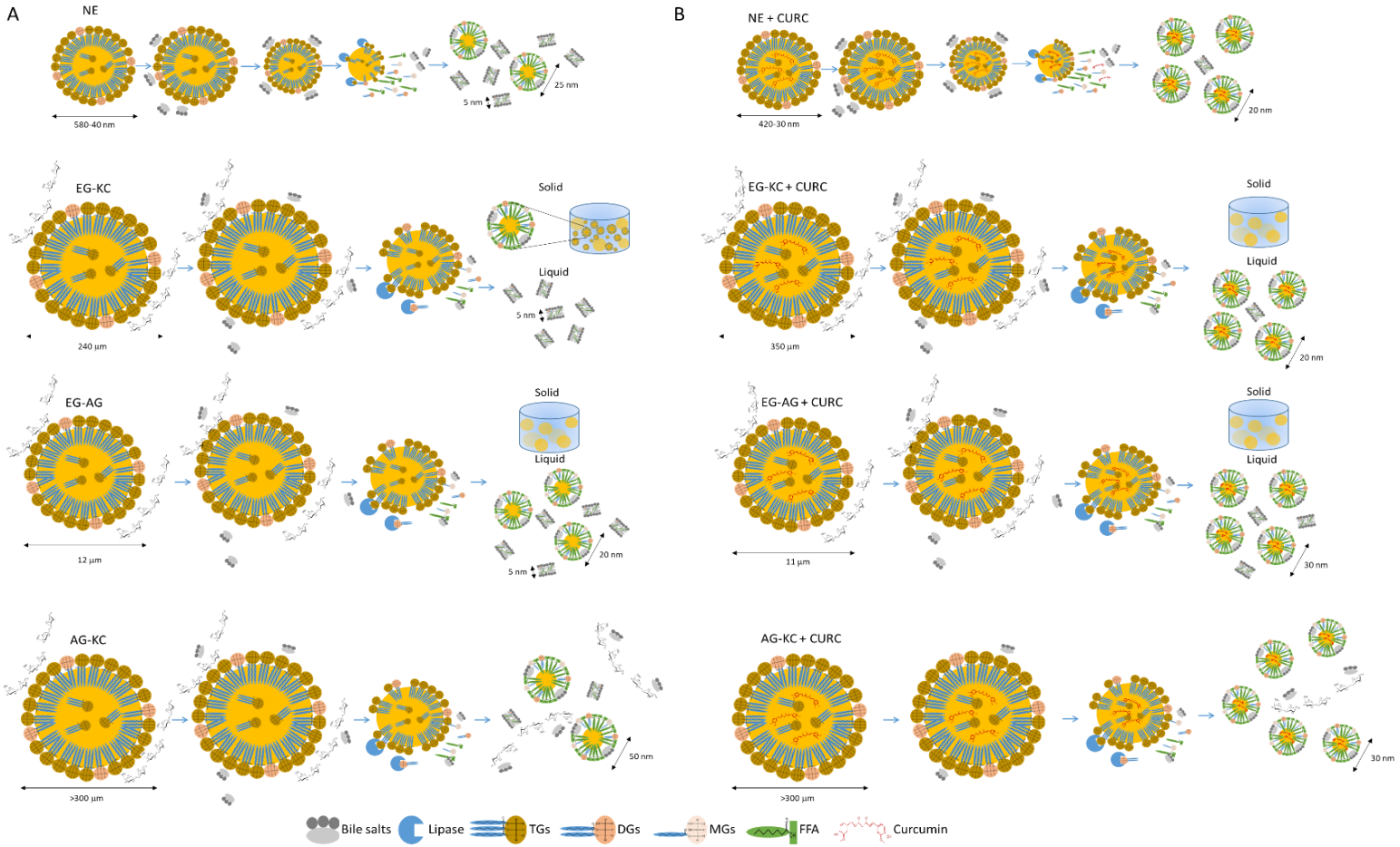

Figure 7. Schematic representation of the type of structures formed as a result of the lipolysis process during the intestinal digestion of the control nanoemulsions and the oil-filled gel-like structures.

5 Conclusions

Gel-like structures from agar and κ-carrageenan, in the form of emulsion-gels and oil-filled aerogels were produced and curcumin was incorporated into the oil phase. The structure and mechanical properties of the gel-like structures were characterized and the effect on the type of structures generated upon *in vitro* gastrointestinal digestion was investigated. Agar emulsion-gels presented smaller and more homogeneously distributed oil droplets than those from κ-carrageenan. Due to the distinct nature of interactions holding together the gelling networks, agar emulsion-gels showed a more rigid behaviour, whereas κ-carrageenan yielded more resistant emulsion-gel structures. On the other hand, freeze-drying produced a collapse in the polysaccharide network and coalesce of oil droplets took place, being able to produce oil-filled aerogels only in the case of κ-carrageenan. In that case, the oil was only physically entrapped within the aerogel structure being easily released upon mechanical forces.

When subjecting the samples to a simulated gastrointestinal digestion process, the type of structures generated as a result of the oil lipolysis was dependent of the polysaccharide type and the physical state. For all the emulsion-gels a solid fraction (mainly non-digested material) remained even after the intestinal phase, whereas in the oil-filled aerogels, due to the lack of interactions between the oil and the polysaccharide phase, the aerogel structure was disrupted during the digestion process. The solid and liquid fractions were separately analysed by SAXS and compared to the digesta from control nanoemulsions. The scattering patterns showed the coexistence of different types of structures in most of the samples, with bile salt lamellae/micelles of ca. 5 nm and larger vesicles of partially digested oil with ca. 20-50 nm being the predominant type of structures. Partially digested emulsified oil was seen to remain trapped in the solid fraction from the κ-carrageenan emulsion-gels, probably due to a lower extent of lipolysis originated by a limited diffusion of bile salts towards the oil droplets through the strong gelling network and the larger droplet size in the initial nanoemulsions. Consequently, a greater amount of free bile salt structures was present in the liquid media. In the case of the κ-carrageenan oil-filled aerogels, the polysaccharide particles released towards the liquid medium seemed to de-stabilize the bile salt small lamellae/micelles and promoted the formation of larger vesicles. The presence of curcumin seems to limit the formation of these

mixed bile salt-digestion products lamellae/micelles. Interestingly, in all the samples the presence of curcumin induced the formation of a greater amount of larger vesicles, with curcumin being most likely located within the interior of these structures.

These results evidence the high relevance of the microstructure and mechanical behavior of oil-filled gel-like structures, as well as the presence of bioactive components such as curcumin, in the behavior upon gastrointestinal digestion. This is of crucial importance, since the formation of different types of structures in the digestion products is expected to affect the intestinal transport and adsoprtion of the generated compounds. Moreover, the incorporation of these strucures into different types of food matrices is expected to have a strong impact on their digestibility and, thus, this should be studied in the future.

6 Acknowledgements

The projects RTI2018-094268-B-C22 was funded by MCIN/AEI/ 10.13039/501100011033 and by "ERDF A way of making Europe". Cynthia Fontes-Candia is recipient of a pre-doctoral grant from CONACYT (MEX/Ref. 306680).

7 References

Ahmed, K., Li, Y., McClements, D. J., & Xiao, H. (2012). Nanoemulsion-and emulsion-based delivery systems for curcumin: Encapsulation and release properties. *Food Chemistry*, *132*(2), 799–807.

Artiga-Artigas, M., Acevedo-Fani, A., & Martín-Belloso, O. (2017). Effect of sodium alginate incorporation procedure on the physicochemical properties of nanoemulsions. *Food Hydrocolloids*, *70*, 191–200. https://doi.org/10.1016/J.FOODHYD.2017.04.006

Artiga-Artigas, María, Lanjari-Pérez, Y., & Martín-Belloso, O. (2018). Curcumin-loaded nanoemulsions stability as affected by the nature and concentration of surfactant. *Food Chemistry*, *266*, 466–474. https://doi.org/https://doi.org/10.1016/j.foodchem.2018.06.043

Bastien Marze, S., Dric Gaillard, C., & Roblin, P. (2015). In vitro digestion of emulsions: high spatiotemporal resolution using synchrotron SAXS †. *Soft Matter*, *11*, 5365. https://doi.org/10.1039/c5sm01205h

Beaucage, G. (1995). Approximations leading to a unified exponential/power-law approach to small-angle scattering. *Journal of Applied Crystallography*, *28*(6), 717–728.

Benito-González, I., López-Rubio, A., Gómez-Mascaraque, L. G., & Martínez-Sanz, M. (2020). PLA coating improves the performance of renewable adsorbent pads based on cellulosic aerogels from aquatic waste biomass. *Chemical Engineering Journal*, 124607.

Brodkorb, A., Egger, L., Alminger, M., Alvito, P., Assunção, R., Ballance, S., Bohn, T., Bourlieu-

Lacanal, C., Boutrou, R., Carrière, F., Clemente, A., Corredig, M., Dupont, D., Dufour, C., Edwards, C., Golding, M., Karakaya, S., Kirkhus, B., Le Feunteun, S., … Recio, I. (2019). INFOGEST static in vitro simulation of gastrointestinal food digestion. *Nature Protocols*, *14*(4), 991–1014. https://doi.org/10.1038/s41596-018-0119-1

Cas, M. D., & Ghidoni, R. (2019). Dietary Curcumin: Correlation between Bioavailability and Health Potential. *Nutrients 2019, Vol. 11, Page 2147*, *11*(9), 2147. https://doi.org/10.3390/NU11092147

Cervantes-Paz, B., Ornelas-Paz, J. de J., Ruiz-Cruz, S., Rios-Velasco, C., Ibarra-Junquera, V., Yahia, E. M., & Gardea-Béjar, A. A. (2017). Effects of pectin on lipid digestion and possible implications for carotenoid bioavailability during pre-absorptive stages: A review. *Food Research International*, *99*, 917–927. https://doi.org/10.1016/J.FOODRES.2017.02.012

Chang, Y., & McClements, D. J. (2016). Influence of emulsifier type on the in vitro digestion of fish oil-in-water emulsions in the presence of an anionic marine polysaccharide (fucoidan): Caseinate, whey protein, lecithin, or Tween 80. *Food Hydrocolloids*, *61*, 92–101. https://doi.org/https://doi.org/10.1016/j.foodhyd.2016.04.047

Espinal-Ruiz, M., Parada-Alfonso, F., Restrepo-Sánchez, L. P., Narváez-Cuenca, C. E., & McClements, D. J. (2014). Impact of dietary fibers [methyl cellulose, chitosan, and pectin] on digestion of lipids under simulated gastrointestinal conditions. *Food & Function*, *5*(12), 3083–3095. https://doi.org/10.1039/C4FO00615A

Fatouros, D. G., Bergenstahl, B., & Mullertz, A. (2007). Morphological observations on a lipid-based drug delivery system during in vitro digestion. *European Journal of Pharmaceutical Sciences*, *31*(2), 85–94. https://doi.org/10.1016/J.EJPS.2007.02.009

Fontes-Candia, C., Lopez-Sanchez, P., Ström, A., Martínez, J. C., Salvador, A., Sanz, T., Trefna, H. D., López-Rubio, A., & Martínez-Sanz, M. (2021). Maximizing the oil content in polysaccharide-based emulsion gels for the development of tissue mimicking phantoms. *Carbohydrate Polymers*, *256*, 117496. https://doi.org/https://doi.org/10.1016/j.carbpol.2020.117496

Fontes-Candia, C., Ström, A., Gómez-Mascaraque, L. G., López-Rubio, A., & Martínez-Sanz, M. (2020). Understanding nanostructural differences in hydrogels from commercial carrageenans: Combined small angle X-ray scattering and rheological studies. *Algal Research*, *47*, 101882. https://doi.org/https://doi.org/10.1016/j.algal.2020.101882

Fontes-Candia, C., Ström, A., Lopez-Sanchez, P., López-Rubio, A., & Martínez-Sanz, M. (2020). Rheological and structural characterization of carrageenan emulsion gels. *Algal Research*, *47*, 101873. https://doi.org/https://doi.org/10.1016/j.algal.2020.101873

Geremias-Andrade, I. M., Souki, N. P. D. B. G., Moraes, I. C. F., & Pinho, S. C. (2017). Rheological and mechanical characterization of curcumin-loaded emulsion-filled gels produced with whey protein isolate and xanthan gum. *LWT*, *86*, 166–173. https://doi.org/https://doi.org/10.1016/j.lwt.2017.07.063

Hewlings, S. J., & Kalman, D. S. (2017). Curcumin: A Review of Its Effects on Human Health. *Foods*, *6*(10), 92. https://doi.org/10.3390/FOODS6100092

Hosseini-Zare, M. S., Sarhadi, M., Zarei, M., Thilagavathi, R., & Selvam, C. (2021). Synergistic effects of curcumin and its analogs with other bioactive compounds: A comprehensive review. *European Journal of Medicinal Chemistry*, *210*, 113072. https://doi.org/10.1016/J.EJMECH.2020.113072

Ilavsky, J., & Jemian, P. R. (2009). Irena: tool suite for modeling and analysis of small-angle scattering. *Journal of Applied Crystallography*, *42*(2), 347–353.

Kieffer, J., & Wright, J. P. (2013). PyFAI: a Python library for high performance azimuthal integration on GPU. *Powder Diffraction*, *28*(S2), S339–S350.

Klinkesorn, U., & McClements, D. J. (2010). Impact of Lipase, Bile Salts, and Polysaccharides on Properties and Digestibility of Tuna Oil Multilayer Emulsions Stabilized by Lecithin–Chitosan. *Food Biophysics*, *5*(2), 73–81. https://doi.org/10.1007/S11483-010-9147-2

Koç, H., Drake, M., Vinyard, C. J., Essick, G., van de Velde, F., & Foegeding, E. A. (2019). Emulsion filled polysaccharide gels: Filler particle effects on material properties, oral processing, and sensory texture. *Food Hydrocolloids*, *94*, 311–325. https://doi.org/https://doi.org/10.1016/j.foodhyd.2019.03.018

Li, J., Xu, L., Su, Y., Chang, C., Yang, Y., & Gu, L. (2020). Flocculation behavior and gel properties of egg yolk/κ-carrageenan composite aqueous and emulsion systems: Effect of NaCl. *Food Research International*, *132*, 108990. https://doi.org/https://doi.org/10.1016/j.foodres.2020.108990

Lopez-Pena, C., Arroyo-Maya, I. J., & McClements, D. J. (2019). Interaction of a bile salt (sodium taurocholate) with cationic (ε-polylysine) and anionic (pectin) biopolymers under simulated gastrointestinal conditions. *Food Hydrocolloids*, *87*, 352–359. https://doi.org/https://doi.org/10.1016/j.foodhyd.2018.08.029

Macierzanka, A., Torcello-Gómez, A., Jungnickel, C., & Maldonado-Valderrama, J. (2019). Bile salts in digestion and transport of lipids. *Advances in Colloid and Interface Science*, *274*, 102045. https://doi.org/10.1016/J.CIS.2019.102045

Mandal, S., Ghosh, S., Banik, D., Banerjee, C., Kuchlyan, J., & Sarkar, N. (2013). An Investigation into the Effect of the Structure of Bile Salt Aggregates on the Binding Interactions and ESIHT Dynamics of Curcumin: A Photophysical Approach To Probe Bile Salt Aggregates as a Potential Drug Carrier. *The Journal of Physical Chemistry B*, *117*(44), 13795–13807. https://doi.org/10.1021/jp407824t

Manzocco, L., Valoppi, F., Calligaris, S., Andreatta, F., Spilimbergo, S., & Nicoli, M. C. (2017). Exploitation of κ-carrageenan aerogels as template for edible oleogel preparation. *Food Hydrocolloids*, *71*, 68–75. https://doi.org/10.1016/J.FOODHYD.2017.04.021

Mao, L., Lu, Y., Cui, M., Miao, S., & Gao, Y. (2020). Design of gel structures in water and oil phases for improved delivery of bioactive food ingredients. *Critical Reviews in Food Science and Nutrition*, *60*(10), 1651–1666.

Martínez-Sanz, M., Ström, A., Lopez-Sanchez, P., Knutsen, S. H., Ballance, S., Zobel, H. K., Sokolova, A., Gilbert, E. P., & López-Rubio, A. (2020). Advanced structural characterisation of agar-based hydrogels: Rheological and small angle scattering studies. *Carbohydrate Polymers*, *236*, 115655. https://doi.org/https://doi.org/10.1016/j.carbpol.2019.115655

Marze, S., Choimet, M., & Foucat, L. (2012). In vitro digestion of emulsions: diffusion and particle size distribution using diffusing wave spectroscopy and diffusion using nuclear magnetic resonance. *Soft Matter*, *8*(42), 10994–11004. https://doi.org/10.1039/C2SM26334C

McClements, D. J., & Rao, J. (2011). Food-Grade Nanoemulsions: Formulation, Fabrication, Properties, Performance, Biological Fate, and Potential Toxicity. *Critical Reviews in Food Science and Nutrition*, *51*(4), 285–330. https://doi.org/10.1080/10408398.2011.559558

Meng, Z., Qi, K., Guo, Y., Wang, Y., & Liu, Y. (2018). Macro-micro structure characterization and molecular properties of emulsion-templated polysaccharide oleogels. *Food Hydrocolloids*, *77*, 17–29. https://doi.org/10.1016/j.foodhyd.2017.09.006

Nordqvist, D., & Vilgis, T. A. (2011). Rheological Study of the Gelation Process of Agarose-Based Solutions. *Food Biophysics*, *6*(4), 450. https://doi.org/10.1007/s11483-011-9225-0

Okuro, P. K., Martins, A. J., Vicente, A. A., & Cunha, R. L. (2020). Perspective on oleogelator mixtures, structure design and behaviour towards digestibility of oleogels. *Current Opinion in Food Science*, *35*, 27–35. https://doi.org/https://doi.org/10.1016/j.cofs.2020.01.001

Palla, C., Giacomozzi, A., Genovese, D. B., & Carrín, M. E. (2017). Multi – objective optimization of high oleic sun fl ower oil and monoglycerides oleogels : Searching for rheological and textural properties similar to margarine. *Food Structure*, *12*, 1–14. https://doi.org/10.1016/j.foostr.2017.02.005

Patel, A. R., Cludts, N., Sintang, M. D. Bin, Lesaffer, A., & Dewettinck, K. (2014). Edible oleogels based on water soluble food polymers: preparation, characterization and potential application. *Food & Function*, *5*(11), 2833–2841.

Patra, D., Ahmadieh, D., & Aridi, R. (2013). Study on interaction of bile salts with curcumin and curcumin embedded in dipalmitoyl-sn-glycero-3-phosphocholine liposome. *Colloids and Surfaces B: Biointerfaces*, *110*, 296–304. https://doi.org/10.1016/J.COLSURFB.2013.04.027

Pilosof, A. M. R. (2017). Potential impact of interfacial composition of proteins and polysaccharides stabilized emulsions on the modulation of lipolysis. The role of bile salts. *Food Hydrocolloids*, *68*, 178–185. https://doi.org/10.1016/J.FOODHYD.2016.08.030

Plazzotta, S., Calligaris, S., & Manzocco, L. (2019). Structure of oleogels from κ-carrageenan templates as affected by supercritical-CO2-drying, freeze-drying and lettuce-filler addition. *Food Hydrocolloids*, *96*, 1–10. https://doi.org/https://doi.org/10.1016/j.foodhyd.2019.05.008

Sabet, S., Rashidinejad, A., Qazi, H. J., & McGillivray, D. J. (2021). An efficient small intestine-targeted curcumin delivery system based on the positive-negative-negative colloidal interactions. *Food Hydrocolloids*, *111*, 106375. https://doi.org/10.1016/J.FOODHYD.2020.106375

Salentinig, S., Phan, S., Darwish, T. A., Kirby, N., Boyd, B. J., & Gilbert, E. P. (2014). PH-responsive micelles based on caprylic acid. *Langmuir*, *30*(25), 7296–7303. https://doi.org/10.1021/LA500835E/SUPPL_FILE/LA500835E_SI_001.PDF

Salvia-Trujillo, L., Verkempinck, S. H. E., Sun, L., Van Loey, A. M., Grauwet, T., & Hendrickx, M. E. (2017). Lipid digestion, micelle formation and carotenoid bioaccessibility kinetics: Influence of emulsion droplet size. *Food Chemistry*, *229*, 653–662. https://doi.org/10.1016/J.FOODCHEM.2017.02.146

Takeshita, S., & Yoda, S. (2015). Chitosan Aerogels: Transparent, Flexible Thermal Insulators. *Chemistry of Materials*, *27*(22), 7569–7572. https://doi.org/10.1021/acs.chemmater.5b03610

Tavernier, I., Patel, A. R., Meeren, P. Van Der, & Dewettinck, K. (2017). Emulsion-templated liquid oil structuring with soy protein and soy protein : k -carrageenan complexes. *Food Hydrocolloids*, *65*, 107–120. https://doi.org/10.1016/j.foodhyd.2016.11.008

Tran, T., Siqueira, S. D. V. S., Amenitsch, H., Rades, T., & Müllertz, A. (2017). Monoacyl

phosphatidylcholine inhibits the formation of lipid multilamellar structures during in vitro lipolysis of self-emulsifying drug delivery systems. *European Journal of Pharmaceutical Sciences*, *108*, 62–70. https://doi.org/10.1016/J.EJPS.2016.11.022

Wang, L., Mutch, K. J., Eastoe, J., Heenan, R. K., & Dong, J. (2008). Nanoemulsions prepared by a two-step low-energy process. *Langmuir*, *24*(12), 6092–6099. https://doi.org/10.1021/LA800624Z/SUPPL_FILE/LA800624Z-FILE004.PDF

Wang, Z., Neves, M. A., Kobayashi, I., Uemura, K., & Nakajima, M. (2013). Preparation, Characterization, and in Vitro Gastrointestinal Digestibility of Oil-in-Water Emulsion–Agar Gels. *Bioscience, Biotechnology, and Biochemistry*, *77*, 120659.

8 Supplementary Material

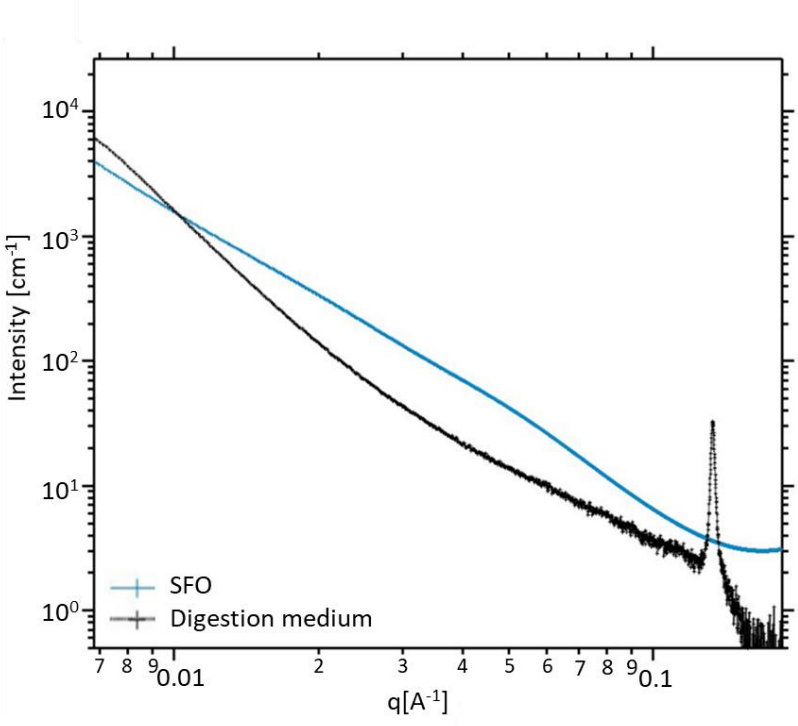

Figure S1. SAXS patterns from the native sunflower oil (SFO) and the digestion medium used during the *in vitro* gastrointestinal digestions.

Table S1. Parameters obtained from the fits of the SAXS data from the gel-like oil-filled structures**.**

Sample	Rg_1	P1	Rg_2	P2
EG-KC	68.8	1.7	7.6	3.1
EG-KC + CURC	67.0	2.0	8.9	2.5
EG-AG	---	2.7	8.2	3.1
EG-AG + CURC	---	2.5	8.2	3.0
OAG-KC	---	3.8	4.8	---
OAG-KC + CURC	---	3.9	5.9	---

3.3.3

MAXIMIZING THE OIL CONTENT IN POLYSACCHARIDE-BASED EMULSION-GELS FOR THE DEVELOPMENT OF TISSUE MIMICKING PHANTOMS

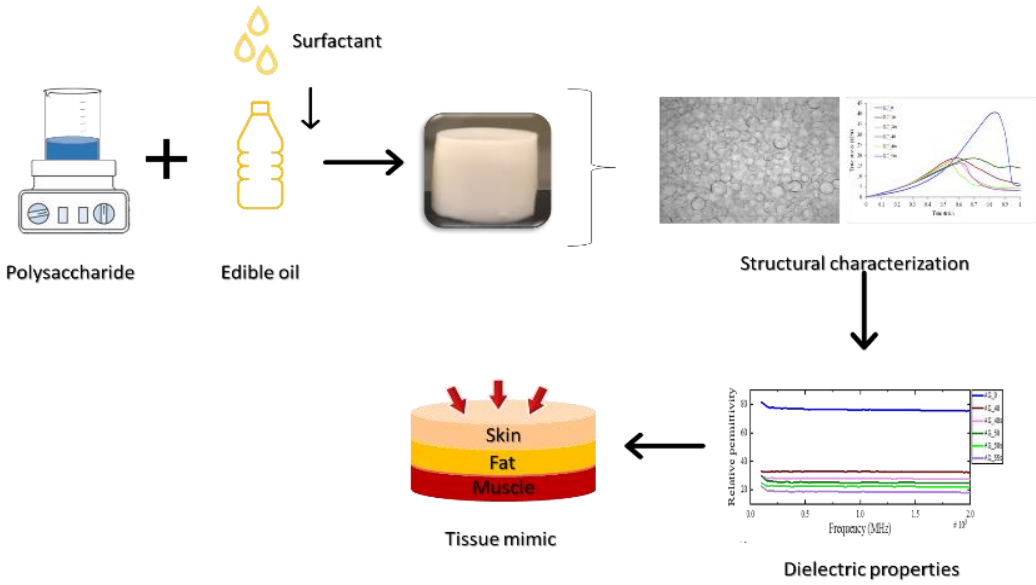

This section is an adapted version of the following published research article:

Fontes-Candia, C., Lopez-Sanchez, P., Ström, A., Martínez, J. C., Salvador, A., Sanz, T., Dobsicek-Trefna, H., López-Rubio, A & Martínez-Sanz, M. (2021). Maximizing the oil content in polysaccharide-based emulsion-gels for the development of tissue mimicking phantoms. Carbohydrate Polymers, 256, 117496

1 Abstract

Formulations based on agar and κ-carrageenan were investigated for the production of emulsion-gels applicable as tissue mimicking phantoms. The effects of the polysaccharide matrix, the oil content and the presence of surfactants on the micro-/nanostructure, rheology, and mechanical and dielectric properties were investigated. Results showed a high capacity of the agar to stabilize oil droplets, producing gels with smaller (10-21 μm) and more uniform oil droplets. The addition of surfactants allowed increasing the oil content and reduced the gel strength and stiffness down to 57% and 34%, respectively. The permittivity and conductivity of the gels were reduced by increasing the oil content, especially in the agar gels (18.8 and 0.05 S/m, respectively), producing materials with dielectric properties similar to those of low-water content tissues. These results evidence the suitability of these polysaccharides to design a variety of tissue mimicking phantoms with a broad range of mechanical and dielectric properties.

2 Introduction

Emulsion-gels are composite soft materials with solid-like behaviour where an oil-phase is dispersed within a continuous hydrogel network. These systems can be classified as emulsion-filled gels, which contain dispersed oil droplets, or as emulsion particulate gels, which contain a network of aggregated oil droplets (Farjami & Madadlou, 2019). Emulsion-gels provide characteristics typical of hydrophobic materials while maintaining structural characteristics similar to hydrogels. Therefore, they are suitable materials for the incorporation and controlled delivery of bioactive compounds with hydrophilic and hydrophobic character. Another advantage of emulsion-gels is that they provide stability to the emulsion phase (Geremias-Andrade et al., 2016; Li et al., 2020). The entrapment of the oil droplets within a continuous hydrogel network limits their aggregation through coalescence and flocculation. Such promising properties make emulsion-gels excellent candidates for the development of materials with applications in the medical, pharmaceutical and food industry fields.

Emulsion-gels can be produced with a wide range of rheological properties, depending on several intrinsic factors such as the nature of the interactions between the components, droplet volume fraction and matrix stiffness (Dickinson, 2012). Furthermore, depending on their

structural behaviour, the rheological properties of emulsion-gels can be determined by the continuous hydrogel network or by the network of aggregated emulsion droplets. Surfactants can also be added to this type of materials to improve the emulsion stability, since interactions between surfactants and polymers may influence the affinity of the oil phase to the hydrogel matrix (Farjami & Madadlou, 2019). All these factors are of considerable practical importance when utilising an emulsion-gel system for pharmaceutical, cosmetic, food and biomedical applications (Farjami & Madadlou, 2019). By varying the ratios of different components of a synergistic mixture, numerous systems can be developed, thus being able to tune the gel characteristics by changing different variables or processing conditions of the system.

Emulsion-gels could be particularly interesting for the development of fat phantom materials for biomedical applications. Phantoms that mimic physical properties of biological tissues are widely used for the evaluation and development of imaging techniques such as ultrasound, magnetic resonance imaging, computed tomography of electromagnetic field distribution in the human body, among others. Biological tissues exhibit a large range of dielectric properties as permittivity (ε_r) and conductivity (σ), which describe the polarization effects on charged particles owing to the applied field and the electrical losses in the material due to the currents driven by the field, respectively. The development of this type of materials requires the use of non-toxic, easy to handle materials, with the capacity to be produced in different forms and with specific mechanical properties. Furthermore, preparation methods should be easy to follow and reproducible, while reducing production costs as much as possible.

Although many different tissue-mimicking phantoms have been developed to simulate the properties of high-water content biological tissues (with ε_r ~ 60-80 and σ ~ 0.4-0.8 S/m), the development of fat phantoms, which mimic low-water content tissues (with ε_r ~ 5-20 and σ ~ 0.05-0.2 S/m) is more complex (Wust et al., 1998). Low permittivity materials are required for the development of fat phantoms and, thus, the development of structured systems with high oil contents is of interest within this field. Most of the fat phantom materials reported in the literature make use of toxic substances such as acrylamide or formaldehyde (Andreuccetti et al., 1988; Davidson & Sherar, 2003; Solanki et al., 2016; Surowiec et al., 1992; Yeh et al., 1998), being therefore unsuitable for biomedical applications. Moreover, most of the described

methodologies require very complex preparation methods, generally involving multistep procedures (Chou et al., 1984; Jónasson et al., 2012). More recently, biopolymers such as gelatin have been used for the development of biocompatible fat phantoms (Solanki et al., 2016); however, the thermal resistance and dielectric properties of these materials are yet to be improved.

We have recently reported on a straightforward methodology to produce emulsion-gels based on sulphated polysaccharides (Martínez-Sanz, M. Fontes-Candia, C. Fabra, M. López-Rubio, 2019). These systems were capable of incorporating significant proportions of oil and their rheological and mechanical properties could be tuned by adjusting the formulations (Fontes-Candia, Ström, Lopez-Sanchez, et al., 2020). Based on these results, our hypothesis is that it is possible to produce emulsion-gels based on sulphated polysaccharides suitable for their application as fat phantoms by tuning the formulations to maximize the oil content. The effect of the polysaccharide matrix (agar and κ-carrageenan), the oil content and the presence of surfactants were evaluated through studying the nanostructure, rheological and mechanical properties of the developed emulsion-gels, thus proving insights on how the properties of these materials can be adapted for each specific application.

3 Materials and methods

3.1 Materials

Commercial κ-carrageenan (Ceamgel 90-093) and agar (PRONAGAR), in the form of powders, were kindly donated by CEAMSA (Pontevedra, Spain) and Hispanagar (Burgos, Spain), respectively. The commercial κ-carrageenan was composed of 92% κ-carrageenan and 8% ι-carrageenan (Fontes-Candia, Ström, Gómez-Mascaraque, et al., 2020). The agar content in the commercial agar was 80% (Martínez-Sanz et al., 2020). KCl, Span 80 and Tween 85 were obtained from Sigma-Aldrich (Spain). Rapeseed oil was purchased in a local market (Coop, Gothenburg, Sweden). The composition of the oil, as provided by the supplier, is shown in Table S1.

3.2 Preparation of emulsion-gels

Emulsion-gels were produced from the commercial κ-carrageenan (KC) and agar (AG). The polysaccharide concentrations in the final emulsions were fixed at 1.3% (w/v) for κ-carrageenan

and 1.6% (w/v) for agar, based on previous experiments (Fontes-Candia, Ström, Lopez-Sanchez, et al., 2020; Martínez-Sanz et al., 2020). The oil phase weight fraction was varied from 0 (in which case hydrogels were produced) to the maximum amount which could be incorporated into the formulations to obtain homogeneous emulsion-gels (i.e. 50% for KC and 55% for AG, as shown in the Table 1). The effect of adding a surfactant into the formulations was also explored. Based on the hydrophilic-lipophilic balance number (HLB) of the rapeseed oil, a mixture of Span 80 and Tween 85 (at a volume ratio of 3:2), presenting a very similar HLB value, was selected. The surfactant blend was dispersed into the oil phase at a fixed concentration of 1% w/w (with respect to the total weight of the formulations) and this mixture constituted the oil phase.

The polysaccharide powder was dispersed in hot water (90°C) for 30 min. For the κ-carrageenan samples, KCl (0.25% (w/v)) was then added to the hot solution which was gently stirred until the salt was completely dissolved. This constituted the aqueous phase. After that, the required amount of oil phase was added and the samples were homogenized with an ultraturrax for 2 min, producing emulsions. Aliquots of the prepared emulsions were directly transferred to quartz capillaries for the temperature-resolved SAXS analyses or to the rheometer plate (pre-heated). For the punctual SAXS measurements and the compression tests, the hot emulsions were transferred to cylindrical moulds (20 mm diameter, 10 mm height) and were cooled down to room temperature and subsequently stored at 4 °C for 24 h prior to the analyses. Figure S1 shows, as an example, the visual appearance of selected hydrogels and emulsion-filled gels with and without the addition of surfactants.

Table 1. Formulations used for the preparation of agar (AG) and κ-carrageenan (KC) emulsion-gels.

Formulation	Polysaccharide	Oil phase (% w/w)	Aqueous phase (% w/w)	Surfactant	Oil phase (%v/v)
AG_0	Agar	0	100	x	0
AG_40		40	60	x	42
AG_40s		40	60	✓	42
AG_50		50	50	x	52
AG_50s		50	50	✓	52
AG_55s		55	45	✓	57
KC_0	κ-carrageenan	0	100	x	0
KC_30		30	70	x	32
KC_30s		30	70	✓	32
KC_40		40	60	x	42
KC_40s		40	60	✓	42
KC_50s		50	50	✓	52

3.3 Uniaxial compression

Uniaxial compression tests were performed using a texture analyser (Stable Micro Systems model TA-XT2, Surrey, UK) equipped with a cylindrical aluminum plunger (3.6 cm diameter) and a load cell of 30 N. Gel disk specimens were compressed to 90 % of the original height, using a crosshead speed of 0.1 mm/s. Experiments were carried out at room temperature (ca. 25ºC). Force (N) and distance (mm) were converted to true stress (σ_T) and true strain (ε_T) using Eqs. (1) and (2). Compression moduli were calculated from the slopes of the initial linear zone of the true stress vs. true strain curves. All the measurements were performed, at least, in triplicate.

$$\sigma_T = \frac{F(t)\,(h_0 - \Delta h(t))}{\pi r^2 h_0} \quad (1)$$

$$\varepsilon_T = \ln \frac{h_0}{h_0 - \Delta h(t)} \quad (2)$$

where F(t) is the force, h_0 is the initial height of the sample, Δh(t) is the change in the height during compression and r is the initial radius of the sample.

3.4 Oscillatory rheological measurements

The rheological measurements were performed on an AR-G2 rheometer from TA instruments (Crawley, England) using a cone-plate geometry (4 cm diameter, 2º angle and 53 µm of gap). Temperature was controlled using a Peltier plate. The cone was equipped with a solvent trap and an evaporation blocker from TA Instruments. In addition, the samples were covered with a layer of paraffin oil. Freshly prepared hot emulsions were loaded onto the pre-heated rheometer plate at 90°C. After an equilibration time of 3 minutes, a cooling step from 90 to 20 °C was performed at a constant rate of 2 ºC/min, followed by an equilibration step of 5 min at 20°C, and a final heating step from 20 °C to 90 °C. The storage (G') and loss (G'') moduli were recorded versus temperature at a strain of 0.1 % (inside the linear viscoelastic region) and a frequency of 6.28 rad/s. Strain amplitude sweeps were also performed at 20 ºC to determine the extension of the linear viscoelastic response (see Figure S2). The samples, initially equilibrated at 90 ºC, were cooled down to 20 ºC (2 ºC/min and 0.1% strain) and equilibrated for 5 minutes at 20 °C; subsequently, a strain sweep within the range of 0.01-100% was carried out, at a constant frequency of 6.28 rad/s. In addition, frequency sweeps (0.1-100 rad/s) were also performed at a fixed 0.1% strain amplitude and 20 °C, after subjecting the samples to the same cooling program used for the strain sweeps.

3.5 Optical microscopy

Optical microscopy was used to visualize the microstructure of the emulsion-gels and to determine oil droplet size distribution. Digital Images were taken using an Eclipse 90i microscope (Nikon Corporation, Japan) equipped with a 5-megapixels cooled digital color microphotography camera Nikon Digital Slight DS-Mc. From each emulsion-gel, two thick sections (ca. 1-2 mm thickness) were carefully cut with the help of a scalpel and placed onto a glass slide. A total of three images were taken for each sample. Oil droplet size was determined by image analysis using the ImageJ software. Measurements were performed from at least 50 well defined droplets on 3 different images and mean and standard deviation values were calculated.

3.6 Confocal Laser Scanning microscopy

Confocal scanning laser microscopy (CLSM) imaging was performed using a Leica TCS SP2 (Leica Microsystems, Germany). A slice was carefully cut from the emulsion-gel (ca. 500 µm thickness) using a scalpel and placed into a sample holder on a glass slide with the cross-section facing upwards. One droplet of Nile Red (0.2% w/w in acetone), which is able to stain fat, was added on top of the sample and covered with a glass coverslip. The light source used was an argon laser with an emission wavelength of 488 nm. An oil immersion objective with a magnification of 40 and a numerical aperture (NA) of 0.50 was used throughout the study.

3.7 Small angle X-ray scattering (SAXS)

SAXS experiments were carried out in the Non Crystalline Diffraction beamline, BL-11, at ALBA synchrotron light source (www.albasynchrotron.es). The polysaccharide emulsion-gels and their corresponding hydrogels were analysed at room temperature (25 ºC). The energy of the incident photons was 12.4 KeV or equivalently a wavelength, λ, of 1 Å. The SAXS diffraction patterns were collected by means of a photon counting detector, Pilatus 1M, with an active area of 168.7 x 179.4 mm^2, an effective pixel size of 172 x 172 μm^2 and a dynamic range of 20 bits. The sample-to-detector distance was set to 7570 mm, resulting in a q range with a maximum value of q = 0.19 $Å^{-1}$. An exposure time of 10 s was selected based on preliminary trials. Additionally, selected formulations were subjected to temperature-resolved SAXS experiments. For the temperature-resolved experiments, aliquots from selected samples were placed in sealed 2 mm quartz capillaries (Hilgenberg GmbH, Germany) and were left to cool down at 25 ºC for 24 h to form gels prior to the experiments. The samples were then heated to 90 ºC until the gels were completely melted and the capillaries were subjected to a cooling ramp from 90 ºC to 20 ºC at a cooling rate of 1 ºC/min. Data were collected in frames of 30 s, followed by a period of 30 s in which the samples were protected from the beam by a fast shutter. Each data frame thus corresponds to a temperature range of 1 ºC. The data reduction was treated by pyFAI python code (ESRF) (Kieffer & Wright, 2013), modified by ALBA beamline staff, to do on-line azimuthal integrations from a previously calibrated file. The calibration files were created from a silver behenate (AgBh) standard. The intensity profiles were then

represented as a function of q using the IRENA macro suite (Ilavsky & Jemian, 2009) within the Igor software package (Wavemetrics, Lake Oswego, Oregon).

The scattering patterns from the polysaccharide gels were properly described using different fitting functions. For the agar gels, a function consisting of the sum of a correlation length model plus a Lorentzian peak was used:

$$I(q) = \frac{A}{q^n} + \frac{C}{1 + (q\xi_L)^m} + \frac{I_0}{1 + \left((q - q_0)/B\right)^2} + bkg \qquad (3)$$

The first and second terms in equation (3) correspond to the correlation length model. This model contains a first term, described by a power-law function, which accounts for the scattering from large clusters in the low q region and a second term, consisting of a Lorentzian function, which describes scattering from polymer chains in the high q region. n is the power-law exponent, A is the power-law coefficient, m is the Lorentzian exponent, C is the Lorentzian coefficient and ξ_L is the correlation length for the polymer chains (which gives an indication of the gel's mesh size). The third term in equation (3) corresponds to the Lorentzian function (where q_0 is the peak position, I_0 is the intensity of the peak and B is the standard deviation of the peak position) and the fourth term accounts for the incoherent background.

Equation (3) did not provide satisfactory fits for the κ-carrageenan gels. Alternatively, a function consisting of a two-leel unified model plus a Lorentzian peak was used:

$$I(q) = \sum_{i=1}^{N} G_i \exp\left(-q^2 \cdot \frac{R_{g,i}^2}{3}\right) + \frac{B_i \left[\operatorname{erf}\left(\frac{qR_{g,i}}{\sqrt{6}}\right)\right]^{3P_i}}{q^{P_i}} + \frac{I_0}{1 + \left(\frac{(q - q_0)}{B}\right)^2} + bkg \qquad (4)$$

The first and second terms in equation (4) correspond to the unified model, which considers that, for each individual level, the scattering intensity is the sum of a Guinier term and a power-law function (Beaucage, 1995). $G_i = c_i V_i \Delta SLD_i{}^2$ is the exponential prefactor (where V_i is the volume of the particle and ΔSLD_i is the scattering length density (SLD) contrast existing between the ith structural feature and the surrounding solvent), $R_{g,i}$ is the radius of gyration describing the average size of the ith level structural feature and B_i is a q-independent prefactor specific to the type of power-law scattering with power-law exponent, P_i. In this particular case,

the largest structural level was modelled only by a power-law ($R_{g1}$was fixed at a value >> q_{min}^{-1} of 5000 Å).

The obtained values from the fitting coefficients are those that minimize the value of Chi-squared, which is defined as:

$$\chi^2 = \sum \left(\frac{y - y_i}{\sigma_i}\right)^2 \quad (5)$$

where y is a fitted value for a given point, y_i is the measured data value for the point and σ_i is an estimate of the standard deviation for y_i. The curve fitting operation is carried out iteratively and for each iteration, the fitting coefficients are refined to minimizeχ^2.

3.8 Dielectric properties

The dielectric properties of the gels were determined by an open-ended coaxial dielectric probe (85070E, Dielectric Probe Kit with Performance Probe, Agilent Technologies, USA) connected to a vector network analyser (VNA) (E8362B, Agilent Technologies, USA). The dielectric probe was calibrated prior to the measurements and distilled water was used to validate the calibration. The properties were measured at 101 points in the frequency range of 100 MHz to 2 GHz. Each examined gel was firmly attached to the probe, to avoid air pockets at the interface between the probe and the gel. Ten measurements were taken for each sample at a different position on the surface.

4 Results and discussions

4.1 Micro- and nanostructural characterization

Commercial κ-carrageenan and agar were used to produce emulsion-gels, increasing the oil content as much as possible to obtain materials suitable for their application as fat phantom systems. The maximum amount of oil phase which could be incorporated into the agar and κ-carrageenan matrices was determined on the basis of preliminary trials. While a weight fraction of 50% oil phase could be incorporated into agar, κ-carrageenan was only able to incorporate a maximum content of 40% oil phase. Greater oil phase contents led to the production of non-homogeneous materials, where the oil phase separated from the aqueous hydrogel phase. The addition of the surfactants blend allowed to incorporate greater oil phase contents of 55% for agar and 50% for κ-carrageenan. To determine the size distribution of the oil droplets within

the gel matrices, the emulsion-gel samples were analysed by CLSM and optical microscopy and representative images are shown in Figure 1. As observed, the oil droplets seemed to be distributed within the continuous gelling polysaccharide aqueous phase (thus indicating the formation of O/W emulsions prior to the gelation process), with the κ-carrageenan samples presenting much larger droplets than the agar samples. This can be explained by two factors: (i) the high emulsifying properties of agar, giving rise to smaller droplets with a more homogeneous size distribution (Ishii et al., 2018) and (ii) the inherent difficulty of dispersing the oil in the κ-carrageenan samples, since they started to form gels at higher temperatures (as later demonstrated by the rheological characterization, cf. Figure 3), becoming much more viscous than the agar samples.

For the agar samples, Figures 1A- E show that the oil droplets were homogeneously distributed within the gel matrix. Even though no significant differences in the measured droplet sizes were observed for the agar samples with different oil contents due to the relatively large standard deviation values (cf. Table 2), increasing the oil content seemed to produce slightly smaller oil droplets, as evidenced by the corresponding CLSM images. Surprisingly, the addition of the surfactants led to the formation of more heterogeneous and larger oil structures. This could be ascribed to a greater coalescence of oil droplets, as demonstrated by the CLSM images from the samples with added surfactants, where oil droplet aggregates with very diffused interface were clearly identified, as previously found in similar systems (agar and κ-carrageenan-locust bean gum gels) with different emulsifiers (Koç et al., 2019). This observation suggests a competition for the droplet interface between the surfactants and the agar, hindering the effect of the agar in stabilizing the oil droplets (Ellis et al., 2017). If the interface is not stabilised prior to gelation of the network, the oil droplets may coalesce and form larger structures.

Table 2. Average oil droplet size of the agar and κ-carrageenan emulsion-gels, measured from the optical microscopy images.

Formulation	Oil droplet size (μm)
AG_40	12.2 ± 3.5 [bc]
AG_40s	20.6 ± 6.9 [a]
AG_50	10.4 ± 2.5 [c]
AG_50s	13.2 ± 5.1 [b]
AG_55s	13.3 ± 7.0 [b]
KC_30	147.1 ± 74.5 [a]
KC_30s	30.1 ± 16.9 [b]
KC_40	183.6 ± 191.2 [a]
KC_40s	18.6 ± 11.7 [b]
KC_50s	21.6 ± 11.9 [b]
KC_30	147.1 ± 74.5 [a]

Values with different letter are significantly different ($p \leq 0.05$) between formulation for each polysaccharide. Data were analysed by ANOVA followed by a Tukey-test.

In the case of the κ-carrageenan samples, Figures 1F and 1H evidence a very heterogeneous distribution of oil droplets, with much larger sizes than those observed in the agar gels. Furthermore, as shown in Table 2, more heterogeneous droplet sizes were originated when increasing the oil content. As previously commented, given their capacity to start the gelation process at higher temperatures, oil dispersion in the κ-carrageenan formulations was more difficult than in the agar samples. This may be the reason for the formation of much larger oil droplets in the κ-carrageenan gels. In this case, the presence of surfactant produced a much more uniform distribution of the oil within the polysaccharide matrix, with smaller average droplet sizes, although a relatively large size variability was still observed. This can be related to a reduction in the viscosity of the κ-carrageenan solutions with the addition of the surfactants. In fact, a decrease in the viscosity of agar solutions in presence of surfactants has been previously reported (Prasad et al., 2005). This allowed a better homogenization of the oil phase and the formation of smaller droplets. As shown in the CLSM images, the large droplet

size variability was due to the effect of the surfactants in promoting the coalescence of oil droplets, just as observed in the agar samples.

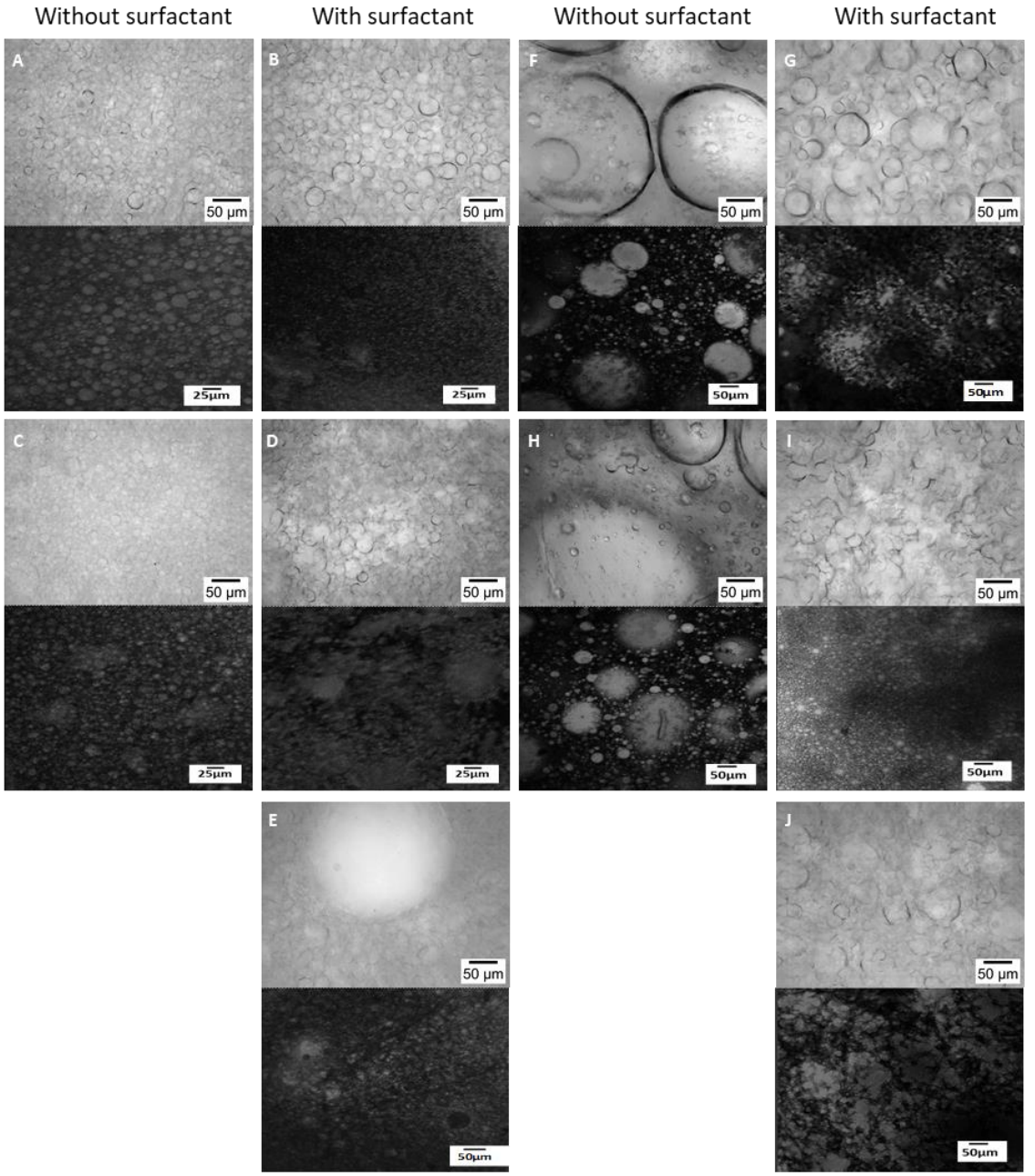

Figure 1. Optical microscopy images of agar (A-E) and κ-carrageenan (F-J) emulsion-gels. (A) AG_40; (B) AG_40s; (C) AG_50 (D) AG_50s and (E) AG_55; (F) KC_30 (G) KC_30s; (H) KC_40 (I) KC_40s and (J) KC_50s. For each sample, optical microscopy images are shown at the top and CLSM images are shown at the bottom.

The nanostructure of the polysaccharide hydrogels and emulsion-gels was also investigated by means of SAXS experiments. The obtained scattering patterns are shown in Figure 2A for the agar samples and in Figure 2B for the κ-carrageenan samples. The greater scattering intensities of the agar samples suggest the formation of stronger (i.e. more strongly interacting) gel networks. Previous studies have demonstrated the potential of SAXS to investigate the structural organization of carrageenan and agar gel systems; however, given the variability of structures which can be formed depending on several parameters such as the polysaccharide molecular structure, the polysaccharide concentration and the valency and concentration of added cationic salts, interpreting the data may be especially complex since suitable theoretical models have to be sought for each specific case (Fontes-Candia, Ström, Gómez-Mascaraque, et al., 2020; Fontes-Candia, Ström, Lopez-Sanchez, et al., 2020; Martínez-Sanz et al., 2020). In general, one should look for the simplest model able to properly describe the experimental data and providing fitting parameters which have physical meaning according to any preliminary knowledge on the samples. After preliminary trials, a correlation length model was seen to provide satisfactory fits for the agar samples, while a more complex two-level unified model (also known as Beaucage model) was selected to fit the experimental data from the κ-carrageenan samples. In both cases, weak scattering peaks were detected within the high q region (as evidenced by the Kratky plots shown in Figure S3) and, thus, an additional term consisting of a Lorentzian function was added to the fitting functions. The most relevant fitting parameters are compiled in Table 3a for the agar gels and Table 3b for the κ-carrageenan gels. The results evidenced stronger structural changes within the studied size range taking place in the κ-carrageenan gels as compared with the agar samples. The agar gels presented power-law exponents of 2.4-2.7 within the low q range, which are characteristic from mass fractal structures, i.e. branched network structures. The Lorentz exponents associated to the lower q range were 2.0-2.7, suggesting that the agar polymeric chains were in a branched conformation. The correlation length, associated to the thickness of the bundles of agar double helices, was 23-29 nm for the samples without surfactant. On the other hand, the real distances corresponding to the weak scattering peak detected within the high q range were 4.9-5.9 nm, which are very similar to the values previously reported for the agar double helices (Fatin-Rouge

et al., 2006; Martínez-Sanz et al., 2020). While the addition of oil did not seem to have a significant impact in the nanostructure of the agar gels, the presence of the surfactant appeared to hinder the association of the agar double helices into bundles, as suggested by the corresponding lower correlation length values.

The κ-carrageenan gels were characterized by greater power-law exponents within the low q region (2.7-3.5) as compared with the agar samples. This indicates the formation of more branched structures within the corresponding size range and may suggest that less rigid structures were formed in the case of κ-carrageenan. The radius of gyration, which was ca. 14 nm for the pure hydrogel, increased with the addition of oil, especially in the presence of the surfactant. It should be noted that the κ-carrageenan hydrogel showed two small peaks located at 0.025 $Å^{-1}$ and 0.050 $Å^{-1}$, indicative of the existence of well-ordered structures with real distances of ca. 25 nm and 13 nm. Similar peaks have been detected in κ-carrageenan hydrogels and emulsion-gels (with oil contents ranging from 0 to 48% w/w) with the addition of KCl (Fontes-Candia, Ström, Gómez-Mascaraque, et al., 2020; Fontes-Candia, Ström, Lopez-Sanchez, et al., 2020) and have been associated to the formation of carrageenan bundles with an ordered periodical structure due to the ionic cross-links formed between the carrageenan sulphate groups and the K^+ ions. These peaks were no longer visible in the emulsion-gels, suggesting that the presence of oil led to the formation of less ordered structures, where the κ-carrageenan double helices were aggregated forming larger but less densely packed bundles. The power-law exponents within the low q region (1.5-2.1) indicated the presence of more rigid swollen linear chains, with carrageenan double helices of ca. 5.6-6.4 nm. It should be noted that the sample with the highest oil content, i.e. KC_50s, presented a distinct scattering pattern, with lower scattering intensity within the whole q range. This can be attributed to the formation of structures with different physical densities within the studied size range (ca. 3-150 nm) (due to a greater concentration of the polysaccharide within the aqueous phase) or to a variation in the scattering length density contrast generated between the polysaccharide and the surrounding liquid medium.

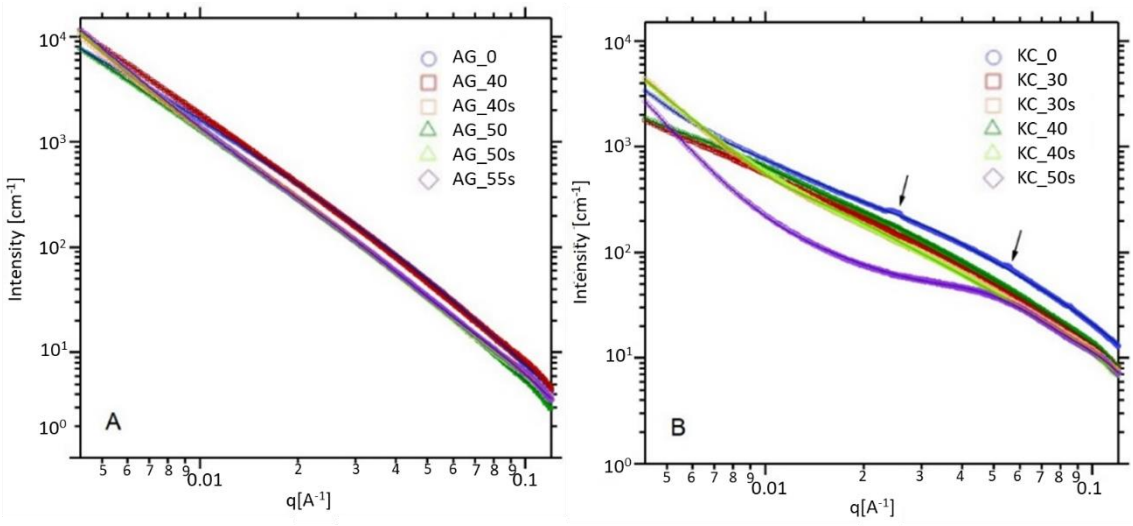

Figure 2. SAXS patterns from the agar (A) and κ-carrageenan (B) hydrogels and emulsion-gels. Markers represent the experimental data and solid lines show the fits obtained using theoretical models.

Table 3. Parameters obtained from the fits of the SAXS data from the agar (a) and κ-carrageenan (b) hydrogels and emulsion-gels.

(a)

Sample	*n*	*m*	ξ_L (nm)	d (nm)
AG_0	2.4	2.0	24.7	4.9
AG_40	2.5	2.0	23.2	5.3
AG_40s	2.7	2.5	7.1	5.9
AG_50	2.5	2.1	28.8	5.0
AG_50s	2.7	2.0	8.8	5.6
AG_55s	2.7	2.7	14.6	5.2

n: power-law exponent; *m*: Lorentzian exponent; ξ_L: correlation length; d: real distance corresponding to the Lorentzian peak.

(b)

Sample	P_1	Rg_2 (nm)	P_2	d (nm)
KC_0	3.1	14.1	1.5	---
KC_30	2.7	19.2	1.6	6.4
KC_30s	2.5	32.1	1.6	6.4
KC_40	2.7	19.2	1.6	6.1
KC_40s	2.7	26.1	1.6	2.1
KC_50s	3.5	7.0	2.1	5.6

P_1: power-law coefficient for the largest structural level; Rg_2: radius of gyration associated to the smallest structural level; P_2: power-law coefficient for the smallest structural level; d: real distance corresponding to the Lorentzian peak.

4.2 Rheological characterization

To investigate the effect of the oil content and the addition of surfactant on the gelation mechanism of agar and κ-carrageenan emulsion-gels, dynamic rheological experiments were carried out, where the elastic (G') and viscous (G'') moduli of the samples were recorded during cooling and heating ramps. Representative results for the different polysaccharide formulations are presented in Figure 3. As observed, the gelation mechanism of the two polysaccharides was clearly different.

Since most of the agar samples did not show a true solution behaviour (G''> G') but rather displayed a behaviour typical of entangled networks at the initial temperature of 90 ºC, the gelation temperature was estimated from the point at which an abrupt rise in G' and G'' took place, which is ascribed to the transition from weak to strong gels (Martínez-Sanz et al., 2020). This transition corresponds to the formation of a well-developed network by aggregation of the agarose helices into larger bundles (Fontes-Candia, Ström, Gómez-Mascaraque, et al., 2020; Fontes-Candia, Ström, Lopez-Sanchez, et al., 2020; Martínez-Sanz et al., 2020). For the agar hydrogel, gelation took place at ca. 36 ºC, which is in agreement with the range of gelling temperatures typically reported in the literature (Aymard et al., 2001; Martínez-Sanz et al., 2020). A distinctive bump was observed in G' and G'' when the temperature was lowered below 30 ºC in the agar hydrogel and emulsion-gels with added surfactants. This behaviour was

observed for these samples when using different measuring parameters, as well as different configurations in the rheometer. It is also worth noting that the viscoelastic moduli estimated at 20 ºC after the cooling ramps agreed well with independent frequency sweeps performed at 20°C. Similar features have been detected in κ-carrageenan hydrogels and emulsion-gels with added KCl and have been ascribed to the formation of a metastable intermediate structure that is disrupted upon cooling (Fontes-Candia, Ström, Lopez-Sanchez, et al., 2020; Hermansson, 1989). This feature has also been reported to appear in very different gels consisting of amphiphilic block copolymer/water/oil systems, where it was associated with structural arrangement caused by thermal and mechanical factors (Rodríguez-Abreu et al., 2007). Nevertheless, this type of features has also been attributed to measurement artefacts in agar gels (Mao et al., 2016). When heating the sample back to 90 ºC, no real melting transition was observed, even though the absolute values of G' and G'' gradually decreased. This indicates that the agar hydrogel network was weakened but the entanglements between the agar molecular chains were not completely disrupted upon heating. Interestingly, a broad bump appeared within the temperature range of 40-70 ºC, suggesting that chain re-organization processes took place (as later confirmed by temperature-resolved SAXS, cf. Figure 4). The incorporation of oil had a marked effect on the rheological behaviour of the agar samples. As observed in Figures 3B and 3D, the AG_40 and AG_50 formulations presented two distinct gelling transitions, the first one taking place at 57 °C in AG_40 and at 51 °C in AG_50, and the second one occurring at 36-37 °C (similarly to the agar hydrogel) (cf. Table 4). The occurrence of these two distinct gelling steps, which were not apparent in the agar hydrogel, may be related to the formation of two different agar domains: (i) the aqueous domain and (ii) the agar located at the surface of the oil droplets. The formation of gelling domains at the surface of oil droplets has been previously reported for protein-based emulsion-gels (Matsumura et al., 1993). These domains were described to behave differently to the protein fraction dispersed within the aqueous phase and produced a reinforcing effect, which was evidenced as an increase in the G' of the emulsion-gels as compared with the protein hydrogel (Matsumura et al., 1993). The behaviour upon heating of the agar emulsion-gels was similar to that of the hydrogel, with no melting transition. Interestingly, the behaviour of the formulations with added surfactants was more

comparable to that of the agar hydrogel, with one single gelling transition taking place at around 38-39 ºC and no melting upon subsequent heating. This may indicate that the added surfactants were selectively adsorbed onto the surface of the oil droplets, preventing the formation of agar domains at the oil/water interface.

Regarding the κ-carrageenan samples, in general, they were able to form gels at higher temperatures than the agar, which is explained by the addition of KCl aiding in the formation of carrageenan helical aggregates by ionic cross-linking. For these samples, the gelling and melting temperature were estimated by the crossover point of G' and G'' in the cooling and heating ramps, respectively. The behaviour was similar for most of the κ-carrageenan formulations, with gelation temperatures ranging from 49 ºC to 56 °C and a small bump appearing when lowering the temperature from 50 ºC to 40 ºC. As already mentioned, this feature has been previously reported for κ-carrageenan gels (Fontes-Candia, Ström, Gómez-Mascaraque, et al., 2020; Hermansson, 1989) and was attributed to the formation of a transient state during the gelation process. This bump was broader in the KC_40s and KC_50s formulations, suggesting that the addition of surfactant somehow affected the gelation mechanism in these samples. Upon subsequent heating, all the κ-carrageenan samples presented a gel-sol transition, with corresponding melting temperatures of 68-76 °C (cf. Table 4). Thermal hysteresis was apparent for the κ-carrageenan and agar samples, which is characteristic from these polysaccharides due to the fact that the agarose/carrageenan bundles remain stable at temperatures much higher than those at which they start associating on cooling (Indovina et al., 1979; Trefná & Ström, 2019).

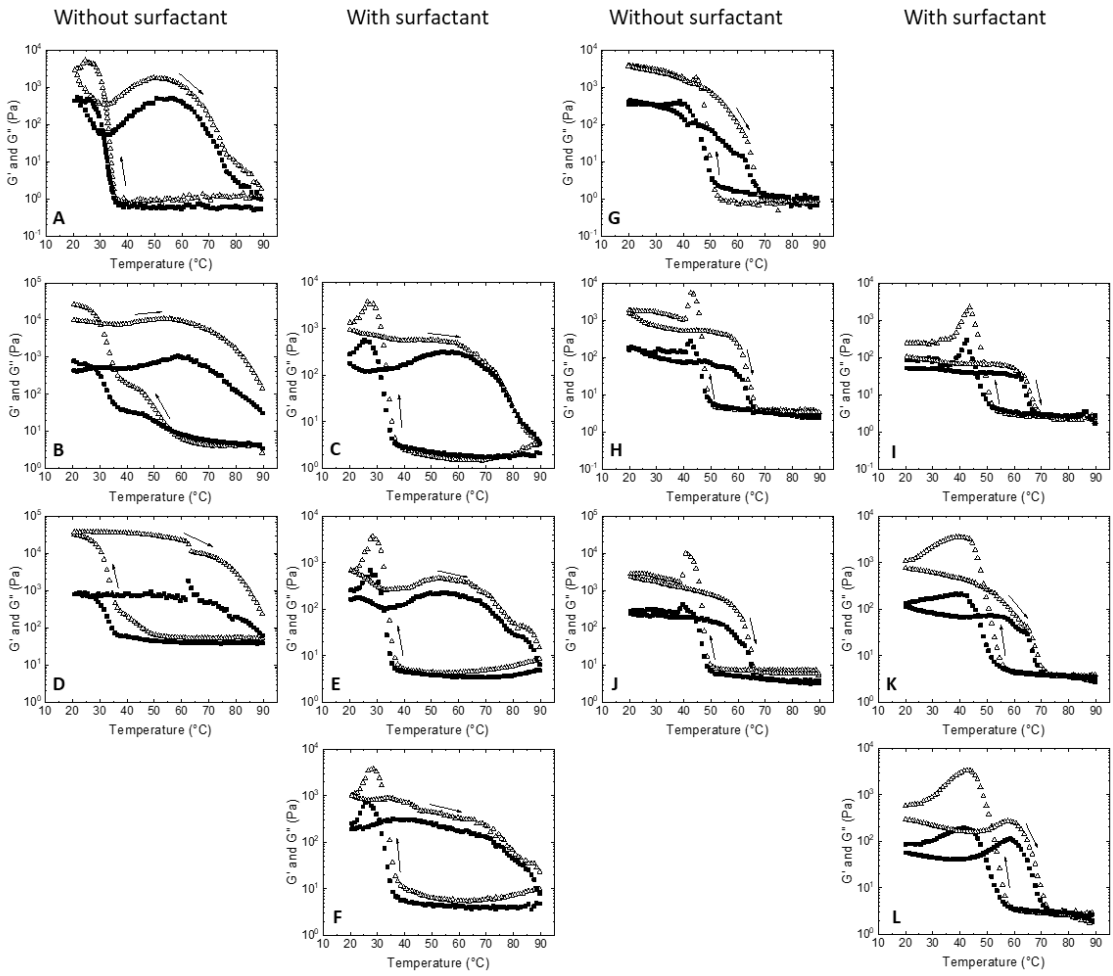

Figure 3. Temperature dependence of G' (open markers) and G'' (filled markers) moduli of agar (A-F) and κ-carrageenan (G-L) gel formulations during cooling and heating ramps (arrows indicate the direction of the temperature ramps). (A) AG_0; (B) AG_40; (C) AG_40s; (D) AG_50; (E) AG_50s; (F) AG_55s; (G) KC_0; (H) AG_30 (I) AG_30s; (J) KC_40 (K) KC_40s and (L) KC_50s.

All the polysaccharide gels were subjected to frequency sweeps at 20 °C and the frequency dependence of G' and G'' was determined. A strain amplitude of 0.1% was selected for these measurements based on the linear viscoelastic region determined for the agar and carrageenan samples, which extended up to 1% as evidenced by the strain amplitude sweeps (cf. Figure S2). As shown in Figure S4, all the samples presented a gel behaviour (G'>G'') along the studied frequency range. Moreover, the values of both moduli were frequency independent. The average G' and G'' values at 20 ºC were estimated and the values, listed in Table 4, evidence

differences in the strength of the different polysaccharide gels. In the case of the agar samples, the incorporation of oil promoted higher values of G'. This can be related to (i) the higher agar concentration in the aqueous phase and (ii) to the higher G' of the oil phase as compared with the agar hydrogel. The storage modulus of liquid droplets is defined using the equation $G' = 2\gamma/r$ in which γ is the interfacial tension of the oil droplets and r is the radius of the droplets (Dickinson, 2012; Van Vliet, 1988). Based on this equation and using a value of 26 mN/m for the interfacial tension of rapeseed oil in aqueous solutions (Gmach et al., 2019) and the average droplet sizes estimated from optical microscopy, the G'of AG_40 and AG_50 were estimated as 5174 Pa and 6078 Pa, respectively. Even though these values should be taken only as an approximation, the results evidence that, in fact, the smaller oil droplets formed in AG_50 were expected to produce a greater reinforcing effect. Surprisingly, as observed in Table 4, the experimental G' values were much larger than anticipated. An unexpectedly marked increase in the G' of protein-based emulsion-gels was also reported by Matsumura et al. (Matsumura et al., 1993), who attributed this to the reinforcing effect of the gelling protein domains formed at the surface of oil droplets. On the other hand, the addition of surfactants resulted in a decrease in the G' and an increase in the frequency dependence, suggesting the formation of weaker structures. In agreement with the results from the temperature sweeps, this seems to indicate that the presence of the surfactants prevented the formation of the agar gelling domains at the surface of the oil droplets, hence having a weakening effect. The same behaviour was reported by (Prasad et al., 2005), who described a decrease in the strength of agar emulsion-gels with the addition of a non-ionic surfactant. The selective adsorption of the surfactants onto the surface of the oil droplets would disrupt the formation of a continuous agar network holding together the structure of the emulsion-gels, which is in line with the results from the SAXS experiments. This would also explain the greater coalescence of oil droplets observed by CLMS (cf. Figure 1).

Contrarily to the agar, the incorporation of oil into the κ-carrageenan gels produced a decrease in G', being this effect more pronounced with the addition of surfactants. This behaviour suggests the presence of a lower number of effective elastic junctions in the κ-carrageenan, which is in agreement with the more loosely packed structures deduced from the SAXS results.

Table 4. Rheological and mechanical properties of agar and κ-carrageenan hydrogels and emulsion-gels.

	T_{gel} (°C)	T_m (°C)	$G'_{20°C}$ (Pa)	$G''_{20°C}$ (Pa)	σ_{max} (kPa)	E (kPa)
AG_0	36 ± 1 ^{b}	-	4739 ± 1024 ^{c}	323 ± 102 ^{bc}	31 ± 2 ^{a}	28 ± 2 ^{c}
AG_40	37 ± 1 ^{ab}	-	9434 ± 1170 ^{b}	387 ± 129 ^{b}	14 ± 2 ^{b}	49 ± 5 ^{a}
AG_40s	39 ± 1 ^{a}	-	1090 ± 127 ^{d}	120 ± 2.0 ^{bc}	6 ± 1 ^{c}	32 ± 1 ^{bc}
AG_50	36 ± 1 ^{b}	-	36342 ± 797 ^{a}	766 ± 5.0 ^{a}	12 ± 1 ^{b}	48 ± 7 ^{a}
AG_50s	38 ± 1 ^{ab}	-	879 ± 72 ^{d}	101 ± 0.9 ^{c}	7 ± 1 ^{c}	35 ± 2 ^{b}
AG_55s	38 ± 1 ^{ab}	-	1031 ± 199 ^{d}	87 ± 7.0 ^{c}	7 ± 1 ^{c}	33 ± 2 ^{bc}
KC_0	52 ± 3 ^{ab}	72 ± 3.0 ^{ab}	4404 ± 302 ^{a}	332 ± 157 ^{a}	46 ± 7 ^{a}	13 ± 2 ^{b}
KC_30	49 ± 1 ^{b}	69 ± 2.0 ^{ab}	1801 ± 48 ^{c}	146 ± 8.0 ^{ab}	20 ± 2 ^{b}	19 ± 1^{a}
KC_30s	50 ± 2 ^{ab}	68 ± 2.0 ^{b}	145 ± 16 ^{d}	31 ± 18 ^{b}	18 ± 1 ^{b}	20 ± 1 ^{a}
KC_40	54 ± 4 ^{ab}	68 ± 1.0 ^{b}	2799 ± 300 ^{b}	212 ± 7.0 ^{ab}	19 ± 1 ^{b}	20 ± 2 ^{a}
KC_40s	55 ± 2 ^{ab}	71 ± 2.0 ^{ab}	940 ± 184 ^{d}	118 ± 27 ^{ab}	17 ± 1 ^{b}	20 ± 2 ^{a}
KC_50s	56 ± 2 ^{a}	76 ± 1.0 ^{a}	760 ± 196 ^{d}	120 ± 19 ^{ab}	17 ± 3 ^{b}	20 ± 3 ^{a}

Values with different letter are significantly different ($p \leq 0.05$) between formulation for each polysaccharide. Data were analysed by ANOVA followed by a Tukey-test. Gelation temperature (T_{gel}), melting temperature (T_m) elastic modulus ($G'_{20°C}$), viscous modulus ($G''_{20°C}$), maximum true stress (σ_{max}) and Young's modulus (E). Values with different letters are significantly different ($p \leq 0.05$). Data were analyzed by ANOVA followed by a Tukey-test.

To investigate the formation of transient structures during the gelation process, the emulsion-gels with the highest oil contents were subjected to temperature-resolved SAXS experiments in which the native gels were melted by rapidly heating the SAXS capillaries at 90 ºC and then cooling them down to 20 ºC at 1ºC/min. Representative scattering curves for AG_55s and KC_50s are shown in Figures 4A and 4B, respectively. As observed, none of the samples showed scattering patterns typical from true polymeric solutions at 90 ºC, since they displayed scattering features indicative of a certain degree of intramolecular association, especially AG_55s, which is in agreement with the lack of melting transition observed for this sample in the rheological characterization. When cooling down the samples, the scattering intensity

showed an increasing trend, confirming the formation of gel networks with greater physical density. In the case of AG_55s, an obvious structural change occurred within the temperature range of 50-40 ºC, which is close to the gelling point of 38 ºC determined from the rheology experiments. The slight difference in the gelling transition observed from SAXS and rheology may be explained by the distinct thermal history of the samples and by the different geometry of the sample containers used in each method. In the case of KC_50s, the scattering intensity also gradually increased, but notably, a new structural feature, corresponding to a real distance of ca. 30 nm, was discerned within the temperature range of 80-50 ºC. This structure may be attributed to the bump detected in the rheology curve from this sample at 60-30 ºC.

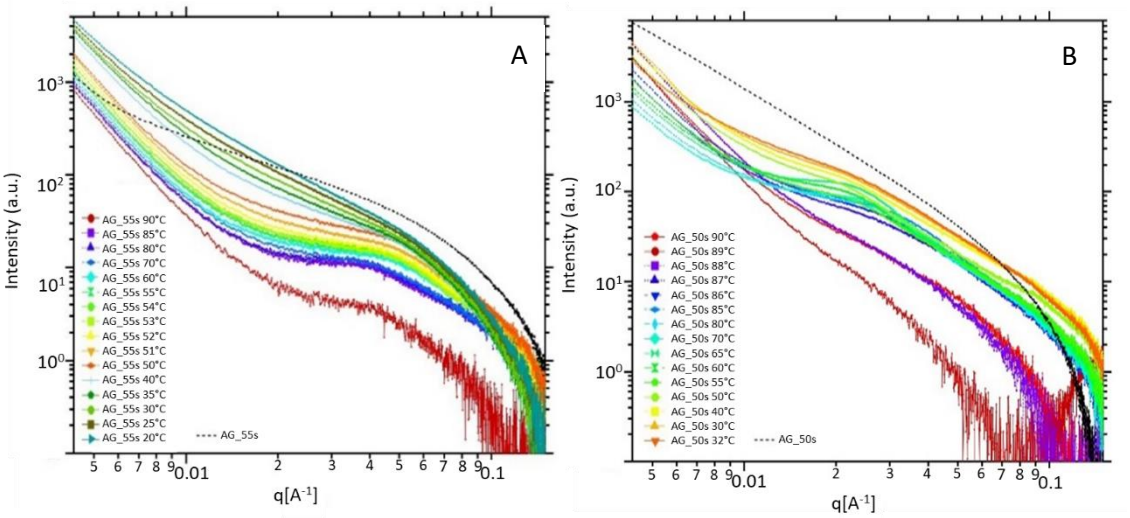

Figure 4. Temperature-resolved SAXS patterns from the AG_50s (A) and KC_55s (B) emulsion-gels at their native state and when subjected to cooling ramps from 90 ºC to 20 ºC. Selected scattering curves are shown to demonstrate the most relevant structural changes taking place during the cooling ramps.

4.3 Mechanical properties

Compression tests were carried out to examine the mechanical behaviour of the emulsion-gels and determine the effect of increasing the oil content in each type of polysaccharide. The data were plotted in the form of stress-strain curves (cf. Figure 5) and the Young's modulus (E) and maximum stress (σ_{max}) were estimated for all the samples (cf. Table 4). As observed in Figure 5,

all the agar emulsion-gels fractured at strains within the range of 20-25 %, similarly to what has been reported for agarose hydrogels (Trefná & Ström, 2019). As deduced from the mechanical parameters, the agar emulsion-gels showed a more rigid behaviour within the linear elastic region than the pure agar hydrogel; however, they were weaker and fractured at lower strain and stress values. The fact that the reinforcement effect shown by the rheology experiments, indicated by the large increase in the G' of the emulsion-gels, was not directly reflected in the large deformation compression behavior, is not surprising given the different length scales proven by each type of measurement. The large deformation behaviour is dominated by the properties of the continuous agar phase, which became more concentrated in the emulsion-gels as compared to the hydrogel. The formation of a more concentrated and less hydrated agar network produced stiffer but less deformable structures. In addition to this, the increase of the modulus with the addition of oil could be related with an oil droplet reinforcing of the network firmness, which could be ascribed to the higher oil modulus. Several reports have shown that if the filler is stiffer than the gel matrix, the larger the filler content the larger the increase in the modulus (Dickinson, 2012; Koç et al., 2019; Sala et al., 2009). The addition of surfactants led to a significant reduction in the strength (two-fold reduction in the maximum stress) and stiffness. This might be related to the more heterogeneous oil distribution, as observed by microscopy, and to a reduced aggregation of agar double helices, as suggested by the SAXS results. The effect of different surfactants in agar gels was investigated by (Prasad et al., 2005), who reported that the presence of non-ionic surfactants decreased the gel strength. Our rheology results also suggest that the presence of surfactants prevents the gelation of agar at the surface of the oil droplets, thus disrupting the formation of a strong and continuous gel network. Moreover, the presence of the surfactants coating the surface of the oil droplets leads to a weakening of the filler, resulting in a decrease in the gel modulus. In light of these results and the previous literature, it would be interesting to carry out further work to investigate the nature of interactions established between agar and different surfactants and how these may affect the gelation mechanism in agar-based gels.

In general, the κ-carrageenan samples presented a more ductile behaviour, i.e. they were less stiff within the linear elastic region, but withstood higher maximum stresses and strains before

fracture, than the agar samples. In fact, the emulsion-gels without added surfactants did not show a clear fracture upon compression, but they just weakened after reaching the maximum stress point. This can be related to the nature of the interactions holding together the polysaccharide gel network. In the case of agar, the gel network was mainly held by hydrogen bonds, while in the case of κ-carrageenan ionic interactions were responsible for the association of the polysaccharide chains (Fontes-Candia, Ström, Gómez-Mascaraque, et al., 2020; Fontes-Candia, Ström, Lopez-Sanchez, et al., 2020; Martínez-Sanz et al., 2020). Furthermore, similarly to agar, the presence of oil droplets in the κ-carrageenan gel matrix gave rise to stiffer but weaker materials. In this case, this can be related to the formation of weaker and less densely packed carrageenan networks, as suggested by the results from the SAXS and rheology experiments. These carrageenan networks were further weakened with the addition of surfactants; however, this did not produce a further decrease in the mechanical performance of the emulsion-gels under compression, which can be attributed to the counteracting positive effect of the surfactants in reducing the average oil droplet size.

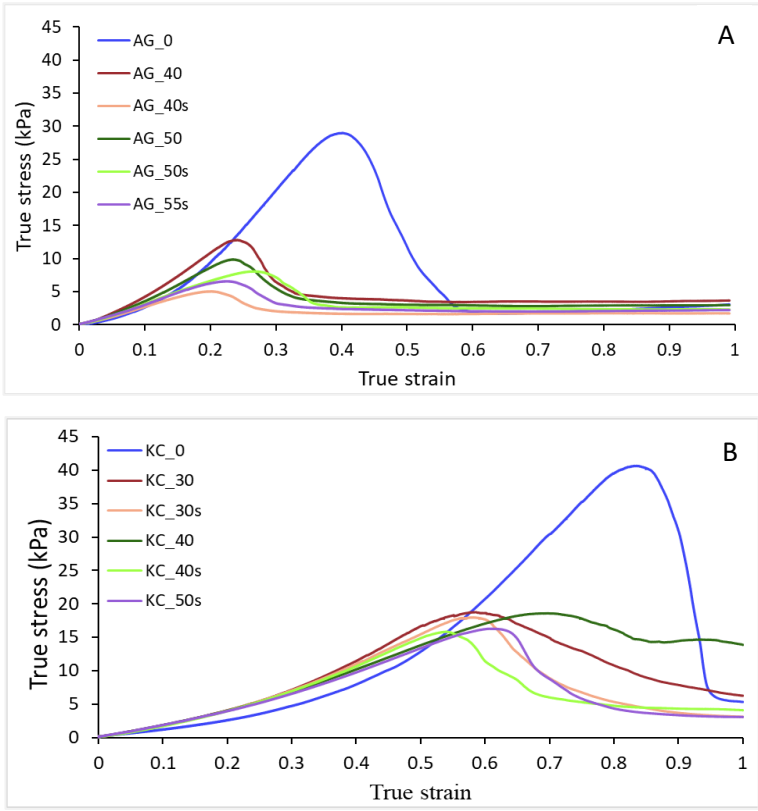

Figure 5. Representative compressive true stress-true strain curves for the (A) agar and (B) κ-carrageenan hydrogels and emulsion-gels.

4.4 Dielectric properties

In order to investigate the effect of the addition of oil and surfactant on the dielectric properties of the obtained emulsion-gels, the permittivity and conductivity of the samples were evaluated and the results are shown in the Figure 6. As expected, increasing the oil content in the gels led to a decrease in the permittivity values. Solanki et al. reported the same behaviour for gelatin emulsion-gels, which was attributed to the low permittivity of the oil phase (ca. 2.5-6 GHz) (Solanki et al., 2016). This effect was more remarkable in the agar samples, which can be related to the greater homogeneity and smaller oil droplet sizes attained in these samples. The permittivity values for the AG_55s formulation were in fact within the range required for phantoms which mimic low-water content tissues (ε_r ~ 5-20) (Wust et al., 1998).

Regarding the conductivity, it was seen to increase slightly with the frequency within the studied range. A similar behaviour was reported for a carrageenan/gellan gum hybrid gel within a frequency range of 5-130 MHz (Kuroda et al., 2005). As already anticipated, due to the presence of KCl in the κ-carrageenan emulsion-gels, these presented higher conductivity values than those formulated with agar. Moreover, a decrease in the conductivity values was observed when increasing the oil content, being this effect more evident in the agar gels. While most of the agar-based emulsion-gels present conductivity values acceptable for the development of fat mimicking phantoms ($\sigma \sim 0.05\text{-}0.2$ S/m) (Wust et al., 1998), only the KC_40 and KC_40s formulations would be suitable for this application.

These results show that the agar emulsion-gels with the highest oil content (AG_55s) are suitable to produce materials mimicking the dielectric properties of low-water content tissues, whereas the remaining formulations could be used to mimic high-water content tissues.

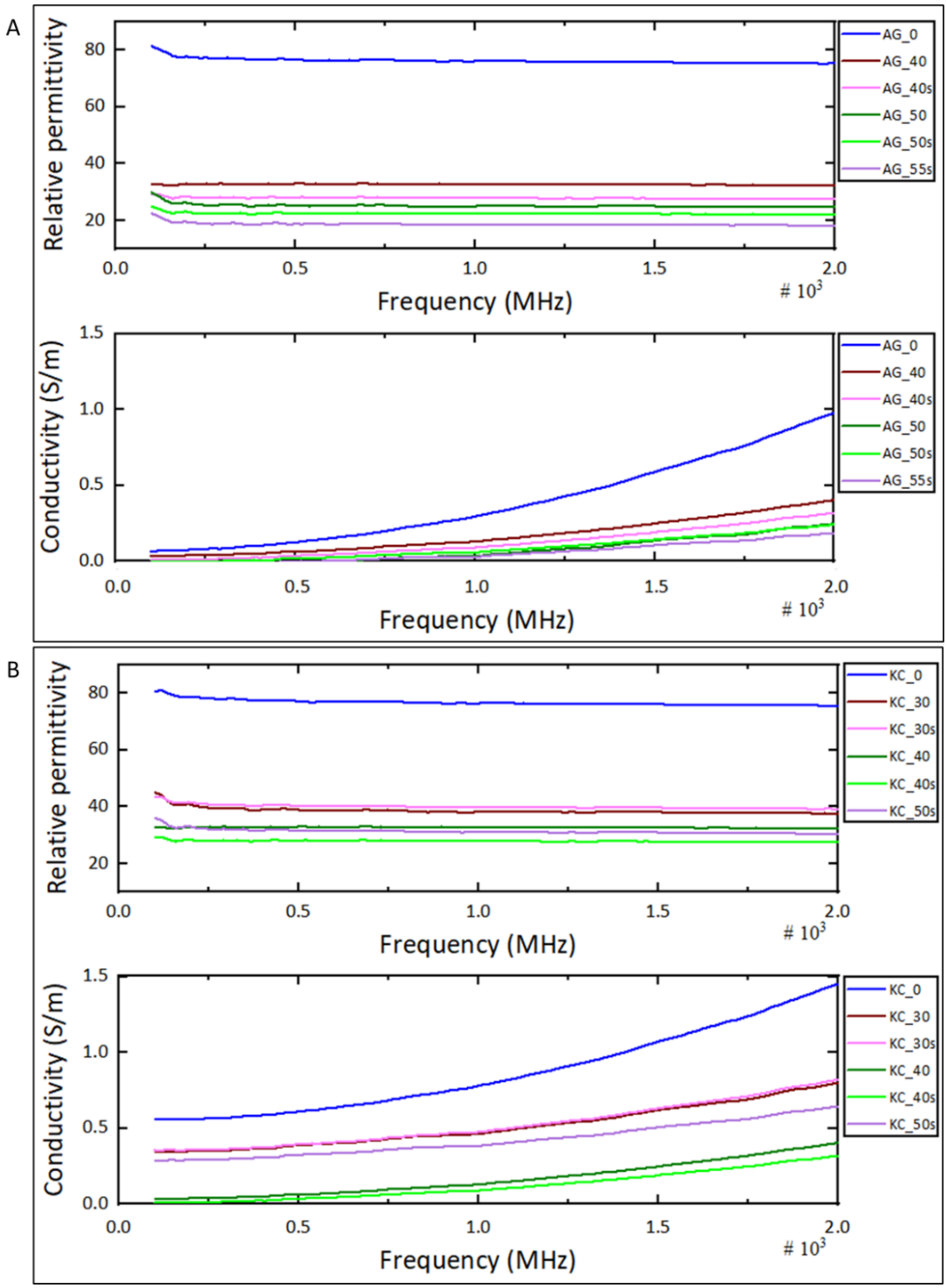

Figure 6. Dielectric properties of (A) agar and (B) κ-carrageenan hydrogels and emulsion-gels.

5 Conclusions

Agar and κ-carrageenan emulsion-gels were produced aiming to maximize the oil content to make them suitable for their use as tissue mimicking phantoms. The results evidenced the capacity of the agar to stabilize the oil droplets in the produced emulsion-gels, being able to incorporate greater amounts of oil phase (50% w/w) than κ-carrageenan (40% w/w) and producing a much more homogeneous distribution of smaller oil droplets. For both polysaccharides, the addition of a blend of non-ionic surfactants allowed to incorporate greater oil phase contents and permitted a better dispersion of the oil within the κ-carrageenan formulations.

The presence of oil in the agar had a reinforcing effect, which was evidenced as an increase in the G' of the emulsion-gels, while the presence of surfactants impeded this reinforcing effect. This was ascribed to the formation of agar gelling domains at the surface of the oil droplets, which could not be formed in the presence of surfactants. The large deformation behaviour of the samples under compression was mostly dominated by the continuous gelling network; as a result, the emulsion-gels were stiffer but weaker than their corresponding hydrogels.

As expected, an increase in the oil content led to materials with lower permittivity and conductivity values, being this effect more obvious in the agar gels due to their greater structural homogeneity and smaller oil droplet sizes. From all the developed formulations, AG_55s seemed to be the most appropriate for fat phantoms, since it showed permittivity and conductivity values within the range of low-water content tissues. These results highlight the suitability of polysaccharide-based emulsion-gels to produce tissue mimicking materials and demonstrate that their dielectric properties can be tuned depending on the requirements by adjusting the formulations.

6 Acknowledgements

Synchrotron experiments were performed at NCD beamline at ALBA Synchrotron with the collaboration of ALBA staff (2019103981 experiment). This work was financially supported by the grant RTI2018-094268-B-C22 (MCIU/AEI/FEDER, UE). Part of this work was supported by the COST Action ES1408 European network for algal-bioproducts (EUALGAE). Cynthia Fontes-Candia is recipient of a pre-doctoral grant from CONACYT (MEX/Ref. 306680).

7 References

Andreuccetti, D., Bini, M., Ignesti, A., Olmi, R., Rubino, N., & Vanni, R. (1988). Use of polyacrylamide as a tissue-equivalent material in the microwave range. *IEEE Transactions on Biomedical Engineering*, *35*(4), 275–277. https://doi.org/10.1109/10.1377

Aymard, P., Martin, D. R., Plucknett, K., Foster, T. J., Clark, A. H., & Norton, I. T. (2001). Influence of thermal history on the structural and mechanical properties of agarose gels. *Biopolymers: Original Research on Biomolecules*, *59*(3), 131–144.

Beaucage, G. (1995). Approximations leading to a unified exponential/power-law approach to small-angle scattering. *Journal of Applied Crystallography*, *28*(6), 717–728.

Chou, C., Chen, G., Guy, A. W., & Luk, K. H. (1984). Formulas for preparing phantom muscle tissue at various radiofrequencies. *Bioelectromagnetics: Journal of the Bioelectromagnetics Society, The Society for Physical Regulation in Biology and Medicine, The European Bioelectromagnetics Association*, *5*(4), 435–441.

Davidson, S. R. H., & Sherar, M. D. (2003). Measurement of the thermal conductivity of polyacrylamide tissue-equivalent material. *International Journal of Hyperthermia*, *19*(5), 551–562.

Dickinson, E. (2012). Emulsion gels: The structuring of soft solids with protein-stabilized oil droplets. *Food Hydrocolloids*, *28*(1), 224–241. https://doi.org/https://doi.org/10.1016/j.foodhyd.2011.12.017

Ellis, A. L., Norton, A. B., Mills, T. B., & Norton, I. T. (2017). Stabilisation of foams by agar gel particles. *Food Hydrocolloids*, *73*, 222–228.

Farjami, T., & Madadlou, A. (2019). An overview on preparation of emulsion-filled gels and emulsion particulate gels. *Trends in Food Science & Technology*, *86*, 85–94. https://doi.org/https://doi.org/10.1016/j.tifs.2019.02.043

Fatin-Rouge, N., Wilkinson, K. J., & Buffle, J. (2006). Combining small angle neutron scattering (SANS) and fluorescence correlation spectroscopy (FCS) measurements to relate diffusion in agarose gels to structure. *The Journal of Physical Chemistry B*, *110*(41), 20133–20142.

Fontes-Candia, C., Ström, A., Gómez-Mascaraque, L. G., López-Rubio, A., & Martínez-Sanz, M. (2020). Understanding nanostructural differences in hydrogels from commercial carrageenans: Combined small angle X-ray scattering and rheological studies. *Algal Research*, *47*, 101882. https://doi.org/https://doi.org/10.1016/j.algal.2020.101882

Fontes-Candia, C., Ström, A., Lopez-Sanchez, P., López-Rubio, A., & Martínez-Sanz, M. (2020). Rheological and structural characterization of carrageenan emulsion gels. *Algal Research*, *47*, 101873. https://doi.org/https://doi.org/10.1016/j.algal.2020.101873

Geremias-Andrade, M. I., Souki, P. B. G. N., Moraes, C. F. I., & Pinho, C. S. (2016). Rheology of Emulsion-Filled Gels Applied to the Development of Food Materials. In *Gels* (Vol. 2, Issue 3). https://doi.org/10.3390/gels2030022

Gmach, O., Bertsch, A., Bilke-Krause, C., & Kulozik, U. (2019). Impact of oil type and pH value on

oil-in-water emulsions stabilized by egg yolk granules. *Colloids and Surfaces A: Physicochemical and Engineering Aspects*, *581*, 123788.

Hermansson, A.-M. (1989). Rheological and microstructural evidence for transient states during gelation of kappa-carrageenan in the presence of potassium. *Carbohydrate Polymers*, *10*(3), 163–181.

Ilavsky, J., & Jemian, P. R. (2009). Irena: tool suite for modeling and analysis of small-angle scattering. *Journal of Applied Crystallography*, *42*(2), 347–353.

Indovina, P. L., Tettamanti, E., Micciancio-Giammarinaro, M. S., & Palma, M. U. (1979). Thermal hysteresis and reversibility of gel–sol transition in agarose–water systemsa. *The Journal of Chemical Physics*, *70*(6), 2841–2847.

Ishii, T., Matsumiya, K., Aoshima, M., & Matsumura, Y. (2018). Microgelation imparts emulsifying ability to surface-inactive polysaccharides—bottom-up vs top-down approaches. *NPJ Science of Food*, *2*(1), 1–12.

Jónasson, S. Þ., Zhurbenko, V., & Johansen, T. K. (2012). Design and characterization of a low-viscous muscle tissue mimicking media at the ISM-band (2.4–2.48 GHz) for easy antenna displacement in in vitro measurements. *2012 Asia Pacific Microwave Conference Proceedings*, 283–285.

Kieffer, J., & Wright, J. P. (2013). PyFAI: a Python library for high performance azimuthal integration on GPU. *Powder Diffraction*, *28*(S2), S339–S350.

Koç, H., Drake, M., Vinyard, C. J., Essick, G., van de Velde, F., & Foegeding, E. A. (2019). Emulsion filled polysaccharide gels: Filler particle effects on material properties, oral processing, and sensory texture. *Food Hydrocolloids*, *94*, 311–325. https://doi.org/https://doi.org/10.1016/j.foodhyd.2019.03.018

Kuroda, M., Kato, H., Hanamoto, K., Shimamura, K., Uchida, T., Wang, Y., Akaki, S., Asaumi, J.-I., Himei, K., & Takemoto, M. (2005). Development of a new hybrid gel phantom using carrageenan and gellan gum for visualizing three-dimensional temperature distribution during hyperthermia and radiofrequency ablation. *International Journal of Oncology*, *27*(1), 175–184.

Li, J., Xu, L., Su, Y., Chang, C., Yang, Y., & Gu, L. (2020). Flocculation behavior and gel properties of egg yolk/κ-carrageenan composite aqueous and emulsion systems: Effect of NaCl. *Food Research International*, *132*, 108990. https://doi.org/https://doi.org/10.1016/j.foodres.2020.108990

Mao, B., Divoux, T., & Snabre, P. (2016). Normal force controlled rheology applied to agar gelation. *Journal of Rheology*, *60*(3), 473–489.

Martínez-Sanz, M. Fontes-Candia, C. Fabra, M. López-Rubio, A. (2019). *PROCEDIMIENTO DE OBTENCIÓN DE OLEOGELES* (Patent No. PCT/ES2019/070530).

Martínez-Sanz, M., Ström, A., Lopez-Sanchez, P., Knutsen, S. H., Ballance, S., Zobel, H. K., Sokolova, A., Gilbert, E. P., & López-Rubio, A. (2020). Advanced structural characterisation

of agar-based hydrogels: Rheological and small angle scattering studies. *Carbohydrate Polymers*, *236*, 115655. https://doi.org/https://doi.org/10.1016/j.carbpol.2019.115655

Matsumura, Y., Kang, I.-J., Sakamoto, H., Motoki, M., & Mori, T. (1993). Filler effects of oil droplets on the viscoelastic properties of emulsion gels. *Food Hydrocolloids*, *7*(3), 227–240.

Prasad, K., Siddhanta, A. K., Rakshit, A. K., Bhattacharya, A., & Ghosh, P. K. (2005). On the properties of agar gel containing ionic and non-ionic surfactants. *International Journal of Biological Macromolecules*, *35*(3–4), 135–144.

Rodríguez-Abreu, C., Shrestha, L. K., Varade, D., Aramaki, K., Maestro, A., Quintela, A. L., & Solans, C. (2007). Formation and properties of reverse micellar cubic liquid crystals and derived emulsions. *Langmuir*, *23*(22), 11007–11014.

Sala, G., Van Vliet, T., Stuart, M. A. C., Van Aken, G. A., & Van de Velde, F. (2009). Deformation and fracture of emulsion-filled gels: effect of oil content and deformation speed. *Food Hydrocolloids*, *23*(5), 1381–1393.

Solanki, L. S., Singh, S., & Singh, D. (2016). Development and modelling of the dielectric properties of tissue-mimicking phantom materials for ultra-wideband microwave breast cancer detection. *Optik*, *127*(4), 2217–2225. https://doi.org/https://doi.org/10.1016/j.ijleo.2015.10.215

Surowiec, A., Shrivastava, P. N., Astrahan, M., & Petrovich, Z. (1992). Utilization of a multilayer polyacrylamide phantom for evaluation of hyperthermia applicators. *International Journal of Hyperthermia*, *8*(6), 795–807.

Trefná, H. D., & Ström, A. (2019). Hydrogels as a water bolus during hyperthermia treatment. *Physics in Medicine & Biology*, *64*(11), 115025. https://doi.org/10.1088/1361-6560/ab0c29

Van Vliet, T. (1988). Rheological properties of filled gels. Influence of filler matrix interaction. *Colloid and Polymer Science*, *266*(6), 518–524.

Wust, P., Fähling, H., Berger, J., Jordan, A., Mönich, G., & Felix, R. (1998). Solid materials with high dielectric constants for hyperthermia applications. *International Journal of Hyperthermia*, *14*(2), 183–193.

Yeh, F., Sokolov, E. L., Walter, T., & Chu, B. (1998). Structure studies of poly (diallyldimethylammonium chloride-co-acrylamide) gels/sodium dodecyl sulfate complex. *Langmuir*, *14*(16), 4350–4358.

8 Supplementary Material

Table S1. Composition of the rapeseed oil (values are expressed per 100g oil).

Total Fat (g)	92
Saturated Fat (g)	7
Monounsaturated Fat (g)	57
Polyunsaturated Fat (g)	28
Carbohydrates (g)	0
Sugars (g)	0
Protein (g)	0
Sodium (g)	0
Vitamin E (mg)	17.5
Vitamin K (mg)	71.3

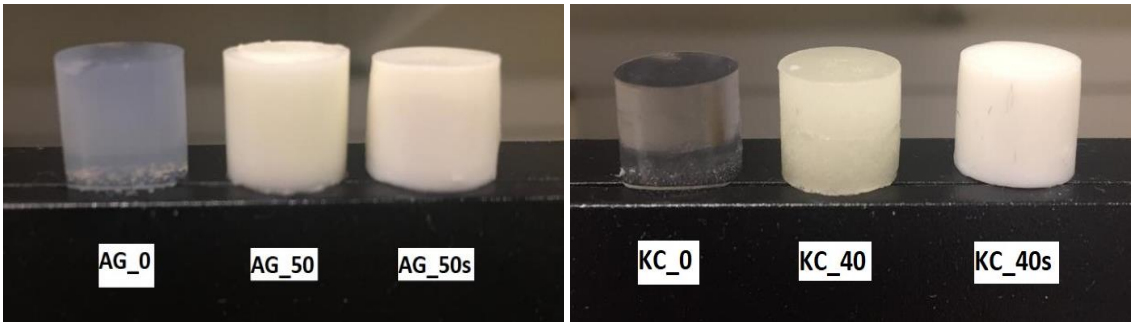

Figure S1. Visual appearance of agar and κ-carrageenan emulsion-filled gels.

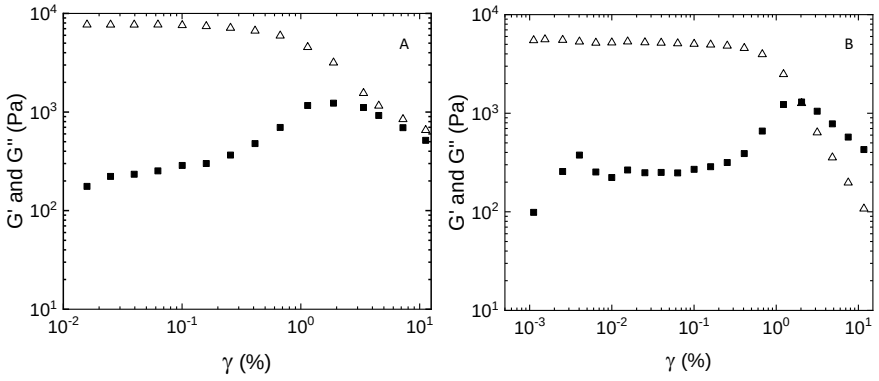

Figure S2. G' (open markers) and G'' (filled markers) as a function of strain amplitude for the (A) agar and (B) κ-carrageenan gel formulations at 20 ºC.

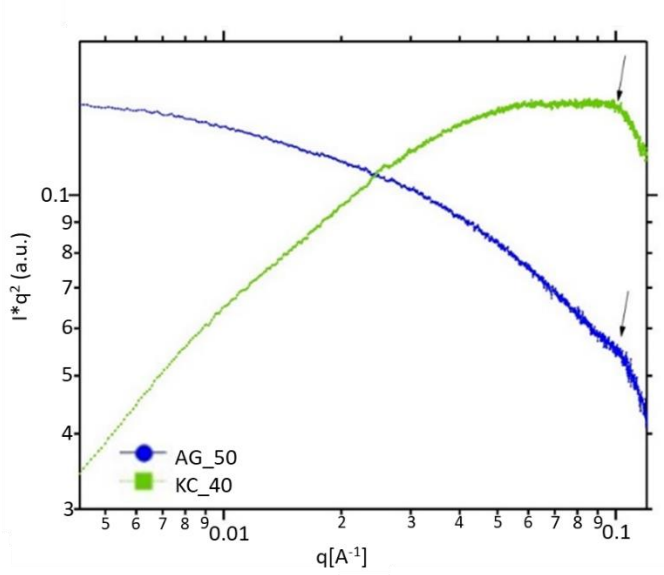

Figure S3. Kratky plots from the SAXS data corresponding to the AG_50 and KC_40 emulsion-gels.

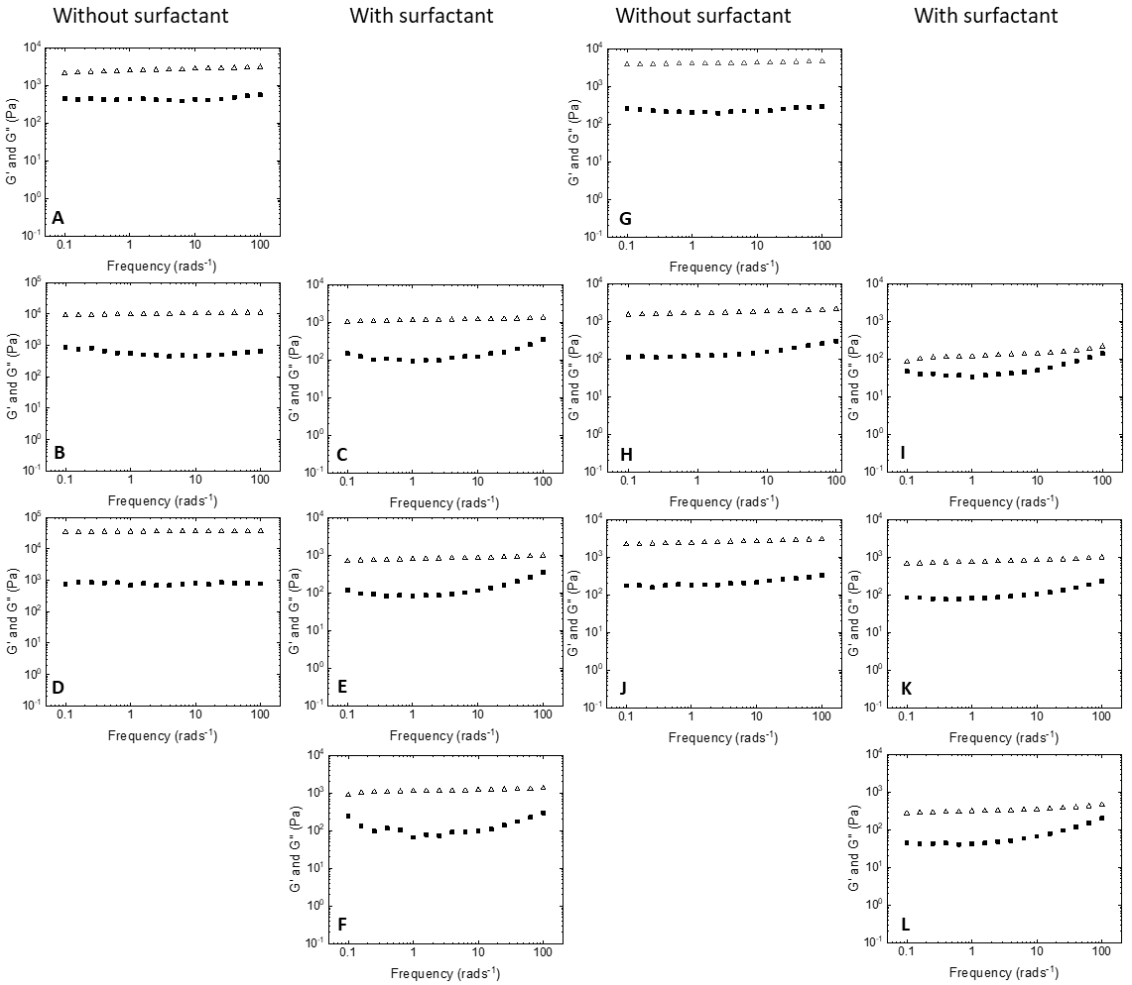

Figure S4. G' (open markers) and G'' (filled markers) as a function of frequency for the agar and κ-carrageenan gel formulations at 20 ºC. (A) AG_0; (B) AG_40; (C) AG_40s; (D) AG_50 (E) AG_50s; (F) AG_55; (G) KC_0; (H) KC_30 (I) KC_30s; (J) KC_40 (K) KC_40s and (L) KC_50s.

IV. GENERAL DISCUSSION

General discussion of the results

4.1 Structure and functional properties of sulphated polysaccharide hydrogels.

In this chapter, the different gelation mechanisms of sulphated polysaccharides and the parameters affecting the structure and functional properties of the obtained hydrogels were investigated and the application of this type of materials as encapsulation and controlled delivery systems was evaluated.

In the first work of this chapter, four different commercial carrageenan grades (κ-C, ι-C, λ↓-C and λ↑-C) were used to produce hydrogels, with and without the addition of two different types of salts (a monovalent salt such as KCl and a divalent salt such as $CaCl_2$). The results evidenced that the amount of sulphate groups in the different carrageenan grades had a strong effect in the gelation mechanism and the mechanical properties of the formed hydrogels. The lower amount of sulphate substitution in κ-C resulted in a strong association of double helices, thus leading to the formation of hydrogels with higher strength than the other carrageenan grades. In that case, stronger hydrogels were obtained when increasing the κ-C and salt concentration, with K^+ having a greater effect than Ca^{2+} on the hydrogel strength due to the formation of more ordered and densely packed networks, as evidenced by SAXS. On the other hand, the greater amount of sulphate groups in ι-C, λ↑-C and λ↓-C hindered the proper association of carrageenan double helices due to repulsive forces, hence making necessary the addition of salts to form hydrogels with good mechanical integrity. In the case of ι-C, all the considered factors had a significant effect on the hydrogel strength. Notably, these systems were seen to behave differently depending on the added salt. While the presence of K^+ ions led to stronger hydrogels when increasing the carrageenan and salt concentrations, the formulations with added Ca^{2+}, showed a maximum strength at intermediate salt concentrations. This was ascribed to the fact that Ca^{2+} ions are more efficient in promoting ι-C gelation, as lower concentrations are required to neutralize the same amount of sulphate groups; however, a very similar network of ionic-bonded carrageenan double helices is formed with both salts, producing soft hydrogels with similar strength values. The complex composition of the λ-C grades, which were a blend of the λ-, κ-, θ- and μ-C forms, yielded more heterogeneous

branched network structures. Interestingly, K^+ yielded stronger hydrogels than Ca^{2+} for both λ-C grades, suggesting that the gelation mechanism was mostly governed by the κ-carrageenan component. All these results point out towards the fact that λ-C gelation took place by means of a very distinct mechanism to that of κ-C and ι-C, forming less ordered structures. The results also showed that the presence of cations and their valency had a strong impact on the rheological behaviour of the hydrogels from the different carrageenan grades studied. In all the grades, the addition of salts increased the gelation temperature and produced hydrogels with higher strength (as suggested by the higher G' values) and increased their elastic character (as indicated by the lower tan δ values). This suggests that the presence of cations facilitated the association of carrageenan molecular chains to originate the network structures responsible for hydrogel formation.

Based on the acquired knowledge on the gelation mechanism of sulphated polysaccharides, the second work of this chapter explored the potential application of agar and κ-carrageenan hydrogels and aerogels to encapsulate a food protein such as casein and evaluated their protective effect against the enzymatic hydrolysis upon simulated gastrointestinal digestions. The polysaccharide type (agar vs. κ-carrageenan), the polysaccharide:casein ratio (25:75 vs. 75:25) and the physical state of the structures (hydrogel vs. aerogels) were all essential factors with an impact on the degree of hydrolysis undergone by casein upon *in vitro* gastrointestinal digestions. In general, the hydrogels from both polysaccharides showed a greater protective effect than the aerogels, with most of the protein remaining in the solid non-digested fraction after the gastric digestion. The polysaccharide:protein ratio of 25:75 resulted in softer gels with less physical integrity and more susceptible to release the protein towards the liquid medium, while the 75:25 showed a great protective effect, with some intact casein being detected even after the intestinal phase. The molecular weight (MW) distribution of the peptides detected in the gastrointestinal digests from the gel-like structures varied depending on the type of polysaccharide, with the agar-based structures providing a greater release of peptides within the range of MW>2 kDa, while a greater percentage of peptides within the range of 0.5-1 kDa were observed in the κ-carrageenan digests. All these results pointed towards HG-A25 (agar

hydrogel with 25% of protein), AG-A75 (agar aerogel with 75% of protein) and HG-KC25 (κ-carrageenan hydrogel with 25% of protein) being the most optimal structures, since they were able to preserve intact casein after the gastric phase while promoting the release of peptides with greater molecular weights during the intestinal phase. These results evidence the potential of polysaccharide-protein gel-like structures to produce satiating dietary products and demonstrate the relevance of their structural properties on their behavior upon digestion.

4.2 Cellulosic aerogels as adsorbent packaging structures.

A different type of structures which can be obtained by subjecting hydrogels to drying processes are the aerogels. As already mentioned in this thesis, the highly porous structure and high sorption capacity of aerogels make them excellent candidates for the replacement of absorbent pads typically used to maintain the quality of packaged fresh food products such as meat and fish. In this chapter, the possibility of developing this type of structures by valorising an underutilized waste biomass source such as *Arundo donax* was evaluated. This biomass was used to generate cellulosic fractions with different purification degrees and water-soluble bioactive extracts, which were subsequently used to produce hybrid bioactive aerogels. Morphological characterization of the aerogels showed that the presence of hemicelluloses in the less purified cellulosic fractions led to less dense and more porous structures, resulting in greater water sorption capacities than the pure cellulose aerogels. In contrast, the pure cellulose fractions yielded aerogels with greater oil sorption capacities. Apart from the cellulosic fractions, water soluble extracts were obtained from *A. donax* leaves and stems, using hot water and ultrasound-assisted extractions. The material extracted from the stems using the hot water treatment showed the highest antioxidant capacity, which could be ascribed to its highest polysaccharide and polyphenol content. This extract was, thus, selected to be combined with selected cellulosic fractions to produce hybrid bioactive aerogels and films. *In vitro* release studies indicated that greater release of the extract took place in the samples containing hemicelluloses and, in particular, in the aerogels, due to their more hydrophilic character and their more porous structure. Finally, the hybrid aerogels were evaluated as absorbent pads for the preservation of red meat and compared with commercial pads. The capacity of these

materials to prevent colour loss and lipid oxidation upon storage was evaluated and the results showed that the less purified cellulosic aerogels incorporating the antioxidant extract had the greatest potential to be used as bioactive absorbent pads to improve the quality of red meat upon storage.

4.3 Structure, properties and applications of emulsion-gels based on sulphated polysaccharides

Emulsion-gels are recognized for their great potential as functional ingredients in the food industry to modify texture and for solid fat replacement. Moreover, they can be used as a delivery vehicle for the controlled release of fat-soluble bioactive compounds. They can also be valuable in biomedical applications for the development of tissue mimicking phantoms. Thus, in this chapter, the nature of interactions between the components in polysaccharide-based emulsion-gel formulations was investigated and related to their structure and mechanical and rheological behavior, with the aim of understanding how the properties of these materials can be modified for specific applications.

In the first work of this chapter, three types of commercial carrageenans (κ-C, ι-C, λ-C) were used to produce emulsion-gels in the presence of an added salt (KCl) and the effect of the carrageenan type and concentration, the salt concentration and the oil:water volume ratio (OWR) on the emulsion-gels strength were evaluated. The strength of the emulsion-gels was determined by the type of network formed by the different carrageenan grades, being the κ-C emulsion-gels the strongest ones. While the carrageenan concentration needed to obtain the maximum strength was higher in the case of ι-C, the salt concentration and OWR needed to form stronger emulsion-gels were very similar for the three carrageenan grades. With regards to the OWR, an increase up to intermediate oil contents enhanced the emulsion-gel strength values; however, further increasing the amount of oil reduced the integrity of the materials leading to softer gels, suggesting that an excessive amount of oil limits the cross-linking between the carrageenan chains. According to the rheological characterization, the emulsion-gel samples presented the same (κ-C) or even higher (ι-C and λ-C) gelation temperature than

the corresponding hydrogels, indicating that the carrageenan coil-helix transition, responsible for the gelation, was somehow facilitated in the case of the emulsions. Moreover, the G' values at 20 °C were higher for the emulsion-gels than for the control hydrogels, suggesting the formation of stronger gel networks in the former ones. Since no evidence of interactions between the carrageenans and the oil phase was found, this was ascribed to a concentration effect of the carrageenans in the aqueous phase from the emulsion-gels. These results provide the basis for a rational design of carrageenan emulsion-gels and demonstrate that the rheological and mechanical behaviour of these materials is governed by the nanostructure and intermolecular associations.

After studying the gelation mechanism of carrageenan emulsion-gels and the implications on their structural and functional properties, these systems were adapted and used for two different applications relevant to the food and biomedicine sectors.

In the second work, oil-filled gel-like structures from agar and κ-carrageenan emulsion-gels and oil-filled aerogels were produced and evaluated as carriers of a lipophilic bioactive such as curcumin, which was incorporated into the oil phase. The structure and mechanical properties of the gel-like structures were characterized, showing that the κ-carrageenan samples presented a much more heterogeneous distribution of oil droplets with larger diameters while in the agar emulsion-gels the oil was more homogeneously dispersed forming smaller droplets. For the oil-filled gels, the κ-carrageenan formulations were able to preserve their physical integrity after the freeze-drying process, whereas that was not the case for the agar formulations, which were not able to form oil-filled aerogels. Due to the distinct nature of the interactions holding together the gelling networks, κ-carrageenan and agar emulsion-gels presented a significantly different mechanical behaviour, with the κ-carrageenan emulsion-gels showing lower rigidity but greater hardness and resistance to breakage. For the κ-carrageenan oil-filled aerogels, the modulus increased seven-fold as compared to the corresponding emulsion-gels, which is due to the formation of more compacted structures upon removal of water by freeze-drying. The incorporation of curcumin into the oil phase did not have a significant effect on the mechanical behaviour of any of the samples. The oil droplets were seen

to be only physically entrapped within the aerogel structure, as evidenced by the low oil binding capacity, in contrast with the emulsion-gels, which showed very high oil binding capacity values.

The different oil-filled gel-like structures were subjected to *in vitro* gastrointestinal digestions and the type of nanostructures generated as a result of the oil lipolysis was investigated by SAXS. The results showed that the polysaccharide type and the physical state of the gel network had an impact on the structure of the digestion products. For all the emulsion-gels a solid fraction (mainly non-digested material) remained even after the intestinal digestion phase, whereas in the case of the oil-filled aerogels the structure was disrupted during the digestion process and one liquid phase with particles in suspension was obtained. The solid and liquid fractions were separately analysed by SAXS and compared to the liquid digesta from control nanoemulsions. The results showed the existence of two different types of structures in most of the samples, bile salt lamellae/micelles of ca. 5 nm and larger vesicles of partially digested oil with ca. 20-50 nm. For the κ-carrageenan emulsion-gels, partially digested emulsified oil was seen to remain trapped in the solid fraction suggesting that the strong gelling networks and the larger size of oil droplets resulted in a lower extent of lipolysis. In the case of the κ-carrageenan oil-filled aerogels, the polysaccharide particles released towards the liquid medium seemed to de-stabilize the bile salt small lamellae/micelles and promoted the formation of larger vesicles. The presence of curcumin seems to limit the formation of mixed bile salt-digestion products lamellae/micelles, inducing the formation of a greater amount of larger vesicles, with curcumin being most likely located within the interior of these structures.
These results evidence the high relevance of the microstructure and mechanical behavior of oil-filled gel-like structures upon gastrointestinal digestion since the formation of different structures in the digestion products is expected to affect the intestinal transport and absorption of the generated compounds.

In the third work from this chapter, the potential of emulsion-gels based on sulphated polysaccharides (κ-carrageenan and agar) for the production of tissue mimicking phantoms was evaluated. In particular, the oil content was increased to the maximum possible with the aim of

obtaining materials suitable as fat phantoms systems. The agar formulations were able to incorporate a greater amount of oil phase (50% w/w) than the κ-carrageenan ones (40% w/w). Furthermore, the addition of a blend of surfactants allowed to further increase the amount of oil in both polysaccharides (up to 55% w/w for agar and up to 50% w/w for κ-carrageenan). The greater emulsifying capacity of agar, together with its rheological behaviour (presenting a lower gelling temperature, which allowed a better dispersion of the oil prior to the gelation step) resulted in smaller and more homogeneously distributed oil droplets within the structure of the emulsion-gels. On the other hand, while the addition of the surfactants permitted a better dispersion of the oil within the κ-carrageenan formulations, yielding smaller and more homogeneous droplets, in the case of the agar it induced the formation of more heterogeneous and larger oil structures. The rheological characterization showed that the incorporation of oil had a marked effect on the behaviour of the agar samples, producing higher G' values. In contrast, the presence of surfactants resulted in a decrease in the G', impeding the reinforcing effect. These results were explained by the formation of agar gelling domains at the surface of the oil droplets, while these domains could not be formed in the presence of surfactants. Contrarily to the agar, the incorporation of oil into the κ-carrageenan gels produced a decrease in G', being this effect more pronounced with the addition of surfactants. This behaviour suggests the presence of a lower number of effective elastic junctions in the κ-carrageenan. The large deformation behaviour of the emulsion-gels under compression was seen to be mostly governed by the properties of the continuous gelling network. Thus, the emulsion-gels were stiffer but weaker than the corresponding hydrogels and the addition of surfactants led to a significant reduction in the strength and stiffness. As already anticipated, increasing the oil content in the emulsion-gels resulted in a decrease in the permittivity and conductivity values, being this effect more remarkable in the agar samples due to the greater homogeneity and smaller oil droplet sizes attained. Regarding the conductivity, the presence of KCl in the κ-carrageenan emulsion-gels increased this parameter. The results showed that the agar emulsion-gels with the highest oil content (55% oil) are suitable to produce materials mimicking the dielectric properties of low-water content tissues, whereas the remaining formulations could be used to mimic high-water content tissues.

V. CONCLUSIONS

Conclusions

- The molecular structure of sulphated polysaccharides such as carrageenans is crucial to determine their gelation mechanism and the properties of the obtained hydrogels. In particular, the amount of sulphate groups seems to be one of the factors with outmost importance. Moreover, it is possible to produce stronger hydrogels with the addition of cationic salts; however, the mechanism through which different salts interact with the carrageenan chains is also determined by the amount and location of sulphate groups.

- Understanding the distinct gelation mechanism of polysaccharide-based hydrogels and their implications in the nanostructure and functional properties of the formed hydrogels opens up the possibility of designing gel-like structures with specific properties for targeted applications within the food industry and any other relevant fields.

- Hydrogels and aerogels from sulphated polysaccharides were able to affect the hydrolysis of casein upon *in vitro* gastrointestinal digestions, being this effect dependent on the polysaccharide type (agar or κ-carrageenan), the polysaccharide:casein ratio and the physical state of the structures. Considering these factors, it was possible to design materials with the capacity of protecting casein during the gastric phase, but allowing the release and hydrolysis during the intestinal phase, hence yielding larger peptide fragments. These materials have a great potential within different food and pharma applications; for instance, they are good candidates for the development of satiating food products.

- Fully bio-based aerogels with great adsorption capacity can be produced by valorising *Arundo donax* waste biomass through the application of simplified extraction protocols for the production of less purified cellulosic fractions and aqueous bioactive extracts. The cellulosic fractions serve as templates for the development of porous structures, while the bioactive extracts are incorporated as additives. These systems have shown

a great potential to be used as alternative absorption pads in fresh meat packages, being able to retard the colour loss and limit lipid oxidation, thus improving the shelf life of red meat products.

- The gelation capacity of sulphated polysaccharides such as agar and κ-carrageenan can be exploited for the development of novel structures known as emulsion-gels, in which an oil phase is dispersed within the gelling polysaccharide network. The results from this thesis evidenced that the polysaccharide concentration, the presence of salt and the oil volume fraction all have a strong impact on the mechanical and rheological behaviour of the obtained emulsion-gels. Accordingly, these factors can be adjusted to produce emulsion-gels with tuned properties. This opens up the possibility of using these emulsion-gel systems in diverse applications within the food industry, such as fat replacement ingredients or encapsulation systems for the controlled release of bioactive compounds.

- Agar and κ-carrageenan emulsion-gels and oil-filled aerogels can be used as carrier systems for the incorporation of lipophilic bioactive compounds, such as curcumin. The results from this thesis indicate that the gelling network structure and the distribution of oil within this structure are crucial to determine the behaviour of these materials upon simulated gastrointestinal digestion. Furthermore, they will determine the type of nanostructures obtained as digestion products. Interestingly, the presence of curcumin was seen to have a marked influence on the type of structures forming the digestion products. This is of high relevance, since different structures are expected to be distinctly transported and absorbed in the intestinal tract.

- The good mechanical properties and the relatively high oil contents which can be incorporated into agar and κ-carrageenan emulsion-gels make them suitable to produce tissue mimicking materials. The addition of surfactants can further increase the maximum amount of oil incorporated, but it also has a strong impact on the

mechanical behaviour of the materials. The dielectric properties of the emulsion-gels can be tuned depending on the oil content and distribution, being the agar-based emulsion-gels more suitable as fat mimicking phantoms.

VI. Annexes

Annex A: List of publications included in this thesis

Algal Research 47 (2020) 101882

Contents lists available at ScienceDirect

Algal Research

journal homepage: www.elsevier.com/locate/algal

Understanding nanostructural differences in hydrogels from commercial carrageenans: Combined small angle X-ray scattering and rheological studies

Cynthia Fontes-Candia[a], Anna Ström[b], Laura G. Gómez-Mascaraque[c], Amparo López-Rubio[a], Marta Martínez-Sanz[a,*]

[a] Food Safety and Preservation Department, IATA-CSIC, Avda Agustín Escardino 7, 46980 Paterna, Valencia, Spain
[b] Applied Chemistry, Chemistry and Chemical Engineering, Chalmers University of Technology, Gothenburg, Sweden
[c] Department of Food Chemistry & Technology, Teagasc Food Research Centre, Moorepark, Fermoy, Co. Cork, Ireland

ARTICLE INFO

Keywords:
Polysaccharide
Seaweed
Gelation
Scattering
Food texture

ABSTRACT

Hydrogels from commercial carrageenans (κ-C, ι-C, λ↑-C (high viscosity) and λ↓-C (low viscosity)) were prepared with and without the addition of salts (KCl and $CaCl_2$). FT-IR and ^{1}H NMR characterization evidenced that while the κ-C and ι-C grades were relatively pure carrageenans, the two λ-C grades were λ-, κ-, θ- and μ-carrageenan hybrids. The effect of carrageenan and salt concentration on the hydrogel strength were evaluated through a response surface design and a detailed structural characterization was carried out by small angle X-ray scattering (SAXS) and rheology. The low amount of sulphate substitution in κ-C enabled intramolecular association, giving rise to strong hydrogels, even in the absence of salts. On the other hand, ι-C, λ↑-C and λ↓-C produced much weaker hydrogels and required the addition of salts to induce intramolecular association by ionic cross-linking. SAXS results suggested the formation of similar structures of double helices in κ-C and ι-C with the addition of salts; however, distinct network structures were attained. In the case of κ-C, a Gauss-Lorentz gel model was suitable to describe the hydrogel structure and the addition of K^+ promoted the formation of more ordered and densely packed structures. On the other hand, larger but weaker aggregates, with marked periodicity, were observed in ι-C, with Ca^{2+} inducing the formation of more densely packed networks. The complex composition of the λ-C grades gave rise to more heterogeneous branched network structures, properly described by a correlation length model, where the gelation mechanism was mostly governed by the κ-carrageenan component.

1. Introduction

Carrageenans are sulphated polysaccharides present in the cell walls and in the intercellular matrix of red seaweeds (*Rhodophyta*). These polysaccharides contain a backbone of alternating disaccharide repeating units of β-D-galactose (G-units) linked at position 3 and α-D-galactose (D-units) or 3,6-anhydro-α-D-galactose (DA-units) linked at position 4. Depending on the content and position of sulphate groups (SO_3^-), they can be classified into different forms, being the kappa (κ)-, iota (ι)- and lambda (λ)-carrageenans, which contain one, two and three sulphate groups per disaccharide unit, respectively, the three main types commercially available. These carrageenans are obtained from different seaweed species and using different extraction procedures. κ-Carrageenan is typically extracted from the *Eucheuma cottonii* seaweed species, while ι-carrageenan is mainly obtained from *Eucheuma spinosum* [1]. Their extraction process involves the application of physical separation methods, followed by alkali treatments at high temperatures to transform the naturally occurring μ- and ν-carrageenans (whose backbones are composed of G- and D-units) into κ- and ι-carrageenans. The alkali treatments produce the removal of one sulphate group from the D-units, originating an anhydride bridge and giving rise to the formation of DA-units. It should be noted that most of the extraction protocols described in the literature typically yield κ-/ι-hybrids rather than pure carrageenans [2–4]. On the other hand, λ-carrageenan is obtained from different species of the *Gigartina* and *Chondrus* genera, although the materials obtained from these seaweeds are typically hybrids of several types of carrageenan [1,5–7].

Carrageenans are widely used in the food industry due to their texturizing properties, highlighting their thickening and gelling capacity and their ability to stabilize proteins [8,9]; additionally, they also find applications in the pharmaceutical [10], cosmetic [11], printing and textile industries [12]. Of special interest is their use for the

* Corresponding author.
E-mail address: mmartinez@iata.csic.es (M. Martínez-Sanz).

https://doi.org/10.1016/j.algal.2020.101882
Received 16 October 2019; Received in revised form 20 February 2020; Accepted 15 March 2020
Available online 21 March 2020

Food Hydrocolloids 96 (2019) 151–160

Contents lists available at ScienceDirect

Food Hydrocolloids

journal homepage: www.elsevier.com/locate/foodhyd

Superabsorbent food packaging bioactive cellulose-based aerogels from *Arundo donax* waste biomass

Cynthia Fontes-Candia[a], Evrim Erboz[a], Antonio Martínez-Abad[b], Amparo López-Rubio[a], Marta Martínez-Sanz[a,*]

[a] Food Safety and Preservation Department, IATA-CSIC, Avda. Agustín Escardino 7, 46980, Paterna, Valencia, Spain
[b] Dept. Analytical Chemistry, Nutrition and Food Sciences, University of Alicante, 03690, San Vicente del Raspeig, Alicante, Spain

ARTICLE INFO

Keywords:
Aquatic biomass
Porous materials
Valorization
Release
Food preservation
Active packaging

ABSTRACT

A. donax waste biomass has been valorized for the extraction of cellulosic fractions with different purification degrees, as well as aqueous bioactive extracts, which were then combined to develop superabsorbent bioactive aerogels. All the developed aerogels presented excellent water and oil sorption capacities; however, the presence of hemicelluloses yielded more porous and hydrophilic aerogels, capable of absorbing more water. With regards to the aqueous extracts, the hot water treatment (HW) of *A. donax* stems promoted the extraction of polysaccharides and polyphenols, producing the extract (S-HW) with the highest antioxidant capacity. This extract was then incorporated into the aerogels produced from the less purified stem fractions (F2A and F3A), which were chosen due to their good water sorption capacity, higher antioxidant potential and lower production costs and environmental impact. The hybrid aerogels showed a great potential to be used as bioactive pads for food packaging. In particular, the F2A + S-HW aerogel would be the most optimum choice since it provides a complete release of the extract in hydrophilic media, as demonstrated by *in-vitro* release and β-carotene bleaching inhibition studies, and it is able to reduce the colour loss and lipid oxidation in red meat upon refrigerated storage to a greater extent.

1. Introduction

In the context of the extremely demanding market within the food industry, packaging plays a crucial role, not only protecting the product from the external environment and maintaining food quality to extend products' shelf life, but also being able to provide added functionalities, such as the incorporation of health-beneficial compounds (e.g. antioxidants) which can improve the nutritional value of the packaged product. Accordingly, strategies based on the controlled release of bioactive compounds from the package towards the food product, are being extensively investigated. For instance, some studies have reported on the incorporation of bioactive extracts into packaging films to preserve meat quality and organoleptic properties (Barbosa-Pereira, Aurrekoetxea, Angulo, Paseiro-Losada, & Cruz, 2014; Bolumar, Andersen, & Orlien, 2011; Camo, Lorés, Djenane, Beltrán, & Roncalés, 2011; Jofré, Aymerich, & Garriga, 2008; Lorenzo, Batlle, & Gómez, 2014), demonstrating that the processes of lipid oxidation and colour loss upon storage could be reduced through the antioxidant activity of the incorporated extracts.

In the particular case of meat packaging, absorption pads are commonly used as moisture control elements, which absorb the excess liquids released by meat upon storage. These pads are typically made of a non-permeable/non-stick synthetic polymer, such as polyethylene and a hydrophilic non-woven bottom layer filled with active substances which prevent bacterial growth, such as citric acid and sodium bicarbonate (McMillin, 2017). Given the severe environmental issues associated to the production and use of synthetic plastics, current trends in the food packaging sector are clearly moving towards the utilization of more sustainable bio-based and renewable materials, i.e. biopolymers. Polysaccharides and, in particular, lignocellulosic materials, have already demonstrated their great potential to develop high performance bio-based packaging structures (Benito-González, López-Rubio, & Martínez-Sanz, 2018; Martínez-Sanz, Erboz, Fontes, & López-Rubio, 2018; Rampazzo et al., 2017; Satyanarayana, Arizaga, & Wypych, 2009). Lignocellulosic materials can be extracted from multiple sources such as terrestrial and aquatic plants, algae and agriculture and forestry-derived waste by-products (Trache, Hussin, Haafiz, & Thakur, 2017). However, the extraction from waste or underutilized resources that do not compete with the food chain is particularly interesting and in line with the principles of circular economy. For instance,

* Corresponding author.
E-mail address: mmartinez@iata.csic.es (M. Martínez-Sanz).

https://doi.org/10.1016/j.foodhyd.2019.05.011
Received 15 January 2019; Received in revised form 3 May 2019; Accepted 6 May 2019
Available online 09 May 2019
0268-005X/

Algal Research 47 (2020) 101873

Contents lists available at ScienceDirect

Algal Research

journal homepage: www.elsevier.com/locate/algal

Rheological and structural characterization of carrageenan emulsion gels

Cynthia Fontes-Candia[a], Anna Ström[b], Patricia Lopez-Sanchez[c], Amparo López-Rubio[a], Marta Martínez-Sanz[a,*]

[a] Food Safety and Preservation Department, IATA-CSIC, Avda Agustín Escardino 7, 46980 Paterna, Valencia, Spain
[b] Applied Chemistry, Chemistry and Chemical Engineering, Chalmers University of Technology, Gothenburg, Sweden
[c] Agrifood and Bioscience, RISE Research Institutes of Sweden, Frans Perssons väg 6, SE-412 76 Gothenburg, Sweden

ARTICLE INFO

Keywords:
Polysaccharide
Seaweed
Gelation
Scattering
Fat replacement

ABSTRACT

Carrageenan emulsion gels containing sunflower oil were prepared using three different commercial carrageenan grades (κ-C, ι-C and λ-C). The effect of the carrageenan and salt content, as well as the oil:water ratio, on the emulsion gel strength was evaluated through a response surface methodology. Moreover, the rheological properties and the micro- and nanostructure from the stronger emulsion gel formulations were investigated and compared to their analogous hydrogel formulations. Interestingly, emulsion gels formed stronger and more thermally stable networks than the hydrogels, being this effect more evident in ι-C and λ-C. The results indicate that this was mainly due to a polysaccharide concentration effect, as no evidence of interactions between the carrageenan and the oil phase was found. Consequently, the rheological behaviour of the emulsion gels was mostly determined by the type of carrageenan. The association of carrageenan molecular chains was favoured in κ-C and λ-C (due to the presence of κ-carrageenan in the latter) and promoted by the addition of KCl. In contrast, a lower degree of chain association, mostly driven by ionic cross-linking, took place in ι-C. These results evidence the relevance of the gelation mechanism on the properties of emulsion gels and provide the basis for the design of these systems for targeted applications within the food industry.

1. Introduction

Emulsion gels are soft-solid materials composed of a three-dimensional network structure formed by a continuous phase consisting of a gel matrix and a dispersed phase consisting of an emulsion [1]. These materials present a great potential within the food industry as functional ingredients to modify food texture [2,3], for solid fat replacement [4,5] or even as templates for the controlled release of bioactive compounds [6]. Fats play a very important role in food processing; however, solid fats contain high amounts of saturated fatty acids which have been associated with several health conditions such as obesity, cancer and cardiovascular diseases [7]. Consequently, the food industry is actively looking for alternative ingredients to replace, at least partially, saturated and trans fats in products such as dairy and processed meats, while preserving their original organoleptic attributes as much as possible to ensure consumers' acceptance. A plausible approach consists in the replacement of solid fats with emulsion gels where an oil is incorporated into the dispersed phase. However, mimicking the rheological and textural properties of solid fats using emulsion gels is not trivial and many factors such as the physicochemical properties of the gelling matrix, the interactions between matrix and oil phase, oil droplet size, volume fraction and distribution, etc., have an impact on the textural and rheological properties of the product [8–10]. Depending on the interactions between the gel and the emulsified phase, the oil droplets can be classified as active (bound to the gel matrix) or inactive (unbound) fillers [11]. Active fillers can increase or decrease the stiffness of the gel depending on the ratio between the modulus of the oil droplets and that of the gel matrix, whereas inactive fillers are thought to cause a reduction on the gel stiffness [12]. Therefore, the properties of emulsion gels can be optimized by means of an adequate selection of the gelling matrices and fillers and a rational structural design of the produced materials.

Ethyl cellulose has been widely used as solid fat replacement in meat and bakery products [13,14], since it can be directly dispersed in edible oils. However, the high temperatures required for its processing promote the oxidation of the oil phase. The use of synthetic polymers such a polyvinylalcohol and polysiloxanes as oil structuring agents has also been reported, but due to their synthetic nature, these compounds are not accepted as edible matrices [15]. As an alternative, natural compounds such as proteins [7,16–18] and polysaccharides [19–23] are

* Corresponding author.
E-mail address: mmartinez@iata.csic.es (M. Martínez-Sanz).

https://doi.org/10.1016/j.algal.2020.101873
Received 20 December 2019; Received in revised form 17 February 2020; Accepted 9 March 2020
Available online 21 March 2020

Carbohydrate Polymers 256 (2021) 117496

Contents lists available at ScienceDirect

Carbohydrate Polymers

journal homepage: www.elsevier.com/locate/carbpol

Maximizing the oil content in polysaccharide-based emulsion gels for the development of tissue mimicking phantoms

Cynthia Fontes-Candia [a], Patricia Lopez-Sanchez [b], Anna Ström [c], Juan Carlos Martínez [d], Ana Salvador [a], Teresa Sanz [a], Hana Dobsicek Trefna [e], Amparo López-Rubio [a], Marta Martínez-Sanz [a,*]

[a] Food Safety and Preservation Department, IATA-CSIC, Avda. Agustín Escardino 7, 46980 Paterna, Valencia, Spain
[b] Agrifood and Bioscience, RISE Research Institutes of Sweden. Frans Perssons väg 6, SE-412 76, Gothenburg, Sweden
[c] Applied Chemistry, Chemistry and Chemical Engineering, Chalmers University of Technology, Gothenburg, Sweden
[d] ALBA Synchrotron Light Facility, Carrer de la Llum 2-26, 08290, Cerdanyola del Vallès, Barcelona, Spain
[e] Signal Processing and Biomedical Engineering, Department of Electrical Engineering, Chalmers University of Technology, Sweden

ARTICLE INFO

Keywords:
Surfactant
Tissue mimicking
Gelation
Seaweed polysaccharides
X-ray scattering

ABSTRACT

Formulations based on agar and κ-carrageenan were investigated for the production of emulsion gels applicable as tissue mimicking phantoms. The effects of the polysaccharide matrix, the oil content and the presence of surfactants on the micro-/nanostructure, rheology, and mechanical and dielectric properties were investigated. Results showed a high capacity of the agar to stabilize oil droplets, producing gels with smaller (10–21 μm) and more uniform oil droplets. The addition of surfactants allowed increasing the oil content and reduced the gel strength and stiffness down to 57 % and 34 %, respectively. The permittivity and conductivity of the gels were reduced by increasing the oil content, especially in the agar gels (18.8 and 0.05 S/m, respectively), producing materials with dielectric properties similar to those of low-water content tissues. These results evidence the suitability of these polysaccharides to design a variety of tissue mimicking phantoms with a broad range of mechanical and dielectric properties.

1. Introduction

Emulsion gels are composite soft materials with solid-like behaviour where an oil-phase is dispersed within a continuous hydrogel network. These systems can be classified as emulsion-filled gels, which contain dispersed oil droplets, or as emulsion particulate gels, which contain a network of aggregated oil droplets (Farjami & Madadlou, 2019). Emulsion gels provide characteristics typical of hydrophobic materials while maintaining structural characteristics similar to hydrogels. Therefore, they are suitable materials for the incorporation and controlled delivery of bioactive compounds with hydrophilic and hydrophobic character. Another advantage of emulsion gels is that they provide stability to the emulsion phase (Geremias-Andrade, Souki, Moraes, & Pinho, 2016; Li et al., 2020). The entrapment of the oil droplets within a continuous hydrogel network limits their aggregation through coalescence and flocculation. Such promising properties make emulsion gels excellent candidates for the development of materials with applications in the medical, pharmaceutical and food industry fields.

Emulsion gels can be produced with a wide range of rheological properties, depending on several intrinsic factors such as the nature of the interactions between the components, droplet volume fraction and matrix stiffness (Dickinson, 2012). Furthermore, depending on their structural behaviour, the rheological properties of emulsion gels can be determined by the continuous hydrogel network or by the network of aggregated emulsion droplets. Surfactants can also be added to this type of materials to improve the emulsion stability, since interactions between surfactants and polymers may influence the affinity of the oil phase to the hydrogel matrix (Farjami & Madadlou, 2019). All these factors are of considerable practical importance when utilising an emulsion gel system for pharmaceutical, cosmetic, food and biomedical applications (Farjami & Madadlou, 2019). By varying the ratios of different components of a synergistic mixture, numerous systems can be developed, thus being able to tune the gel characteristics by changing

* Corresponding author.
E-mail address: mmartinez@iata.csic.es (M. Martínez-Sanz).

https://doi.org/10.1016/j.carbpol.2020.117496
Received 22 September 2020; Received in revised form 23 November 2020; Accepted 7 December 2020
Available online 14 December 2020
0144-8617/

Annex B: List of patents

MINISTERIO
DE INDUSTRIA, ENERGIA
Y TURISMO

Oficina Española
de Patentes y Marcas

TRATADO DE COOPERACIÓN EN MATERIA DE PATENTES
NOTIFICACIÓN DE LA RECEPCIÓN DE LOS DOCUMENTOS QUE CONSTITUYEN SUPUESTAMENTE UNA SOLICITUD INTERNACIONAL PRESENTADA DE FORMA ELECTRÓNICA.
(Instrucciones Administrativas del PCT, Parte Séptima)

1.-Se notifica al solicitante que la Oficina Receptora ha recibido en la fecha de recepción indicada más abajo, los documentos que supuestamente constituyen una solicitud internacional.
2.-Se llama la atención del solicitante sobre el hecho de que la Oficina Receptora no ha comprobado aún si estos documentos satisfacen las condiciones del art. 11.1, es decir, si cumple los requisitos para que le sea atribuida una fecha de presentación internacional. En cuanto la Oficina Receptora haya comprobado los documentos, avisará al solicitante.
3.-El número de la supuesta solicitud internacional indicado más abajo ha sido otorgado automáticamente a estos documentos. Se invita al solicitante a mencionar este número en toda la correspondencia con la Oficina Receptora.

Número de presentación	300374604
Solicitud Número PCT	PCT/ES2020/070486
Fecha de recepción	27 julio 2020
Oficina Receptora	Oficina Española de Patentes y Marcas, Madrid
Referencia del expediente del solicitante o mandatario	PCT16411406b
Solicitante	CONSEJO SUPERIOR DE INVESTIGACIONES CIENTÍFICAS
Número de solicitantes	1
País	ES
Título de la invención	PROCEDIMIENTO DE OBTENCIÓN DE OLEOGELES

MINISTERIO
DE INDUSTRIA, ENERGÍA
Y TURISMO

Oficina Española
de Patentes y Marcas

TRATADO DE COOPERACIÓN EN MATERIA DE PATENTES
NOTIFICACIÓN DE LA RECEPCIÓN DE LOS DOCUMENTOS QUE CONSTITUYEN SUPUESTAMENTE UNA SOLICITUD INTERNACIONAL PRESENTADA DE FORMA ELECTRÓNICA.
(Instrucciones Administrativas del PCT, Parte Séptima)

1.-Se notifica al solicitante que la Oficina Receptora ha recibido en la fecha de recepción indicada más abajo, los documentos que supuestamente constituyen una solicitud internacional.

2.-Se llama la atención del solicitante sobre el hecho de que la Oficina Receptora no ha comprobado aún si estos documentos satisfacen las condiciones del art. 11.1, es decir, si cumple los requisitos para que le sea atribuida una fecha de presentación internacional. En cuanto la Oficina Receptora haya comprobado los documentos, avisará al solicitante.

3.-El número de la supuesta solicitud internacional indicado más abajo ha sido otorgado automáticamente a estos documentos. Se invita al solicitante a mencionar este número en toda la correspondencia con la Oficina Receptora.

Número de presentación	300328864
Solicitud Número PCT	PCT/ES2019/070530
Fecha de recepción	26 julio 2019
Oficina Receptora	Oficina Española de Patentes y Marcas, Madrid
Referencia del expediente del solicitante o mandatario	PCT1641.1406
Solicitante	CONSEJO SUPERIOR DE INVESTIGACIONES CIENTÍFICAS
Número de solicitantes	1
País	ES
Título de la invención	PROCEDIMIENTO DE OBTENCIÓN DE OLEOGELES

Annex C: List of additional publications

Carbohydrate Polymers 199 (2018) 276–285

Contents lists available at ScienceDirect

Carbohydrate Polymers

journal homepage: www.elsevier.com/locate/carbpol

Valorization of *Arundo donax* for the production of high performance lignocellulosic films

Marta Martínez-Sanz*, Evrim Erboz, Cynthia Fontes, Amparo López-Rubio

Food Safety and Preservation Department, IATA-CSIC, Avda. Agustín Escardino 7, 46980 Paterna, Valencia, Spain

ARTICLE INFO

Keywords:
Arundo donax
Biomass
Valorization
Lignocellulose
Packaging

ABSTRACT

This work reports on the valorization of the biomass from the aquatic invasive species *Arundo donax* for the extraction of lignocellulosic fractions and the development of films with interest in food packaging. Stems and leaves were separately evaluated, with the stems producing higher yields and better properties for the extracted fractions.

The purification of cellulose by removing hemicelluloses led to more crystalline and thermally stable fractions, which were more homogeneously dispersed in water and produced films with enhanced transparency, mechanical and water barrier properties.

The application of a simplified extraction protocol, avoiding the use of organic solvents, led to the presence of minor amounts of lipidic impurities in the fractions, which, surprisingly, had a positive impact in the properties of the films. In particular, the film obtained from the purified cellulose without Soxhlet treatment (F3A) outperforms biopolymeric materials such as starch and PLA in terms of mechanical and water barrier performance.

1. Introduction

Plastics are ubiquitous with more than 300 million metric tons produced annually. Despite the tremendous benefits of using plastics for packaging, their single-use character results in an enormous stream of waste with an extremely negative impact on the environment. This hazardous waste not only accumulates in landfills but also leaks towards the ocean (Eriksen et al., 2014). Furthermore, over 90% of plastics are derived from virgin fossil feedstocks, representing about 6% of global oil consumption (Plastics - the Facts, 2015, 2015). Circular economy strategies are required to overcome these sustainability and environmental issues. Only 14% of plastic packaging is currently recycled (Plastics - the Facts, 2015, 2015) and there is a clear consensus that the industry needs to shift to biodegradable plastics from renewable resources. As a result, research efforts are being focused on the development of competitive bioplastics (Wróblewska-Krepsztul et al., 2018).

Lignocellulosic biomass is one of the most abundantly available raw materials on Earth and it represents a cheap feedstock for the extraction of different biopolymers such as cellulose, hemicelluloses and lignin. Lignocellulosic fractions can be extracted from multiple sources: virgin resources such as terrestrial and aquatic plants, algae and aquatic animals (tunicates), or agriculture and forestry-derived waste by-products (Trache, Hussin, Haafiz, & Thakur, 2017). However, sourcing it from waste or underutilized resources that do not compete with the food chain is particularly interesting and in line with the principles of circular economy.

Arundo donax (commonly known as giant reed) is an aquatic plant belonging to the *Poaceae* family that grows spontaneously in temperate areas and is able to adapt to very different environments (Corno, Pilu, & Adani, 2014). Its larger biomass yields occur in freshwater environments such as rivers, lakes and ponds. This plant is native to Asia, but it has been widespread all around the world, especially in southern Europe (Mediterranean area), as a consequence of human activity. Due to their excellent mechanical properties, the stems have been typically used for building and carpentry applications (Flores et al., 2011; Pilu, Badone, & Michela, 2012), but more recently they are also being evaluated as reinforcing fillers in composite materials (Fiore, Botta, Scaffaro, Valenza, & Pirrotta, 2014; Fiore, Scalici, & Valenza, 2014) and as a source of biomass for hydrothermal conversion and production of biofuels (Antonetti, Bonari, Licursi, Nassi o Di Nasso, & Raspolli Galletti, 2015; Corno et al., 2014; Di Girolamo, Grigatti, Barbanti, & Angelidaki, 2013; Licursi et al., 2015; Pilu et al., 2012; Scordia, Cosentino, Lee, & Jeffries, 2011).

Due to its great adaptability to diverse environments and its high growth rate, *A. donax* has become a very problematic invasive species,

* Corresponding author.
E-mail address: mmartinez@iata.csic.es (M. Martínez-Sanz).

https://doi.org/10.1016/j.carbpol.2018.07.029
Received 30 April 2018; Received in revised form 3 July 2018; Accepted 9 July 2018
Available online 11 July 2018
0144-8617/

Valorización de biomasa acuática para el desarrollo de estructuras biopoliméricas de uso alimentario (2): aplicaciones como texturizantes de alimentos

Autores: Cynthia Fontes-Candia, Marta Martínez-Sanz, Isaac Benito-González, Vera Cebrian-Lloret, Antonio Martínez-Abad, Amparo López-Rubio*

Food Safety and Preservation Department, IATA-CSIC, Avda. Agustín Escardino 7, 46980 Paterna, Valencia, Spain

Interdisciplinary Platform for Sustainable Plastics towards a Circular Economy- Spanish National Research Council (SusPlast-CSIC), Madrid, Spain

*amparo.lopez@iata.csic.es

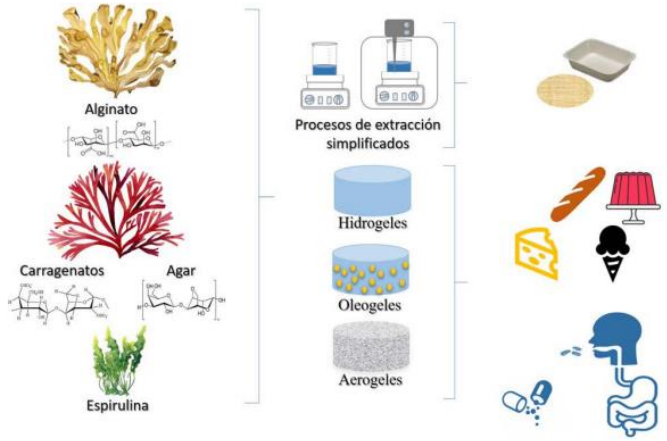

Resumen

Ficocoloides como agar, carragenatos o alginatos, extraídos a partir de algas rojas y marrones, se utilizan ampliamente en la industria alimentaria como texturizantes y pueden estructurarse para formar distintos tipos de geles (hidrogeles, oleogeles y aerogeles). Frente a los métodos tradicionales de extracción utilizados a nivel industrial, se están explorando métodos más eficientes que dan lugar a extractos menos purificados, pero con funcionalidades adicionales. Entender los procesos de gelificación y cómo la composición afecta a la estructuración de estos biopolímeros es clave para el correcto diseño en función de la aplicación final deseada. En este artículo se describen, por un lado, metodologías simplificadas para la extracción de estos ficocoloides y, por otro lado, el uso de los mismos como ingredientes texturizantes.

Palabras clave: algas; *Gelidium sesquipedale*; biomasa acuática; ficocoloides; capacidad antioxidante; geles.

Abstract

Phycocolloids like agar, carrageenan or alginates, extracted from red and brown seaweed, are broadly used in the food industry as texturizing ingredients and they can be structured giving rise to different types of gels (hydrogels, oleogels and aerogels). In order to make phycocolloids extraction processes more efficient industrially, alternative protocols are being established which give rise to less purified extracts, but with additional functionalities. Understanding the gelling processes and how composition affects biopolymer structuring is key for the rational design aiming for a certain application. In this manuscript we describe, on one hand, simplified methodologies to extract the phycocolloids from seaweeds and, on the other hand, the use of the extracted biopolymers as texturizing food ingredients.

Keywords: seaweed; *Gelidium sesquipedale*; aquatic biomass; phycocolloids; antioxidant capacity; gels.

Valorización de biomasa acuática para el desarrollo de estructuras biopoliméricas de uso alimentario (1): materiales para envases biodegradables

Autores: Isaac Benito-González, Marta Martínez-Sanz, Cynthia Fontes-Candia, Vera Cebrian-Lloret, Antonio Martínez-Abad, Amparo López-Rubio*

Food Safety and Preservation Department, IATA-CSIC, Avda. Agustín Escardino 7, 46980 Paterna, Valencia, Spain

Interdisciplinary Platform for Sustainable Plastics towards a Circular Economy- Spanish National Research Council (SusPlast-CSIC), Madrid, Spain

*amparo.lopez@iata.csic.es

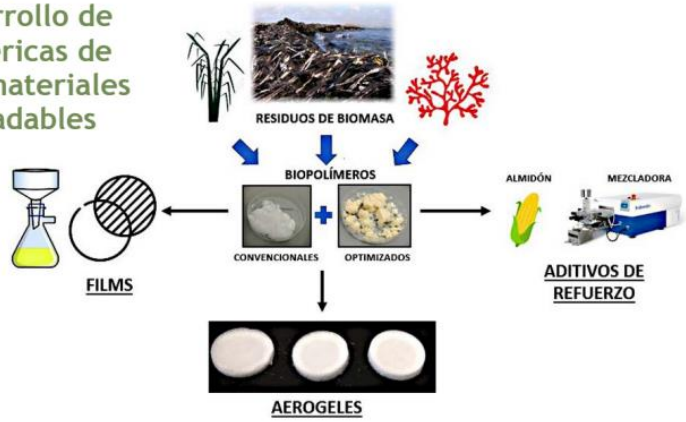

Resumen

La biomasa acuática representa un recurso altamente inexplorado y con un tremendo potencial para el desarrollo de estructuras biopoliméricas con aplicación en el área de envasado alimentario. En general, la celulosa es el biopolímero más ampliamente utilizado como aditivo en estructuras de envase alimentario, pero las hemicelulosas presentes en la biomasa vegetal en general y, más concretamente, en la biomasa acuática, pueden aportar propiedades muy interesantes a los materiales. Por ello, en este artículo se describen metodologías simplificadas para la obtención de distintas fracciones a partir de algas y plantas acuáticas y su utilización para el desarrollo de distintos tipos de estructuras y/o aditivos de envase biodegradables y sostenibles.

Palabras clave: algas; *Gelidium sesquipedale*; biomasa acuática; envases biodegradables; celulosa.

Abstract

Aquatic biomass represents a highly unexplored resource with a tremendous potential for the development of biopolymeric structures with application in the food packaging area. In general, cellulose is the most widely used biopolymer as additive in food packaging structures, but hemicelluloses present in vegetable biomass in general and, more particularly, in aquatic biomass, can provide very interesting properties to the materials. Therefore, in this manuscript we describe simplified methodologies to obtain different fractions from seaweed and aquatic plants and their use for developing different types of food packaging structures and/or additives which are biodegradable and sustainable.

Keywords: seaweed; *Gelidium sesquipedale*; aquatic biomass; biodegradable packaging; cellulose.

GOBIERNO DE MÉXICO | CONACYT Consejo Nacional de Ciencia y Tecnología

GOBIERNO DE ESPAÑA | MINISTERIO DE CIENCIA E INNOVACIÓN

CSIC
CONSEJO SUPERIOR DE INVESTIGACIONES CIENTÍFICAS